

Modular Modification of Polymeric Microspheres

Zur Erlangung des akademischen Grades eines
DOKTORS DER NATURWISSENSCHAFTEN
(Dr. rer. nat.)

Fakultät für Chemie und Biowissenschaften
Karlsruher Institut für Technologie (KIT) - Universitätsbereich

genehmigte
DISSERTATION
von

Dipl. Chem. Michael Kaupp

aus
Nagold, Deutschland

Dekan: Prof. Dr. Peter Roesky
Referent: Prof. Dr. Christopher Barner-Kowollik
Korreferent: Prof. Dr. Manfred Wilhelm
Tag der mündlichen Prüfung: 17.04.2014

Hiermit erkläre ich wahrheitsgemäß, dass ich die vorliegende Doktorarbeit im Rahmen der Betreuung durch Prof. Dr. Christopher Barner-Kowollik, selbständig verfasst und keine anderen als die angegebenen Quellen und Hilfsmittel verwendet habe. Des Weiteren erkläre ich, dass ich mich derzeit in keinem laufenden Promotionsverfahren befinde, und auch keine vorausgegangenen Promotionsversuche unternommen habe.

Karlsruhe, den 17.04.2014

.....

(Michael Kaupp)

Die vorliegende Arbeit wurde von Januar 2011 bis März 2014 unter Anleitung von Prof. Dr. Christopher Barner-Kowollik am Karlsruher Institut für Technologie (KIT) – Universitätsbereich angefertigt.

No 9000 computer has ever made a mistake.

HAL 9000 (2001 – A Space Odyssey)

Always look on the bright side of life.

Eric Idle (Life of Brian)

Abstract

Polymeric microspheres are established as versatile substrates for a wide range of applications, notably in chromatographic systems and as carrier materials. Current research focuses not only on the synthesis of novel microparticles, yet in particular on the effective and versatile modification of existing and facile to synthesize spheres, thereby intensifying present or introducing novel properties.

The current thesis describes several techniques for the modular modification of porous polymeric microspheres and further exploits the possibilities of the developed grafting techniques. All the tethering strategies have in common that the grafted polymers were generated by reversible addition fragmentation chain transfer (RAFT-)polymerization, featuring high end group fidelity as a requirement for successful grafting.

The second commonality of the employed approaches is the utilization of 'grafting-to' techniques, permitting the thorough examination of the polymer chains preceding the immobilization reaction. The primary substrates employed in the current work are porous polymeric microparticles based on glycidyl methacrylate. The motif required for the subsequent ligation was introduced to the spheres in one facile modification step. The conjugation of the polymer chains onto the particle was followed by a thorough investigation utilizing diverse instrumentations such as scanning electron microscopy, X-ray photoelectron spectroscopy, inverse size exclusion chromatography, elemental analysis, fluorescence microscopy, and high resolution attenuated total reflectance FT-IR-microscopy allowing qualitative as well as quantitative insights into the modified particles and the achieved grafting densities.

As a thermally-induced ligation strategy RAFT hetero Diels-Alder was employed – a mild cycloaddition utilizing electron deficient thiocarbonyls originating from RAFT-agents – to immobilize a glycopolymer on cyclopentadiene-functional microspheres. The modification afforded a grafting density of $0.16 \text{ chains} \cdot \text{nm}^{-2}$.

The remaining work describes the precise ligation of polymers onto microspheres via photo-induced conjugation reactions, an unexplored concept for the modification of microparticles. Two novel light-sensitive RAFT-agents were developed, containing func-

tional motifs previously unknown in the structures of RAFT-mediators. The novel RAFT-agents can be utilized to generate a wide variety of different polymers, including glycopolymers, in a controlled fashion.

The primary RAFT-agent contains an ortho-quinodimethane or photo-enol precursor, which forms a highly reactive diene for Diels-Alder reactions upon irradiation ($\lambda_{\text{max}} = 320 \text{ nm}$). The end-functional polymers are capable of generating block copolymers in minutes and can be photo-grafted onto previously maleimide-functionalized particles. Furthermore, the light-triggered reaction allows for the generation of Janus-microspheres utilizing a Pickering emulsion approach.

The second novel RAFT-agent gives rise to a thioaldehyde upon irradiation ($\lambda_{\text{max}} = 355 \text{ nm}$), which can react with dienes as well as nucleophiles. Cylopentadiene-functional microparticles can be photo-grafted with RAFT-polymers generated with the aforementioned RAFT-mediator. The two light-induced ligation techniques lead to grafting densities up to $0.12 \text{ chains} \cdot \text{nm}^{-2}$ (photo-enol) and $0.10 \text{ chains} \cdot \text{nm}^{-2}$ (thioaldehyde-ligation), respectively.

In combination with a direct laser writing setup the latter RAFT-agent can further be utilized to generate patterns of polymers on nucleophilic surfaces, such as PDA interfaces, with submicrometer resolution, which can be imaged via time-of-flight secondary ion mass spectrometry.

Zusammenfassung

Polymere Mikrokugeln sind ein etablierter Werkstoff in einer Vielzahl von Anwendungsbereichen, vor allem im Bereich von Chromatographiesystemen und als Trägermaterial. Aktuelle Forschungsbemühungen konzentrieren sich nicht nur auf die Synthese neuartiger Mikropartikel, sondern insbesondere auf die effektive und vielseitige Funktionalisierung existierender und leicht herzustellender Kugeln, wodurch vorhandene Eigenschaften verstärkt, beziehungsweise neue Eigenschaften generiert werden können. Die vorliegende Dissertation beschreibt verschiedene Techniken für die modulare Funktionalisierung von porösen, polymeren Mikrokugeln, sowie weitere Einsatzmöglichkeiten der entwickelten Verknüpfungsmethoden. Den entwickelten Methoden ist gemein, dass die aufzubringenden Polymere durch die reversible Addition-Fragmentierung-Kettentransfer- (RAFT-) Polymerisation generiert werden, was zu einem hohen Funktionalisierungsgrad der Kettenenden führt, welcher eine Voraussetzung für das erfolgreiche Aufpfropfen der Makromoleküle ist.

Ein weitere Gemeinsamkeit der benutzten Ansätze ist die Anwendung von Aufpfropfungstechniken, wodurch eine detaillierte Analyse der Polymerketten vor dem Aufbringen ermöglicht wird. Als Ausgangsmaterial wurden in dieser Arbeit poröse, polymere Mikropartikel verwendet, die auf Glycidylmethacrylat basieren und auf deren Oberfläche die für das Aufpfropfen benötigte Funktionalität in einem unkomplizierten Reaktionsschritt eingeführt werden konnte. Auf die Verknüpfung der Polymere mit den Partikeln folgte eine umfassende Untersuchung mit verschiedensten Analysesystemen, unter anderem Rasterelektronenmikroskopie, Röntgen-Photoelektronen-Spektroskopie, inverser Größenausschlusschromatographie, Elementaranalyse, Fluoreszenzmikroskopie und hochauflösender, abgeschwächte-Totalreflektions-FT-Infrarotmikroskopie. Durch die verschiedenen Analysemethoden erhält man sowohl qualitative als auch quantitative Informationen über die modifizierten Partikel und die erreichte Funktioanalisisierungsdichte. Der RAFT-hetero-Diels-Alder-Ansatz wurde als eine wärmeinduzierte Verknüpfungsmethode verwendet – eine Cycloaddition, bei der die elektronenarme Schwefel-Kohlenstoff Doppelbindung, die in einigen RAFT-Reglern beinhaltet ist, genutzt wird

– um ein Glucopolymer auf mit Cyclopentadien versehene Mikropartikel aufzubringen. Hierbei wurde eine Funktionalisierungsdichte von 0,16 Molekülen pro nm^{-2} erzielt.

Der verbleibende Teil der Dissertation befasst sich mit der exakten Verknüpfung von Polymeren mit Mikrokugeln durch lichtinduzierte Aufpfropfungstechniken. Dieses Konzept hat in der Literatur für Mikropartikelmodifikation bisher wenig Beachtung gefunden. Zu diesem Zweck wurden zwei neuartige RAFT-Regler entwickelt – die funktionelle Einheiten tragen die zuvor nicht bei RAFT-Molekülen bekannt waren – und für die kontrollierte Polymerisation einer großen Bandbreite an Monomeren, darunter auch Glucomonomeren, geeignet sind.

Einer der RAFT-Regler enthält den Vorläufer für ein ortho-Chinodimethan (oder Photo-Enol-Gruppe), welcher unter Bestrahlung ($\lambda_{\text{max}} = 320 \text{ nm}$) ein in Diels-Alder-Reaktionen überaus reaktives Dien bildet. Die kettenendfunktionalisierten Polymere können innerhalb von Minuten Blockcopolymer bilden und mit Hilfe von Licht auf mit Maleimid funktionalisierte Mikropartikel aufgebracht werden. Darüber hinaus ermöglicht die lichtinduzierte Reaktion die Bildung von Janus-Mikrokugeln (mit zwei sich unterscheidenden Hemisphären) mit Hilfe eines Pickering-Emulsions-Ansatzes.

Der andere neue RAFT-Regler formt bei Bestrahlung ($\lambda_{\text{max}} = 355 \text{ nm}$) ein Thioaldehyd, welches sowohl mit Dienen, als auch mit Nukleophilen, Reaktionen eingehen kann. RAFT-Polymere, die unter Zuhilfenahme des soeben genannten Reglers hergestellt wurden, können bei Bestrahlung auf mit Cyclopentadien funktionalisierte Mikropartikel aufgebracht werden.

Die beiden lichtinduzierten Reaktionen erreichen eine Funktionalisierungsdichte von 0,12 Molekülen pro nm^{-2} (Photo-Enol) bzw. 0,10 Molekülen pro nm^{-2} (Thioaldehyd).

Durch die Verwendung eines Aufbaus für direktes Laser-Schreiben kann der letztgenannte RAFT-Regler darüber hinaus auch für die Erzeugung von beliebigen Mustern aus polymeren Einheiten auf nukleophilen Oberflächen, wie zum Beispiel Poly(Dopamin)-Schichten, herangezogen werden. Die Auflösung der Strukturen liegt dabei im sub-Mikrometerbereich, was mit Hilfe der Flugzeit-Sekundärionen-Massenspektrometrie visualisiert werden konnte.

Publications Arising from the Thesis

1. **Modular Design of Glyco-Microspheres via Mild Pericyclic Reactions and their Quantitative Analysis**

M. Kaupp, A. P. Vogt, J. C. Natterodt, V. Trouillet, T. Gruending, T. Hofe, L. Barner, C. Barner-Kowollik, *Polym. Chem.* **2012**, 3, 2605–2614.

2. **Photo-Sensitive RAFT-Agents for Advanced Microparticle Design**

M. Kaupp, T. Tischer, A. F. Hirschbiel, A. P. Vogt, U. Geckle, V. Trouillet, T. Hofe, M. H. Stenzel, C. Barner-Kowollik, *Macromolecules* **2013**, 46, 6858–6872.

3. **Photo-Induced Functionalization of Spherical and Planar Surfaces via Caged Thioaldehyde End-Functional Polymers**

M. Kaupp, A. Quick, C. Rodriguez-Emmenegger, A. Welle, V. Trouillet, O. Pop-Georgievski, M. Wegener, C. Barner-Kowollik, *Adv. Funct. Mater.* **2014**, DOI: 10.1002/adfm.201400609.

Additional Publications*

- 1. Photo-Induced Conjugation of Dithioester- and Trithiocarbonate-Functional RAFT Polymers with Alkenes[§]**
T. Gruending, M. Kaupp, J. P. Blinco, C. Barner-Kowollik, *Macromolecules* **2011**, *44*, 166–174.
- 2. Orthogonal Ligation to Spherical Polymeric Microparticles: Modular Approaches for Surface Tailoring**
A. S. Goldmann, L. Barner, M. Kaupp, A. P. Vogt, C. Barner-Kowollik, *Prog. Polym. Sci.* **2012**, *37*, 975–984.
- 3. A Facile Route to Boronic Acid Functional Polymeric Microspheres via Epoxide Ring Opening**
A. P. Vogt, V. Trouillet, A. M. Greiner, M. Kaupp, U. Geckle, L. Barner, T. Hofe, C. Barner-Kowollik, *Macromol. Rapid Commun.* **2012**, *33*, 1108–1113.
- 4. (Ultra-)Fast Catalyst-Free Macromolecular Conjugation in Aqueous Environment at Ambient Temperature**
M. Glassner, G. Delaittre, M. Kaupp, J. P. Blinco, C. Barner-Kowollik, *J. Am. Chem. Soc.* **2012**, *134*, 7274–7277.
- 5. Access to Intrinsically Glucoside-Based Microspheres with Boron Affinity**
A. P. Vogt, T. Tischer, U. Geckle, A. M. Greiner, V. Trouillet, M. Kaupp, L. Barner, T. Hofe, C. Barner-Kowollik, *Macromol. Rapid Commun.* **2013**, *34*, 916–921.
- 6. Photochemical Design of Functional Fluorescent Single-Chain Nanoparticles**
J. Willenbacher, K. Wuest, J. O. Mueller, M. Kaupp, H.-A. Wagenknecht, C. Barner-Kowollik, *ACS Macro Lett.* **2014**, *3*, 574–579.

*The publications marked with a § were accomplished during the Diploma thesis. All other publications originate from projects the author was involved in the course of the current thesis.

Contents

Table of Contents	I
List of Figures	V
Abbreviations	XV
1 Introduction	1
1.1 Motivation and Aim of the Thesis	1
2 Background	3
2.1 Polymeric Microspheres – A Literature Overview	4
2.1.1 Synthesis	4
2.1.2 Modification of Microspheres	10
2.1.3 Applications	14
2.2 Reversible Addition Fragmentation Chain Transfer (RAFT) Polymerization	15
2.2.1 Introduction	15
2.2.2 Mechanism of the RAFT-Process	15
2.2.3 Applications	18
2.2.4 RAFT-HDA	21
2.3 Glycopolymers	24
2.4 Light-Induced Grafting Reactions	29
2.4.1 Nitrile Imine Mediated Tetrazole-Ene Coupling (NITEC)	29
2.4.2 Photo-Enol Chemistry	30
2.4.3 Thioaldehyde Ligation	32
2.4.4 Other Techniques	33
3 Modular Design of Glyco-Microspheres via Mild Pericyclic Reactions	35
3.1 Introduction	36
3.2 Results and Discussion	37

3.2.1	Preparation of RAFT-Glycopolymer with HDA End Group	37
3.2.2	Preparation of Cp-Functional Microspheres	38
3.2.3	Small Molecule Model Study of RAFT-HDA Reactions on Cp- Functional Microspheres	42
3.2.4	RAFT-HDA Reaction of Cp-Functional Microspheres with Gly- copolymer	45
3.3	Conclusions	50
3.4	Experimental Part	51
3.4.1	Materials	51
3.4.2	Synthesis of the Poly(Glycidyl Methacrylate) Microspheres	51
3.4.3	Synthesis of Cp-Functional Microspheres	51
3.4.4	Labeling with <i>N</i> -(1-Pyrene)Maleimide	52
3.4.5	RAFT-HDA Model-Reaction	52
3.4.6	RAFT-Polymerization	53
3.4.7	RAFT-HDA Reaction with the Glycopolymer	55
4	Photo-Sensitive RAFT-Agents for Advanced Microparticle Design	57
4.1	Introduction	58
4.2	Results and Discussion	60
4.2.1	Photo-RAFT-Agent Design	60
4.2.2	Model Reaction and Stability Assay	61
4.2.3	RAFT-Polymerizations	63
4.2.4	Block Copolymer Formation	64
4.2.5	Grafting onto Microspheres	67
4.3	Conclusions	81
4.4	Experimental Part	82
4.4.1	Materials	82
4.4.2	Synthesis of 1-((3-Hydroxypropoxy)Carbonyl)Ethyl Dodecyl Carbonotrithioate (DoPATOH)	82
4.4.3	Synthesis of DoPAT-Photo-Enol (DoPATPE)	84
4.4.4	Synthesis of 2-(2',3',4',6'-Tetra- <i>O</i> -Acetyl- β -D-Mannosyloxy) Ethylacrylate (AcManEA)	86
4.4.5	RAFT-Polymerizations	90
4.4.6	Maleimide-Functionalization of PGMA Microspheres	96
4.4.7	Model Photo-Reaction	97
4.4.8	Photo-Induced Block Copolymer Formation	97

4.4.9	Photo-Induced Grafting Reactions and Control Reaction on Microspheres	98
4.4.10	Photo-Induced Synthesis of Janus-Particles	98
5	Functionalization of Microspheres with Photo-Reactive RAFT-Polymers Em- ploying NITEC	101
5.1	Introduction	102
5.2	Results and Discussion	103
5.2.1	RAFT-Polymerization	103
5.2.2	Microsphere Modification	104
5.3	Conclusions	113
5.4	Experimental Part	114
5.4.1	Materials	114
5.4.2	RAFT-Polymerizations	114
5.4.3	Photo-Reactions	119
6	Photo-Induced Functionalization of Spherical and Planar Surfaces via Caged Thioaldehyde End-Functional Polymers	121
6.1	Introduction	122
6.2	Results and Discussion	123
6.2.1	Photo-RAFT-Agent Design	123
6.2.2	RAFT-Polymerization	124
6.2.3	Functionalization of Microspheres	125
6.2.4	Spatially Resolved Grafting via Direct Laser Writing	136
6.3	Conclusions	139
6.4	Experimental Part	140
6.4.1	Materials	140
6.4.2	Synthesis of DoPAT-Phenacysulfid (DoPATPAS)	140
6.4.3	RAFT-Polymerizations	143
6.4.4	Functionalization of Silicon Wafers and Glass Slides with Poly- dopamin (PDA)	149
6.4.5	Photo-Reactions	149
7	Concluding Remarks and Outlook	151
8	Characterization Methods	155
8.1	Scanning Electron Microscopy (SEM)	155
8.2	Gel Permeation Chromatography (GPC)	155

8.3	Electrospray Ionization – Mass Spectrometry (ESI–MS)	156
8.4	Density Measurements	156
8.5	Nuclear Magnetic Resonance (NMR) Spectroscopy	156
8.6	Inverse Size Exclusion Chromatography (iSEC)	156
8.7	Gel Permeation Chromatography – Electrospray Ionization – Mass Spectrometry (GPC–ESI–MS)	157
8.8	X-Ray Photoelectron Spectroscopy (XPS)	157
8.9	Attenuated Total Reflectance (ATR) FT-IR-Microscopy Imaging	158
8.10	Ultraviolet-Visible (UV-Vis) Spectroscopy	158
8.11	Confocal Fluorescence Microscopy	158
8.12	Elemental Analysis (EA)	159
8.13	Time-of-Flight Secondary Ion Mass Spectrometry (ToF-SIMS)	159
8.14	Spectroscopic Ellipsometry	159
A	Appendix	161
A.1	Additional SEM Images from Chapter 4	168
A.2	SEM Images from Chapter 5	177
A.3	SEM Images from Chapter 6	183
	Bibliography	203
	Curriculum Vitae	205
	Publications and Conference Contributions	207
	Acknowledgements	211

List of Figures

2.1	Schematic depiction of the suspension polymerization technique.	5
2.2	Schematic description of the stages of precipitation polymerization for porous particle production.	6
2.3	Schematic description of the stages of dispersion polymerization.	7
2.4	Schematic representation of the mechanism of emulsion polymerization.	8
2.5	Schematic microfluidic capillary co-flow device as an example for the various microfluidic systems.	9
2.6	Schematic representation of the general difference between the 'grafting-from' and the 'grafting-to' approach.	10
2.7	Mechanism of reversible addition fragmentation chain transfer polymerization.	16
2.8	Mechanism of nitroxide mediated polymerization.	17
2.9	Mechanism of atom transfer radical polymerization.	17
2.10	Guidelines for the selection of the R- and Z-group of RAFT agents for various polymerizations.	18
2.11	Processes for RAFT-end group transformation.	19
2.12	Overview of macromolecular compositions and architectures that are accessible via the RAFT-process.	20
2.13	Mechanism of RAFT-HDA. Right: Available Z-groups promoting RAFT-HDA.	21
2.14	RAFT-HDA reaction between the glycopolymer PAGlc and cyclopentadiene-functional PEG in aqueous solution	22
2.15	RAFT-HDA reaction between cyclopentadiene-functionalized cellulose and poly(isobornyl acrylate).	22
2.16	HDA reaction between polymeric microparticles and diene-functionalized poly(ϵ -caprolactone).	23
2.17	Exemplary overview of glycomonomers polymerizable with RDRP techniques.	24

2.18	Synthetic approach for the preparation of <i>S-co</i> -HEAGI statistical glycopolymers by FRP. Atomic force microscopy image of films obtained by spin coating of the copolymer and polystyrene. Fluorescence image obtained by recognition between the glycopolymer and fluorescein-conjugated concanavalin A within the pores.	25
2.19	Structure of seven-arm β -cyclodextrin-((poly(hydroxyethyl acrylate) ₁₀ - <i>b</i> -(poly(<i>N</i> -acryloyl glucose) ₁₀) ₇).	26
2.20	Synthetic method to achieve intrinsically glucoside-based microspheres via water in olive oil inverse suspension polymerization.	27
2.21	Synthesis of glycopolymer-grafted DVB microspheres.	28
2.22	Synthetical procedure to pattern a PDA coated silicon wafer with anti-fouling brushes. ToF-SIMS imaging of the successful surface modification. Stained cell pattern after 7 h culture proving the anti-fouling behaviour.	30
2.23	Photo-patterning of biosurfaces with a model peptide and PTFEMA employing photo-enol chemistry.	31
2.24	Photo-patterning of silicon wafers with nucleophiles employing thioaldehyde ligation.	32
3.1	Schematic illustration of the synthetic steps for the grafting of glycopolymers onto porous microspheres via the RAFT-HDA approach.	37
3.2	Z-groups presently available for RAFT-agents that are able to undergo hetero Diels-Alder (HDA) reactions.	37
3.3	GPC-ESI-MS spectra of a representative repetition unit of the protected glycopolymer PAIpGlc synthesized via RAFT-polymerization.	39
3.4	Overview of the functionalization and grafting reactions on microspheres.	40
3.5	Photograph of suspensions of microspheres with different pore sizes after Cp-functionalization and fluorescent marking with <i>N</i> -(1-pyrene) maleimide.	41
3.6	False color high-resolution ATR FT-IR-microscopy images of a single 1000 Å PGMA microsphere before and after Cp-functionalization, and after RAFT-HDA reaction with glycopolymer, respectively.	41
3.7	Overview of the loading capacity achieved via HDA chemistry as a function of the reaction time and the average pore size of the employed substrate.	43
3.8	SEM images of the non-modified PGMA microspheres with an average pore size of 1000 Å and the same spheres after Cp-functionalization and RAFT-HDA reaction with glycopolymer.	46

3.9	N 1s and S 2p XP spectra of Cp-functionalized microspheres before and after HDA reaction.	47
3.10	Evolution of the ratio of oxygen to carbon determined by elemental analysis.	47
3.11	GPC trace in DMAc of PAIpGlc polymerized with BPDF.	53
3.12	GPC trace in THF of PAIpGlc polymerized with BPDF.	54
3.13	¹ H-NMR spectrum of PAIpGlc polymerized with BPDF	55
3.14	GPC trace in DMAc of PAGlc polymerized with BPDF.	56
3.15	¹ H-NMR spectrum of PAGlc polymerized with BPDF	56
4.1	Schematic illustration of the synthetic strategy employing the RAFT-photo-enol agent based on DoPAT.	59
4.2	Synthesis and structural information of the photo-enol RAFT-agent DoPATPE.	60
4.3	Comparison of ¹ H-NMR spectra of DoPATPE before and after irradiation for 30 min.	61
4.4	Model reaction between DoPATPE and a maleimide-functionalized poly(ethylene glycol) (PEG-Mal).	62
4.5	Light-triggered block copolymer formation between PacManEA and PEG-Mal.	65
4.6	Light-triggered block copolymer formation between PDMAA and PEG-Mal.	66
4.7	Comparison of the GPC traces of pure PacManEA, the block copolymer of PacManEA and PEG formed after 10 min of UV-irradiation and the control reaction of pure PacManEA irradiated for 30 min.	66
4.8	Maleimide-functionalization of PGMA microspheres.	68
4.9	S 2p XP spectra of maleimide-functional microspheres grafted with DoPATPE and the control reaction between PGMA microspheres and DoPATPE.	70
4.10	Light-induced grafting reactions of RAFT-polymers onto maleimide functionalized microspheres.	72
4.11	S 2p XP spectra of maleimide-functional microspheres and spheres grafted with PS , PDMAA and PacManEA.	72
4.12	N 1s XP spectra of untreated PGMA microspheres, maleimide-functionalized spheres, and spheres photo-grafted with PDMAA.	73
4.13	C 1s XP spectra of maleimide-functionalized microspheres and spheres photo-grafted with PS, PacManEA, and PDMAA.	74

4.14	Comparison of the amount of carbon bound to oxygen or nitrogen and carbon bound to carbon or hydrogen based on the deconvolution of the carbon peak in the XP spectra and the oxygen to carbon ratio determined via EA.	75
4.15	False color high resolution FT-IR-microscopy images of a GMA microsphere functionalized with maleimide and after photo-grafting of PDMAA.	77
4.16	SEM images of wax spheres covered with PGMA microspheres.	79
4.17	False color high resolution FT-IR-microscopy images of a maleimide-functionalized microsphere after photo-grafting of PDMAA on one-half of the sphere employing a Pickering emulsion approach.	80
4.18	Comparison of IR spectra extracted from the mapping in Figure 4.17 to illustrate the difference generated by the spatial resolved photo-induced grafting of PDMAA onto microparticles partially protected by wax.	80
4.19	¹ H-NMR spectrum of 1-((3-hydroxypropoxy)carbonyl)ethyl dodecyl carbonotrithioate (DoPATOH).	83
4.20	¹³ C-NMR spectrum of 1-((3-hydroxypropoxy)carbonyl)ethyl dodecyl carbonotrithioate (DoPATOH).	84
4.21	¹ H-NMR spectrum of DoPATPE.	85
4.22	¹³ C-NMR spectrum of DoPATPE.	86
4.23	¹ H-NMR spectrum of β-D-mannose pentaacetate.	87
4.24	¹³ C-NMR spectrum of β-D-mannose pentaacetate.	87
4.25	¹ H-NMR spectrum of 2-(2',3',4',6'-tetra-O-acetyl-β-D-mannosyloxy)ethylacrylate (AcManEA).	89
4.26	¹³ C-NMR spectrum of 2-(2',3',4',6'-tetra-O-acetyl-β-D-mannosyloxy)ethylacrylate (AcManEA).	89
4.27	GPC trace of polystyrene polymerized with DoPATPE.	90
4.28	¹ H-NMR spectrum of polystyrene polymerized with DoPATPE.	91
4.29	Zoom into the ESI-MS spectrum of polystyrene polymerized with DoPATPE.	91
4.30	GPC trace of poly(<i>N,N</i> -dimethylacrylamide) polymerized with DoPATPE.	92
4.31	¹ H-NMR of poly(<i>N,N</i> -dimethylacrylamide) polymerized with DoPATPE.	93
4.32	Zoom into the ESI-MS spectrum of poly(<i>N,N</i> -dimethylacrylamide) polymerized with DoPATPE.	93
4.33	GPC trace in THF of PAcManEA polymerized with DoPATPE.	95
4.34	GPC trace in DMAc of PAcManEA polymerized with DoPATPE.	95
4.35	¹ H-NMR spectrum of PAcManEA polymerized with DoPATPE.	96

5.1	General reaction strategy to graft RAFT-polymers onto polymeric microspheres via NITEC.	102
5.2	Test and control reaction for the UV-induced grafting on microspheres employing DoPATTET.	105
5.3	Fluorescence microscopy images of test and control reaction of UV-induced grafting reactions of DoPATTET on microspheres.	107
5.4	Light-induced grafting of RAFT-polymers onto maleimide-functionalized microspheres employing NITEC.	108
5.5	N 1s XP spectra of maleimide functionalized PGMA particles and microspheres photo-grafted with PS and PDMAA.	109
5.6	S 2p XP spectra of maleimide functionalized PGMA particles and microspheres photo-grafted with PS and PDMAA.	109
5.7	False color high resolution FT-IR-microscopy images of a microsphere functionalized with maleimide and after UV-grafting of PDMAA.	111
5.8	Fluorescence microscopy images of UV-induced grafting reactions of PS and PDMAA on microspheres.	112
5.9	Comparison of the spectra of poly(<i>N,N</i> -dimethylacrylamide) polymerized with DoPATTET before and after the UV-induced grafting reaction.	113
5.10	GPC trace of polystyrene polymerized with DoPATTET.	115
5.11	¹ H-NMR spectrum of polystyrene polymerized with DoPATTET.	115
5.12	Zoom into the ESI-MS spectrum of polystyrene polymerized with DoPATTET.	116
5.13	GPC trace of poly(<i>N,N</i> -dimethylacrylamide) polymerized with DoPATTET.	117
5.14	¹ H-NMR spectrum of poly(<i>N,N</i> -dimethylacrylamide) polymerized with DoPATTET.	117
5.15	Zoom into the ESI-MS spectrum of poly(<i>N,N</i> -dimethylacrylamide) polymerized with DoPATTET.	118
6.1	Synthesis and reactivity of the novel photo-reactive RAFT-agent DoPATPAS.	123
6.2	Cp-functionalization of PGMA microspheres employing sodium cyclopentadienide; Control reaction between PGMA spheres and DoPATPAS; Test reaction between Cp-functional spheres and DoPATPAS.	126
6.3	S 2p XP spectra of Cp-microspheres photo-grafted with DoPATPAS and of PGMA spheres subjected to the same reaction conditions.	127
6.4	Photo-triggered grafting reactions of RAFT-polymers onto Cp-functionalized microspheres.	129

6.5	S 2p XP spectra of Cp-microspheres, spheres photo-grafted with PAcManEA, PDMAA and PS.	130
6.6	N 1s XP spectra of non-modified PGMA particles, Cp-functionalized microspheres and microspheres photo-grafted with PDMAA.	130
6.7	C 1s XP spectra of Cp-functionalized microspheres and microspheres photo-grafted with PS, PAcManEA, and PDMAA.	132
6.8	Comparison of the amount of carbon bound to oxygen or nitrogen and carbon bound to carbon or hydrogen based on the deconvolution of the carbon peak in the XP spectra.	133
6.9	False color high resolution FT-IR-microscopy images of a cyclopentadiene functionalized PGMA microsphere before and after photo-grafting of PDMAA.	134
6.10	Comparison of the nitrogen contents derived from elemental and XPS analysis of all microsphere samples.	135
6.11	Comparison of the sulfur contents derived from elemental and XPS analysis of all microsphere samples.	136
6.12	Synthetic route for the photo-patterning of PDA-interfaces.	137
6.13	ToF-SIMS imaging of PDA-functionalized surfaces photo-grafted with PS via DLW.	138
6.14	¹ H-NMR spectrum of DoPATPAS.	141
6.15	¹³ C-NMR spectrum of DoPATPAS.	142
6.16	UV-Vis spectrum of DoPATPAS in acetonitrile.	142
6.17	GPC trace of polystyrene polymerized with DoPATPAS.	143
6.18	¹ H-NMR spectrum of polystyrene polymerized with DoPATPAS.	144
6.19	Zoom into the ESI-MS spectrum of polystyrene polymerized with DoPATPAS.	144
6.20	GPC trace of poly(<i>N,N</i> -dimethylacrylamide) polymerized with DoPATPAS.	145
6.21	¹ H-NMR spectrum of poly(<i>N,N</i> -dimethylacrylamide) polymerized with DoPATPAS.	146
6.22	Zoom into the ESI-MS spectrum of poly(<i>N,N</i> -dimethylacrylamide) with DoPATPAS.	146
6.23	GPC trace of PAcManEA polymerized with DoPATPAS.	148
6.24	¹ H-NMR spectrum of PAcManEA polymerized with DoPATPAS.	148
A.1	Illustration of the employed photo-reactor.	162
A.2	Zoom into the ESI-MS spectrum of PEG-Mal.	162

A.3	Zoom into the ESI-MS spectrum of the photo-adduct between PEG-Mal and DoPATPE after 60 min irradiation.	163
A.4	Zoom into the single charged region of the ESI-MS spectrum of the model reaction between DoPATPE and PEG-Mal.	164
A.5	Picture of the suspension of maleimide-functionalized microspheres in a solution of RAFT-polymer in DCM.	164
A.6	Excerpt of the $^1\text{H-NMR}$ spectrum of the photo-addition of DoPATPE to PEG-Mal.	165
A.7	$^1\text{H-NMR}$ spectrum of PEG-Mal.	165
A.8	Overlay of GPC traces in THF showing the formation of the photo-adduct between PEG-Mal and DoPATPE.	166
A.9	Image of the wax sphere decorated with maleimide-functionalized microspheres.	166
A.10	C 1s XP spectrum of Cp-functionalized microspheres photo-grafted with DoPATPAS and the control reaction of PGMA spheres applied to the same reaction conditions.	167
A.11	'Intensity profile' for the C_7H_7^+ signal across an edge of the DLW patterned structure shown in Figure 6.13 right.	167
A.12	SEM image of the maleimide-functionalized microspheres. Overview image.	168
A.13	SEM image of the maleimide-functionalized microspheres. Zoom image.	168
A.14	SEM image of the maleimide-functionalized microspheres. Surface morphology image.	169
A.15	SEM image of the maleimide-functionalized microspheres grafted with PS. Overview image.	169
A.16	SEM image of the maleimide-functionalized microspheres grafted with PS. Zoom image.	170
A.17	SEM image of the maleimide-functionalized microspheres grafted with PS. Surface morphology image.	170
A.18	SEM image of the maleimide-functionalized microspheres grafted with PacManEA. Overview image.	171
A.19	SEM image of the maleimide-functionalized microspheres grafted with PacManEA. Zoom image.	171
A.20	SEM image of the maleimide-functionalized microspheres grafted with PacManEA. Surface morphology image.	172
A.21	SEM image of the maleimide-functionalized microspheres grafted with PDMAA. Overview image.	172

A.22 SEM image of the maleimide-functionalized microspheres grafted with PDMAA. Zoom image.	173
A.23 SEM image of the maleimide-functionalized microspheres grafted with PDMAA. Surface morphology image.	173
A.24 SEM image of a wax sphere covered with maleimide-functionalized microspheres.	174
A.25 SEM image of the surface of a wax sphere covered with maleimide-functionalized microspheres.	174
A.26 SEM image of the maleimide-functionalized microspheres half grafted with PDMAA. Overview image.	175
A.27 SEM image of the maleimide-functionalized microspheres half grafted with PDMAA. Zoom image.	175
A.28 SEM image of the maleimide-functionalized microspheres half grafted with PDMAA. Surface morphology image.	176
A.29 SEM image of the maleimide-functionalized microspheres. Overview image.	177
A.30 SEM image of the maleimide-functionalized microspheres. Zoom image.	177
A.31 SEM image of the maleimide-functionalized microspheres. Surface morphology image.	178
A.32 SEM image of the maleimide-functionalized microspheres grafted with DoPATTET. Overview image.	178
A.33 SEM image of the maleimide-functionalized microspheres grafted with DoPATTET. Zoom image.	179
A.34 SEM image of the maleimide-functionalized microspheres grafted with DoPATTET. Surface morphology image.	179
A.35 SEM image of the maleimide-functionalized microspheres grafted with PS. Overview image.	180
A.36 SEM image of the maleimide-functionalized microspheres grafted with PS. Zoom image.	180
A.37 SEM image of the maleimide-functionalized microspheres grafted with PS. Surface morphology image.	181
A.38 SEM image of the maleimide-functionalized microspheres grafted with PDMAA. Overview image.	181
A.39 SEM image of the maleimide-functionalized microspheres grafted with PDMAA. Zoom image.	182
A.40 SEM image of the maleimide-functionalized microspheres grafted with PDMAA. Surface morphology image.	182

A.41 SEM image of the Cp-functionalized microspheres photo-grafted with DoPATPAS. Overview image.	183
A.42 SEM image of the Cp-functionalized microspheres photo-grafted with DoPATPAS. Zoom image.	183
A.43 SEM image of the Cp-functionalized microspheres photo-grafted with DoPATPAS. Surface morphology image.	184
A.44 SEM image of the Cp-functionalized microspheres photo-grafted with PS. Overview image.	184
A.45 SEM image of the Cp-functionalized microspheres photo-grafted with PS. Zoom image.	185
A.46 SEM image of the Cp-functionalized microspheres photo-grafted with PS. Surface morphology image.	185
A.47 SEM image of the Cp-functionalized microspheres photo-grafted with PDMAA. Overview image.	186
A.48 SEM image of the Cp-functionalized microspheres photo-grafted with PDMAA. Zoom image.	186
A.49 SEM image of the Cp-functionalized microspheres photo-grafted with PDMAA. Surface morphology image.	187
A.50 SEM image of the Cp-functionalized microspheres photo-grafted with PacManEA. Overview image.	187
A.51 SEM image of the Cp-functionalized microspheres photo-grafted with PacManEA. Zoom image.	188
A.52 SEM image of the Cp-functionalized microspheres photo-grafted with PacManEA. Surface morphology image.	188

Abbreviations

AcManEA	2-(2',3',4',6'-Tetra-O-Acetyl- β -D-Mannosyloxy) Ethylacrylate
AIPGlc	3-O-Acryloyl-1,2:5,6-Di-O-Isopropylidene- α -D-Glucopyranoside
AIBN	2,2'-Azobis(2-methylpropionitrile)
AM	Acrylamide
AN	Acrylonitrile
AOI	Angle of Incidence
AROP	Anionic Ring-Opening Polymerization
ATR	Attenuated Total Reflectance
ATRP	Atom Transfer Radical Polymerization
BE	Binding Energy
BPDF	Benzyl Pyridin-2-Yldithioformate
CAE	Constant Analyzer Energy
CuAAC	Copper Catalyzed Azide-Alkyne Cycloaddition
Cp	Cyclopentadiene
DCM	Dichloromethane
DLW	Direct Laser Writing
DMAA	<i>N,N</i> -Dimethylacrylamide
DMAC	<i>N,N</i> -Dimethylacetamide
DMF	<i>N,N</i> -Dimethylformamide
DMSO	Dimethyl Sulfoxide
DoPAT	2-((Dodecylsulfanyl)Carbonothioyl)Sulfanyl Propanoic Acid
DoPATOH	1-((3-Hydroxypropoxy)Carbonyl)Ethyl Dodecyl Carbonotrithioate
DoPATPAS	DoPAT-Phenacylsulfid
DoPATPE	DoPAT-Photo-Enol
DoPATET	DoPAT-Tetrazole
DVB	Divinylbenzene
e.g.	for Example (exempli gratia)
EA	Elemental Analysis

EAL	Effective Attenuation Length
ESI	Electrospray Ionization
FT	Fourier Transformation
FPA	Focal Plane Array
FRP	Free Radical Polymerization
GD	Grafting Density
GMA	Glycidyl Methacrylate
GPC	Gel Permeation Chromatography
HDA	Hetero Diels-Alder
HEAGI	2-[(D-Glucosamin-2-N-yl) Carbonyl]oxyethyl Acrylate
HEMA	Hydroxyethyl Methacrylate
HPLC	High-Performance Liquid Chromatography
HPMAM	N-(2-Hydroxypropyl)Methacrylamide
i.e.	that is (id est)
IR	Infrared
iSEC	Inverse Size Exclusion Chromatography
LC	Loading Capacity
MA	Methyl Acrylate
MCT	Mercury Cadmium Telluride
MMA	Methyl Methacrylate
MRFA	Met-Arg-Phe-Ala Acetate
MS	Mass Spectrometry
MWCO	Molecular Weight Cut Off
NA	Numerical Aperture
NBR	Nitrile-Butadiene Rubber
NITEC	Nitrile Imine Mediated Tetrazole-Ene Coupling
NMP	Nitroxide Mediated Polymerization
NMR	Nuclear Magnetic Resonance
NVC	N-Vinylcarbazole
NVP	N-Vinylpyrrolidone
PAcManEA	Poly(2-(2',3',4',6'-Tetra-O-Acetyl-β-D-Mannosyloxy)- Ethylacrylate
PAGlc	Poly(3-O-Acryloyl-α,β-D-Glucopyranoside)
PAIpGlc	Poly(3-O-Acryloyl-1,2:5,6-Di-O-Isopropylidene-α-D- Glucofuranoside)
PDA	Poly(Dopamine)
PDMAA	Poly(N,N-Dimethylacrylamide)

PDVB	Poly(Divinyl Benzene)
PEG	Poly(Ethylene Glycol)
PEG-Mal	Maleimide-Functionalized Poly(Ethylene Glycol)
PGMA	Poly(Glycidyl Methacrylate)
PHEMA	Poly(Hydroxyethyl Methacrylate)
ppm	Parts per Million
PS	Polystyrene
PSS	Polymer Standards Service
PTFEMA	Poly(Trifluoro Ethyl Methacrylate)
RAFT	Reversible Addition Fragmentation Chain Transfer
RDRP	Reversible Deactivation Radical Polymerization
RI	Refractive Index
SBR	Styrene-Butadiene Rubber
SEC	Size Exclusion Chromatography
SEM	Scanning Electron Microscopy
SIMS	Secondary Ion Mass Spectrometry
S	Styrene
TEMPO	2,2,6,6-Tetramethylpiperidine-1-Oxyl
TFA	Trifluoroacetic Acid
Tfa	Trifluoroacetate
THF	Tetrahydrofuran
ToF	Time-of-Flight
UV	Ultraviolet
VAc	Vinylacetate
XPS	X-Ray Photoelectron Spectroscopy

1

Introduction

Spherical polymeric microparticles play an important role in many applications, ranging from solid supports for catalysts^[1,2] or synthesis^[3,4] to being the solid state material in a variety of chromatographic techniques such as GPC^[5] and HPLC.^[6] Many parameters of these particles can be adjusted during their synthesis as they can be fully cross-linked, porous,^[7] hollow,^[8] contain (magnetic) nanoparticles^[9] and can range in size from less than one to several hundred micrometers, depending on the synthesis procedure. Although a multitude of functionalities and properties of the microparticles can already be introduced during the synthesis, a research focus lies on the grafting of polymeric structures onto facile to manufacture precursor microparticles,^[10] thus imparting novel properties onto the particles, which is interesting from a commercial point of view as well.

1.1 Motivation and Aim of the Thesis

The aim of the current thesis is to improve established and find novel grafting techniques for the functionalization of microparticles with polymeric chains and to add spatial control to the grafting reaction. Several requirements are desired for the ligation techniques: First, the to-be grafted chains should be facile and universal to synthesize and be thoroughly characterized prior to the attachment. Second, the reaction conditions should be mild and metal free, allowing the grafting to not only be conducted on microparticles

but for other substrates, including bio-substrates as well in the future. In addition, the functionalized microspheres should be characterized comprehensively with various techniques, leading to qualitative and – more important – quantitative information about the grafting.

In the current thesis the base materials are porous polymeric microspheres consisting of poly(glycidyl methacrylate) synthesized via suspension polymerization. The epoxide moiety of glycidyl methacrylate can subsequently be employed for further functionalization reactions. In the present thesis the diene cyclopentadiene and dienophile/dipolarophile maleimid was immobilized on the surface of the particles. These functionalizations allowed for several pericyclic grafting reactions to be conducted on the particles, also tethering challenging structures such as glycopolymers. The grafted macromolecules were in all cases polymerized via reversible addition fragmentation chain transfer (RAFT) polymerization, the most versatile controlled polymerization technique^[11–15] and could be grafted onto the microspheres without any further treatment, since the reactive moieties were already incorporated by the polymerization. The applied grafting strategies were the well known thermally-induced RAFT hetero Diels-Alder approach,^[16] UV-triggered nitrile imine mediated tetrazole-ene coupling^[17] – where existing RAFT-agents were employed – and two light-induced reactions based on photo-generated ortho-quinodimethanes or photo-enols^[18] and thioaldehydes,^[19] which were combined with RAFT-polymerization for the first time. The functionalized particles as well as the to-be grafted polymers were thoroughly analyzed via SEM, elemental analysis, mass spectrometry, GPC, inverse size exclusion chromatography, NMR spectroscopy, confocal fluorescence microscopy, high resolution attenuated total reflectance FT-IR-microscopy, and XPS, leading to qualitative as well as quantitative information about the grafting success. The novel photo-reactive RAFT-agents were furthermore utilized to generate challenging structures, such as block copolymers, Janus-microspheres exhibiting two different hemispheres, and various patterns on flat surfaces via a direct laser writing setup.

2

Background

The current chapter will give an overview about the topics the thesis combines. All the following chapters will describe how porous polymeric microspheres based on PGMA can be modified via the grafting of polymers that were synthesized with the RAFT-process. Chapter 3 deals with the decoration of microparticles with small molecules as well as a glycopolymers. Chapter 4 to 6 will describe the tethering of several polymers, including a glycopolymers (except for Chapter 5). For the immobilization of the polymeric chains a thermally-triggered and several light-induced grafting reactions are utilized, two of which (photo-enol^[18] and thioaldehyde ligation^[19]) were not combined with RAFT before. All of the aforementioned topics are well investigated and/or in the focus of research – which can be seen by the current and total number of publications (Table 2.1 on the following page) – so here merely an overview with some groundbreaking and remarkable examples can be given, and the reader is referred to the cited literature for more details. For light induced grafting reactions a comprehensive publication list is hard to generate due to the difficulty in finding search terms which would exclude studies from similar topics. For polymeric microspheres, their different synthesis methods as well as their applications will be described. In addition, the modification of microparticles via the grafting of polymers, especially via 'grafting-to' methods will be presented. RAFT-polymerization will be introduced with its mechanism and manifold possibilities, together with a short comparison to other RDRP techniques. A special focus will lie on the RAFT-HDA

technique,^[16] which was developed and thoroughly investigated by our group. The topic of glycopolymers will be summarized before the last section will focus on light-induced grafting reactions, which can be employed for spatially controlled grafting on surfaces.

Table 2.1: Topics addressed in the current thesis with corresponding publications in 2013 and in total.¹

topic	publications 2013	total publications
microspheres ²	918	13,681
RAFT-polymerization ³	786	5,379
glycopolymers ⁴	115	1046

¹Search on February 10th, 2014 in SciFinder[®], duplicates removed if possible. Search terms:

²microspheres + polymer; ³RAFT + polymerization; ⁴glycopolymer.

2.1 Polymeric Microspheres – A Literature Overview

Polymeric microparticles consist of crosslinked polymeric structures in the size range of close to one to several hundred micrometers and are spherical in most cases, although a variety of shapes, spanning and surpassing the range of discs to rods,^[20,21] is known as well. Spherical shapes predominate, as spheres offer the highest volume to surface ratio, thereby minimizing the surface tension. Due to their versatility in form, size, functionalities and other properties microparticles have been employed in a wide repertoire of applications for decades (Section 2.1.3).

2.1.1 Synthesis

The commonality of all manufacturing processes for polymeric microparticles is the immiscibility of two phases. The most common techniques are suspension, precipitation, dispersion, and emulsion polymerization as well as microfluidic approaches and other more special techniques. The aforementioned approaches will be discussed below, yet the interested reader is also referred to excellent reviews by Arshady,^[22] Kawaguchi,^[23] and Du Prez^[7] to obtain in-depth insight into the reaction mechanisms and possibilities during the synthesis of the microparticles.

Suspension Polymerization

Most commonly the suspension polymerization entails the polymerization of a hydrophobic divinyllic/vinyllic monomer mixture in water as the continuous phase, although the

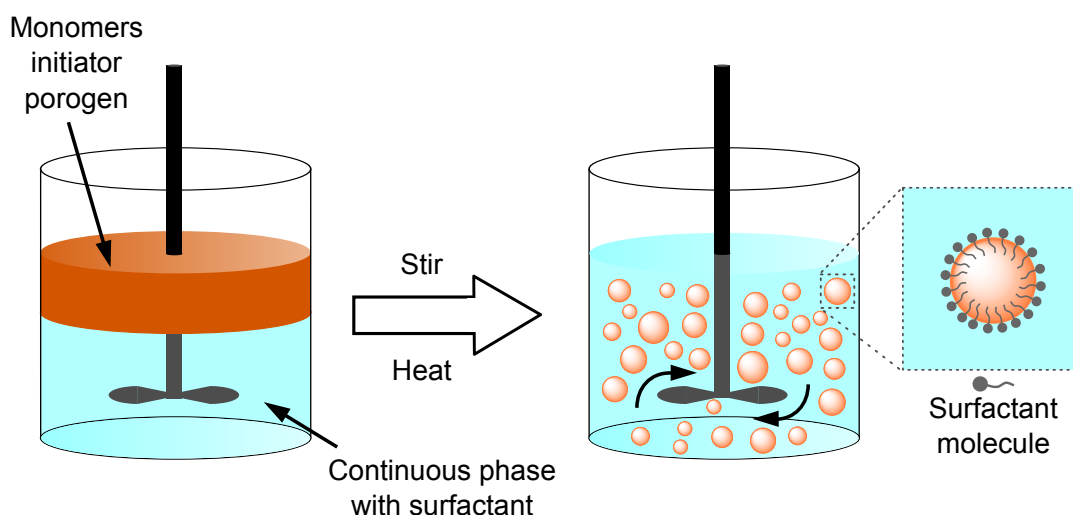


Figure 2.1: Schematic depiction of the suspension polymerization technique. Adapted with permission from [7].

inverse case is well known, too. The size of the produced microspheres reaches up to several hundred micrometers and – with the addition of porogens such as solvents or polymers – porosity can be achieved. The size of the particles is tuneable by changing the agitation speed as well as the shape of the reaction vessel and the stirrer. The degree of porosity is adjustable over several orders of magnitude by varying the concentration and kind of the porogen. A radical initiator not soluble in water needs to be added and the polymerization occurs only in the organic phase. Surfactants or stabilizers are often added to the reaction mixture to stabilize the suspension. During and before the polymerization a continuous agitation is required to form and maintain the suspension, leading to collisions of the droplets, thus being the major reason for the polydispersity observed in most particles derived from suspension polymerization. Suspension polymerization allows for the synthesis of intrinsically glucoside-based microspheres.^[24] With the addition of hydrophobic magnetic nanoparticles to the reaction, microspheres with magnetic properties can be achieved.^[9] With suspension polymerization even hollow spheres can be prepared,^[8] and with water as the porogen and blowing agent, pores with diameters of up to 100 μm on millimeter sized beads have been achieved.^[25]

Precipitation Polymerization

Microparticles produced by precipitation polymerization, introduced by the group of Stöver, are mostly based on divinylbenzene (DVB) as crosslinker and monomer, range in size between 2 and 10 μm and are monodisperse.^[26] No additional surfactants and stabilizers are required, leading to very pure particles. The reaction starts in a homogeneous mixture of the reactants and the phase separation between the nuclei and the poor solvent –

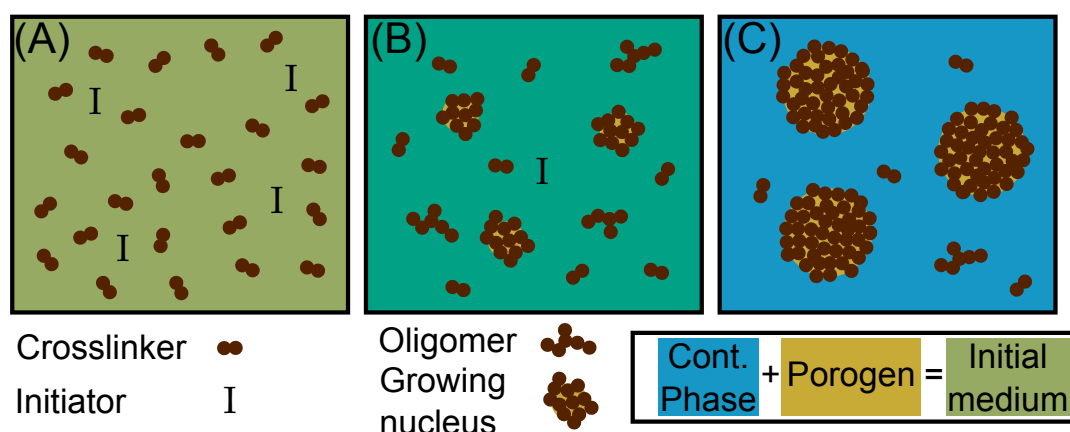


Figure 2.2: Schematic description of the stages of precipitation polymerization for porous particle production. (A) Initially, only crosslinker and initiator molecules are in the medium. (B) Oligomers and nuclei are being formed due to radical polymerization. (C) As the reaction continues, nuclei grow by adding monomers and oligomers from the medium. In reality, there is a swollen layer of oligomers around the nuclei. Adapted with permission from [7].

mostly the near Θ -solvent acetonitrile – occurs in an early state of the polymerization, followed by the growth of the nuclei. The size of the particles can be adjusted by controlling the reaction time/conversion and the content of the monomer as well as of the initiator. An interesting variety is the so-called distillation precipitation polymerization.^[27] Porosity can be achieved by the addition of a porogen, such as a good co-solvent for the monomer – toluene in the case of divinylbenzene – a non-solvent or a polymer. The crosslinking agent is often polymerized on its own, yet other monomers can be added in low quantities. Gentle to no agitation is sufficient to prevent the particles from coagulating, as they are protected by a layer of oligomers during the reaction. Non-reacted double-bonds remain on the surface of the particles and can be employed in further functionalization reactions.

Dispersion Polymerization

Dispersion polymerization is comparable to the precipitation polymerization approach in many aspects, e.g., both techniques start from a homogeneous phase and the reaction consists of nuclei formation with subsequent growth. The main differences between dispersion polymerization and precipitation polymerization is that for the former the addition of a stabilizer is required, yet the amount of crosslinking agent can be significantly lower. The achievable sizes range from less than 1 μm up to around 15 μm . Monodispers particles can be achieved with the addition of the crosslinker after the nucleation,^[28] without this approach the particles exhibit dispersity. In the majority of cases the particles are non-porous, yet the utilization of a porogen is possible to achieve porosity. The contin-

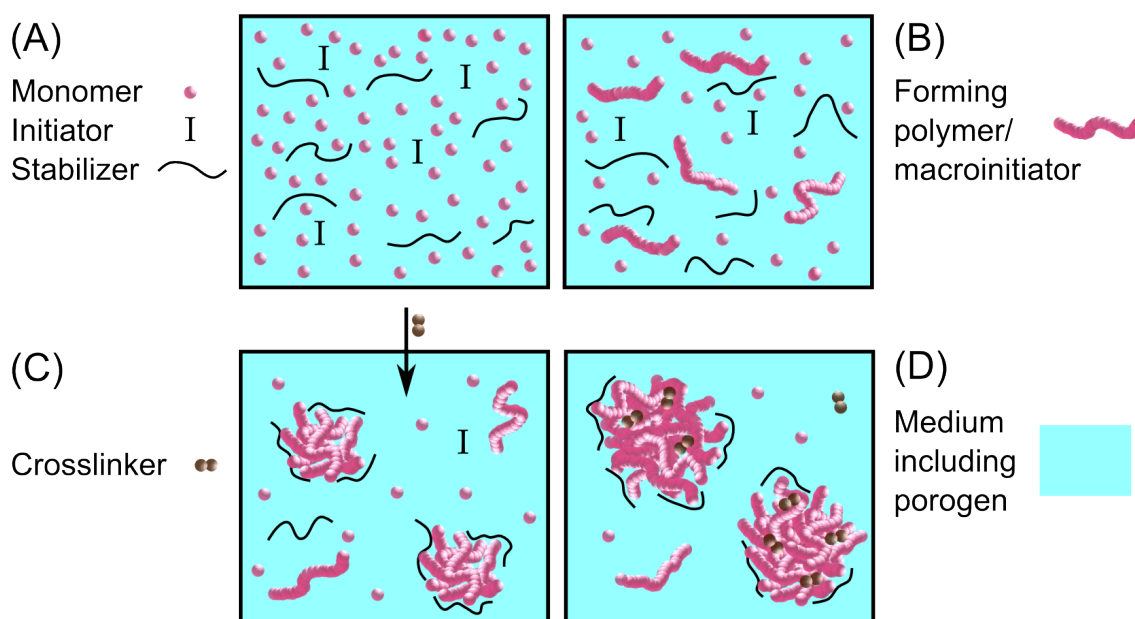


Figure 2.3: Schematic description of the stages of dispersion polymerization. **(A)** Initially monomer, initiator, porogen and polymeric stabilizer are dissolved in the medium. **(B)** Oligomers are forming, which are still soluble in the medium. **(C)** Nucleation stage at around 1 % monomer conversion. As their length increase, polymer chains precipitate and form the nuclei that are stabilized by the stabilizer. At this stage, a crosslinker may be added if desired. **(D)** Particles grow by capturing monomers and oligomers from the medium. Adapted with permission from [7].

uous phase is a precipitant for the polymer, usually a short alcohol such as methanol or ethanol.

Emulsion Polymerization

Particles synthesized via emulsion polymerization can be described as nanoparticles, as they normally feature a size range of 0.05 to 0.2 μm . Depending on the solubility of the monomer, the polymerization is conducted as an oil-in-water emulsion, or for hydrophilic monomers, as a water-in-oil emulsion. In both cases a surfactant is added to keep the phases emulsified, which is supported by intensive stirring. The chosen initiator has to be soluble in the surrounding medium, not in the monomer, leading to the initiation taking place in the surrounding medium, which contains dissolved traces of the monomer. The synthesized particles are non-porous and relatively disperse. If the monomer is diluted with a solvent, the reaction is termed diluted emulsion polymerization. In reactions without added emulsifier (emulsifier free emulsion polymerization) the particles are stabilized in the lattices by steric effects, solvated surface layers or electrorepulsive forces between ionic fragments. Since these forces are less effective stabilizers than an emulsifier, the final particles reach up to 1 μm in size. Synthesis of nano- and microparticles via emulsion

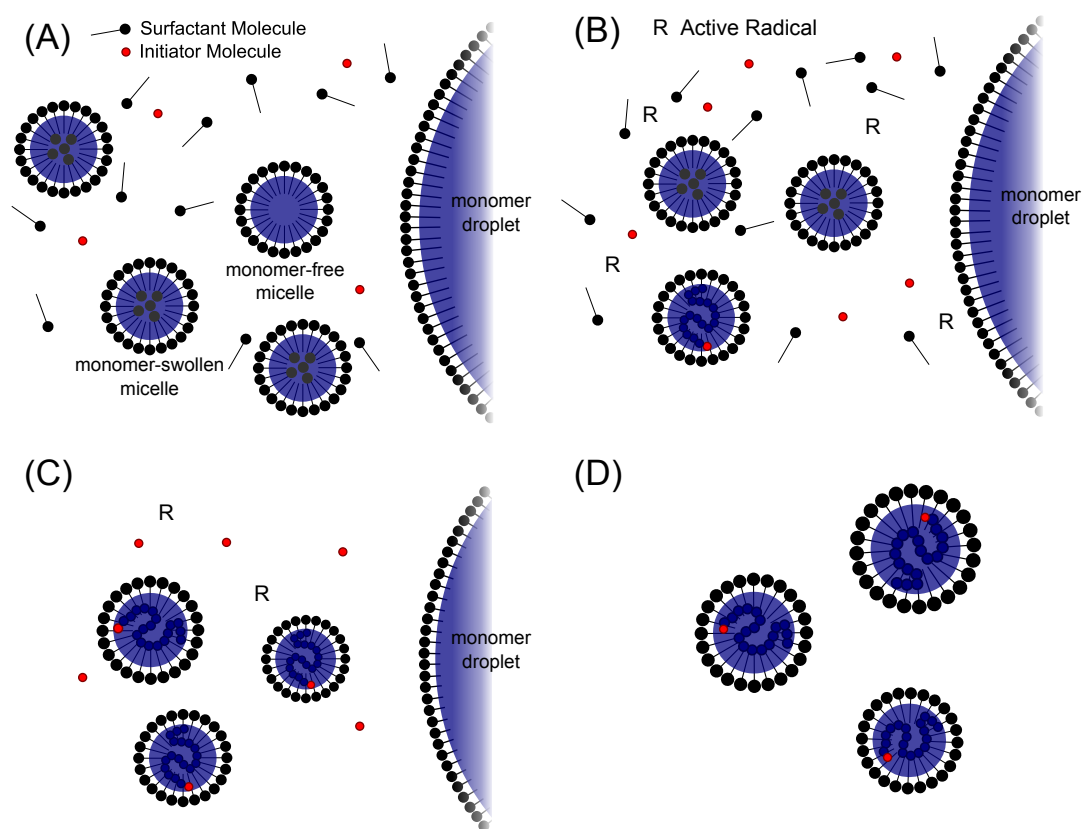


Figure 2.4: Schematic representation of the mechanism of emulsion polymerization. (A) before the reaction; (B) nucleation; (C) growth; (D) after the reaction; Adapted with permission from [29] where more details can be found.

polymerization is a very versatile and extensively investigated area of research. Since the current thesis is rather covering the modification of microparticles, the reader is instead referred to the general reviews and books by Landfester,^[30] Ballauff and Lu,^[31] Thickett and Gilbert,^[32] as well as Mittal.^[33]

Microfluidics

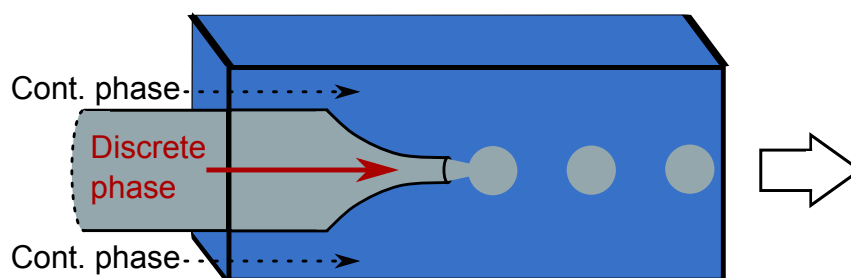


Figure 2.5: Schematic microfluidic capillary co-flow device as an example for the various microfluidic systems. Adapted with permission from [7].

Microfluidics offer the highest degree of control over the size and dispersity of microparticles. Uniform monomer droplets are produced in the center of a flowing continuous phase by a nozzle, which are subsequently crosslinked, most of the time with the help of UV-sensitive initiators. The sophisticated and miniaturized design of microchannel emulsification reactors allows not only for the synthesis of monodisperse spherical particles yet also structures – e.g., regular nonspherical particles^[34,35] and Janus-particles^[36,37] – that were hardly achievable before or only with significant effort. A great number of possibilities were already achieved and a wide field is yet to be explored for microfluidic device based microsphere generation,^[7] yet the major drawback of small achievable sample amounts hinders mass production and commercial use.

Other Techniques

In addition to the aforementioned synthesis strategies there exists a range of more specialized, yet not less interesting possibilities, which can – for the sake of space – not all be mentioned or covered in detail here. Seeding polymerization^[38] utilizes particles formed by emulsion or dispersion polymerization, which are reacted with a second monomer to form larger spheres, featuring the monodispersity stemming from the seeds and are able to incorporate more functionalities or porosity. Monodisperse seeds can be assembled to larger spheres, termed supraballs.^[39] A high control with regard to size, morphology, and other properties of the spheres, such as functionality or porosity, can be gained by electrospraying^[40] or electrohydrodynamic (co-)jetting,^[20] where a high voltage is applied to generate an aerosol. Co-jetting is a facile approach for the synthesis of Janus-particles, exhibiting two different hemispheres.^[41]

2.1.2 Modification of Microspheres

Although a wide range of properties and functionalities can already be introduced to the microspheres during their synthesis, a strong focus currently lies on the modification of preformed microspheres with facile and upscalable approaches, enabling their surface modification with polymers.^[10,42] With the addition of polymeric chains onto the particles, functional core-shell entities can be produced that can be utilized in a wide range of applications (refer to Section 2.1.3).

There are three fundamental approaches for the functionalization of microspheres with polymers: the 'grafting-to', 'grafting-from', and the 'grafting-through' approach. The 'grafting-through' approach can be described as a copolymerization of a monomer with the functionalized particles acting as a macromonomer.^[43] Since it offers the least control over the reaction, it will not be discussed here.

The wide field of molecularly imprinted polymeric microspheres introduced by Mosbach and coworkers,^[44] is not covered here in-depth as it is not matching the scope of the thesis. In molecular imprinting a complex formed between a functional monomer and a template molecule is embedded during the synthesis of the polymeric particle, thereby forming a recognition site for the imprinted molecule.^[45,46] After removal of the template the microsphere can rebind the original template very specifically, making it applicable e.g., in affinity separation applications.^[47]

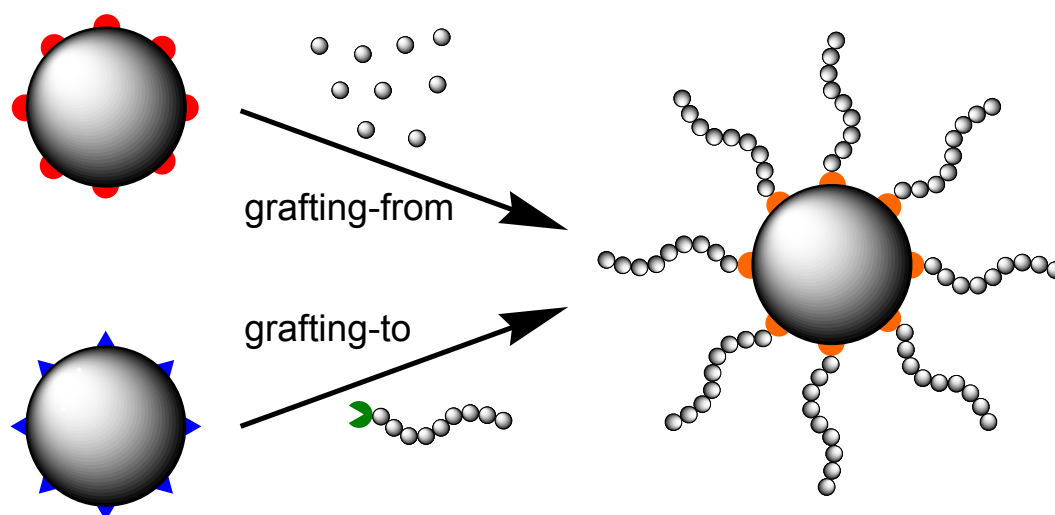


Figure 2.6: Schematic representation of the general difference between the 'grafting-from' and the 'grafting-to' approach.

Grafting-From

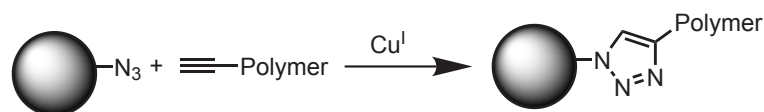
In a 'grafting-from' approach a moiety able to initiate has to be immobilized on the surface of a particle, from which the polymer can subsequently grow. The main benefit of the 'grafting-from' approach is that there is less steric hindrance, which theoretically leads to a higher achievable grafting density. Polymerization techniques that can be employed for grafting range from ring-opening polymerizations,^[48] ionic polymerizations, such as anionic ring-opening polymerization (AROP),^[49] to the controlled radical polymerization techniques termed reversible deactivation radical polymerizations (RDRP), including atom transfer radical polymerization (ATRP) and RAFT-polymerization (discussed in Section 2.2). RAFT-functionalities can be incorporated into PDVB-particles during the synthesis and are active for subsequent grafting.^[50] Sometimes 'grafting-through' processes employing initially dissolved RAFT-agents are also described as 'grafting-from', since a higher degree of control is achieved than for a free radical grafting process.^[51] Via the RAFT-process also challenging structures such as poly(vinyl alcohol) (via the growth of poly(vinyl pivalate) and subsequent hydrolysis)^[52] and glycopolymers can be grafted from microparticles.^[53]

ATRP initiators can be attached to non-reacted double-bonds,^[54] hydroxy moieties of co-polymerized hydroxyethyl methacrylate (HEMA)^[55] or by functionalization of the epoxide groups of glycidyl methacrylate particles.^[56] Disadvantages of the 'grafting-from' process are coupling reactions between the particles during radical polymerization processes and difficulties in gaining information about the structure and length of the grafted molecules.

Grafting-To

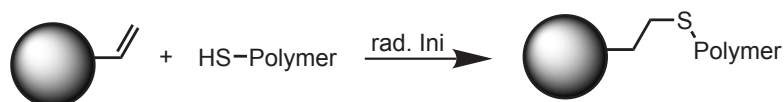
'Grafting-to' processes allow for the tethered molecules as well as the microparticles to be thoroughly characterized prior to the grafting reaction. In addition, the chemical nature of the functional moieties immobilized on the particles for the grafting does not influence which kind of polymer chemistry is utilized to generate the polymeric chains, strongly increasing the diversity of polymers which can be grafted onto the particles. In theory, the achievable grafting density for 'grafting-to' techniques is lower than in 'grafting-from' as already attached chains lead to a steric hindrance for subsequent chains to diffuse to the surface.^[57] In practice the difference in achieved grafting densities is often negligible (Chapter 3). Many of the applied grafting strategies adhere to the concept of click chemistry introduced by Sharpless^[58] and adapted for polymeric ligations by Barner-Kowollik et al.^[59] Some of the different grafting techniques for polymers as well as some selected other modifications will now be discussed.

Copper Catalyzed Azide-Alkyne Cycloaddition (CuAAC)



The prime example of a click ligation reaction is the copper(I) mediated cycloaddition between azides and terminal alkynes, which was first introduced by Huisgen^[60] and later modified to adhere to the click criteria by Meldal^[61] and Sharpless.^[62] The first example of CuAAC on polymeric microspheres is from 2006, where short aliphatic chains were grafted onto particles previously functionalized with azide as well as alkyne groups.^[6] Glycomoiety can be grafted on microspheres as a monolayer or on polymeric chains previously grafted from the spheres by ATRP.^[63] Natural polymers, such as previously alkyne-functionalized proteins, can also be grafted on microspheres via CuAAC.^[64] Azide functionalized spheres were grafted with several polymers synthesized via RDRP techniques. Goldmann et al. grafted PHEMA chains polymerized via ATRP onto microparticles pre-functionalized with azide motifs via a thiol-ene reaction.^[65] Poly(methyl ether oligo(ethylene glycol) methacrylate) prepared with an alkyne containing RAFT-agent^[66] as well as several polymers derived from ATRP were also grafted onto microparticles via CuAAC.^[67,68]

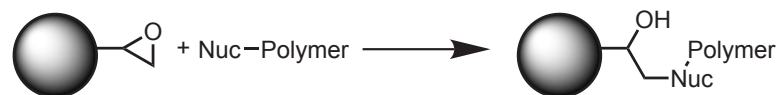
Thiol-Ene Chemistry



Since RAFT-polymers can be functionalized with thiol moieties by the simple addition of an amine to the dissolved polymer (aminolysis), ligations utilizing thiols are ideal for the grafting of polymers prepared via RAFT-polymerization onto microspheres exhibiting double (or triple) bonds, e.g., microspheres synthesized from DVB by precipitation polymerization. When the reaction occurs between thiols and triple bonds, it is termed thiol-yne chemistry. Per triple bond two thiols can be attached. The addition to non-Michael systems proceeds via radical pathways, utilizing thermal or photo-initiators. In the first published report employing thiol-ene chemistry, poly(*N*-isopropylacrylamide) prepared via RAFT was tethered onto the double bonds of PDVB microspheres, after previous reduction of one terminus to a thiol.^[65] Small thiol-functionalized sugar molecules^[69–71] as well as glycopolymers^[53] can also be grafted onto vinyl functionalized particles. Du Prez and coworkers showed that thiol-ene chemistry can be utilized to synthesize microparticles via a microfluidic approach.^[72] These authors furthermore conducted several reactions on thiol-functionalized particles and compared the grafting density reached on

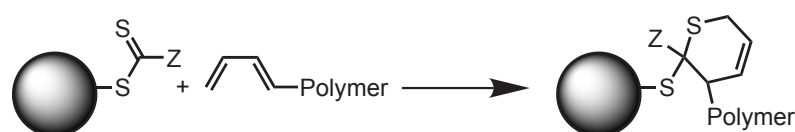
alkyne functionalized spheres via thiol-yne chemistry and CuAAC, of which thiol-yne ligation was superior.^[73]

Ring-Opening of Epoxides



The possibility to synthesize microspheres mainly based on the epoxide containing monomer GMA or copolymerized with GMA makes ring-opening of epoxides a facile and versatile grafting reaction on microparticles. Due to the ring strain, the three-membered ring is very reactive and can react with a range of nucleophiles as well as electrophiles.^[74] Boronic acid can be attached to the glycidyl group, leading to interactions with sugar moieties.^[75] Commercially available polymers such as poly(ethylene glycol) (PEG) or poly(ethylene imine) can directly be grafted onto particles containing GMA utilizing their nucleophilic end groups.^[76,77] A range of proteins and enzymes can be immobilized on GMA containing or epoxide functionalized microparticles, too.^[78–81] Poly(sulfopropyl methacrylate) synthesized via iniferter polymerization was – after hydrolysis of the end group to a thiol – tethered to previously treated spheres.^[82] Ring opening of epoxides – as well as the above mentioned techniques CuAAC and thiol-yne – can be combined with microcontact printing to form Janus-particles.^[83,84]

RAFT Hetero Diels-Alder (RAFT-HDA)



The RAFT hetero Diels-Alder approach is the reaction between a C=S double bond of the thiocarbonyl thio moiety, stemming from special RAFT-agents, and a diene. It will be discussed in detail in Section 2.2.4 on page 21. RAFT-functionalities can be tethered to microparticles with the addition of a RAFT-agent during the manufacturing process of the particles. Since the RAFT-HDA concept is rather novel, there are not many reports in the literature yet. Nebhani et al. grafted diene-functionalized poly(ϵ -caprolactone) synthesized via ring-opening polymerization on RAFT-functionalized spheres.^[85] In a second approach polystyrene – produced via the RAFT-process – was grafted onto cyclopentadiene-functional microspheres (three steps were necessary to attach the cyclopentadiene). Poly(isobornyl acrylate) was directly immobilized onto PDVB particles,

employing the most reactive HDA-capable RAFT-agent, which contains a sulfonyl as Z-group. The sulfonyl enables the C=S bond to even react with many vinylic monomers, thus strongly minimizing its area of application.^[86]

In summary, there already exists a significant range of possibilities to functionalize microspheres with small molecules and polymeric chains, of which some clearly adhere to click criteria, such as CuAAC or RAFT-HDA. Yet, so far the amount of light-induced reactions that could lead to even more orthogonal grafting applications, as well as temporal and spatial control about it, is limited to the utilization of UV-initiators for thiol-ene/yne reactions, where radicals are generated, thus more or less leading to a poorly controlled reaction. Spatial resolved grafting is limited to microcontact printing, having the disadvantage of being non-trivial to upscale.^[83,84]

2.1.3 Applications

The most striking properties of polymeric microspheres are their immense surface area, especially for porous particles, and their insolubility, which makes them an ideal substance class to be used as carrier materials as well as the stationary phase in chromatographic systems. The fields where microspheres are applied to are so manifold that for the sake of space only an overview can be given here. The interested reader is, once more, referred to the comprehensive reviews by Kawaguchi^[23] and Du Prez.^[7]

Polymeric microparticles are employed as the stationary phase in various chromatographic systems^[87] ranging from the interactionless gel permeation chromatography (GPC)^[88,89] to different forms of high-performance liquid chromatography (HPLC) including chiral,^[90,91] affinity, reverse phase chromatography^[6,92,93] and more.

Microspheres play an important role in synthetical applications, acting as solid supports for organic^[4,94] and peptide synthesis.^[94–96] Furthermore, the particles are utilized for the immobilization of inorganic and organic catalysts,^[1,97,98] including enzymes, the biological catalysts.^[79–81,99] Microbeads are also used as ion exchange material^[100,101] and consequently ion exchange chromatography.^[102] Utilization of microspheres for scavenging^[103,104] and in extraction^[105,106] is also worth mentioning.

In addition, microparticles are also utilized in many medical and biological applications such as drug delivery, tissue engineering and for diagnostic kits.^[23,107]

For the future even more promising applications seem possible such as hydrogen storage systems^[108] and microsensing,^[109,110] thus keeping polymeric microspheres in the focus of research for a long time.

2.2 Reversible Addition Fragmentation Chain Transfer (RAFT) Polymerization

2.2.1 Introduction

Radical polymerization techniques are from an academical as well as a commercial point of view the most important avenue for generating polymeric materials. In the last decades several reversible deactivation radical polymerization (RDRP) techniques were developed, offering more control over the reaction than conventional free radical polymerization (FRP) and furthermore showing some characteristics that are normally associated with living polymerization techniques,^[111] which typically are very laborious. RDRP techniques feature excellent control over the molecular weight – due to a linear increase of the degree of polymerization with conversion – as well as the micro-structure of the polymer, show high end group fidelity, lead to low polydispersities and offer the possibility of being reactivated, e.g., for the formation of block copolymers. The most common RDRP techniques are NMP,^[112,113] ATRP,^[114,115] and RAFT^[116] of which RAFT is arguably the most versatile one.^[11–15]

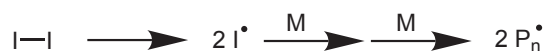
2.2.2 Mechanism of the RAFT-Process

The mechanism of RAFT-polymerization is comparable to the FRP process. In a free radical polymerization the reaction can be divided in three fundamental parts, which are initiation, propagation, transfer and termination. During the initiation an initiator generates radical species due to heat or irradiation. The vinylic monomer reacts with the initiating radical species and forms a propagating radical species, which adds monomer units until it is terminated by reacting with a second radical. The propagation time of a radical in FRP is in the range of 1 s.^[117] Transfer reactions occur when the radical reactivity is passed on from a propagating chain to a different molecule.

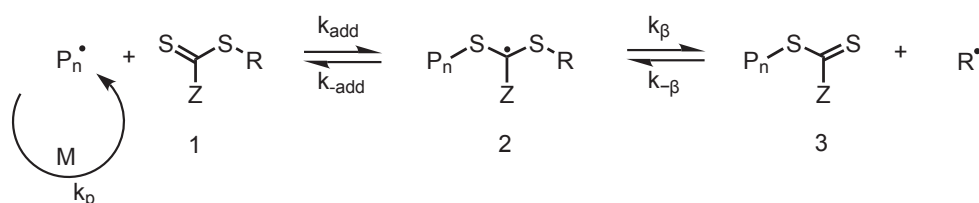
For a RAFT-polymerization typically a thiocarbonyl-thio species – the so-called RAFT-agent – is added to the reaction mixture. Thiocarbonyl-thio classes include dithioesters, trithiocarbonates, xanthates, and dithiocarbamates. The mechanism of the RAFT-polymerization is depicted in Figure 2.7 on the following page and resembles the FRP-mechanism with two additional equilibria.

Control over the polymerization is gained via a degenerative chain transfer, not via a reduction in the concentration of radicals. An initiating molecule generates radicals and subsequently propagating radical chains \mathbf{P}_n^\bullet . In the pre-equilibrium the propagating radical adds to the RAFT-agent (**1**) and expels the **R** or leaving group via β -scission. The **R**-group then forms a new propagating chain \mathbf{P}_m^\bullet . In the chain equilibrium a rapid exchange

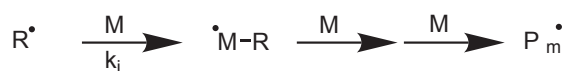
Initiation



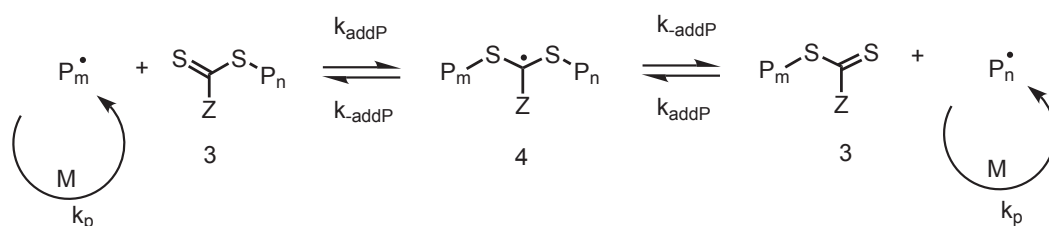
Reversible Chain Transfer (Pre-equilibrium)



Reinitiation



Chain Equilibrium



Termination

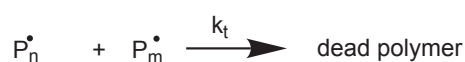


Figure 2.7: Mechanism of reversible addition fragmentation chain transfer polymerization. Adapted with permission from [11].

of an active radicals and dormant macro-RAFT-agents (**3**) takes place. The rapid exchange leads to the control, as it generates an equal probability for each chain to grow. The **Z** or stabilizing group stays on the (macro-)RAFT-agent during the polymerization reaction. The radical intermediates (**2** and **4**) fragment rapidly, thus the amount of propagating chains is almost constant throughout the polymerization. The formation of termination products is strongly suppressed due to the alternative reaction pathway for the propagating chains, yet still can occur. In an ideal RAFT-polymerization there should be no difference in the polymerization rate compared to an analogous FRP, yet inhibition periods and a decrease in the polymerization rate can sometimes be observed,^[118] which can in part be attributed to the chain length dependency of k_p ,^[119] slow fragmentation of the intermediate radicals or intermediate radical termination.

Comparison with other RDRP Techniques

In contrast to the RAFT process – where a degenerative chain transfer is utilized to gain control – the two other widely used RDRP techniques (NMP and ATRP) rely on reversible chain deactivation. In the current thesis these techniques were not employed, thus they are mentioned here only in short to complete the picture given recording RDRP.

In NMP the propagating radicals are deactivated by reacting with a nitroxide to form an alkoxyamine, which can be cleaved by heat (Figure 2.8).

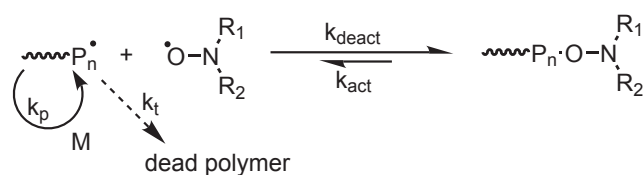


Figure 2.8: Mechanism of nitroxide mediated polymerization. Adapted with permission from [120]. Copyright 2001 American Chemical Society.

The control over the polymerization is gained via the decrease of radical concentration. Since the termination reaction is a bimolecular reaction between two radicals and propagation adheres to a first order kinetic law, the reduction of radicals strongly suppresses termination events in favor of propagation. However, the polymerization is decelerated as well.

First reports employed the addition of 2,2,6,6-tetramethylpiperidine-1-oxyl (TEMPO) to a FRP of styrene, requiring high temperatures.^[121] Later, unimolecular NMP-initiators – decomposing during the reaction to a nitroxide and initiating radical – were developed, leading to a more versatile approach, as these are applicable at only slightly elevated temperatures and allow for the utilization of a wider range of monomers.^[122, 123]

ATRP utilizes redox active transition metal complexes for the reversible deactivation of propagating radicals, and its principle mechanism and way of controlling the polymerization is comparable to NMP (Figure 2.9).

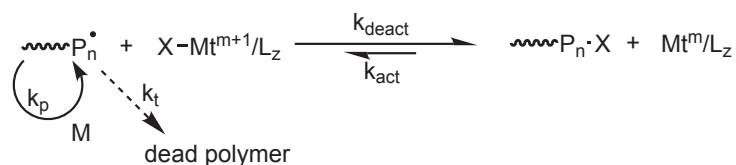


Figure 2.9: Mechanism of atom transfer radical polymerization. Adapted with permission from [120]. Copyright 2001 American Chemical Society.

The metal **Mt** – commonly copper – is stabilized with a ligand **L** and **X** is an halogenide, which is reversibly transferred to the radical, thus changing the oxidation state of the

metal. Other metals can be employed for ATRP as well, e.g., Ni, Fe, Ru and Os.^[124] The most common ligands are bi- and multi-dentate nitrogen ligands and as initiators halogenated organic molecules are utilized.^[125] Drawbacks of ATRP are the utilization of often cytotoxic metals, which prevents the application in many medical and biological fields as well as the incompatibility with some monomers.

2.2.3 Applications

The RAFT-process is a very versatile polymerization procedure. Nearly every vinylic monomer class can be polymerized, including e.g., styrenes, acrylates, methacrylates, acrylamides, and vinyl esters and it can be conducted in bulk, solution (organic and aqueous) and heterogeneous media. The versatility stems from the possible functionalities that can act as the R- or Z-group of the RAFT-agents (Figure 2.10), which match the reactivity of the desired monomers,^[126] with the exception of switchable RAFT-agents, which are applicable for a wider range of monomer classes.^[127]

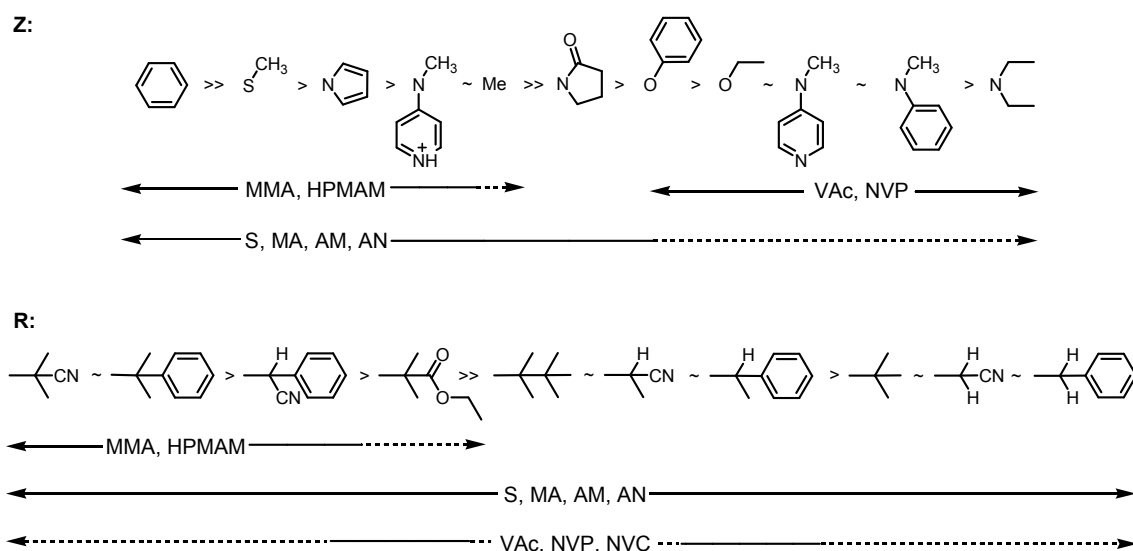


Figure 2.10: Guidelines for the selection of the R- and Z-group of RAFT agents for various polymerizations. A dashed line indicates partial control (i.e., control of molar mass but poor control over dispersity or substantial retardation in the case of less activated monomers such as vinyl acetate (VAc) or *N*-vinylpyrrolidone (NVP)). St: styrene; MMA: methyl methacrylate; MA: methyl acrylate; AM: acrylamide; AN: acrylonitrile; HPMAM: *N*-(2-hydroxypropyl)methacrylamide; NVC: *N*-vinylcarbazole. Figure adapted with permission from [126]. Copyright 2012 American Chemical Society.

RAFT-polymerization leads to end-functional chains and with the addition of desired moieties to the R- or Z-group of the controlling agent these moieties are tethered to the α or ω -end of the chain, respectively. In addition, there exists a range of transformation reactions to generate new functionalities from the Z-group^[128] (Figure 2.11).

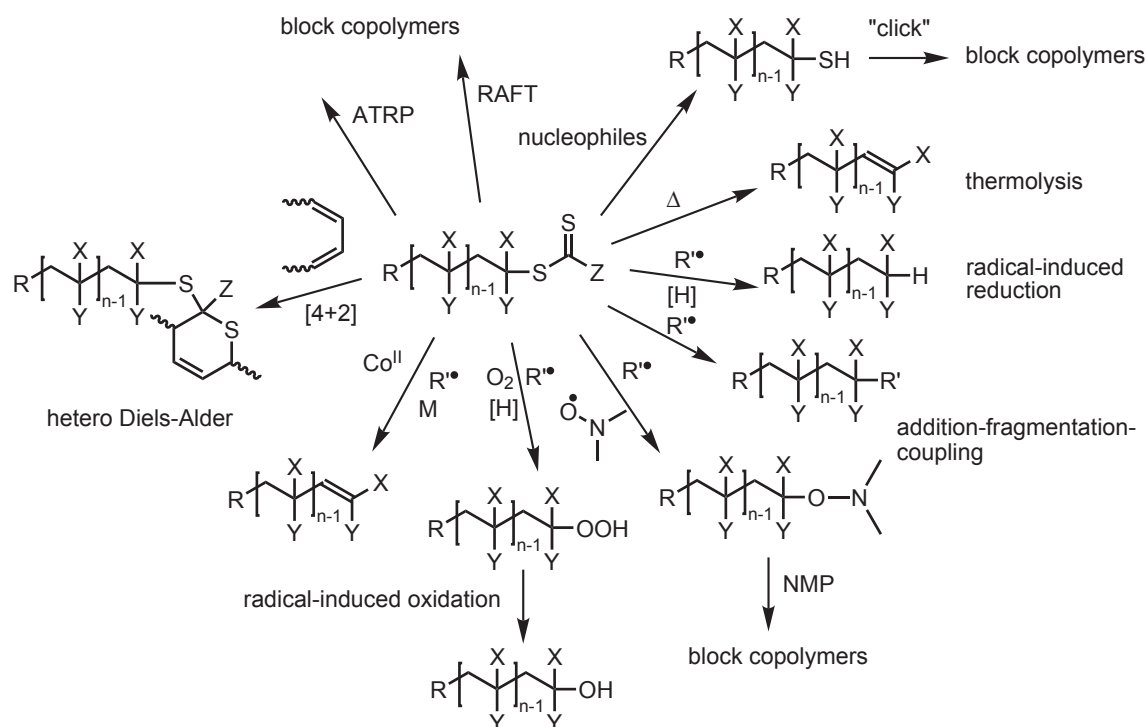
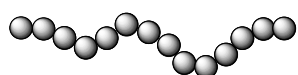


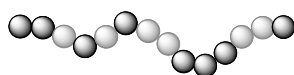
Figure 2.11: Processes for RAFT-end group transformation (R^\bullet = radical; $[H]$ = hydrogen donor; M = monomer). Figure adapted with permission from [128].

Transformations of the end group allow for the formation of block copolymers not only by sequential RAFT-polymerization, yet also with a subsequent non-radical polymerization.^[129] The RAFT-technique can also be employed for the synthesis of highly specialized polymers such as glycopolymers^[130] and the realization of complex macromolecular architectures such as multiblock,^[131] star-^[132] or combpolymers^[133] and more^[134] (Figure 2.12 on the next page) as well as the grafting of polymeric chains from surfaces,^[135] ranging from microspheres,^[50] and cellulose^[136] to graphene oxide.^[137] The range of applications of the RAFT-technique is much longer as can be depicted here, and the interested reader is referred to the RAFT Handbook^[11] and the excellent reviews by Moad, Rizzardo and Thang,^[12–15] already mentioned in the Introduction section 2.2.1.

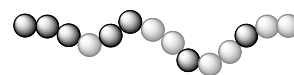
Composition



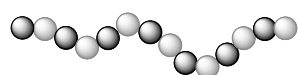
homopolymer



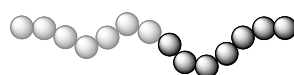
random copolymer



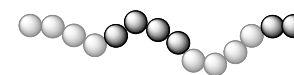
gradient copolymer



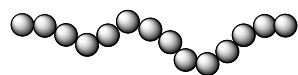
alternating copolymer



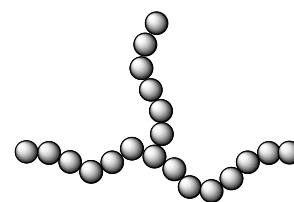
block copolymer

multi-segment
blockcopolymer

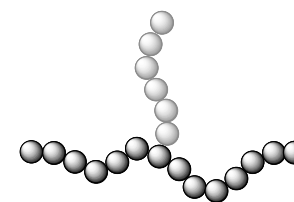
Topology



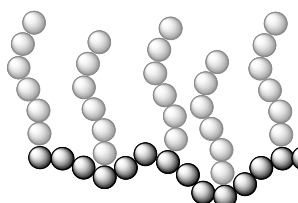
linear



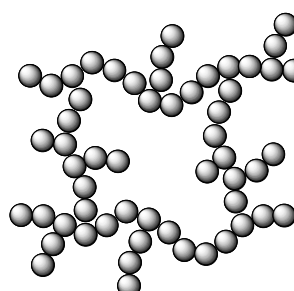
star



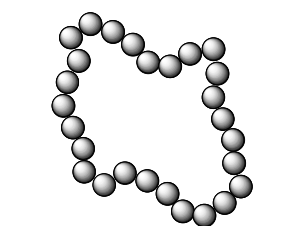
miktoarm star



brush/comb



network/branched



cyclic

Figure 2.12: Overview of macromolecular compositions and architectures that are accessible via the RAFT-process.

2.2.4 RAFT-HDA

An alternative and very elegant way to generate block copolymers or to graft polymers onto surfaces is the RAFT hetero Diels-Alder (RAFT-HDA) approach, which was introduced by our team in 2008.^[16,138] In RAFT-HDA, the C=S double bond inherent in the thiocarbonyl-thio group of the RAFT-agent or the end group of a RAFT-polymer, respectively, is able to react with a diene in a [4+2] Diels-Alder cycloaddition (Figure 2.13).

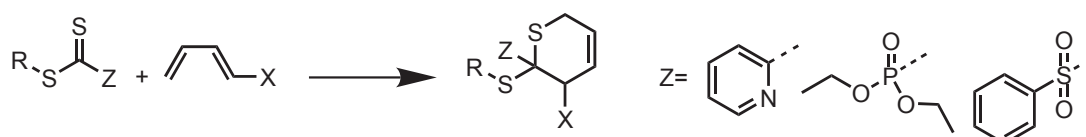


Figure 2.13: Mechanism of RAFT-HDA. Right: Available Z-groups promoting RAFT-HDA.

Special electron deficient Z-groups are required to withdraw electron density from the thiocarbonyl moiety. The reaction is very rapid, even at ambient conditions, as it can reach full conversion in the matter of seconds to minutes (depending on the diene). In addition, it adheres to the click criteria.^[139] RAFT-HDA has been utilized for the formation of block copolymers,^[138] block copolymers with high molecular weight,^[140] star polymers,^[16] star-shaped block copolymers^[141] and the grafting of poly(methyl methacrylate) onto single-walled carbon nanotubes.^[142]

The glycopolymer poly(3-*O*-acryloyl- α,β -D-glucopyranoside) (PAGlc) can be synthesized via a controlled polymerization utilizing a RAFT-agent which is able to undergo HDA reactions (and subsequent deprotection). Glassner et al. employed the unprotected glycopolymer and other water soluble RAFT-polymers to form block copolymers with diene-functional PEG in aqueous solution in the matter of minutes,^[143] which can be seen by the distinct shift in the GPC signal (Figure 2.14 on the next page). Neither residual starting material nor a shoulder can be observed.

Goldmann et al. functionalized cellulose sheets with cyclopentadiene moieties employing nickelocene via a preceding tosylation. HDA was utilized to immobilize poly(isobornyl acrylate) generated via the RAFT-process. The successful tethering of the polymeric chains was proven via X-ray photoelectron spectroscopy, scanning electron microscopy (SEM) and elemental analysis. In addition, high-resolution FT-IR microscopy was able to visualize single cellulose fibers with the grafted poly(isobornyl acrylate) (Figure 2.15 on the following page).^[144]

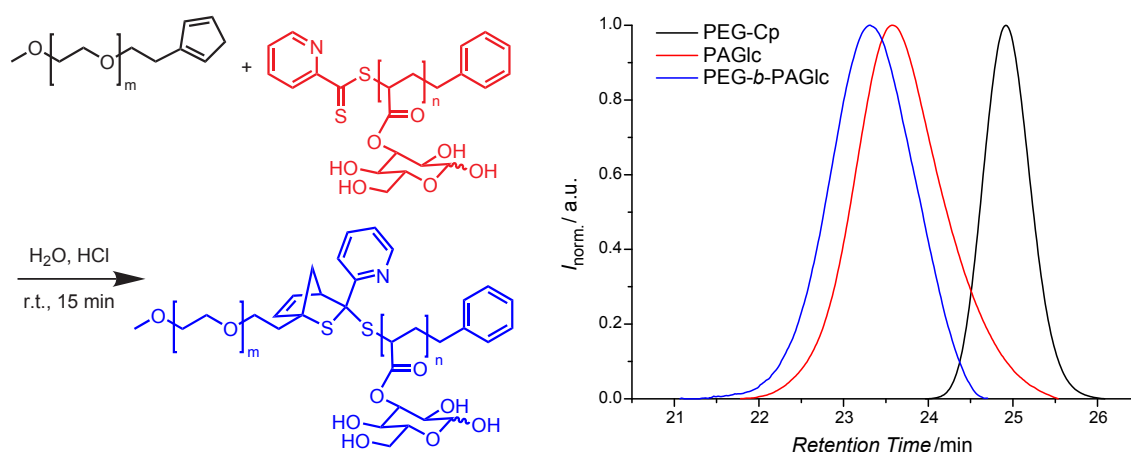


Figure 2.14: RAFT-HDA reaction between the glycopolymer PAGlc and cyclopentadiene-functional PEG in aqueous solution. The GPC traces (right) show the formation of the block copolymer via a distinct shift. Figure adapted with permission from [143]. Copyright 2012 American Chemical Society.

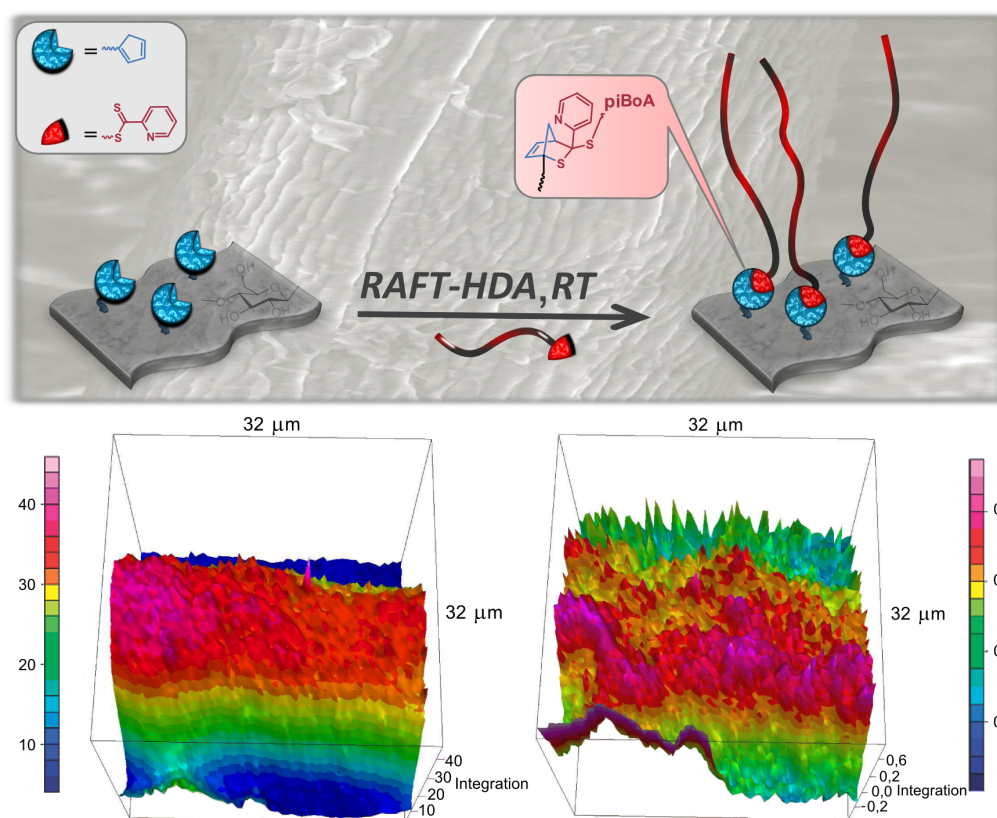


Figure 2.15: RAFT-HDA reaction between cyclopentadiene-functionalized cellulose and poly(isobornyl acrylate). High resolution FT-IR microscopy (right) depicts the evenly distributed grafting of a cellulose fibre. Figure adapted with permission from [144]. Copyright 2011 American Chemical Society.

Nebhani et al. utilized RAFT-HDA to graft polymer chains onto microspheres.^[85,86] They functionalized the particles with the RAFT-moieties and corresponding diene, respectively, and immobilized polystyrene, poly(isobornyl acrylate), and poly(ϵ -caprolactone). The grafted spheres were analyzed qualitatively as well as quantitatively with SEM, IR-spectroscopy and elemental analysis. If the RAFT-moieties are expressed on the surface of the microparticles the successful grafting is even observable with the naked eye, as the spheres lose their color, which stems from the dithioester (Figure 2.16).

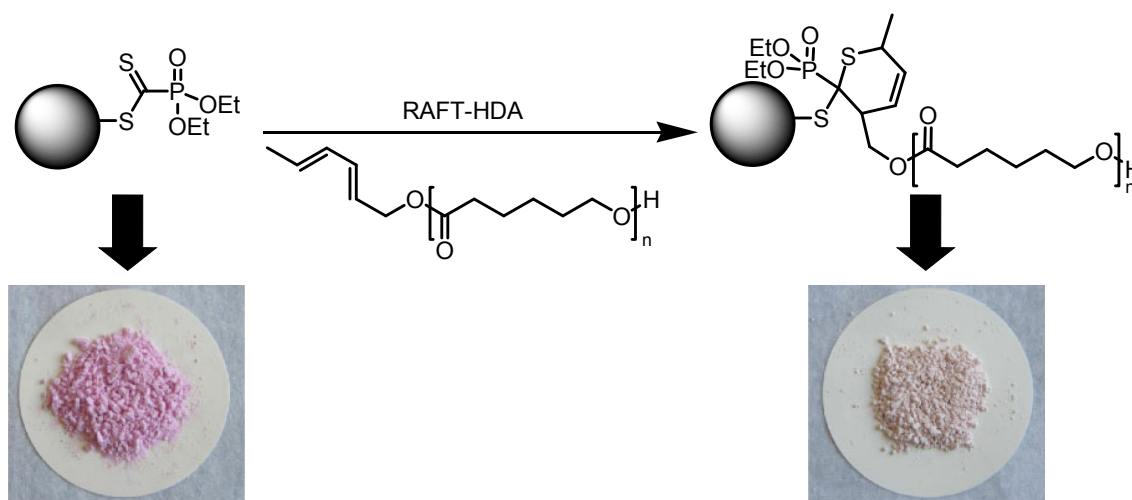


Figure 2.16: HDA reaction between polymeric microparticles and diene-functionalized poly(ϵ -caprolactone). The successful grafting can be recognized by the decoloration as the dithioester moieties are reacted. Figure adapted with permission from [85].

Despite already having generated a long list of published applications with remarkable results, the potential of RAFT-HDA seems not to be exhausted yet.

2.3 Glycopolymers

The term glycopolymer is employed for a variety of polymeric structures, covering modified natural polymers grafted to synthetic polymers as well as synthetic polymers containing sugar moieties. The current section will concentrate on the latter, specifically on synthetic polymers that carry sugar moieties in the majority of the repeating units.

Glycopolymers can be synthesized by all common polymerization reactions – radical, ionic, ring-opening polymerization (ROP), and ring-opening metathesis polymerization as well as by polymer analogous reactions introducing the carbohydrates to preformed polymers.^[145–148] The majority of synthetical glycopolymers, especially if generated by radical polymerization, carry the sugar moiety in the side chain. The preparation of glycomonomers is often tedious, due to the high number of similar functional groups in carbohydrates, demanding protecting group chemistry and multi-step synthesis, yet is preferable to post-polymerization modification, with often limited conversions due to steric hindrance. Utilization of enzymes often circumvents the use of protecting groups.^[149, 150] Although FRP can and has been employed to generate glycopolymers,^[151] in recent years RDRP techniques are employed more and more, with RAFT becoming the most applied strategy,^[148] as end-functional and thereby further transformable chains offer a wide variety of synthetic opportunities. Glycomonomers that can be polymerized via RDRP techniques include all major monomer classes in their protected and unprotected form (Figure 2.17).

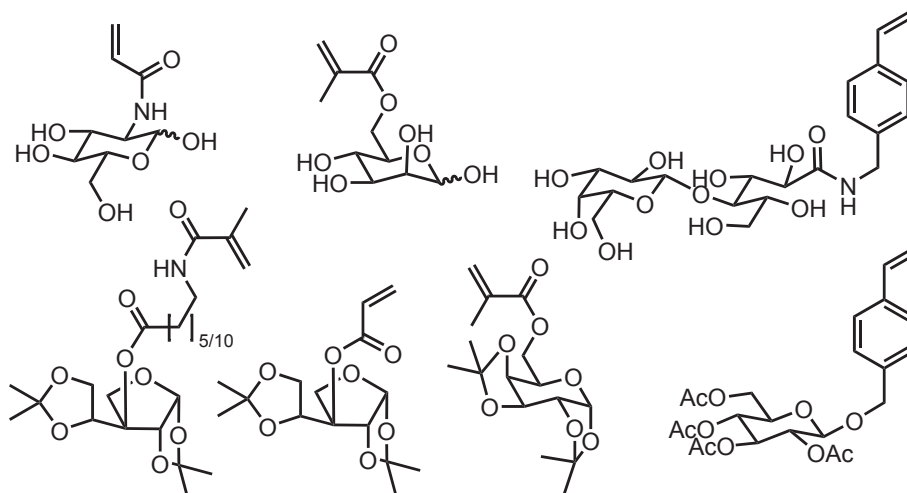


Figure 2.17: Exemplary overview of glycomonomers polymerizable with RDRP techniques.

Glycopolymers exhibit an outstanding and unique combination of properties. Glycopolymers can be generated from renewable resources, possess high polarity and solubility in water, are biocompatible and show specific interaction with boronic acids and

biomolecules, particularly lectins.^[152]

The above mentioned properties make glycopolymers interesting candidates for medical applications, such as drug delivery^[153] and macromolecular drugs^[154] as well as biological usage in cell culturing,^[155] enzyme containing hydrogels^[156] and biological model systems.^[157]

A range of novel glyco(co-)polymers was introduced, analyzed and tested for interactions with lectins by Fernández-García and coworkers.^[158–160] The monomers are based on glucosamine and functionalized with acrylic and methacrylic moieties without the aid of protecting groups. Polymerization was conducted via FRP and ATRP. Copolymers of styrene with 2-[(D-glucosamine-2-N-yl) carbonyl]oxyethyl acrylate (HEAGI) spincoated with polystyrene lead – after annealing – to films with expressed glycofunctionalities and uniform pores (Figure 2.18). The porosity was imaged with atomic force microscopy and the active glycofunctionalities were shown via fluorescence imaging of rhodamine immobilization and lectin interaction.^[161]

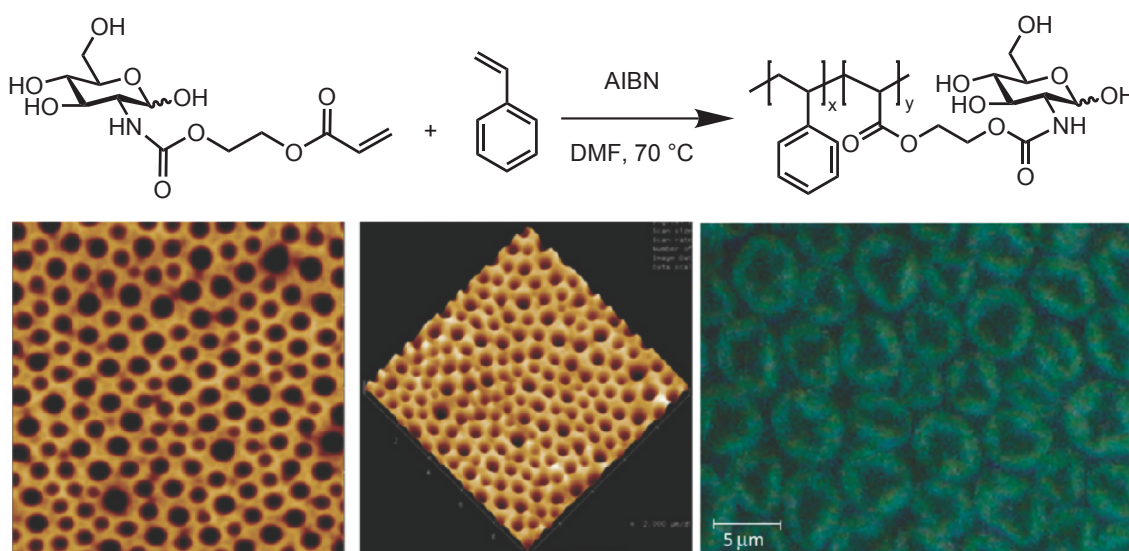


Figure 2.18: Top: Synthetic approach for the preparation of *S-co*-HEAGI statistical glycopolymers by FRP. Bottom left: Atomic force microscopy image of films obtained by spin coating of the copolymer and polystyrene ($10\ \mu\text{m} \times 10\ \mu\text{m}$). Bottom right: Fluorescence image obtained by recognition between the glycopolymer and fluorescein-conjugated Concanavalin A within the pores. Figure adapted with permission from [161]. Copyright 2010 American Chemical Society.

The group of Stenzel conducts comprehensive research in the field of synthesizing glycopolymers via RDRP techniques, particularly RAFT-polymerization. They generated an impressive list of novel glycomonomers which were employed to synthesize homo and copolymers,^[149,150,162] including challenging architectures such as hollow nanoparticles^[163] and star-polymers.^[164] A noteworthy example is the synthesis of

2. Background

a seven-arm star-copolymer. A water soluble RAFT-agent was synthesized via the attachment of seven trithiocarbonates to a β -cyclodextrin and subsequent polymerization of ten 2-hydroxyethyl acrylate units per branch. The RAFT-agent was then employed for the controlled polymerization of *N*-acryloyl glucose to result in a seven-arm glyco-star-polymer (Figure 2.19).^[165] In the same study the synthesis of thermoreponsive core-shell particles based on block copolymers of *N*-isopropyl acrylamide and *N*-acryloyl glucose was described, too. The block copolymers self-assembled into micelles and were subsequently cross-linked.

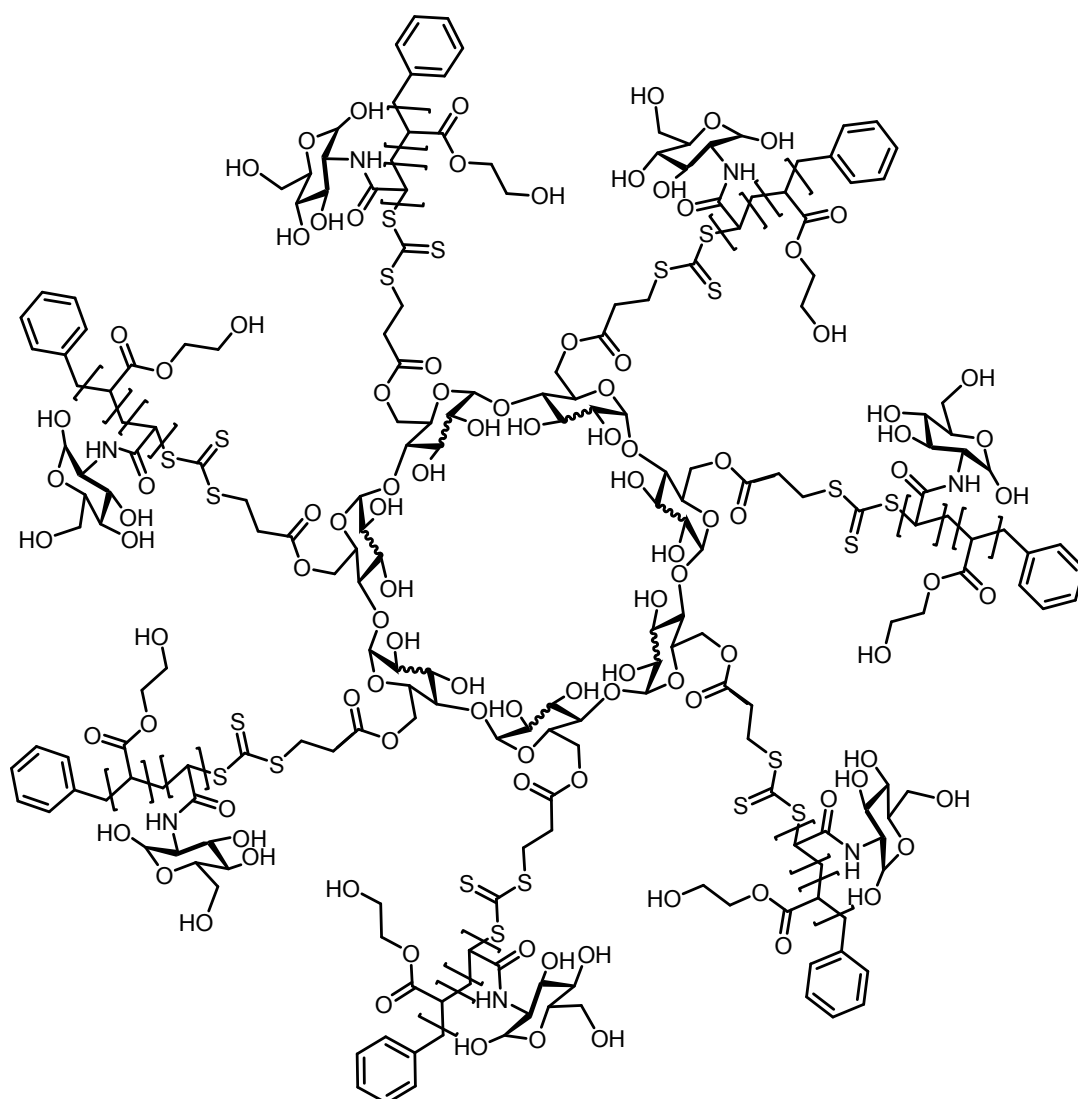


Figure 2.19: Structure of seven-arm β -cyclodextrin–((poly(hydroxyethyl acrylate)₁₀–*b*–(poly(*N*-acryloyl glucose)₁₀)₇). Figure reproduced with minor changes in formatting under creative commons license CC BY-NC-ND 3.0 from [165].

In the realm of microspheres there exist two main strategies in combination with glycopolymers. Microparticles can be synthesized consisting of or containing glycomonomers or existing microspheres can be decorated with glycopolymers subsequent to the particle synthesis. The first approach was conducted in our group, where microspheres were synthesized via water in olive oil inverse suspension polymerization to generate particles consisting of more than 40 % glucose acrylamide. Characterization consisted of SEM, FT-IR microscopy and XPS. In addition, the interaction between the glucose moieties and a fluorescent molecule containing boronic acid was utilized to visualize the spheres via fluorescent microscopy (Figure 2.20).^[24]

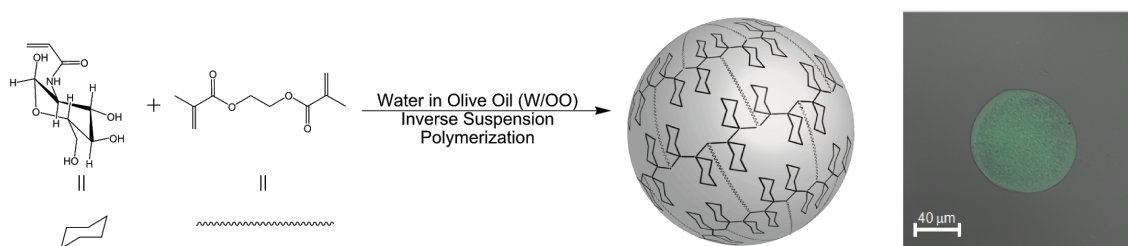


Figure 2.20: Synthetic method to achieve intrinsically glucoside-based microspheres via water in olive oil inverse suspension polymerization. Right: Fluorescence microscopy image of the glycomicrosphere with fluorescent boronic acid. Figure adapted with permission from [24].

Müller and coworkers decorated PDVB microparticles prepared via distillation polymerization with glycopolymers via 'grafting-through', 'grafting-from' and 'grafting-to'.^[53,166] They immobilized a RAFT-agent on the surface of the spheres for 'grafting-from'. ATRP and RAFT were applied for the 'grafting-through' of linear and hyperbranched chains derived from protected and unprotected glycomonomers onto the particles (Figure 2.21 on the following page). For the 'grafting-to' approach a thiol-ene approach was employed after aminolysis of the RAFT-end group. High grafting densities up to $0.43 \text{ chains} \cdot \text{nm}^{-2}$ were reached – calculated from the oxygen content determined via elemental analysis – for the 'grafting-through' approach, 'grafting-from' and 'grafting-to' reached 0.20 to $0.35 \text{ chains} \cdot \text{nm}^{-2}$. The spheres were also tested for interactions with lectins, which was positive for spheres grafted with glucose and galactose moieties, whereas the mannose derived polymers failed due to the functionalization of the OH-groups.

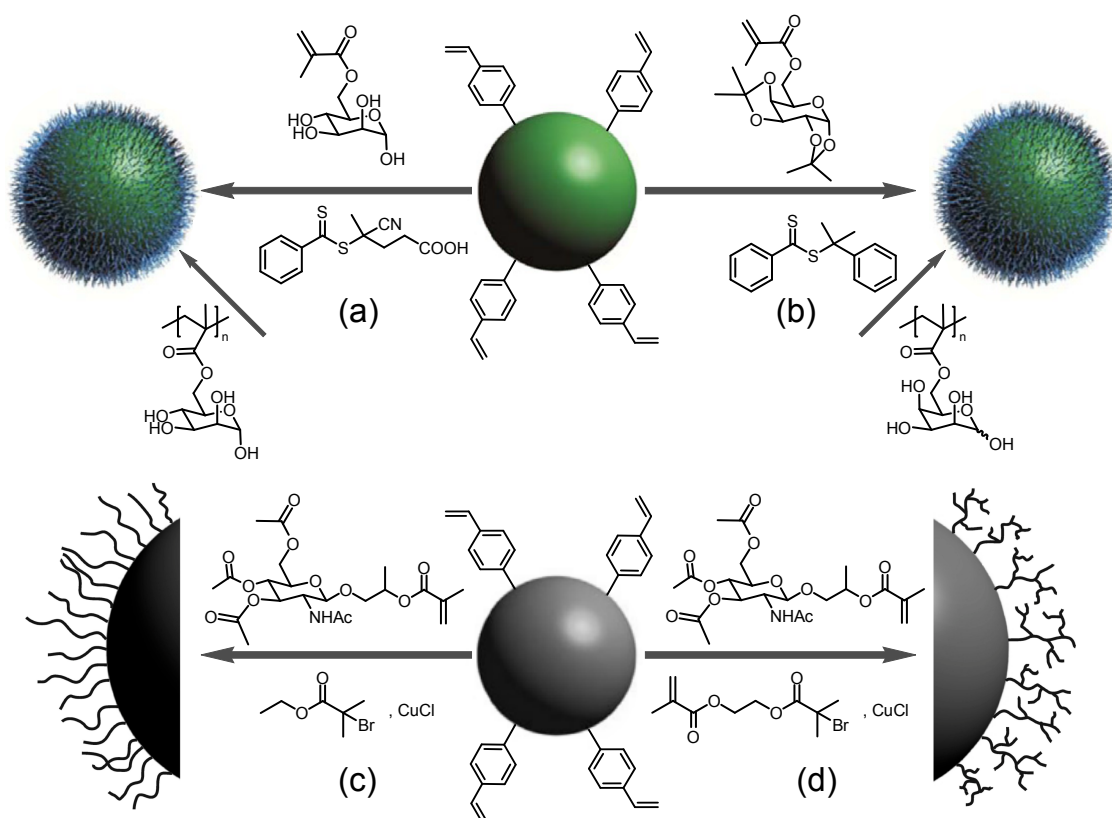


Figure 2.21: Synthesis of glycopolymer-grafted DVB microspheres. Top line: 'Grafting-through' employing RAFT-polymerization of 6-*O*-methacryloyl mannose **(a)** and 6-*O*-methacryloyl-1,2;3,4-di-*O*-isopropylidene-galactopyranose **(b)**. Bottom line: Synthesis of linear **(c)** and hyperbranched **(d)** glycopolymer-covered microspheres applying ATRP. Figures adapted with permission from [166] and [53] (Copyright 2011 American Chemical Society).

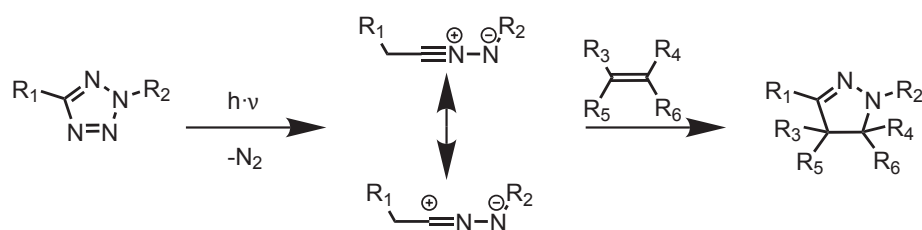
Alternative substrates can also be grafted with glycopolymers, including challenging substrates such as poly(ethyleneterephthalate) membranes,^[167] multi-walled carbon nanotubes,^[168] magnetic nanoparticles,^[169] and more.

2.4 Light-Induced Grafting Reactions

Light-induced 'grafting to' reactions offer some remarkable advantages in comparison to thermally triggered grafting reactions. In addition to being conducted at ambient conditions, the utilization of light offers a temporal and – more importantly – spatial control over the grafting reactions. To the best of the candidates knowledge, no light-triggered grafting reactions were conducted on polymeric microspheres so far, with the exception of radical thiol-ene coupling with UV-sensitive initiators, where the aforementioned benefits do not apply.

In the last years a 'tool box' of light-triggered grafting reactions has been developed and applied for macromoleclar grafting reactions, not alone yet particularly in the authors re-search group, some of which will be discussed below.

2.4.1 Nitrile Imine Mediated Tetrazole-Ene Coupling (NITEC)



Huisgen and coworkers revealed that 2,5-tetrazoles can undergo a cycloreversion to form molecular nitrogen and an 1,3-dipole, which can react in a pericyclic reaction with suitable dipolarophiles, including many double bonds.^[170] The cycloreversion can be conducted under UV-irradiation at ambient conditions to modify membranes.^[171] The substituted pyrazoline which is formed via the grafting reaction exhibits fluorescence, making it possible to examine the success of the reaction with fluorescence detection. NITEC is a robust approach, as it is not sensitive to oxygen or traces of water. The absorbance of the tetrazole can be tuned by varying the substituents, in the majority of cases aromatic functionalities are employed, leading to an absorbance of around 300 nm and below.

Dürr et al. proved that NITEC is compatible with RAFT-polymerization^[172], additionally NITEC was utilized in biological applications by Lin and coworkers.^[173] The photo-induced cycloaddition has been further applied in our group to graft poly(methyl methacrylate) prepared via ATRP onto silicon wafers and cellulose (filter paper) in a spatially controlled manner^[174] as well as to generate patterned light-responsive surfaces via the immobilization of azo-benzene containing molecules.^[175]

Rodriguez-Emmenegger and Preuss et al. employed NITEC to pattern a silicon wafer with anti-fouling brushes of poly(oligoethylene glycol methyl ether methacrylate) via 'grafting from'.^[176] A silicon wafer was coated with poly(dopamine) (PDA) and a tetrazole

containing molecule ligated to the surface. With the help of a shadow mask an ATRP-initiator was patterned onto the surface and subsequently the anti-fouling brushes were grafted from the surface (Figure 2.22). The successful spatially resolved modification was confirmed via XPS and imaged via ToF-SIMS. Cell tests proved the active anti-fouling behaviour.

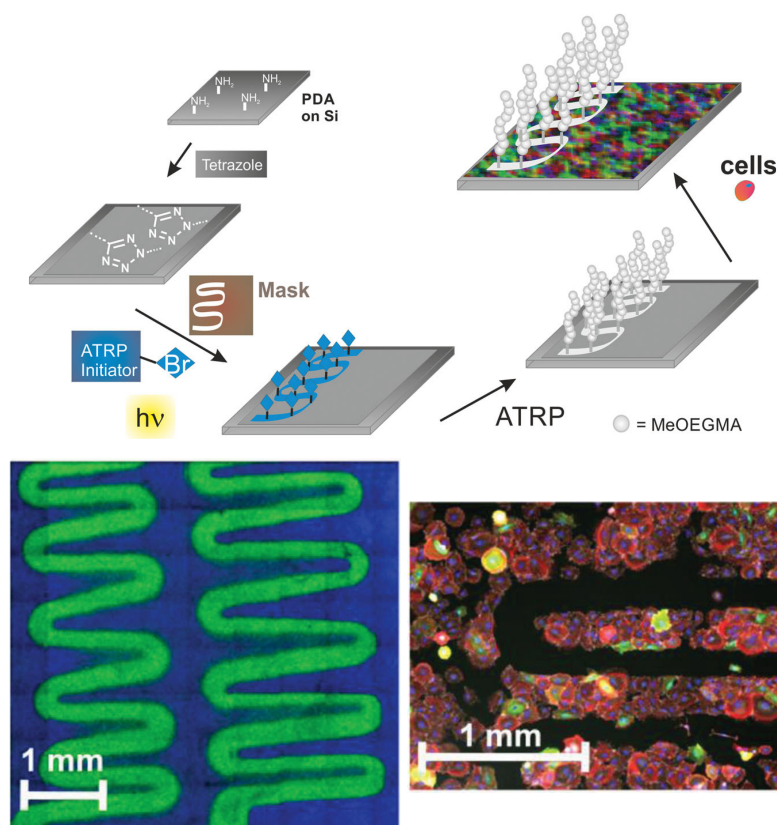
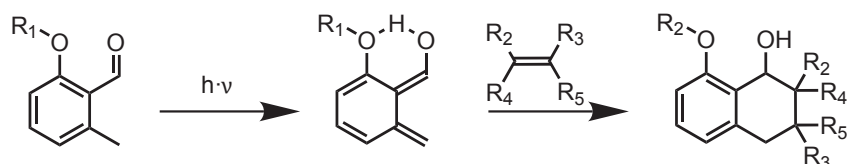


Figure 2.22: Synthetical procedure to pattern a PDA coated silicon wafer with anti-fouling brushes (top). ToF-SIMS imaging of the successful surface modification (bottom left). Stained cell pattern after 7 h culture proving the anti-fouling behaviour (bottom right). Figure adapted with permission from [176].

2.4.2 Photo-Enol Chemistry



When irradiated with light ortho-methylbenzaldehyde and analogous structures form ortho-quinodimethanes – so-called photo-enols – that are extremely reactive dienes for Diels-Alder reactions,^[18] which has been intensively studied by our group. The formed

diene can even react with the C=S double bond of conventional dithioester RAFT-agents and their corresponding polymers^[177] as well as acrylic double bonds^[178] to form block copolymers. To generate the photo-enol, irradiation close to 320 nm is applied. The light-induced reaction is highly orthogonal, even thermally-triggered Diels-Alder reactions can be conducted in the presence of the photo-enol precursor.^[179]

Spatially resolved grafting has successfully been conducted with peptides and polymers on diverse and challenging surfaces. Functionalized PEG and peptides were tethered to silicon wafers.^[180] In addition, poly(DOPA) on carrier materials such as gold, poly(ethylene terephthalate), and graphite was decorated with PTFMA, PEG, and a peptide.^[181] Tischer et al. immobilized a peptide and poly(trifluoro ethyl methacrylate) (PTFEMA) on hyaluronan films and cellulose sheets in a photo-pattern.^[182] The biosubstrates were functionalized with the photo-enol precursor. Subsequently, the maleimide-functional peptide or PTFEMA generated via ATRP were tethered to the surface by irradiation through a meander shadow mask (Figure 2.23). The successful functionalization was proven by XPS and illustrated via ToF-SIMS imaging.

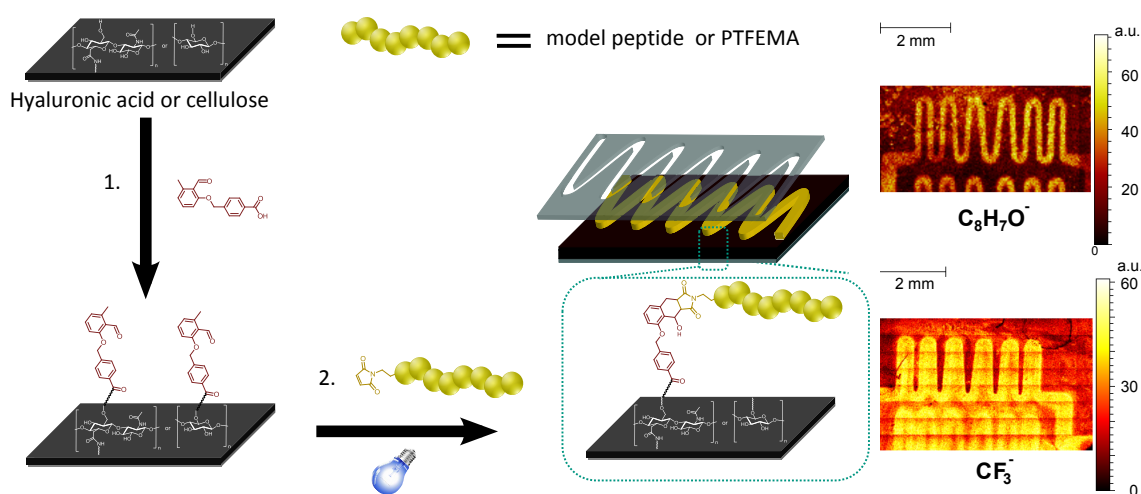
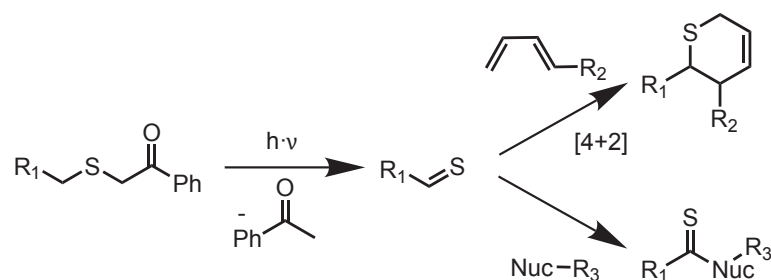


Figure 2.23: Photo-patterning of biosurfaces with a model peptide and PTFEMA employing photo-enol chemistry. Top right: ToF-SIMS imaging of the model peptide on hyaluronan. Bottom right: ToF-SIMS imaging of PTFEMA on cellulose. Figure adapted with permission from [182]. Copyright 2013 American Chemical Society.

2.4.3 Thioaldehyde Ligation



A very versatile light-induced reaction is the formation of thioaldehydes from phenacyl-sulfides. The photo-generated thioaldehyde is very reactive and undergoes [4+2] cycloadditions with dienes as well as addition to a range of nucleophiles. Nucleophilic moieties are ubiquitous in chemistry and nature, making the thioaldehyde ligation on the one hand very versatile yet on the other hand less specific. To generate the thioaldehyde from the phenacylsulfide light with the longest wavelength of the here described techniques is needed (close to 355 nm). In addition, the precursor (phenacylthio)acetic acid can readily be synthesized from commercially available, low cost materials (mercaptoacetic acid and 2-chloroacetophenone) in just one facile step via a nucleophilic reaction.^[183]

The thioaldehyde ligation has been utilized in our group to generate patterns of cyclopentadiene-functional PEG on a silicon wafer.^[19] Pauloehrl et al. generated photo-patterns of several nucleophiles in a similar approach.^[184] The reactivity of the photo-generated thioaldehyde was earlier studied in solution and analyzed via ESI-MS measurements. For patterning silicon wafers were fully functionalized with a thioaldehyde precursor. Subsequently, parts of the wafer were irradiated in the presence of a nucleophile leading to an immobilization on the surface, which was subsequently imaged via ToF-SIMS imaging (Figure 2.24).

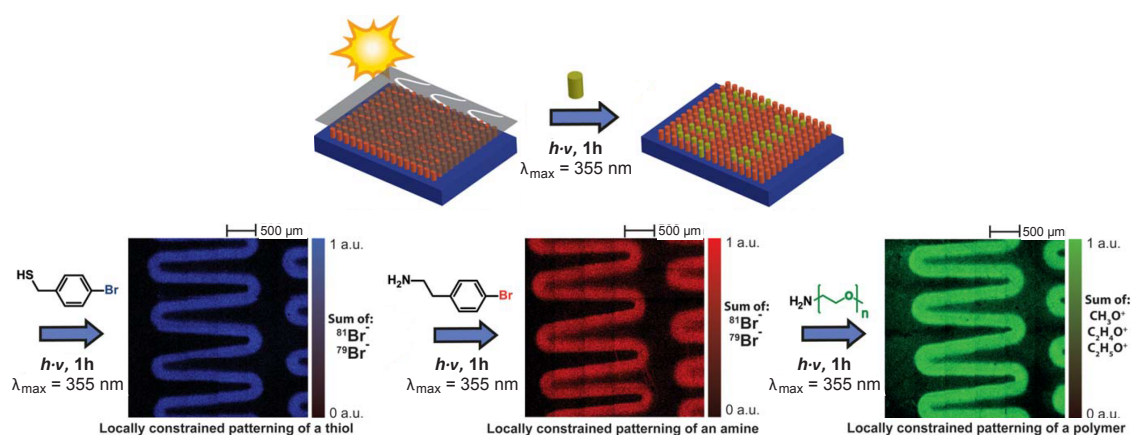


Figure 2.24: Photo-patterning of silicon wafers with nucleophiles employing thioaldehyde ligation imaged via ToF-SIMS. Figure adapted with permission from [184].

Current research on various surfaces proving the versatility of the approach is conducted in the author's research group.

In all aforementioned cases the photo-active group has been immobilized onto the surface of the substrate and the patterning was achieved with the utilization of a shadow mask during the light-triggered ligation process.

2.4.4 Other Techniques

Several other light-induced grafting reactions have been utilized to graft macromolecules on various surfaces in a spatially controlled manner. Aldehydes can be protected with a photo-labile group and immobilized on a silicon surface. Under irradiation the aldehyde is deprotected and active for oxime ligation with a peptide.^[185] In a similar fashion immobilized phencyclones can be employed to photo-pattern a silicon wafer with non-modified peptides.^[186]

Popik and Arumugam introduced the 3-(hydroxymethyl)naphthalene-2-ol structure, which upon irradiation generates o-naphthoquinone methides as reactive dienes for Diels-Alder or thiol-ene reactions. The immobilization of the precursor on surfaces allows for the photo-patterning with peptides, which are removable as well as replaceable when thiols are utilized for the covalent linking.^[187-191]

More insight into light-induced grafting reactions and photo-triggered click reactions can be gained from the review from Tasdelen and Yagci.^[192]

The immense range of light-triggered grafting reactions already allows for a diverse set of macromolecules to be tethered onto several substrates. Further research aims at a more universal and/or milder approach. The ideal light-induced grafting reaction utilizes ambient (sun-)light, can be applied to graft in general all polymer classes and employs surfaces that do not require tedious pre-functionalization.

Two of the aforementioned problems – the limited universality and the need for surface pre-functionalization – will be solved by the approach described in Chapter 6, preceding a comprehensive thermally-induced grafting study (Chapter 3). In addition, two precise/orthogonal light-induced grafting reactions on microspheres will be discussed (Chapter 4 and 5).

3

Modular Design of Glyco-Microspheres via Mild Pericyclic Reactions

The current chapter describes the first original findings of the thesis. Porous polymeric particles based on GMA were functionalized with a cyclopentadiene moiety in one facile step, making them a suitable counterpart for reversible addition fragmentation chain transfer hetero Diels-Alder (RAFT-HDA) cycloaddition. Utilizing a HDA capable RAFT-agent as a test-molecule, a comprehensive study of achievable loading capacities on Cp-functionalized microspheres – with pore sizes ranging over several orders of magnitude – was conducted. Elemental analysis was employed for quantification and loading capacities of up to $180 \mu\text{mol} \cdot \text{g}^{-1}$ were reached.

In addition, the first grafting of a glycopolymer onto microparticles via RAFT-HDA chemistry was conducted on a representative substrate. Poly(3-*O*-acryloyl-1,2:5,6-di-*O*-isopropylidene- α -D-glucofuranoside) was grafted onto the Cp-functionalized spheres, subsequently – and in one-pot – a deprotection of the grafted glycopolymer followed. The successful grafting was confirmed via SEM, XPS, inverse SEC, FT-IR-microscopy and elemental analysis to gain qualitative as well as quantitative information about the grafting process. A grafting density of $0.16 \text{ chains} \cdot \text{nm}^{-2}$ was determined.

Parts of this chapter were reproduced from M. Kaupp, A. P. Vogt, J. C. Natterodt, V. Trouillet, T. Gruending, T. Hofe, L. Barner, C. Barner-Kowollik, *Polym. Chem.* **2012**, **3**, 2605–2614 by permission from The Royal Society of Chemistry.

3.1 Introduction

Modification of porous polymeric microspheres can introduce new or alter existing properties of the particles, thus making them employable in various applications. As discussed in Section 2.1.3, microspheres are already utilized in chromatographic systems,^[87] as solid carrier materials for synthesis^[95] and catalysis,^[97] in biological, medicinal and pharmaceutical applications,^[23,107] and more. By the introduction of new functionalities, e.g., strongly hydrophilic groups, the field of applications can be expanded or particles previously not matching the desired field of usage can now be employed.

Current research strongly focuses on the modification of particles via 'grafting-to' techniques (Section 2.1.2), which allows for an in-depth characterization of the to be grafted molecules before the immobilization reaction.^[10] To achieve high grafting densities, very efficient reactions should be employed, such as the click reactions (modular ligations) described by Sharpless^[58] and modified for polymer conjugations by Barner-Kowollik.^[59] One of the tethering reactions matching these strict criteria is the RAFT-HDA cycloaddition (Section 2.2.4), where the RAFT-agent has two purposes: First, it controls the polymerization and thereby the molecular weight distribution and end groups of the polymer. Second, the thiocarbonyl originating from the Z-group of the RAFT-agent, which is tethered to one of the chain ends after the polymerization, acts as a highly reactive dienophile. A very well known and very reactive diene is cyclopentadiene,^[193] which has been introduced onto polymeric microspheres before,^[86] and reacts in RAFT-HDA reactions without metal containing catalysts at slightly elevated to ambient temperatures.^[194] By the introduction of glycopolymers (Section 2.3) onto hydrophobic particles, the surface properties are changed to very hydrophilic, forming functional core shell-particles, as described by Müller et al.^[53,166] Thus, the functionalized particles are employable in applications the initial particles were not suitable for.

The current chapter describes the first-time functionalization of microspheres with a glycopolymer via a mild cycloaddition based on RAFT-HDA chemistry. Cp-functionalization of the particles was conducted in one facile step beforehand. The general synthesis strategy for the decoration of microspheres with glycopolymers is depicted in Figure 3.1 on the opposite page.

3. Modular Design of Glyco-Microspheres via Mild Pericyclic Reactions

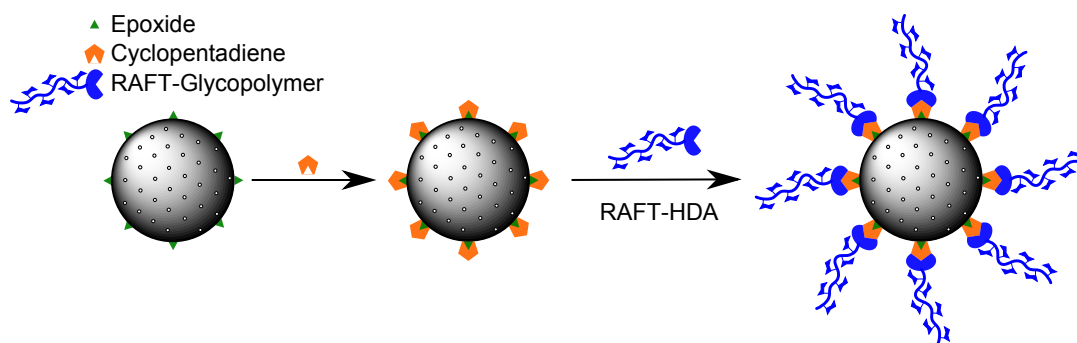


Figure 3.1: Schematic illustration of the synthetic steps for the grafting of glycopolymers onto porous microspheres via the RAFT-HDA approach.

3.2 Results and Discussion

In the following the synthetic steps and analytical results will be discussed in detail, covering the entire sequence from the glycopolymer preparation to the surface analysis of the final microspheres decorated with the glycopolymer. For a successful (RAFT-)HDA reaction between polymers and microspheres one reaction partner has to be functionalized with a dienophile, whereas the other one needs to contain a diene. Although it is possible to synthesize polymeric chains^[16,193] as well as microspheres^[85,86] with each desired functionality, RAFT-HDA simplifies this approach very elegantly as – by the inherent polymerization process – the dienophilic RAFT-end group is incorporated on one end of the polymeric chain.

3.2.1 Preparation of RAFT-Glycopolymer with HDA End Group

So far, three basic RAFT-agent structures are available, which can undergo HDA reactions, because of the electron-withdrawing nature of their Z-groups (Figure 3.2).^[16,86]

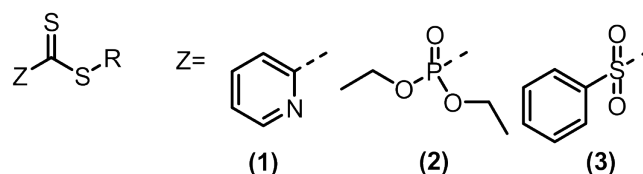


Figure 3.2: Z-groups presently available for RAFT-agents that are able to undergo hetero Diels-Alder (HDA) reactions.

RAFT-agents carrying the sulfonyl moiety (3) as Z-group are labile and react readily even with vinylic monomers in [2+4] cycloadditions,^[195] thereby making them unsuitable for the controlled polymerization of some monomers. The phosphonate group (2) has been employed in the grafting of RAFT-polymers onto microspheres before.^[86] However, phosphorus cannot be detected by most elemental analyzers, leading to a disadvan-

3. Modular Design of Glyco-Microspheres via Mild Pericyclic Reactions

tage as in the current study elemental analysis provides the only quantitative information about the grafting density. Therefore, utilization of a phosphorous-carrying RAFT-agent would lead to grafting densities which are based on elemental analyses that are always disputable, as the mass balance would never be closed. Thus, a RAFT-agent with a pyridinyl-based Z-group (**1**) was selected. The one and only disadvantage when employing (**1**) is the need for an acid catalyst, e.g., trifluoroacetic acid, for facile and fast RAFT-HDA conversion, however the acidic catalyst may be removed simply in vacuo. The water solubility of such pyridinyl RAFT-agents could be adjusted by the variation of the R-group, yet establishing the synthesis of a well water soluble RAFT-agent with the Z-group required for RAFT-HDA would be very tedious. Moreover, several protected glycomonomers are reported in the literature which are readily soluble in organic solvents. Therefore, the polymerizations were conducted in toluene. The chosen monomer was 3-O-acryloyl-1,2:5,6-di-O-isopropylidene- α -D-glucofuranoside (AIPGlc) which was synthesized according to the literature from commercially available acetyl protected glucose in one simple step.^[196] It was found that for a reasonable reaction time a high amount of radical initiator (up to 0.3 equiv. corresponding to the RAFT-agent) and a rather high concentration of monomer (close to $1 \text{ mol} \cdot \text{L}^{-1}$) were needed. Under the aforementioned conditions the polymerization reached 25 % conversion at 75 °C in 4 h, resulting in poly(3-O-acryloyl-1,2:5,6-di-O-isopropylidene- α -D-glucofuranoside) (PAIPGlc) with a number-average molecular weight (M_n) of $4200 \text{ g} \cdot \text{mol}^{-1}$ and a low dispersity ($D = 1.2$). Further analysis of the generated glyco-RAFT-polymer via electrospray ionization mass spectrometry allowed for an in-depth investigation of its end group functionality (Figure 3.3 on the opposite page). The subscripted letters refer to the end groups of the polymeric chains. The vast majority of chains exhibit the Z-group stemming from the RAFT-agent (highlighted with a black box), which is the end group necessary for a successful subsequent RAFT-HDA reaction. The other chain ends also originate from the RAFT-agent (P_{RZ}) or from the radical initiator (P_{IZ}). A negligible amount of side products could also be identified, e.g., a product without any functional end groups (P) derived from transfer to monomer or saturated chain ends (S) derived from radical disproportionation. The polymerization was quenched between 20 and 30 % of conversion to retain the desired high thiocarbonylthio end group functionalization, as the amount of transfer reactions increases with conversion.

3.2.2 Preparation of Cp-Functional Microspheres

The porous microspheres consist of 80 % GMA and 20 % of a commercial crosslinker and were synthesized via suspension polymerization. Due to the presence of a reactive ring-strained epoxide, PGMA based microspheres are an ideal substrate for further

3. Modular Design of Glyco-Microspheres via Mild Pericyclic Reactions

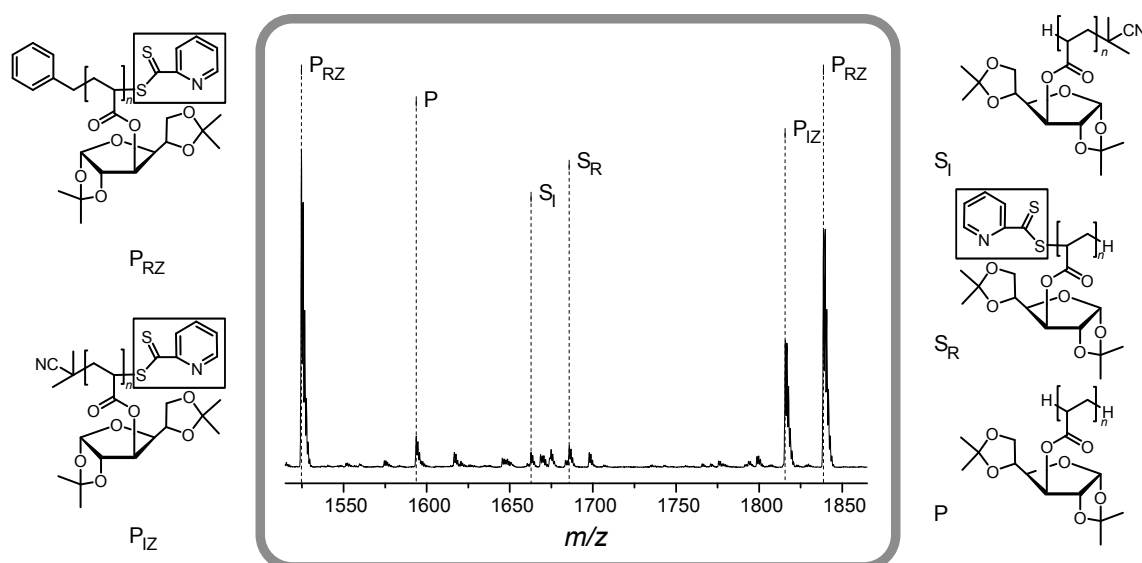


Figure 3.3: GPC-ESI-MS spectra of a representative repetition unit of the protected glycopolymer PAIpGlc synthesized via RAFT-polymerization. The subscripted letters describe the end groups of the polymer (R = R-group, Z = Z-group, I = initiator fragment). The capital S describes a saturated side product derived from disproportionation. A side product without any end groups – originating from transfer to monomer – is labeled as P. The Z-group, which is needed for a successful HDA reaction, is highlighted with a black box.

functionalizations. Initially, the microspheres were thoroughly characterized via scanning electron microscopy (SEM), inverse size exclusion chromatography (iSEC), X-ray photoelectron spectroscopy (XPS), attenuated total reflectance (ATR) FT-IR-microscopy, and elemental analysis. SEM gives information about the morphology, size, porosity, and dispersity of the particles, which exhibited a disperse size distribution with an average diameter of about 7-10 μm . The elevated dispersity was intended, as with disperse spheres the packing density is increased in potential later chromatographic applications. The porosity of the microspheres is adjustable over several orders of magnitude with the amount of employed precipitating agent and solvent during the synthetic process, yielding pores that match macromolecules of a contour length between 1 nm and 500 nm. X-ray photoelectron spectroscopy and FT-IR-microscopy allow for a qualitative monitoring of the functionalization whereas elemental analysis allows for quantification of the grafting reactions. Via iSEC the surface area and porosity of the particles could be determined.^[197] The full data of the iSEC measurements can be found in the Appendix in Table A.1 on page 161.

One of the most reactive dienes for the Diels-Alder reactions is cyclopentadiene (Cp). Although there is a previously reported procedure for the functionalization of polymeric microspheres with Cp-moieties, it was exclusively conducted on PDVB-based particles in a three step process.^[86] The PGMA microspheres employed in the current

3. Modular Design of Glyco-Microspheres via Mild Pericyclic Reactions

work were functionalized with Cp-moieties in just one facile step by suspending the substrate in anhydrous THF and subsequently adding a solution of sodium cyclopentadienide (Figure 3.4).

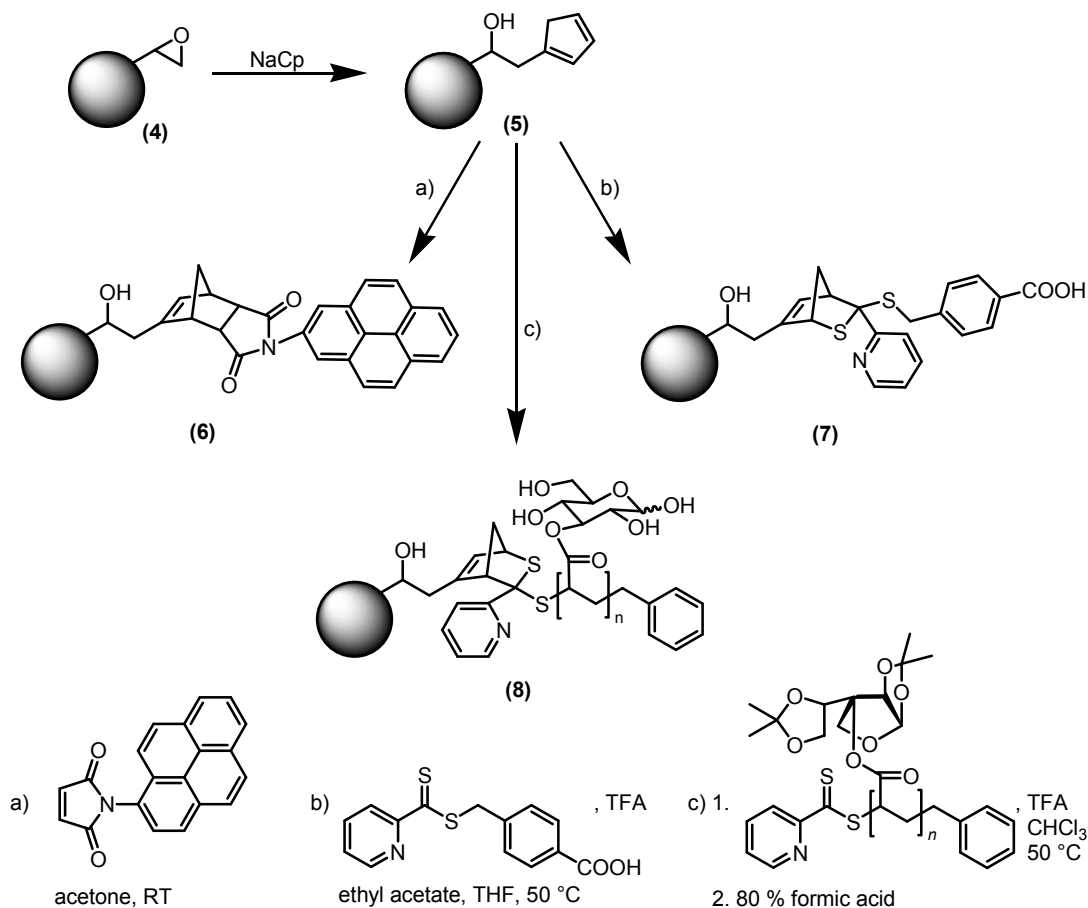


Figure 3.4: Overview of the functionalization and grafting reactions on microspheres. PGMA microspheres (4) were functionalized with cyclopentadiene by the reaction with sodium cyclopentadienide solution in anhydrous THF. The Cp-functionalized particles (5) can undergo Diels-Alder reactions with the fluorescence marker *N*-(1-pyrene) maleimide (6), HDA with a RAFT-agent (7), and RAFT-HDA with the protected glycopolymer (with subsequent one-pot deprotection) (8).

The nucleophilic cyclopentadienide anion rapidly undergoes addition to the epoxide. After just 4 h the reaction was quenched in a saturated solution of ammonium chloride and by filtration and extensive washing the Cp-functionalized microspheres were isolated. A proof for a successful reaction can be given indirectly via the reaction of the Cp-functionalities with the fluorescent marker *N*-(1-pyrene) maleimide in a Diels-Alder reaction in just 2.5 h at slightly elevated temperatures (40 °C). Only microparticles that were functionalized with Cp show a blue fluorescence upon irradiation with UV-light ($\lambda_{\text{max}} = 366 \text{ nm}$), which can be seen in Figure 3.5 on the opposite page. Spheres from a control reaction (PGMA particles undergoing an analogous treatment) did not fluoresce.

3. Modular Design of Glyco-Microspheres via Mild Pericyclic Reactions

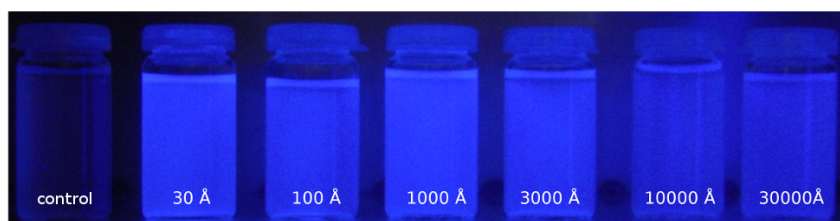


Figure 3.5: Photograph of suspensions of microspheres with different pore sizes after Cp-functionalization and fluorescent marking with *N*-(1-pyrene) maleimide and one control sample of 1000 Å PGMA-microspheres without Cp-functionalization under irradiation with UV-light ($\lambda_{\text{max}} = 366 \text{ nm}$). 2 mg of microspheres were suspended in ca. 6 mL of acetone. Fluorescence is observed for every sample, except for the control.

High resolution ATR FT-IR-microscopy can give a second proof for the success of the functionalization process, as it is able to determine the spatial distribution of an IR-active functionality on a given substrate.^[198] By the nucleophilic ring-opening of the epoxide on the microspheres an OH-group is formed, whose vibration can be detected and thereby its distribution on the spheres is visualized via FT-IR-microscopy as shown in Figure 3.6.

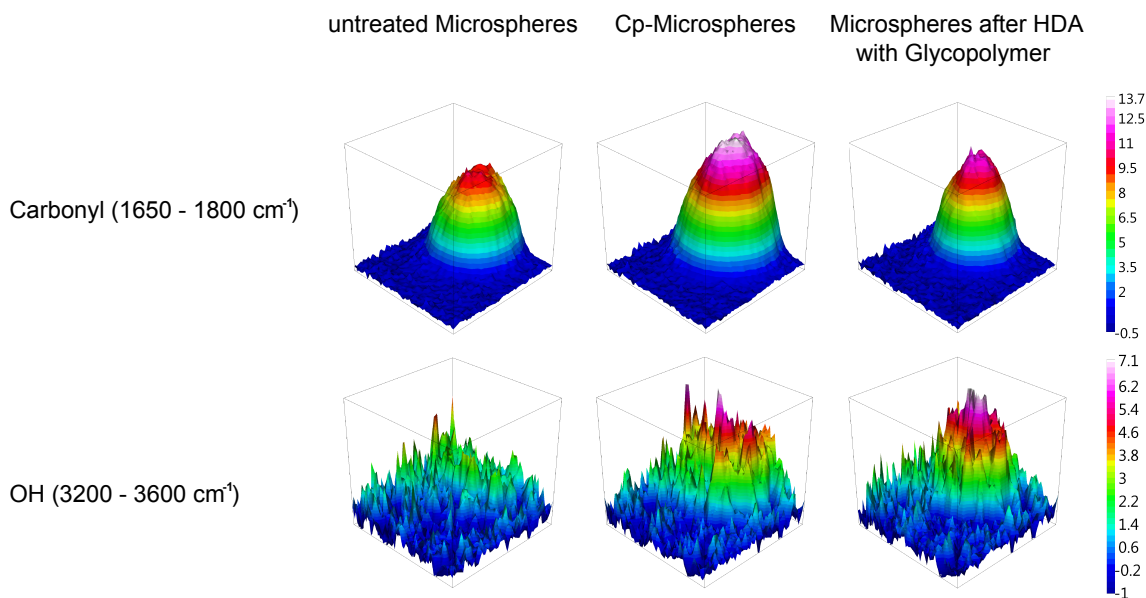


Figure 3.6: False color high-resolution ATR FT-IR-microscopy images (4 cm^{-1} spectral resolution with a pixel resolution of $0.25 \mu\text{m}^2$) of a single 1000 Å PGMA microsphere before and after Cp-functionalization, and after RAFT-HDA reaction with glycopolymer, respectively. The measured area is $32 \mu\text{m} \times 32 \mu\text{m}$. Red color corresponds to a high degree of functionalization. In the top row the intensities of bands corresponding to the C=O stretching vibration are visualized, in the bottom row a broad OH peak was integrated. Each row of spectra was normalized to the same scale for comparability.

3. Modular Design of Glyco-Microspheres via Mild Pericyclic Reactions

The FT-IR-microscopy technique was able to depict the shape and functionalization density of the microspheres as can be seen by the mapping of the C=O stretching vibration between 1650 and 1800 cm^{-1} for PGMA (Figure 3.6, top row). Although the integration of the broader OH peak between 3200 and 3600 cm^{-1} resulted in somewhat noisy spectra, in the area of the sphere a clear change in functionalization could be evidenced. For the untreated microspheres no OH-vibration was detected. In contrast, the Cp-functionalized particles displayed a maximum intensity for the OH signal that spatially coincided with the maximum in the carbonyl signal. The last column in Figure 3.6 will be discussed below. The combined results of FT-IR-microscopy and the fluorescence marking unambiguously demonstrate that the reactive Cp-diene was incorporated onto the surface of the microspheres.

3.2.3 Small Molecule Model Study of RAFT-HDA Reactions on Cp-Functional Microspheres

For the quantification of the grafting density elemental analysis was employed. Sulfur is covalently bound to the spheres via the HDA reaction with a RAFT-agent or with a polymer synthesized via RAFT-polymerization. In addition, sulfur is a new element in the composition of the PGMA microspheres (also after Cp-functionalization) and therefore the loading capacity (the number of grafted chains) could be determined directly via the quantification of the amount of sulfur without any bias of the chain length of the grafted polymeric material.

A broad study was conducted with substrates of varying pore sizes to establish the ideal conditions for the HDA reaction on the Cp-functionalized microspheres. The RAFT-agent 4-((pyridine-2-carbodithiyl)methyl)benzoic acid was chosen as a simple test molecule. The reaction was conducted for up to 96 h at slightly elevated temperatures (50 °C) in a mixture of ethyl acetate and THF with trifluoroacetic acid (TFA) as the catalyst. The successful reaction was evidenced by elemental analysis as the sulfur content increased with reaction time, up to 1.34 wt%. This means that 1 g of grafted microspheres contained up to 0.0134 g of sulfur. The full data of the elemental analysis can be found in in Table 3.1 on page 44.

The sulfur content can be converted to a loading capacity via Equation 3.1: ^[86]

$$LC = \frac{W(S)}{n(S) \cdot M(S)} \quad (3.1)$$

3. Modular Design of Glyco-Microspheres via Mild Pericyclic Reactions

where LC is the loading capacity (in $\text{mol} \cdot \text{g}^{-1}$), $W(S)$ is the weight of sulfur per 1 g of microspheres obtained via elemental analysis, $n(S)$ is the number of sulfur atoms per grafted molecule (here 2) and $M(S)$ is the molecular weight of sulfur. The LC results are shown in Figure 3.7.

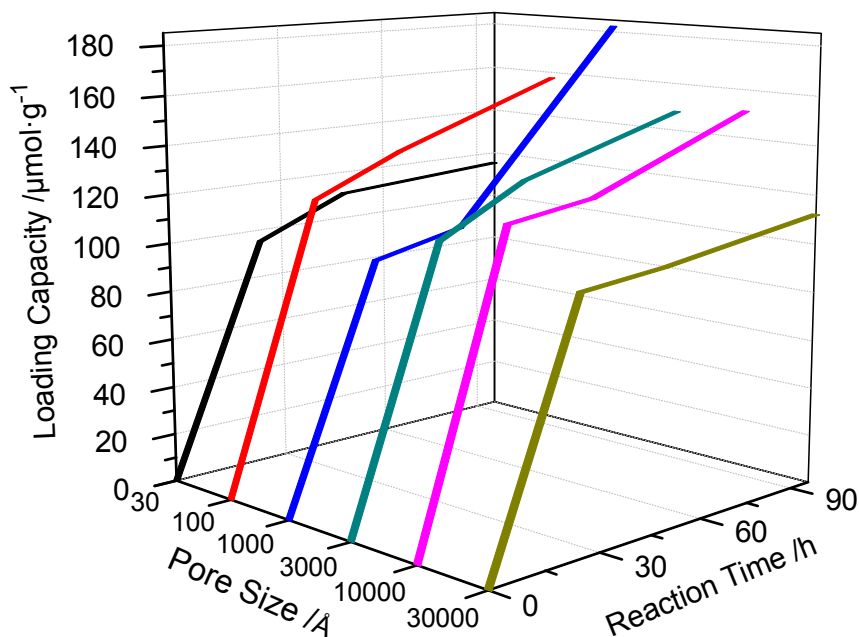


Figure 3.7: Overview of the loading capacity achieved via HDA chemistry as a function of the reaction time and the average pore size of the employed substrate. The Cp-functionalized microspheres were reacted with 4-((pyridine-2-carbodithiyl)methyl)benzoic acid at 50 °C with TFA as a catalyst (the exact reaction conditions can be found in the Experimental Section 3.4.5 on page 52). The elemental constitution was analyzed and the loading capacity was calculated from the sulfur content according to Equation 3.1.

During the first 24 h of the grafting reaction the main conversion took place, yet for a maximized loading capacity a longer reaction time of several days was necessary. The highest loading capacity was achieved for the 1000 Å sample. For the microspheres with the smallest (30 Å) and largest (30000 Å) pores a lower maximum sulfur content was observed – the reason being the morphology of the spheres. For the smallest pore size (30 Å) the lower loading capacity is assumed to be due to small pores making much of the internal sphere surface inaccessible for the reactant. The result for the particles with the highest pore diameters is expected as the surface to volume ratio decreases with the pore diameter, leaving less surface to react with.

3. Modular Design of Glyco-Microspheres via Mild Pericyclic Reactions

Table 3.1: Collected data from elemental analysis of all samples described in Chapter 3.

Sample	N [wt%] ¹	C [wt%]	H [wt%]	S [wt%] ²	O [wt%] ³
PGMA 30 Å	0.27	55.68	6.90	0.00	32.60
Cp-functionalized	0.28	54.65	6.80	0.00	31.23
24 h HDA	0.31	51.11	6.29	0.57	34.45
48 h HDA	0.38	50.87	6.20	0.65	34.02
96 h HDA	0.36	50.40	6.02	0.67	33.31
PGMA 100 Å	0.00	58.66	7.41	0.00	33.89
Cp-functionalized	0.00	57.98	7.23	0.00	33.46
24 h HDA	0.22	52.77	6.53	0.70	33.71
48 h HDA	0.21	52.07	6.40	0.79	33.82
96 h HDA	0.21	51.50	6.23	0.94	34.30
PGMA 1000 Å	0.19	55.77	6.88	0.00	32.84
Cp-functionalized	0.00	57.79	7.24	0.00	31.88
24 h HDA	0.23	58.28	7.08	0.62	34.25
48 h HDA	0.30	52.51	6.39	0.63	33.94
96 h HDA	0.33	52.01	6.19	1.09	33.63
90 h HDA ⁴	0.39	51.75	6.26	1.34	32.75
HDA with glycopolymer	0.37	51.90	6.57	0.24	35.11
HDA with glycopolymer (repeated)	0.45	54.41	6.13	0.31	35.67
control	0.00	55.73	6.88	0.00	34.91
PGMA 3000 Å	0.00	58.63	7.27	0.00	32.93
Cp-functionalized	0.00	58.34	7.23	0.00	31.92
24 h HDA	0.00	53.04	6.36	0.66	34.03
48 h HDA	0.00	52.41	6.26	0.76	33.81
96 h HDA	0.10	51.94	6.12	0.88	33.61
PGMA 10000 Å	0.00	58.37	7.35	0.00	32.75
Cp-functionalized	0.00	57.67	7.10	0.00	31.16
24 h HDA	0.00	53.47	6.38	0.72	33.21
48 h HDA	0.00	53.31	6.33	0.75	32.80
96 h HDA	0.22	52.76	6.26	0.90	32.85

3. Modular Design of Glyco-Microspheres via Mild Pericyclic Reactions

PGMA 30000 Å	0.00	59.70	7.41	0.00	32.89
Cp-functionalized	0.00	58.37	7.21	0.00	32.41
24 h HDA	0.00	54.26	6.47	0.60	32.03
48 h HDA	0.09	53.50	6.37	0.62	33.63
96 h HDA	0.09	52.81	6.25	0.67	33.29

¹ The nitrogen found in the untreated and Cp-functionalized microspheres can be explained by fragments from the nitrogen containing initiator, stabilizer or gaseous nitrogen trapped in the porous surface morphology of the microspheres. Since the nitrogen value is not used for any further calculations, this does not lead to an error for the calculated loading capacity or grafting density values.

² Content measured independently, employing a water-trap.

³ Content measured independently.

⁴ The reaction was performed separately. Why a higher loading capacity was reached is still under investigation.

3.2.4 RAFT-HDA Reaction of Cp-Functional Microspheres with Glycopolymer

The grafting of the glycopolymer onto the Cp-functionalized microspheres was performed with experimental conditions similar to those established in the model study with the small molecule RAFT-agent. Due to the solubility of the polymer the solvent was changed to chloroform, a well-known solvent for (RAFT-)HDA reactions between polymers.^[16] The reaction was conducted for 5 days at a slightly elevated temperature (50 °C) with TFA as catalyst. Subsequently – in the same reaction vessel and with no work up, except for removal of the solvent via a rotary evaporator – the deprotection of the grafted polymer to poly(3-*O*-acryloyl- α,β -D-glucopyranoside) (PAGlc) was performed by adding formic acid and shaking at ambient temperature for another two days. The functionalized microspheres were thoroughly analyzed via XPS, FT-IR-microscopy, SEM, and elemental analysis.

The first indication of a successful grafting reaction was an increase in the dry mass of the microspheres of almost 16 %, which was measured after a small but inevitable loss of substance associated with washing over a sintered glass filter. The SEM micrographs (Figure 3.8 on the following page) show first and foremost that the porosity and spherical shape of the particles was preserved throughout the reaction sequence.

Detailed inspection of the SEM images reveals a change in the surface morphology after the grafting of glycopolymer, whereby the edges before grafting appear sharp, and

3. Modular Design of Glyco-Microspheres via Mild Pericyclic Reactions

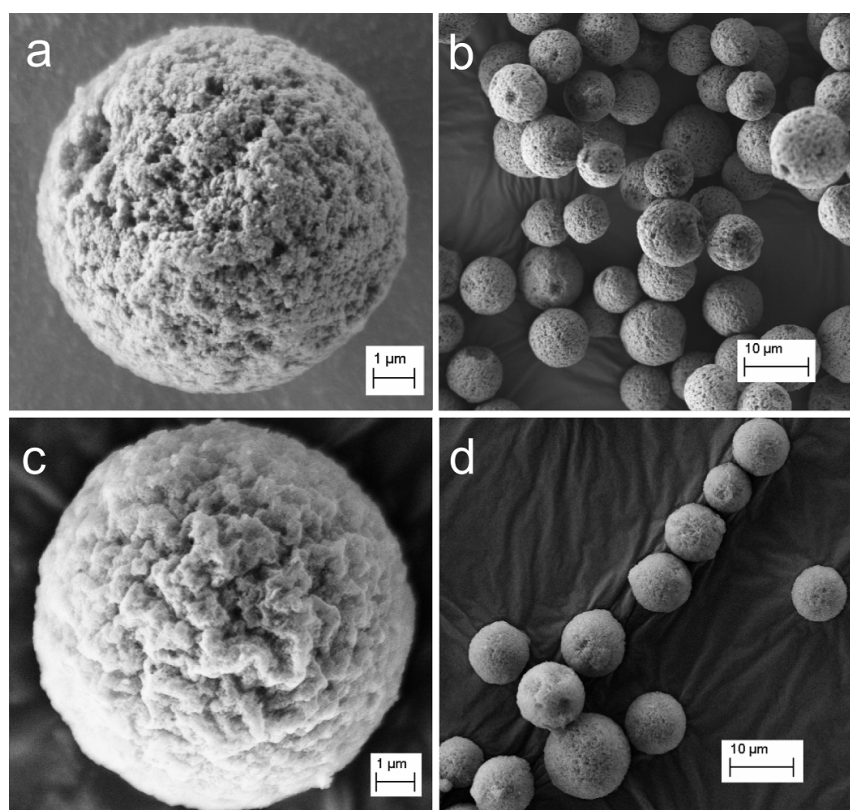


Figure 3.8: SEM images of the non-modified PGMA microspheres with an average pore size of 1000 Å (a and b) and the same spheres after Cp-functionalization and RAFT-HDA reaction with glycopolymer (c and d).

after the reaction they appear much softer. Furthermore, FT-IR-microscopy (Figure 3.6 on page 41) showed the highest degree of OH-functionalization after the HDA reaction, which is localized to the area of the sphere again. Taking into account that the integral for the carbonyl functionality is higher for the Cp-functionalized sphere (due to the slightly larger diameter of the examined particle) than for the microsphere after the grafting reaction, the increase in functionality is even more persuasive.

Further proof of a successful reaction is given by XP spectroscopy. Cp-functionalized microspheres do not show any nitrogen or sulfur signals whereas the spectra of the spheres after the HDA reaction (Figure 3.9 on the opposite page) clearly confirm the presence of nitrogen (at 400.0 eV) and sulfur. The S 2 $p_{3/2}$ signal at 163.6 eV evidences the presence of S-C bonds while the S 2 $p_{3/2}$ signal at 168.7 eV is assigned to some oxidized species (sulfur in the oxidation state +6).^[199] The oxidized species have been observed in XP spectra of polymers grafted via RAFT-HDA before and do not affect the grafting efficiency.^[144]

Analysis of the elemental constitution of the grafted microspheres gains quantitative information about the loading capacity. As described above, the sulfur content can directly be used as a measure of how many polymeric chains were successfully attached to the

3. Modular Design of Glyco-Microspheres via Mild Pericyclic Reactions

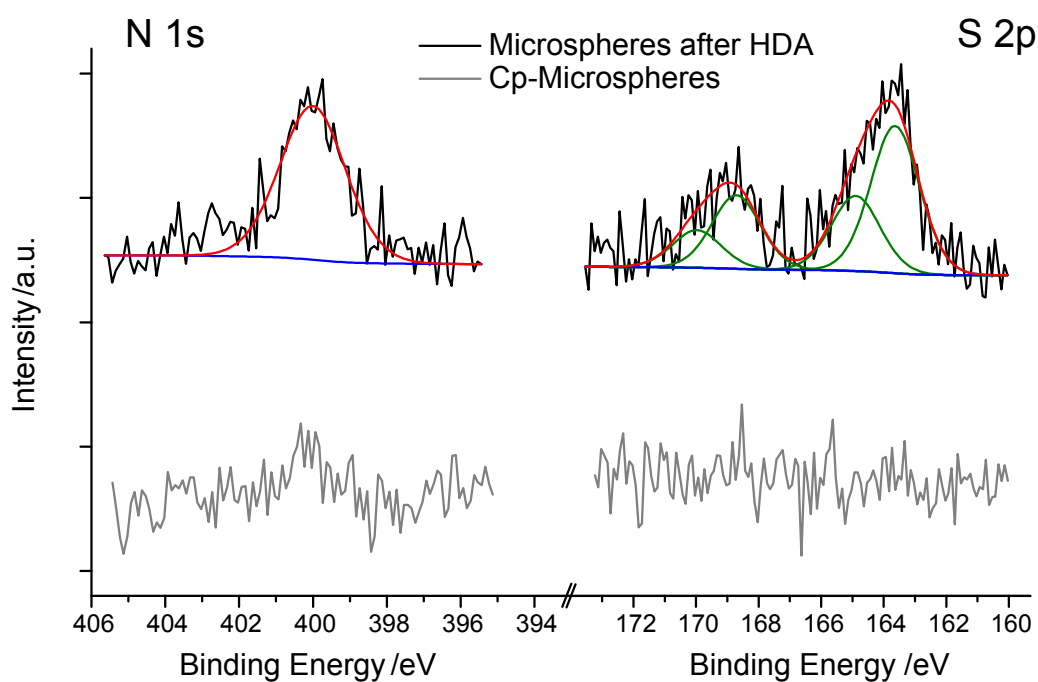


Figure 3.9: N 1s and S 2p XP spectra of Cp-functionalized microspheres before and after HDA reaction. The presence of nitrogen and sulfur after the successful grafting reaction is clearly shown.

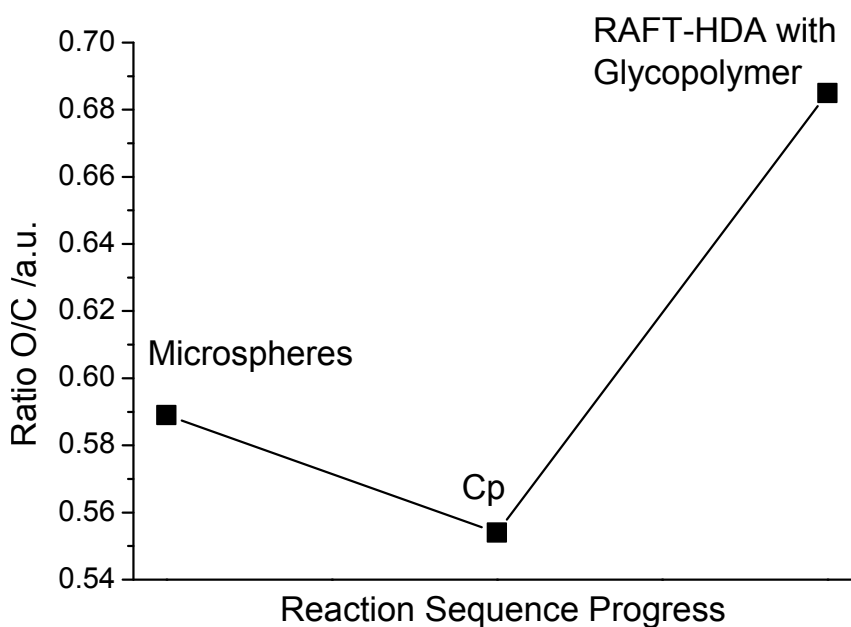


Figure 3.10: Evolution of the ratio of oxygen to carbon determined by elemental analysis in the reaction sequence untreated PGMA microspheres, Cp-functionalization with sodium cyclopentadienide, and RAFT-HDA reaction with glycopolymer.

3. Modular Design of Glyco-Microspheres via Mild Pericyclic Reactions

microspheres' surface. Since sulfur is only contained in the end groups of the polymer chains, the values for the grafting density and loading capacity are not affected by a possible bias in the chain length values determined via SEC. During the reaction process the content of sulfur increases from 0.0 wt% for the untreated and Cp-functionalized particles to 0.28 wt% (averaged) after the grafting reaction. By employing Equation 3.1 on page 42 the content of sulfur can be converted to a loading capacity of $44 \mu\text{mol} \cdot \text{mol}^{-1}$ or via multiplication with Avogadro's number to $2.63 \cdot 10^{19}$ chains per g. In addition, the elemental analysis can be employed to underpin that the whole glycopolymer has been grafted onto the spheres, and not merely a fragment of the RAFT-agent, thus indicating that the polymer was not destroyed by the applied reaction conditions. The weight ratio of oxygen to carbon in the untreated spheres (0.589) matches that of PGMA (0.571) (it is slightly higher due to the crosslinker). The ratio decreases to 0.554 after the Cp-functionalization as the introduced cyclopentadiene functionality only contains carbon and hydrogen but no oxygen. After the grafting reaction with the RAFT-glycopolymer the oxygen to carbon weight ratio increases to 0.685 (averaged) (Figure 3.10 on the preceding page), which can be associated with the unprotected glycopolymer containing more oxygen than carbon (weight ratio: 1.036).

Via inverse SEC the relative surface area of the untreated PGMA microspheres was determined to be close to $225.4 \text{ m}^2 \cdot \text{cm}^{-3}$ under the assumption of cylindrical pores. iSEC allows the determination of all physical pores reachable for polymers. The density of the microspheres swollen in THF can be measured to be $1.39 \text{ g} \cdot \text{cm}^{-3}$ with a procedure described by Barner and coworkers.^[49] The relative surface area can be converted to an area per mass by employing the density value, yielding an accessible microsphere surface area of $162 \text{ m}^2 \cdot \text{g}^{-1}$ or $1.62 \cdot 10^{20} \text{ nm}^2 \cdot \text{g}^{-1}$. These measured surface areas are deemed much more accurate than the estimated values often applied in previous publications which only accounted for the nominal surface area of the spheres using the diameter of the microsphere, thereby neglecting any surface roughness and porosity. Employing a more accurately determined surface area also explains why the surface area in the current work increased around two orders of magnitude compared to the area assumed by Nebhani et al.^[86] and therefore the analogous grafting density is decreased by two orders of magnitude. The grafting density can be calculated according to Equation 3.2:

$$GD = \frac{W(S) \cdot N_A}{n(S) \cdot M(S) \cdot A} \quad (3.2)$$

where GD is the grafting density in chains per unit area; $W(S)$ is the weight of sulfur in 1 g of microspheres obtained via elemental analysis, N_A is Avogadro's number, $n(S)$ is

3. Modular Design of Glyco-Microspheres via Mild Pericyclic Reactions

the number of sulfur atoms per polymer chain (here 2), $M(S)$ is the molecular weight of sulfur, and A is the surface area of the microspheres as determined via iSEC and converted with the measured density value. The thus obtained grafting density is close to $0.16 \text{ chains} \cdot \text{nm}^{-2}$. There are three potential sources of error in determining the grafting density, i.e. the accuracy of the determined surface area – which has been discussed above – the accuracy of the data obtained via elemental analysis, and a potential overestimation of the grafting due to physically trapped chains. The data obtained from elemental analysis are very accurate, as the sulfur contents are determined with a built-in water-trap in an additional experiment, so that the high hydrogen and oxygen contents do not affect the value obtained for sulfur. Furthermore, the mass balance (the experimentally determined net weights of all elements in proportion to the sample weight) is close to 100 % for all the elemental analyses, demonstrating a reproducible and complete combustion of the samples. As noted above, a problem might lay in the morphology of the microspheres. It could not be undisputably proven whether the polymeric chains are covalently bound to the particles or are merely trapped within their porous morphology. To exclude chain trapping, the spheres were repetitively and extensively washed with variable solvents. For a control reaction untreated PGMA microspheres were employed instead of Cp-functionalized particles and exposed to identical conditions and no sulphur could be detected after the reaction.

The values obtained for the loading capacity can be compared subsequently to those obtained in previously reported studies applying a quantification of the loading capacity. Nebhani et al. [86] reported up to $1.2 \cdot 10^{20} \text{ chains} \cdot \text{g}^{-1}$, exceeding the current loading capacities by a factor of more than four. The authors employed the thermally induced RAFT-HDA approach as well, yet grafted polystyrene chains onto non-porous PDVB microparticles. The reactants in the current work were chemically and sterically more demanding, underlining the versatility and robustness of the RAFT-HDA approach. Joso et al. [49] grafted poly(ethylene glycol) from PDVB microspheres obtaining a loading capacity of $3.1 \cdot 10^{19} \text{ chains} \cdot \text{g}^{-1}$, which is merely higher than the loading capacity in the present work. However, they applied a 'grafting from' process, which benefits from a higher achievable grafting density, but lacks the opportunity to thoroughly characterize the grafted polymers. A third study – where elemental analysis was employed for the quantification of the grafting efficiency – is provided by Irgum and coworkers [82] where thiol-terminated polymer chains were grafted onto PDVB microspheres previously functionalized with epoxy moieties. A loading capacity was not determined, yet with sulfur contained in the repeating unit and not only at the chain end, a sulfur content of only 0.6 % was achieved, which is similar to the sulfur contents observed in the present work – where sulfur is only contained in the chain ends – and suggests that the obtained grafting

3. Modular Design of Glyco-Microspheres via Mild Pericyclic Reactions

densities are significantly lower than via the approach described here.

A grafting density of $0.16 \text{ chains} \cdot \text{nm}^{-2}$ might seem low when compared to other values achieved on microparticles at first glance, however this is primarily due to the high (measured) surface area employed for the calculations in the present work. The reason for the observed – and desired – high surface area lies in the high porosity and surface morphology, which is neglected in other publications. Pfaff et al. employed a nominal surface area and achieved a grafting density of $0.20 \text{ chains} \cdot \text{nm}^{-2}$ by grafting a glycopolymer prepared via the RAFT-process onto PDVB with thiol-ene chemistry after aminolysis.^[53] By grafting from other substrates, for which surface data are easier to obtain, such as silicon, Ejaz et al. obtained grafting densities for glycopolymers via a 'grafting from' polymerization approach of about $0.1 \text{ chains} \cdot \text{nm}^{-2}$.^[200] These numbers are in excellent agreement with the data reported in the current study. It is noteworthy – and somewhat surprising – that the 'grafting to' approaches reported herein and in the references by Nebhani^[86] and Pfaff^[53] lead to even higher loading capacities and grafting densities than some 'grafting from' approaches.

3.3 Conclusions

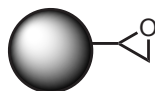
The first successful grafting of a glycopolymer via RAFT-HDA chemistry onto Cp-functionalized microspheres was carried out at mild temperatures with TFA as a readily removable catalyst. The grafted polymer is a PAIPGlc polymerized by RAFT with a M_n of $4200 \text{ g} \cdot \text{mol}^{-1}$ and a D of 1.2. Cp-functionalization of the microparticles was conducted in one facile step. Deprotection of the glycopolymer to PAGlc was conducted in one pot subsequent to grafting. The obtained core-shell particles were thoroughly characterized via inverse SEC, scanning electron microscopy, high resolution ATR FT-IR-microscopy, XPS, and elemental analysis. The in-depth analysis not only allowed qualitative characterization but also the quantification of the loading capacity and grafting density, which reach $2.63 \cdot 10^{19} \text{ chains} \cdot \text{g}^{-1}$ and $0.16 \text{ chains} \cdot \text{nm}^{-2}$, respectively. The data presented in the current chapter demonstrates the versatility and robustness of the RAFT-HDA approach for glycopolymer grafting and demonstrates that the obtained grafting densities are close to – or even exceed – the values reached by other 'grafting to' and 'grafting from' approaches.

3.4 Experimental Part

3.4.1 Materials

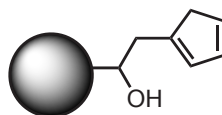
2,2'-Azobis(2-methylpropionitrile) (AIBN, Sigma-Aldrich) was recrystallized twice from methanol and stored at -19 °C. CHCl₃ (VWR) was dried over CaCl₂. Benzyl pyridin-2-ylidithioformate (BPDF),^[201] 4-((pyridine-2-carbodithiyl)methyl)benzoic acid and 3-*O*-acryloyl-1,2:5,6-di-*O*-isopropylidene- α -D-glucofuranoside (AIPGlc)^[196] were synthesized according to the literature. All other chemicals were used as supplied by the manufacturers.

3.4.2 Synthesis of the Poly(Glycidyl Methacrylate) Microspheres*



The PGMA particles were synthesized by suspension polymerization with AIBN as initiator in a commercial 20 L Buechi steel reactor with temperature and stirring control. The particle size is controlled by the stirring speed. GMA and a commercial crosslinker were mixed to adjust the network density and the mechanical stability of the particles and reacted at 65 °C. The pore size is determined by the employed amount of solvent and precipitation agent. The reaction runs over night. After washing and cleaning with various organic and aqueous solvents, the raw material is classified with a commercial particle classifier from Hosokawa. The synthesized porosities are 30 Å, 100 Å, 1000 Å, 3000 Å, 10000 Å and 30000 Å and the classified particle size is 10-12 μ m.

3.4.3 Synthesis of Cp-Functional Microspheres



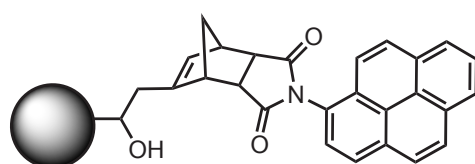
PGMA microspheres (2.00 g) were suspended in 70 mL of dry tetrahydrofuran (THF) in a Schlenk-tube and cooled in an ice-salt bath to -10 °C. A solution of sodium cyclopentadienide (1.00 g, 11.4 mmol) in 15 mL of dry THF was added dropwise to the microspheres. After 1 h the ice-salt-bath was removed and the mixture was slightly stirred for another

*The poly(glycidyl methacrylate) (PGMA) microspheres were synthesized by the Polymer Standards Service (PSS) GmbH, Mainz.

3. Modular Design of Glyco-Microspheres via Mild Pericyclic Reactions

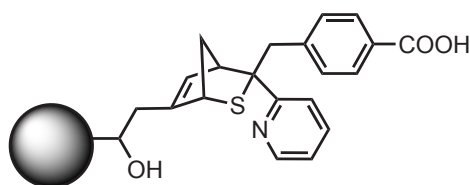
3 h at ambient temperature. The reaction was quenched by pouring the reaction mixture into 150 mL of saturated NH_4Cl -solution. Subsequently, the microspheres were filtered off and washed with 150 mL of acetone, ethanol/water (50:50), 3 %-HCl in water, water, THF and hexane and dried in a vacuum oven at 50°C for 48 h before analysis. The approach above was employed for the 1000 Å microspheres - for the other pore sizes the reaction was scaled down by a factor of 5.

3.4.4 Labeling of Cp-Functionalized Microspheres with *N*-(1-Pyrene)Maleimide



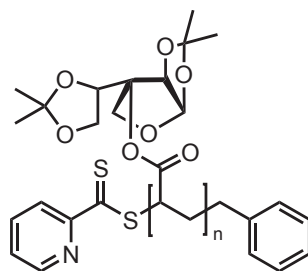
To the Cp-functionalized microspheres (2.0 mg) a solution of *N*-(1-pyrene)maleimide (1.0 mg, $3.4 \cdot 10^{-3}$ mmol) in 1 mL of acetone was added. The reaction was shaken at 40°C for 2.5 h. The microspheres were filtered off and washed four times with 5 mL of acetone.

3.4.5 RAFT-HDA Model-Reaction with a Small Molecule



For each data point to a sample of the Cp-functional microspheres (70 mg) 7.8 mL of a solution of 4-((pyridine-2-carbodithiyl)methyl)benzoic acid (720 mg, 2.49 mmol, 1 equiv) and trifluoroacetic acid (TFA) (1920 μL , 2840 mg, 24.9 mmol, 10 equiv) in a mixture of ethyl acetate (100 mL) and THF (39 mL) was added. The reaction was shaken at 50°C for predetermined time intervals after which the microspheres were filtered off and washed with 5 mL of THF four times. The microspheres were subsequently dried in a vacuum oven at 50°C for 48 h before analysis.

3.4.6 RAFT-Polymerization



A solution of AIBN (12.4 mg, 0.075 mmol, 0.3 equiv), BPDF (62.4 mg, 0.25 mmol, 1 equiv) and the protected glycomonomer (4.00 g, 12.73 mmol, 49 equiv) in toluene ($1 \text{ mol} \cdot \text{L}^{-1}$ according to the glycomonomer) was deoxygenated by three consecutive freeze-pump-thaw cycles. The flask was placed into a preheated oil-bath at $75 \text{ }^\circ\text{C}$ for 4 h. The reaction was stopped by cooling in an ice-bath and exposing the reaction mixture to oxygen. The solvent was removed in vacuo and the residual employed without further purification. $M_n = 4200 \text{ g} \cdot \text{mol}^{-1}$ (GPC in DMAc), $D = 1.2$ (GPC in DMAc), conversion: 25 % (NMR).

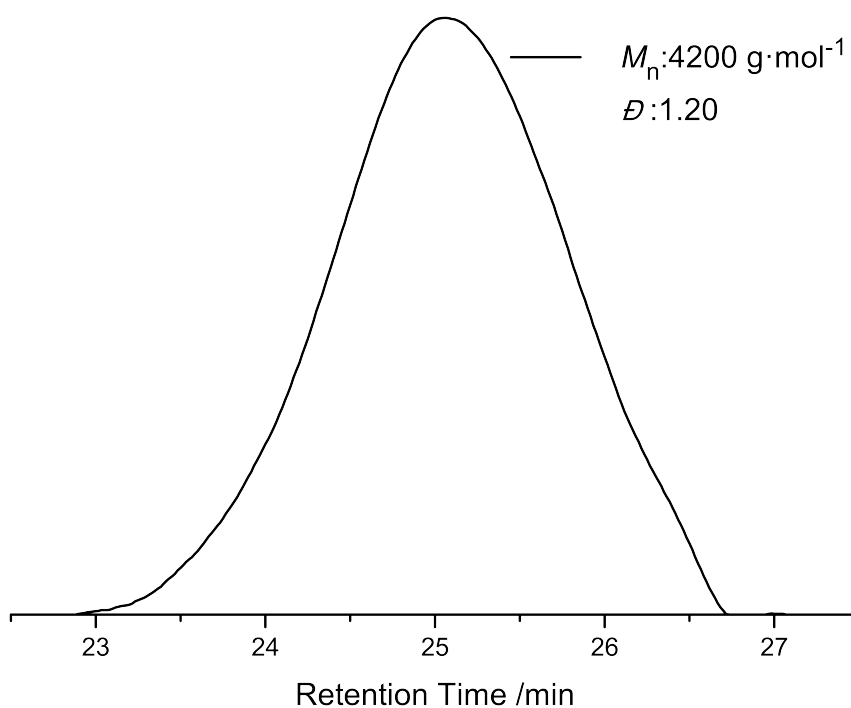


Figure 3.11: GPC trace (PS-Calibration) in DMAc of PAIpGlc polymerized with BPDF.

3. Modular Design of Glyco-Microspheres via Mild Pericyclic Reactions

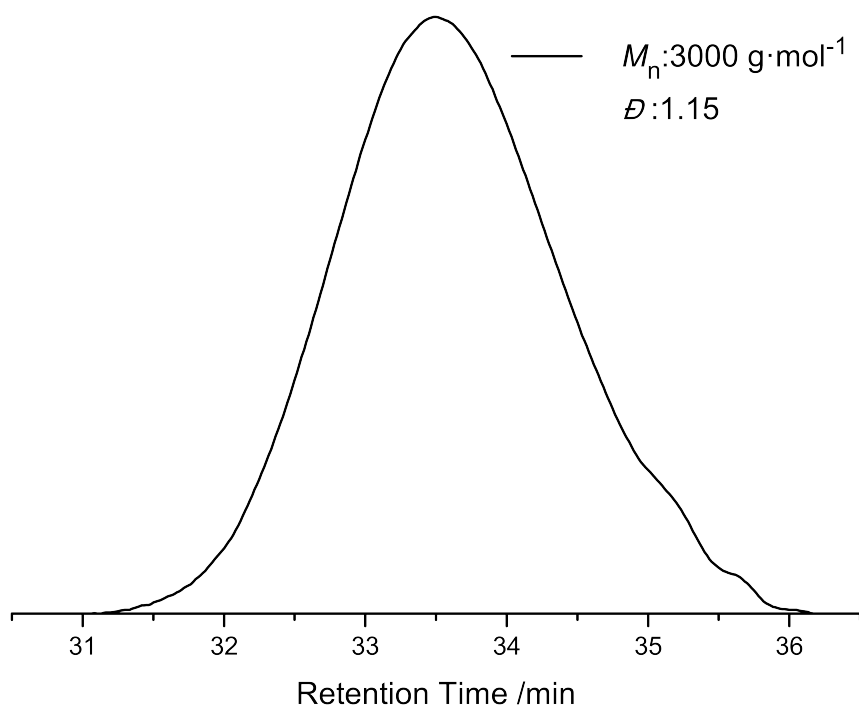


Figure 3.12: GPC trace (PS-Calibration) in THF of PAIpGlc polymerized with BPDF. The inaccuracy of the M_n does not affect the accuracy of the values for the loading capacity or grafting density, as only the sulfur in the chain end is needed for the calculation which is determined separately via elemental analysis. The values for M_n and \bar{D} obtained from the analysis in DMAc are reported throughout this thesis, as the M_n is closer to the theoretical expected value for a controlled RAFT-polymerization at the conversion determined via $^1\text{H-NMR}$ spectroscopy (M_n of approximately $4000 \text{ g} \cdot \text{mol}^{-1}$ for a conversion of 25 %).

Table 3.2: Experimental and theoretical m/z values for the labeled peaks in Figure 3.3 on page 39.

m/z_{exp}	assignment	formula	m/z_{theo}	$\Delta m/z$
1524.67	P_{RZ}	$[\text{C}_{73}\text{H}_{99}\text{NO}_{28}\text{S}_2\text{Na}]^+$	1524.57	0.10
1593.75	P	$[\text{C}_{75}\text{H}_{110}\text{O}_{35}\text{Na}]^+$	1593.67	0.08
1662.75	S_{I}	$[\text{C}_{79}\text{H}_{117}\text{NO}_{35}\text{Na}]^+$	1662.73	0.02
1685.75	S_{R}	$[\text{C}_{82}\text{H}_{118}\text{O}_{35}\text{Na}]^+$	1685.73	0.02
1815.75	P_{IZ}	$[\text{C}_{85}\text{H}_{120}\text{N}_2\text{O}_{35}\text{S}_2\text{Na}]^+$	1815.70	0.05

3. Modular Design of Glyco-Microspheres via Mild Pericyclic Reactions

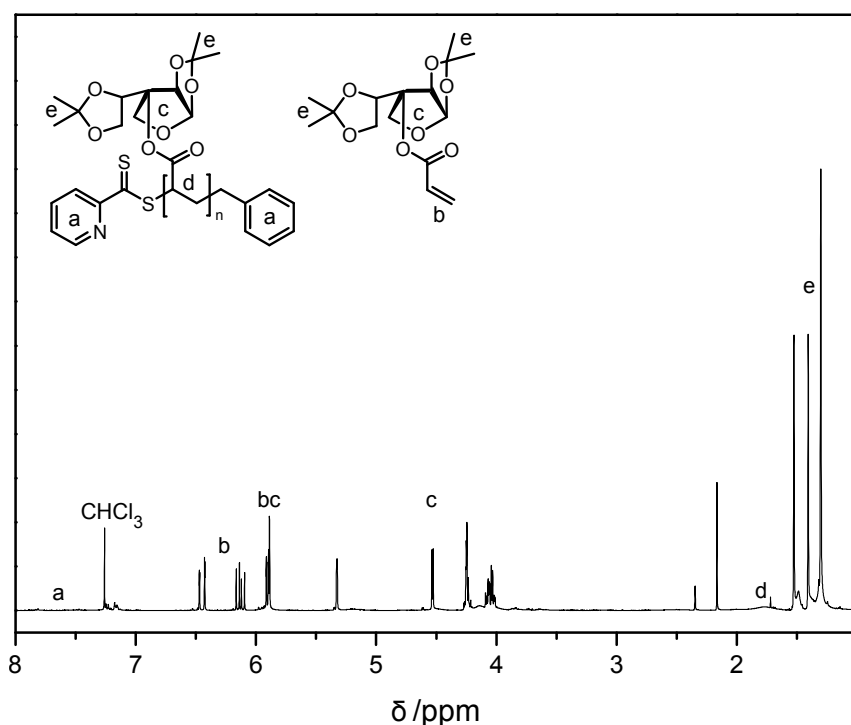
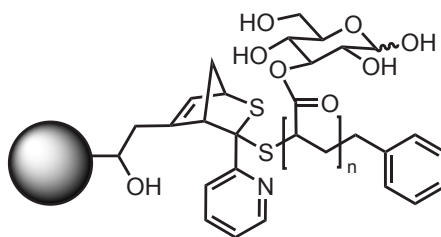


Figure 3.13: ¹H-NMR spectrum of PAIpGlc polymerized with BPDF in CDCl₃ at 400 MHz with unreacted monomer.

3.4.7 RAFT-HDA Reaction with the Glycopolymer on Cp-Functionalized Microspheres and Deprotection



To the Cp-functional microspheres (200 mg) a solution of the polymer monomer mixture from the RAFT-polymerization (2000 mg, corresponds to 31.7 mg, 0.13 mmol, 1 equiv of employed BPDF) in CHCl₃ (15 mL) was added. After the addition of TFA (200 μL, 296 mg, 2.59 mmol, 20 equiv) the reaction mixture was shaken at 50 °C for 5 days. The solvent was subsequently removed in vacuo and 80 % formic acid (80 mL) was added. The mixture was shaken for an additional two days at ambient temperature. The microspheres were then filtered off and washed with water, saturated Na₂CO₃-solution, acetone, water, acetone, and THF – followed by drying in a vacuum oven at 50 °C for 48 h before analysis.

3. Modular Design of Glyco-Microspheres via Mild Pericyclic Reactions

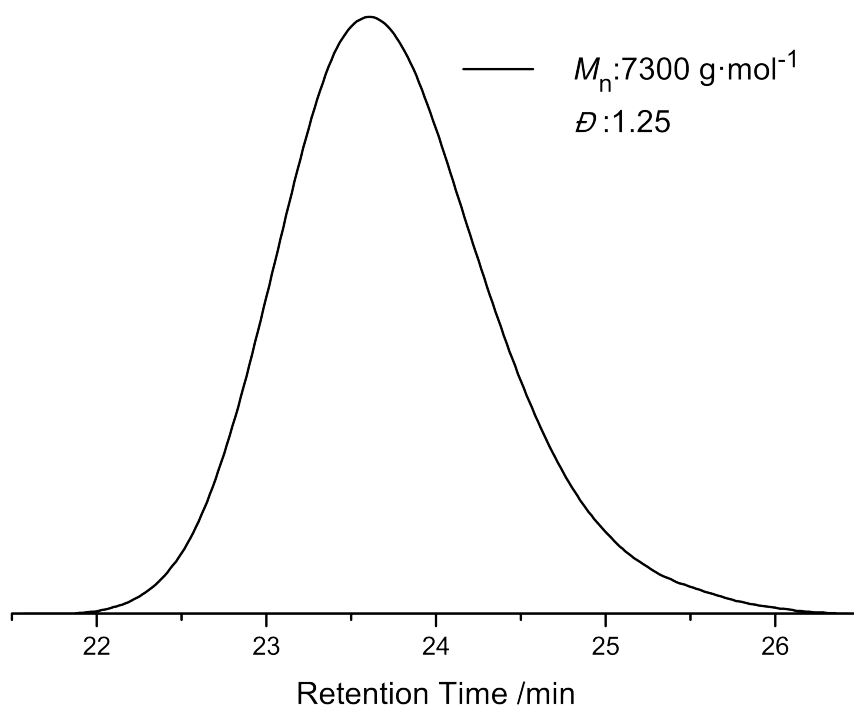


Figure 3.14: GPC trace (PS-Calibration) in DMAc of PAGlc polymerized with BPDF. The polymer was recovered from the grafting reaction by dialyzing the filtrate and the first 50 mL of wash water against distilled water (utilizing a SpectraPor3 membrane (MWCO = 1000 Da)) and subsequent freeze drying.

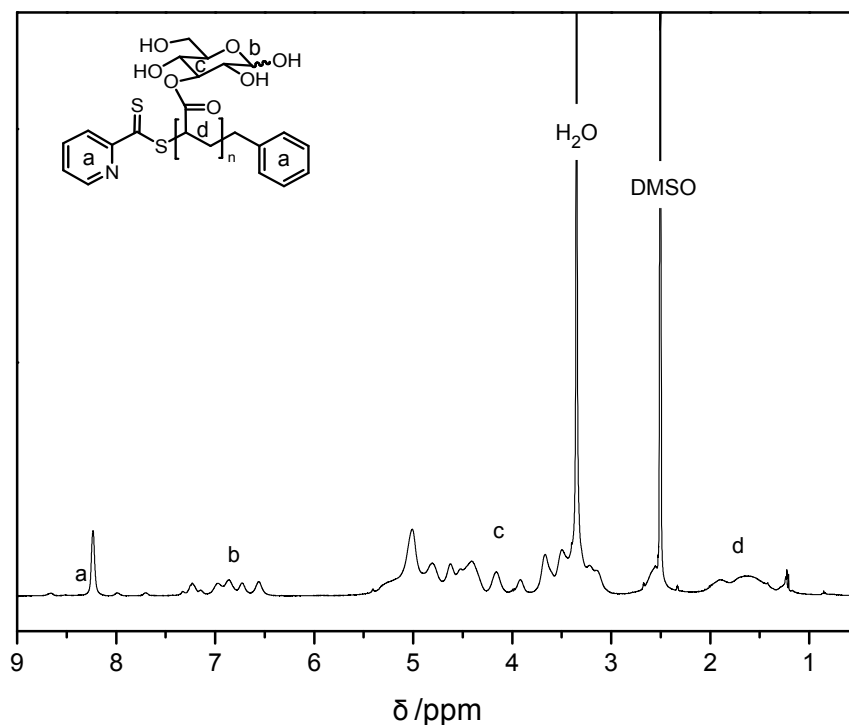


Figure 3.15: ¹H-NMR spectrum of PAIpGlc polymerized with BPDF in DMSO-d₆ at 400 MHz.

4

Photo-Sensitive RAFT-Agents for Advanced Microparticle Design

A novel RAFT-agent was synthesized, which is able to form a highly reactive diene for cycloadditions – a photo-enol – under irradiation with UV-light ($\lambda_{\text{max}} = 320 \text{ nm}$). The RAFT-agent is able to mediate controlled polymerizations for a wide range of monomers. The photoadduct with a suitable dienophile was formed in less than 60 min and was stable under the applied irradiation, as evidenced via ESI-MS. The photo-active RAFT-end group allows for the formation of block copolymers in minutes, which was proven via GPC analysis. The novel photo-sensitive RAFT-agent can additionally be utilized to graft RAFT-polymers onto previously maleimide-functionalized porous polymeric microspheres, which was evidenced qualitatively as well as quantitatively via SEM, XPS, IR-microscopy, and elemental analysis. Grafting densities up to 0.12 molecules per nm^2 were achieved. The light-induced reaction can further be applied to generate Janus-microspheres, exhibiting two different hemispheres with a Pickering emulsion approach, which was visualized via IR-microscopy.

Parts of this chapter were reproduced with permission from M. Kaupp, T. Tischer, A. F. Hirschbiel, A. P. Vogt, U. Geckle, V. Trouillet, T. Hofe, M. H. Stenzel, C. Barner-Kowollik, *Macromolecules* **2013**, *46*, 6858–6872. Copyright 2013 American Chemical Society.

4.1 Introduction

Light-induced grafting reactions (refer to Section 2.4 for details) offer a high degree of control over the ligation process, as light can act as a spatial and temporal trigger. Our group has applied an entire 'tool-box' of light-triggered reactions, of which each has its advantages. In the current chapter a reaction based on the light-induced formation of ortho-quinodimethanes – the so-called photo-enol – is applied, which are highly reactive dienes for Diels-Alder reactions.^[18,179] Photo-enol ligation has been applied to modify various surfaces in a spatially controlled manner, such as silicon wafers,^[180] hyaluronan films and cellulose.^[182] In addition, poly(DOPA) on diverse carrier materials such as graphite, poly(ethylene terephthalate) and gold was patterned with polymers and a peptide.^[181] The photo-enol is so reactive that it can even react with conventional RAFT-polymers^[177] – yet still highly orthogonal^[179] – thus the reaction adheres to click criteria.^[58,59]

Photo-enol-ligation has not been combined with RAFT-polymerization (Section 2.2) or other RDRP-techniques before. The combination of RDRP-techniques with light triggered grafting reactions paves the way to many new opportunities in the modification of surfaces. These surfaces do not require to be flat, as the ones noted above, yet can also be spherical like porous polymeric microspheres (Section 2.1). Many properties of these microparticles can already be introduced during their synthesis (Section 2.1.1), however a major interest lies in the modification of particles with polymers to generate core-shell entities with more or enhanced functionalities (Section 2.1.2).

The current chapter describes the synthesis and application of a novel RAFT-agent exhibiting a photo-active ligation moiety as well as its use in several photo-induced grafting reactions. The RAFT-agent was employed in several controlled polymerizations – including the formation of a glycopolymer (Section 2.3) – and the kinetics and stability of the light-triggered reaction were investigated via several test reactions and the formation of various block copolymers. Importantly, the photo-induced immobilization of RAFT-polymers on porous polymeric microspheres was carried out. The benefit of employing a light-induced grafting reaction was exploited by the generation of Janus-microparticles with the utilization of a Pickering emulsion approach. The general reaction strategy of the current chapter is depicted in Figure 4.1 on the opposite page.

4. Photo-Sensitive RAFT-Agents for Advanced Microparticle Design

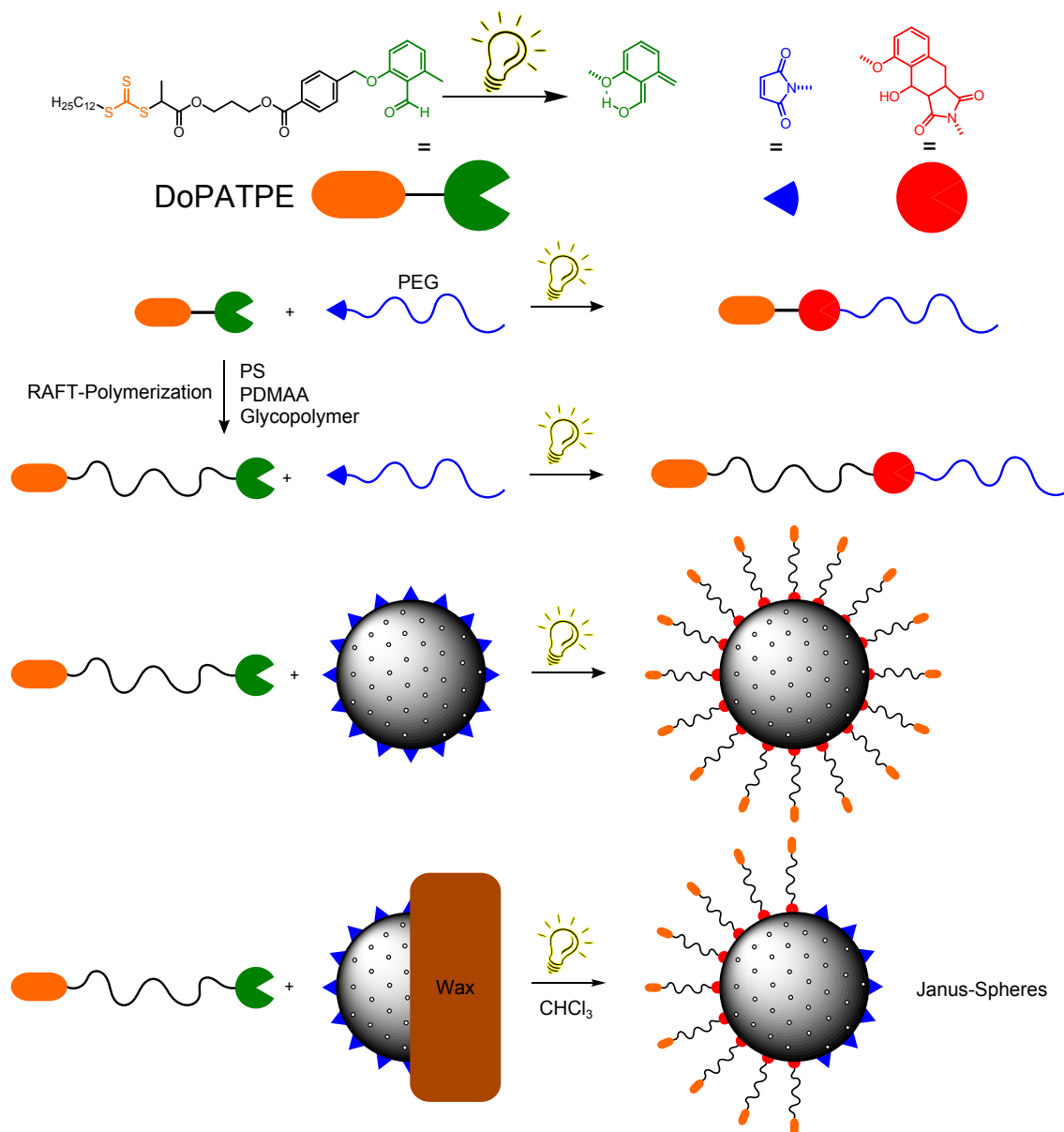


Figure 4.1: Schematic illustration of the synthetic strategy utilizing the RAFT-photo-enol agent based on 2-((dodecylsulfanyl)carbonothioyl)sulfanyl propanoic acid (DoPAT). The versatility and robustness of the applied approach are demonstrated as are the opportunities of employing light-triggered grafting reactions on spherical objects by synthesizing Janus-particles.

4.2 Results and Discussion

4.2.1 Photo-RAFT-Agent Design

The novel molecule combining a photo-enol precursor and a RAFT-moiety is based on a widely used trithiocarbonate (2-((dodecylsulfanyl)carbonothioyl)sulfanyl propanoic acid, DoPAT) and a motif forming a very reactive, well-known ortho-quinodimethane under UV-irradiation, connected by a short spacer preventing any interactions between the two functional groups. The synthesis consists of two facile Steglich-esterifications^[202] (Figure 4.2).

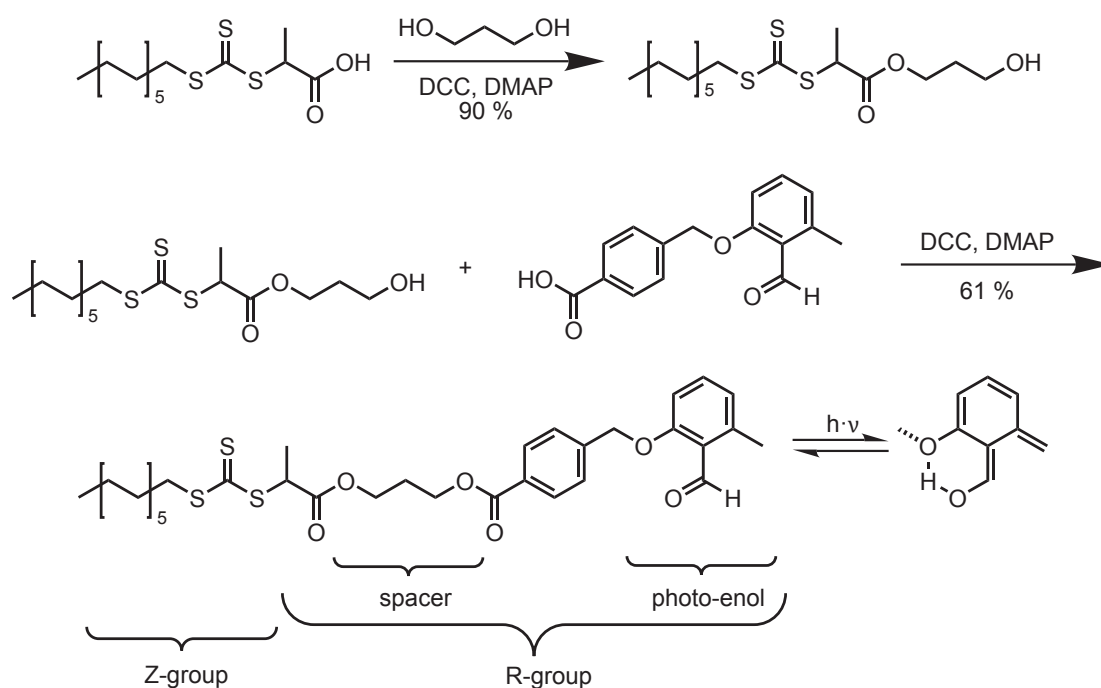


Figure 4.2: Synthesis and structural information of the photo-enol RAFT-agent DoPATPE.

All basic RAFT-agent groups (dithioesters, xanthates, and dithiocarbamates) could have been utilized in principle, yet trithiocarbonates do not undergo a cycloaddition with the highly reactive diene formed by the ortho-quinodimethane under UV-irradiation^[177] and have proven to be stable under the here applied reaction conditions (close to 320 nm irradiation).^[203,204] Nevertheless, the photo-active group was attached to the so called R-group of the RAFT-agent, implying that even if the trithiocarbonate degrades during the photo-triggered reaction, the polymeric chain does not lose the connection to the photo-enol group. Furthermore, attaching the photo-enol moiety to the above mentioned classes of RAFT-agents could be employed in the future for the combination with the RAFT

hetero-Diels-Alder approach^[16] or for the formation of cyclic polymers, based on a reaction between the α - and ω -end of RAFT-polymers.^[177]

4.2.2 Model Reaction and Stability Assay

To evaluate if the reactivity of the photo-enol and/or stability of the product are influenced by the trithiocarbonate, a range of test reactions was carried out. Irradiation of dissolved DoPATPE for 30 min does not lead to degradation as no change in in the mass spectrum nor the NMR spectrum is observable (Figure 4.3 for the a comparison of the NMR spectra of DoPATPE before and after irradiation).

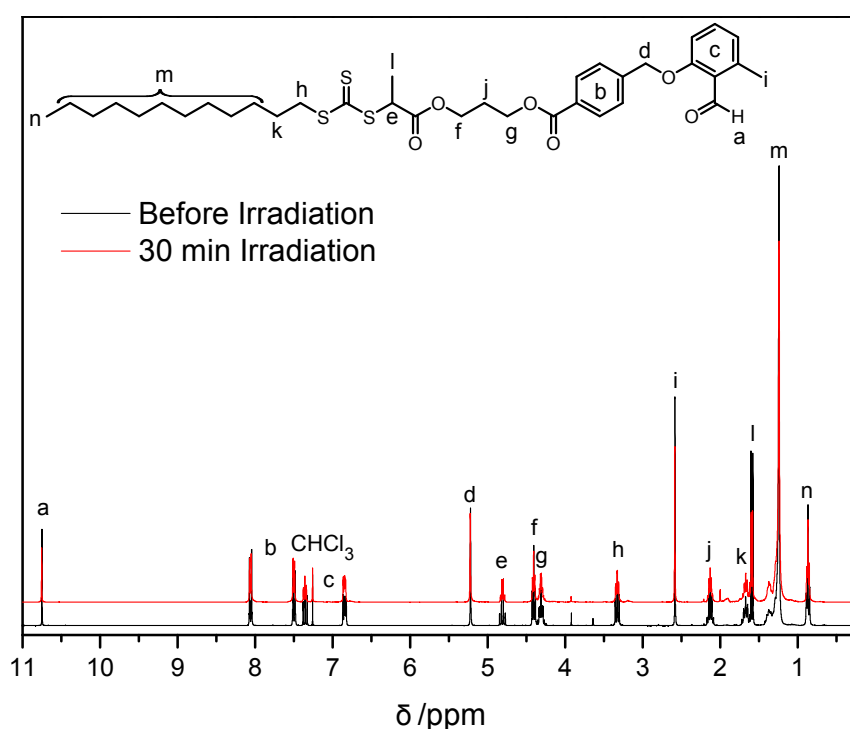


Figure 4.3: Comparison of ^1H -NMR spectra of DoPATPE before and after irradiation for 30 min, measured in CDCl_3 at 400 MHz. No change is observable.

For an initial reactivity test a suitable counterpart was needed. A poly(ethylene glycol) functionalized with maleimide (PEG-Mal) with a molecular weight of around $1300 \text{ g} \cdot \text{mol}^{-1}$ was chosen, as it has shown before to be a reactive dienophile in various Diels-Alder reactions.^[179] In addition, choosing PEG-Mal of $1300 \text{ g} \cdot \text{mol}^{-1}$ readily allows for analysis of the starting material, the product, and potential side products via ESI-MS (Figure 4.4 on the next page).

For a kinetic study of the photo-addition, a solution of PEG-Mal and DoPATPE in acetonitrile was deoxygenated and separated into five vials, which were irradiated for 10, 20, 30, 40, and 60 min, respectively. To determine the conversion, the samples were analyzed

4. Photo-Sensitive RAFT-Agents for Advanced Microparticle Design

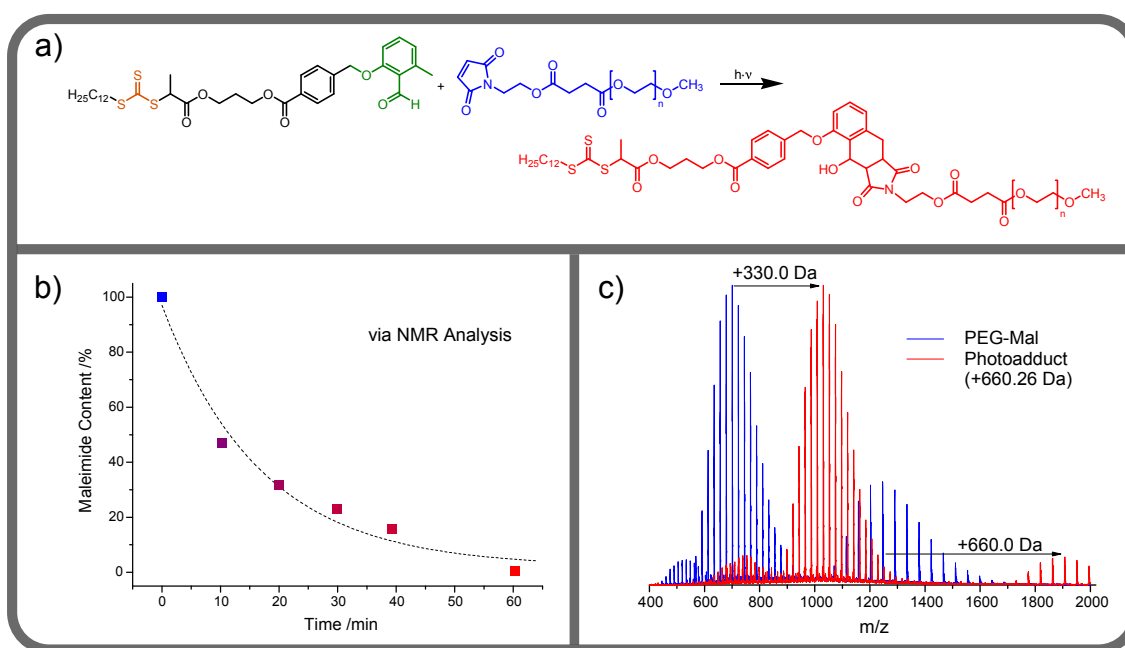


Figure 4.4: Model reaction between DoPATPE and a maleimide-functionalized poly(ethylene glycol) (PEG-Mal): a) Chemical reaction scheme; b) Kinetic investigation; Comparison of the NMR integrals of the maleimide double bond (6.72 ppm) and the methyl ether (3.36 ppm); after 60 min no maleimide can be observed. The dashed line is an exponential decay fit, but should be considered as a guide to the eye only; c) ESI-MS comparison of the starting material (PEG-Mal) and the photo-adduct after 60 min. The shift of the peaks matches the mass of DoPATPE (660 Da for single charged peaks, 330 Da for double charged peaks). No other species are observed, underlining full conversion and stability of the photo-adduct. For peak assignments and more detailed mass spectra refer to the Appendix (Figure A.2-A.4 and Table A.2).

via NMR spectroscopy and the integrals of the methyl ether resonances (at 3.36 ppm) were compared to the integrals of the maleimide double bond resonances (at 6.72 ppm) (Figure 4.4 b). After already 10 min, 53 % conversion is achieved and after 60 min there is no more maleimide resonance observable in the NMR-spectrum (Figure A.6 on page 165 in the Appendix). The dashed line in 4.4 b is an exponential decay fit, yet should be considered as a guide to the eye only. Results discussed later indicate that irradiation times of 30 min or even less are sufficient to achieve full conversion for reactions employing end-functionalized polymers and lower concentrations. Additionally to analysis via NMR, the reaction was analyzed via ESI-MS (Figure 4.4 c and Figure A.2-A.4 in the Appendix). No left-over starting material can be found in the spectrum after 60 min. An unambiguous shift of the main peak by 660 Da for single charged ions and 330 Da for double charged ions, respectively, further underpins the addition of DoPATPE (exact mass: 660.26 Da). Some smaller signals in the spectra are associated with triple charged ions. No other species can be observed, proving again the stability of the product. In addition, the in-

crease in mass (and therefore hydrodynamic volume) can be observed via GPC analysis (Figure A.8 on page 166). Once more, no unreacted PEG-Mal can be observed via GPC, and the signal associated with the product block is clearly shifted to a higher retention time with no tailing or shoulders which would indicate side reactions.

4.2.3 RAFT-Polymerizations

The novel photo-reactive RAFT-agent was tested in polymerizations of dimethylacrylamide, styrene, and a protected glycomonomer (AcManEA) demonstrating its versatility in mediating a wide range of polymerizations. The polymerization reactions were conducted in solution, as well as in bulk, in the case of styrene. The resulting polymers were analyzed via GPC, NMR and ESI-MS. The GPC traces show narrow dispersities, all well below 1.2 (Figure 4.27, 4.30, 4.33, and 4.34 in the Experimental Section 4.4.5). Only in the case of PDMAA, at higher retention times a small shoulder can be found, probably because of transfer to polymer reactions. In the $^1\text{H-NMR}$ spectra all resonances associated with the RAFT-end groups and the photo-enol can be observed (provided that they are not covered by signals from the polymeric chain) (Figure 4.28, 4.31, and 4.35 in the Experimental Section), which allows to determine the (number averaged) molecular weight of the polymer. The molecular weights determined via NMR and GPC are in excellent agreement for the PS sample, as they both yield in $3900 \text{ g} \cdot \text{mol}^{-1}$. In the case of PDMAA, the results are similar, yet they differ substantially for PAcManEA (refer to Section 4.4.5). The discrepancy can be explained in both of these cases, as for the given analytical conditions no MHKS parameters are available, requiring the results to be interpreted as PS samples. Furthermore, in the case of PAcManEA, it is difficult to integrate the signals in the NMR spectrum, as the side group signals are very broad and the ^1H resonances of the end groups overlap with several resonances of the lateral chain. A thorough analysis of the PDMAA and PS samples via ESI-MS reveals that there exists only one species of polymeric chains in the spectrum, namely chains with the end groups stemming from the fragments of the RAFT-agent (labeled P_{RZ} in Figure 4.29 and 4.32 in the Experimental Section). No signals from chains initiated by the radical initiator or occurring from termination events can be identified. As there is a potential bias of the ionization efficiency with molecular weight, no information regarding the length of the polymer can or should be obtained from these measurements. The relatively high chain length of the PAcManEA ($M_n = 10100 \text{ g} \cdot \text{mol}^{-1}$) did not allow for an ESI-MS analysis, yet the narrow polydispersity as well as the NMR analysis indicate a high end group fidelity. In addition, the results from the block copolymer formation (see below) indicate that the molecular weights derived via DMAc GPC are accurate as for a successful conjugation reaction the

stoichiometry has to be precise.

All of the analytical results of the polymers demonstrate that the novel RAFT-agent is capable of controlling a polymerization featuring living characteristics without disturbance by or degradation of the photo-enol group.

4.2.4 Block Copolymer Formation

To verify the reactivity of the ortho-quinodimethane group – when installed at a polymer chain end via the RAFT-process – it was investigated if these RAFT-polymers were able to undergo photo-triggered block copolymer formation with a suitable counterpart. Similar to the model reaction described above, a poly(ethylene glycol) functionalized with maleimide (PEG-Mal) was employed. The synthesis of this PEG-Mal is identical to the one noted above, with the exception that the starting material featured double the molecular weight ($2000 \text{ g} \cdot \text{mol}^{-1}$, yielding a molecular mass of $2300 \text{ g} \cdot \text{mol}^{-1}$ after the functionalization) to achieve a larger shift in the GPC-trace for a successful block copolymer formation. The reaction itself is straight-forward: a 1:1 mixture of the PEG-Mal and the photo-enol end-capped RAFT-polymer in a suitable solvent is freed from oxygen and aliquoted into several Pyrex glass vials. The vials are subsequently irradiated for a predetermined time interval and (after removal of the solvent) analyzed via GPC. A successful reaction is indicated by a shift of the signal to lower retention times (implying a higher hydrodynamic volume due to the higher molecular weight) and a disappearance of traces associated with the starting material. ^[205,206]

For the PAcManEA the exact molecular weight was difficult to determine. So several weigh-ins had to be conducted, and analysis after the reaction indicated which reaction partner was added in excess. Finally, an equimolar ratio was achieved and the results of the successful reaction are shown in Figure 4.5 on the opposite page.

After the reaction the signal is clearly shifted to lower retention times revealing a successful block copolymer formation. A small shoulder in the GPC trace at higher retention times is noticeable, indicating left over PEG-Mal. The left over material is not caused by a non-equimolar reactant ratio, as several reactions were conducted and for the reactions with less PEG-Mal, no improved result was achieved. A kinetic investigation of the block copolymer formation (Figure 4.5c) shows that the main reaction is completed after close to 3 min and no change can be observed in the GPC trace after 20 min.

The results of the photo-induced block copolymer formation between PDMAA and PEG-Mal are shown in Figure 4.6 on page 66 and are very similar to the results achieved with PAcManEA. In the GPC diagram the peak is clearly shifted to lower retention times, indicating a successful block copolymer formation. A small shoulder at higher retention

4. Photo-Sensitive RAFT-Agents for Advanced Microparticle Design

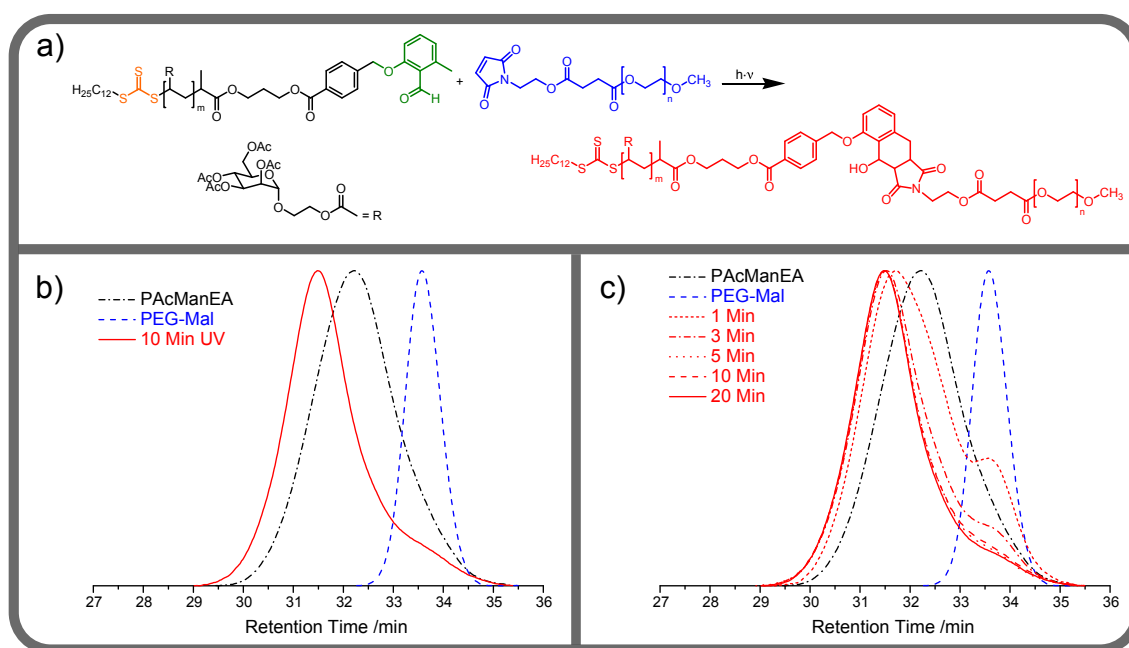


Figure 4.5: Light-triggered block copolymer formation between PAcManEA and PEG-Mal; a) Chemical reaction scheme; b) Comparison of the GPC traces in THF of the starting materials and the block copolymer formed after 10 min irradiation; a clear shift to higher retention times underpins the successful photo-induced formation of the PAcManEA-*b*-PEG block copolymer; c) Kinetic investigation: The main reaction is completed after 5 min, no change can be observed after 20 min.

times is noticeable, indicating remaining PDMAA. Again, remaining PDMAA is observed not because the 1:1 ratio was not met, as several reactions were conducted and for the reaction with less PDMAA a significant signal of left over PEG-Mal was observed. A kinetic investigation of the reaction (Figure 4.6c) indicates that the main grafting reaction is finished after close to 30 min and no change can be observed in the GPC trace after 40 min. The shoulder at higher retention times might be explained with a side reaction pathway, which consumes the photo-enol group without leading to a block copolymer, although no such side reaction was observed in the model reaction, stability study or the block copolymer formation employing PAcManEA.

To underpin that the achieved shift in the GPC trace is due to the formation of a block copolymer, a control reaction was conducted. PAcManEA was exposed to the identical reaction conditions as for a block formation, except for the addition of the PEG-Mal. The results can be found in Figure 4.7 on the following page.

4. Photo-Sensitive RAFT-Agents for Advanced Microparticle Design

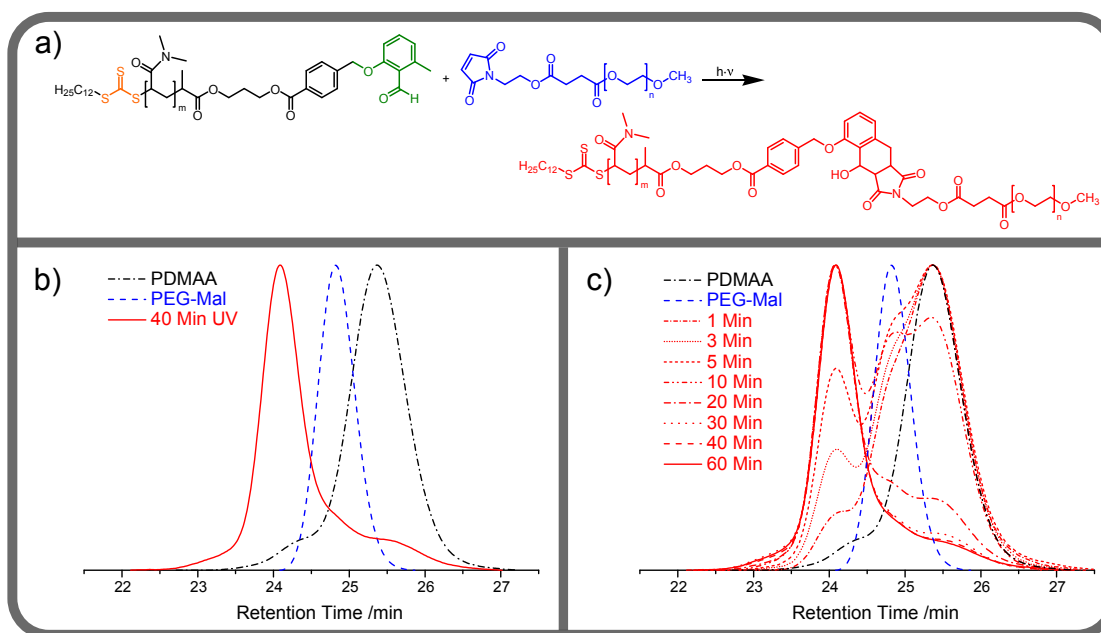


Figure 4.6: Light-triggered block copolymer formation between PDMAA and PEG-Mal; a) Chemical reaction scheme; b) Comparison of the GPC traces in DMAc of the starting materials and the block copolymer formed after 40 min irradiation; a clear shift to higher retention times underpins the successful formation of the PDMAA-*b*-PEG block copolymer; c) Kinetic investigation: The main reaction is completed after 30 min, no change can be observed after 40 min.

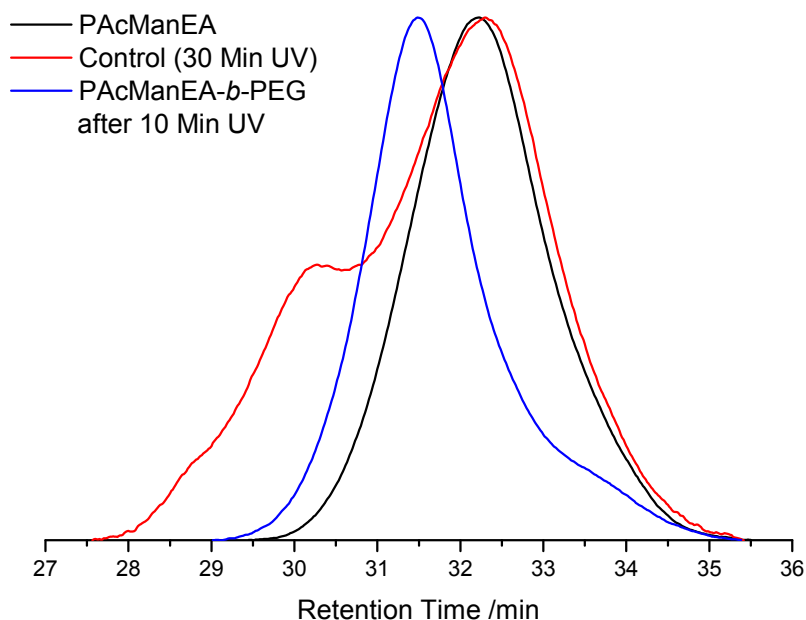


Figure 4.7: Comparison of the GPC traces in THF of pure PAcManEA, the block copolymer of PAcManEA and PEG formed after 10 min of UV-irradiation and the control reaction (pure PAcManEA irradiated for 30 min). The shoulder at lower retention times in the signal of the control reaction approximately corresponds to double the molecular weight of the main peak.

4. Photo-Sensitive RAFT-Agents for Advanced Microparticle Design

For the control reaction, a shoulder can be observed at lower retention times, which does not match the signal of the PAcManEA-*b*-PEG block copolymer. Instead it approximately matches the result one would expect for a block consisting of two PAcManEA chains, indicating that a very reactive species is formed during the irradiation which can react with other polymer chains. The reactive species is most likely the photo-enol, yet the analytical results cannot rule out if a sulfur carbon bond is cleaved to form radicals. In the presence of PEG-Mal, no such side reaction is observed, as it provides an alternate and rapid reaction pathway for the reactive intermediate. As a consequence, no GPC traces matching PAcManEA-*b*-PAcManEA or PAcManEA-*b*-PEG-*b*-PAcManEA can be found in the results of the block copolymer formation reactions.

4.2.5 Grafting onto Microspheres

The photo-enol process has been utilized to graft biomolecules and polymers onto planar surfaces with spatial control.^[180] The employed surfaces were flat silicon wafers, prefunctionalized with the photo-enol group and the dienophile (maleimide) was attached to the grafted molecules. In the present work the grafting macromolecules are carrying the photo-enol groups, so – in contrast to the previously reported study – the substrate has to carry a dienophile on the surface. To evidence the versatility of the photo-enol approach, the substrates employed in the current study were porous polymeric microspheres, based on poly(glycidyl methacrylate) (PGMA), which are more interesting but also more challenging to analyze. The epoxide groups of the PGMA can be used directly to graft macromolecules onto the surface of microspheres^[75,78] or can be functionalized in many ways,^[74] e.g., also with dienes that can undergo (hetero) Diels-Alder reactions (Chapter 3). There exists a multitude of different and interesting macromolecules, such as glycopolymers,^[53] which have been grafted onto microspheres with various techniques,^[10] yet to the best of the candidates' knowledge no example of a light-triggered process with the ability to allow spatial resolution.

Microsphere Pre-Functionalization

The functionalization of the PGMA spheres with a dienophile maleimide moiety is straightforward. The epoxide moieties of the microspheres undergo a nucleophilic attack by a hydroxyl group attached to a furan protected maleimide under Lewis acid ($\text{BF}_3 \cdot \text{OEt}_2$) catalysis in a heated shaker at slightly elevated temperatures (60 °C). Subsequently, the maleimide is deprotected via heating to 90 °C, which induces a retro Diels-Alder reaction, thus removing the furan, in one pot and without intermediate purification (Figure 4.8 on the next page).

4. Photo-Sensitive RAFT-Agents for Advanced Microparticle Design

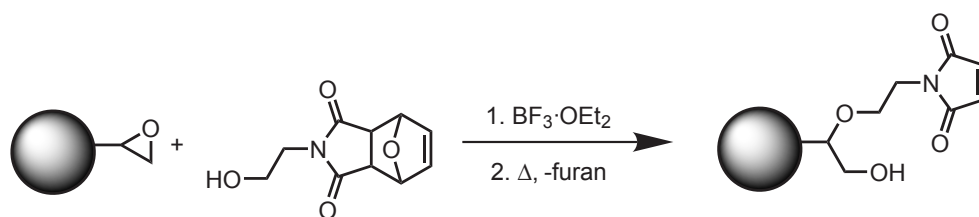


Figure 4.8: Maleimide-functionalization of PGMA microspheres.

The functionalized particles were analyzed – after washing and drying – via X-ray photoelectron spectroscopy (XPS), scanning electron microscopy (SEM), and elemental analysis (EA), showing their successful decoration with maleimide species. The SEM pictures evidence that the surface morphology of the spheres is maintained and the spherical shape of the particles is not altered (Figure A.12 - A.14 in the Appendix). It is always important to check the morphology of the spheres as sometimes their structural integrity can even be affected by stirring with a magnetic stirring bar.^[75] EA as well as XPS illustrate that compared to the initial PGMA spheres, a distinct increase in nitrogen content is detected, demonstrating the successful functionalization. XPS shows only noise in the typical region for nitrogen signals for the untreated particles and a weak but distinct peak for the maleimide-functionalized microspheres (Figure 4.12 on page 73). For the untreated PGMA particles the elemental analysis shows a nitrogen content of 0.19 wt%, which probably stems from the stabilizer or radical initiator employed during the synthesis of the particles. After the maleimide-functionalization, the nitrogen content increases to 0.97 wt% (refer to Table 4.1 on the opposite page for the complete EA results). The increase in the nitrogen content can be correlated to a reaction of approximately one out of five epoxide groups. At first glance, functionalization of close to 20 % might seem low, but many of the epoxide groups are difficult to access as they are buried inside the porous microsphere structure.

4. Photo-Sensitive RAFT-Agents for Advanced Microparticle Design

Table 4.1: Collected data from the elemental analysis of all samples described in Chapter 4.

Sample	N [wt%] ¹	C [wt%]	H [wt%]	S [wt%] ²	O [wt%] ³	mass balance [wt%]
PGMA	0.19	55.77	6.88	0.00	32.84	95.69
±	0.012	0.260	0.035	0.000	0.259	
Mal	0.97	57.96	8.31	0.00	32.65	99.89
±	0.017	2.917	0.800	0.000	0.943	
DoPATPE	1.05	57.30	7.94	0.40	33.40	100.09
±	0.001	0.148	0.452	0.029	0.109	
Control	0.57	57.86	7.44	0.00	34.46	100.33
±	0.045	0.528	0.213	0.000	0.166	
PS	1.14	59.49	6.77	0.29	32.17	99.86
±	0.010	1.080	0.242	0.003	0.237	
PAcManEA	1.08	55.12	6.66	0.00	34.63	97.49
±	0.046	0.808	0.061	0.000	0.242	
PDMAA	1.39	54.89	6.79	0.31	35.26	98.64
±	0.079	0.142	0.178	0.002	0.658	

¹ The nitrogen found in the untreated microspheres and the control sample can be explained by fragments from the nitrogen containing initiator, stabilizer or gaseous nitrogen trapped in the porous surface morphology of the microspheres.

² Content measured independently, employing a water-trap.

³ Content measured independently.

Light-Induced Modification of Microparticles – Pre-Test

To evidence the light-triggered modification of the microspheres – based on the photo-enol group reacting with the maleimide moieties – a simple grafting reaction and a control reaction were conducted. The maleimide-functionalized spheres as well as the untreated PGMA particles were mixed with the photo-active RAFT-agent DoPATPE in dichloromethane (DCM). DCM was chosen because of its density. As the densities of the microspheres and DCM approximately match, the spheres are evenly distributed within the solution and do not sink to the bottom or float on top (refer to Figure A.5 in the Appendix). Subsequently, the suspensions were deoxygenated and irradiated for 30 min. Analysis via XPS reveals that only for the spheres previously functionalized with maleimide sulfur can be detected after the reaction (Figure 4.9).

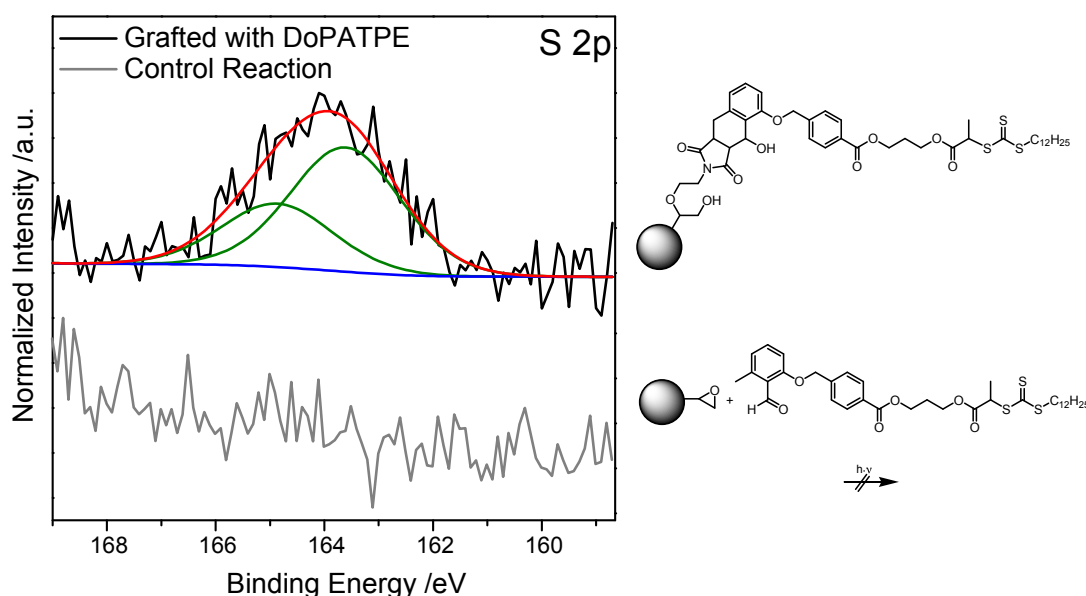


Figure 4.9: S 2p XP spectra of maleimide-functional microspheres grafted with DoPATPE (top) and the control reaction between PGMA microspheres and DoPATPE (bottom). The presence of sulfur after the successful grafting reaction can only be observed for the maleimide-functionalized spheres.

The results of EA lead to the same conclusion as the ones based on XPS. No sulfur can be found for the control reaction on non-functionalized spheres, underpinning the fact that the light-induced Diels-Alder reaction between the photo-enol and the maleimide moieties on the particles leads to the attachment of the DoPATPE. After the photo-reaction between maleimide-functionalized microspheres and DoPATPE, the sulfur content increases to 0.40 wt%, implying that 1 g of microspheres contains 4.0 mg of sulfur. The sulfur content can be converted to a loading capacity via Equation 3.1 on page 42, which is repeated here for clarity:

4. Photo-Sensitive RAFT-Agents for Advanced Microparticle Design

$$LC = \frac{W(S)}{n(S) \cdot M(S)} \quad (4.1)$$

where LC is the loading capacity (in $\text{mol} \cdot \text{g}^{-1}$), $W(S)$ is the weight of sulfur per 1 g of microspheres obtained via elemental analysis, $n(S)$ is the number of sulfur atoms per grafted molecule (here 3) and $M(S)$ is the molecular weight of sulfur. A loading capacity of $41.6 \mu\text{mol} \cdot \text{g}^{-1}$ is reached. Since the relative surface area was measured via inverse size exclusion chromatography to be close to $225.4 \text{ m}^2 \cdot \text{cm}^{-3}$ and the density of the spheres is known as well ($1.39 \text{ g} \cdot \text{cm}^{-3}$) the surface area of the spheres is $1.62 \cdot 10^{20} \text{ nm}^2 \cdot \text{g}^{-1}$ (refer to Section 3.2.4). With a known surface area the grafting density can be calculated via Equation 3.2 on page 48, which is also repeated here for clarity:

$$GD = \frac{W(S) \cdot N_A}{n(S) \cdot M(S) \cdot A} \quad (4.2)$$

where GD is the grafting density in chains per unit area; $W(S)$ is the weight of sulfur in 1 g of microspheres obtained via elemental analysis, N_A is the Avogadro's number, $n(S)$ is the number of sulfur atoms per polymer chain, $M(S)$ is the molecular weight of sulfur and A is the surface area of the microspheres. A grafting density of more than $0.15 \text{ chains} \cdot \text{nm}^{-2}$ is reached. The photo-induced reaction leads to a loading capacity in the same order of magnitude as achieved on porous PGMA microspheres via the heat-triggered RAFT-HDA reaction (RAFT-HDA; refer to Section 3.2.4).

Light-Induced Grafting of RAFT-Polymers onto Microparticles

The light-induced grafting of RAFT-polymers onto microspheres proceeds analogous to the test reaction. The polymers and the particles were mixed in DCM (in which the microspheres float, see above and Figure A.5), deoxygenated and irradiated for 30 minutes. In addition to the analysis via XPS, SEM, and EA, high resolution ATR FT-IR-microscopy can be used in the case of grafted-on PDMAA, as the amide features an additional band in the IR-spectra.

SEM analysis evidences that the surface morphology as well as the spherical shape of the particles is maintained (Figure A.15 - A.23 in the Appendix).

Analysis via XPS yields a whole range of information. For grafted PS, as well as PDMAA, sulfur stemming from the RAFT-end group can be detected. For grafted PAcManEA, sulfur cannot be detected (Figure 4.11 on the next page), indicating that a

4. Photo-Sensitive RAFT-Agents for Advanced Microparticle Design

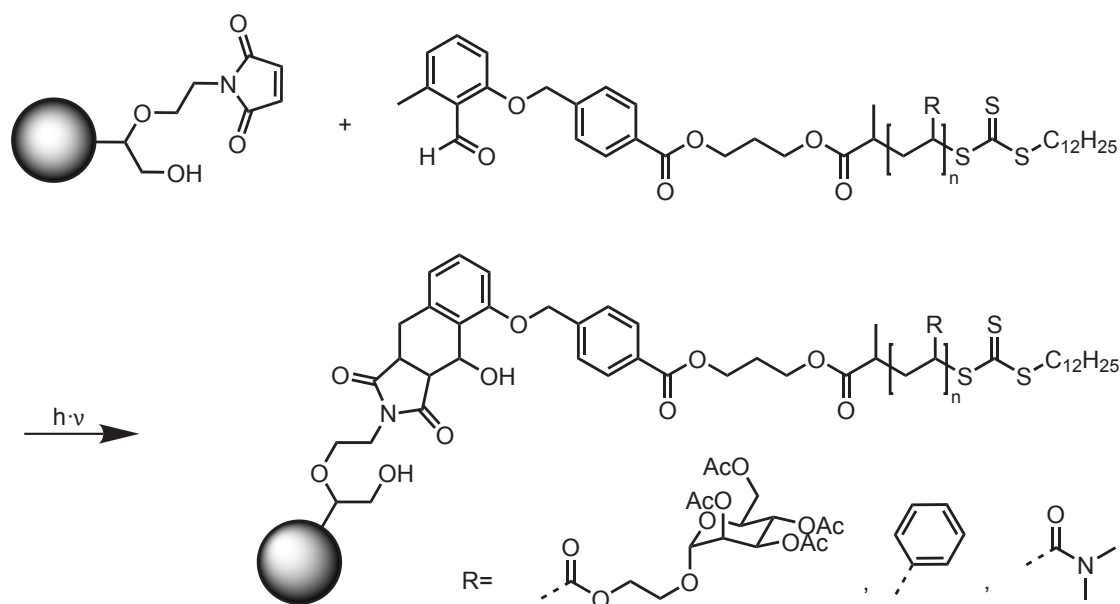


Figure 4.10: Light-induced grafting reactions of RAFT-polymers onto maleimide functionalized microspheres.

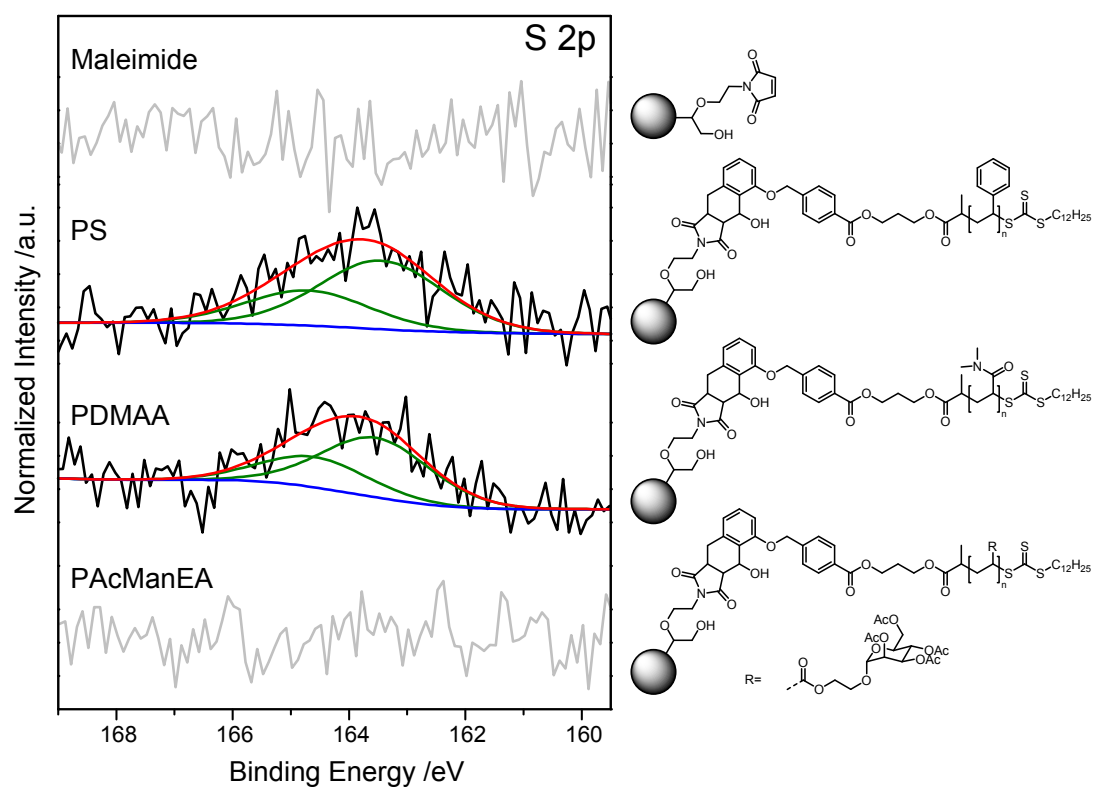


Figure 4.11: S 2p XPS spectra of maleimide-functional microspheres (top) and spheres grafted with PS (2nd row), PDMAA (3rd row), and PAcManEA (bottom). The small, yet distinct sulfur peaks for PS and PDMAA grafted spheres evidence a successful grafting.

4. Photo-Sensitive RAFT-Agents for Advanced Microparticle Design

lower grafting density was achieved, probably due to the longer chain length and therefore more steric hindrance, thus decreasing the sulfur content below the detection limit. In the case of grafted PDMAA, also the nitrogen signal is much stronger (Figure 4.12). Nitrogen is contained in the repetition unit of PDMAA, therefore the nitrogen content increases more significantly than the sulfur content. Integration of the entire spectrum yields 2.7 at% nitrogen for the spheres grafted with PDMAA and merely 0.7 at% nitrogen for the maleimide-functionalized spheres. Unfortunately, numbers derived from XPS are not suitable for the calculation of grafting densities, as XPS only analyzes the surface of the samples and it is often insufficiently accurate especially for minor components.

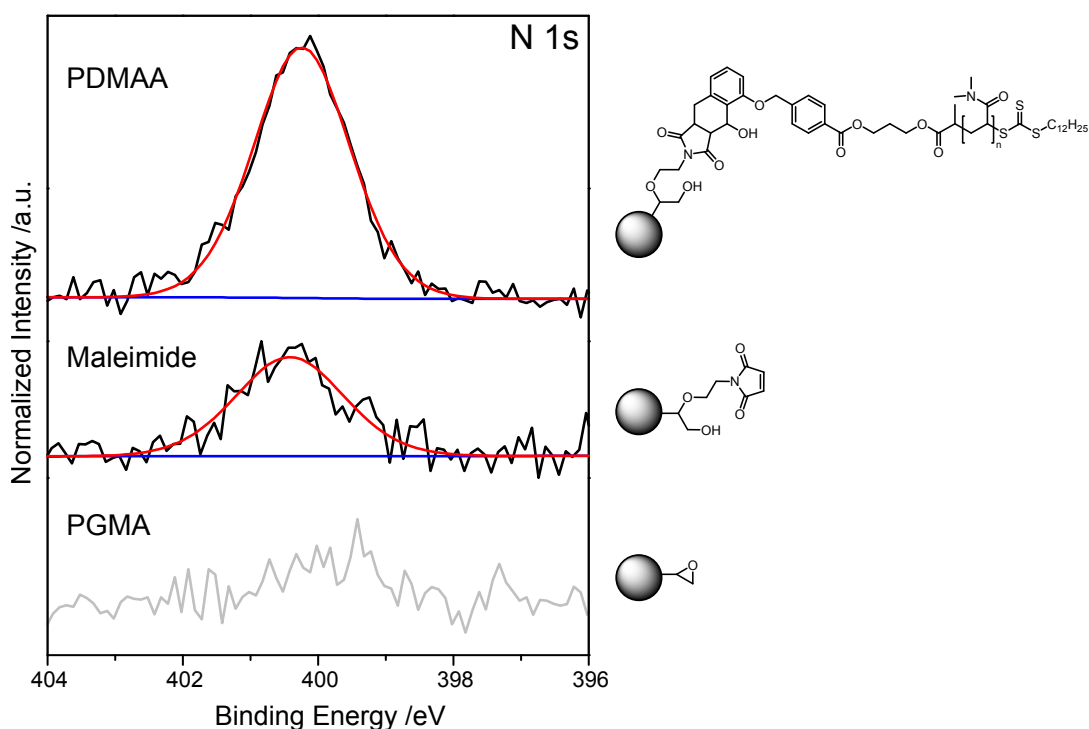


Figure 4.12: N 1s XP spectra of untreated PGMA microspheres (bottom), maleimide-functionalized spheres (middle), and spheres photo-grafted with PDMAA (top). As expected, no nitrogen peak can be observed for the untreated spheres. After the functionalization with maleimide, a small yet distinct nitrogen peak is observable. After the grafting of PDMAA, the signal intensity increases significantly. The increase of nitrogen content evidences the successful molecular functionalization as well as successful macromolecular grafting.

4. Photo-Sensitive RAFT-Agents for Advanced Microparticle Design

In addition, the C 1s peak in the XP spectra can be deconvoluted into several components associated with chemically different carbon species (Figure 4.13): one at 285.0 eV (C–C, C–H), a second one at 286.5 eV (C–O, C–N), and a third one at 288.9 eV (O–C=O, N–C=O).^[24]

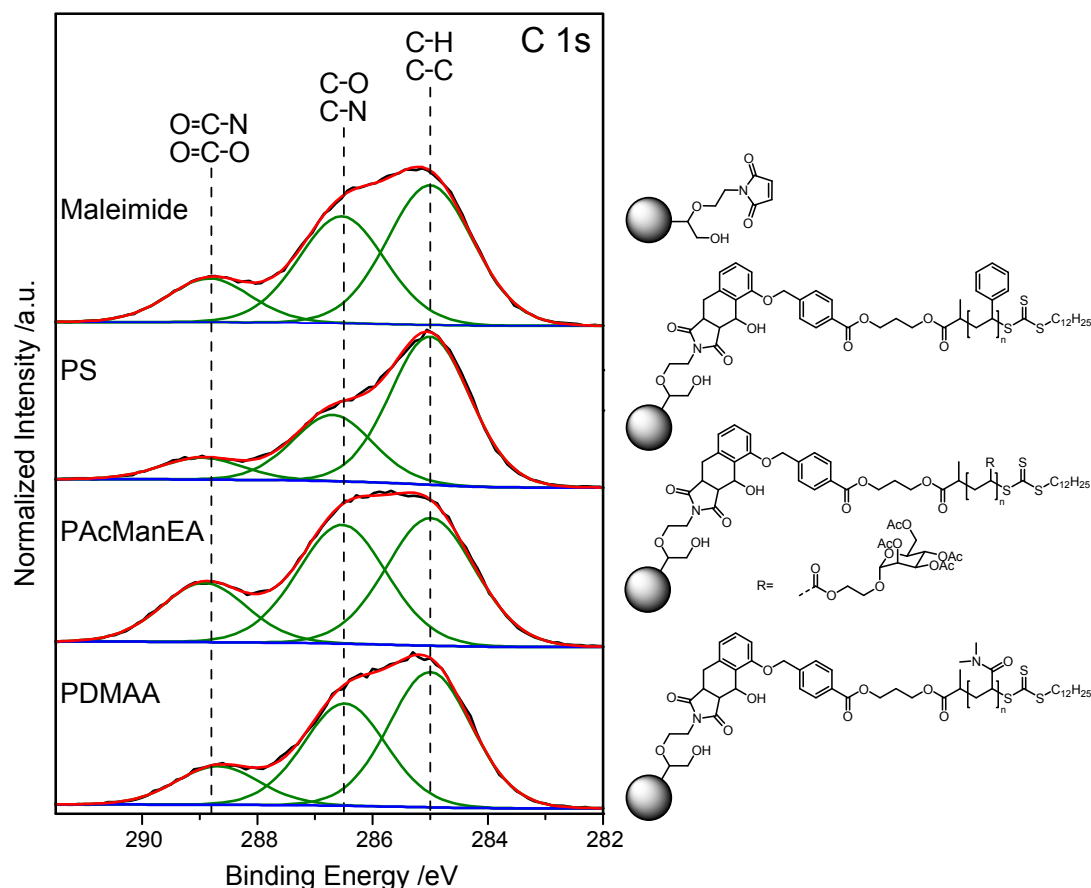


Figure 4.13: C 1s XP spectra of maleimide-functionalized microspheres (top) and spheres photo-grafted with PS (2nd row), PAcManEA (3rd row), and PDMAA (bottom).

The ratios of the intensities of the carbon peaks at 285.0 eV (C–C, C–H) and 286.5 eV (C–O, C–N) is depicted in Figure 4.14 on the opposite page together with additional results from EA which will be discussed in detail below.

Both analysis techniques show similar results: For the modifications involving small molecules only negligible changes in the ratio of the oxygen to carbon ratio determined via EA as well as the ratio of carbon bound to carbon or hydrogen and carbon bound to oxygen or nitrogen from the XP spectra are observable or the changes are within the error margins (for the EA results the standard deviation was used to calculate an error and for XPS the error is estimated to be around 10 %, refer to Figure 4.14). When polystyrene, which only consists of carbon and hydrogen, is grafted onto the particles the ratio of carbon bound to oxygen or nitrogen to carbon bound to carbon or hydrogen determined via

4. Photo-Sensitive RAFT-Agents for Advanced Microparticle Design

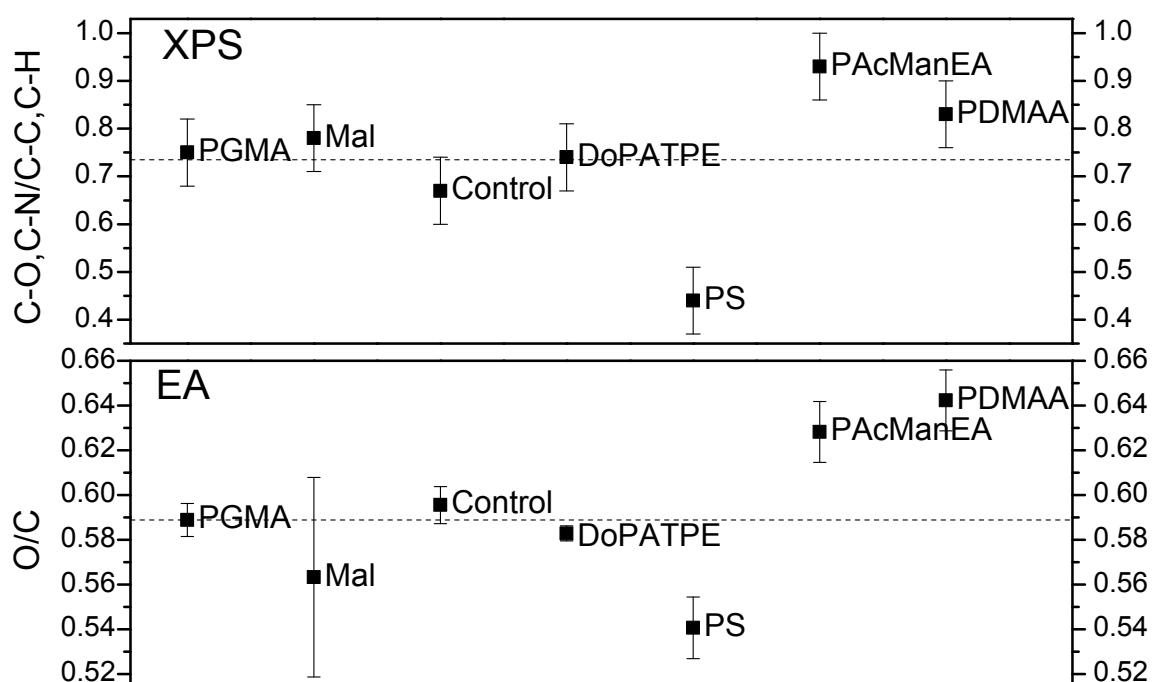


Figure 4.14: Comparison of the amount of carbon bound to oxygen or nitrogen and carbon bound to carbon or hydrogen based on the deconvolution of the carbon peak in the XP spectra (top) (also refer to Figure 4.13) and the oxygen to carbon ratio determined via EA (bottom). The values are non-changing for all modifications involving small molecules and show the theoretically expected changes for grafted-on polymers, indicating a successful reaction (for details, see text).

XPS and the oxygen to carbon ratios determined via EA decrease as expected. In the case of grafted PAcManEA (19 carbon atoms and 12 oxygen atoms per repetition unit) the O/C ratio rises compared to the PGMA (7 carbon and 3 oxygen atoms) microspheres. The same tendency is found in XPS: the signals for C–O, C–N and O–C=O, N–C=O rise in intensity compared to the peak attributed to C–C, C–H (refer to Figure 4.13), as the repeat unit of PAcManEA carries many carbon atoms that are bound to oxygen via single or double bonds. For grafted-on PDMAA no change in the ratios is expected, yet a small change is visible via XPS. Considering the error in XPS this change is negligible. The strong increase in the O/C ratio determined via EA is associated with traces of residual water or oxygen trapped in the porous structure of the particles. These results further underpin the successful light-triggered grafting of RAFT-polymers onto microparticles. Since EA is very accurate and analyzes the whole sphere, it provides – in contrast to XPS, which mainly analyzes the surface – quantitative information about the grafting efficiency. By employing the sulfur value from EA, loading capacities and grafting densities can be determined, which are not influenced by any inaccuracies of the chain length analysis of the polymeric chains, as sulfur is only contained in the chain ends of the polymer. For

4. Photo-Sensitive RAFT-Agents for Advanced Microparticle Design

grafted-on PDMAA the sulfur content reaches 0.31 at% and for PS 0.29 at%, respectively. Employing the above-mentioned equations, the sulfur content can be further converted to loading capacities of $32.2 \mu\text{mol} \cdot \text{g}^{-1}$ (PDMAA) and $30.2 \mu\text{mol} \cdot \text{g}^{-1}$ (PS) (Equation 4.1 on page 71) and grafting densities of 0.12 chains per nm^2 (PDMAA) and 0.11 chains per nm^2 (PS) (Equation 4.2). The photo-induced grafting reactions of RAFT-polymers lead to grafting densities which are similar to the grafting densities achieved on porous PGMA microspheres via thermally induced reactions (0.16 chains per nm^2 , Section 3.2.4).

For grafted-on PDMAA the nitrogen content reaches 1.39 wt%; for the maleimide-functionalized spheres it reads 0.97 wt%. The increase in nitrogen was not used to determine the grafting density, as this value would be biased by inaccuracies in the chain length value of PDMAA as nitrogen is contained in every repetition unit.

In the case of grafted-on PACManEA no sulfur can be detected, thus no quantitative analysis of the grafting is possible. However, the change in the O/C ratio indicates a successful grafting reaction. A potential reason for the weak sulfur signal may be the bulkiness and particularly the length of the glycopolymer chains, which lead to a higher steric hindrance, therefore a lower grafting density, and thus a lower sulfur content are reached. Yet, the fewer but longer chains lead to a sufficient change detectable in the O/C ratio.

For grafted-on PDMAA amide groups are introduced on the microparticles. In the IR spectrum amide vibrations provide a band which can be distinguished from the ester vibrations.^[24] Therefore, high resolution attenuated total reflectance (ATR) FT-IR-microscopy can be utilized to not only show the successful grafting, yet also its spatial distribution. ATR FT-IR-microscopy has been employed before to evidence the successful grafting onto microspheres (Section 3.2.4 and Figure 3.6), and can furthermore even give quantitative information about grafting reactions.^[207]

The results of the IR imaging are depicted in Figure 4.15 on the opposite page. As the particles are based on GMA – which carries an ester group in the repeating unit – the shape of the microspheres is accurately depicted by mapping of the ester vibration between 1680 and 1800 cm^{-1} for the maleimide-functionalized spheres as well as for the ones photo-grafted with PDMAA. On the contrary, mapping the vibration of the amide bond between 1615 and 1660 cm^{-1} gives no signal for the particles functionalized with maleimide, whereas the spherical shape can clearly be evidenced a second time for the microspheres grafted with PDMAA. Thereby the FT-IR-microscopy results not only underpin the successful grafting again, yet also evidence that the grafting is distributed evenly over the whole sphere.

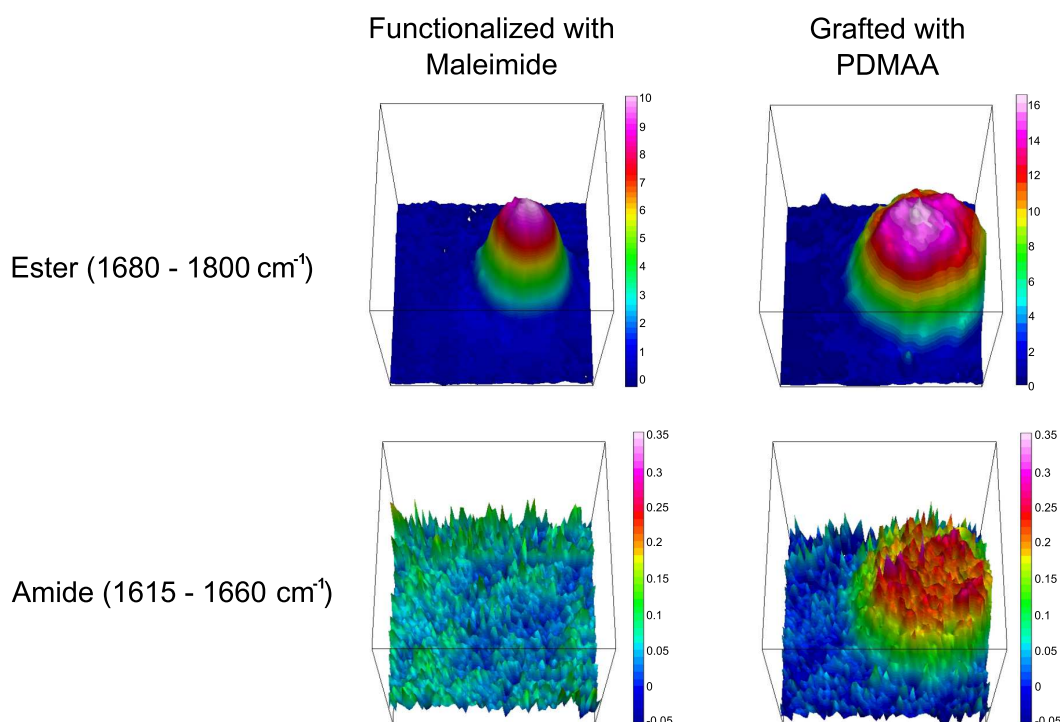


Figure 4.15: False color high resolution FT-IR-microscopy images (4 cm^{-1} spectral resolution with a pixel resolution of $0.25\text{ }\mu\text{m}^2$) of a GMA microsphere functionalized with maleimide and after photo-grafting of PDMAA. The measured area is $32\text{ }\mu\text{m} \times 32\text{ }\mu\text{m}$. Red color corresponds to a high degree of functionalization. In the top row, the intensity of bands corresponding to the O–C=O stretching vibration is visualized, in the bottom row the N–C=O bands.

Synthesis of Janus-Particles

The principal benefit of utilizing light-triggered reactions for the grafting of molecules onto surfaces is the possibility of spatial control over the grafting process. When flat surfaces – such as silicon wafers – are the chosen substrate, shadow masks protecting parts of the surface from the irradiation are employed to generate various patterns.^[19,180] When microparticles are the substrate such an approach is not accomplishable. Instead, Janus-particles – exhibiting two different hemispheres – were synthesized via a Pickering emulsion approach. The Pickering effect describes the stabilization of an emulsion via the aggregation of particles at the interface between the two immiscible liquids.^[208,209] If the hydrophobic liquid is molten paraffin wax – after subsequent cooling down – the microparticles are trapped on the surface of the now solidified wax spheres. Thus, only the part of the trapped particles that is not covered by the wax can be chemically modified, resulting in Janus-particles, which can be isolated after dissolving the wax in a suitable solvent.^[210,211]

In the present work a Pickering emulsion was established in a round-bottom flask

4. Photo-Sensitive RAFT-Agents for Advanced Microparticle Design

equipped with a magnetic stirring bar. In the presence of the microparticles 1 g of paraffin wax was molten and water (10 mL) was added subsequently. The emulsion was kept at an elevated temperature for 1 h and subsequently allowed to slowly reach ambient temperature. The wax spheres were filtered off, washed thoroughly and dried. Although the size of the wax droplets is difficult to control and adjust, this small and simple approach is sufficient. If a precise control over the size of the wax spheres is necessary, a mechanical stirrer or a commercial reactor with stirring control is recommended.

A Pickering emulsion was conducted as described above with maleimide-functionalized microparticles, resulting in wax spheres of close to 5 mm diameter. These wax spheres were analyzed via SEM, yet the SEM images show a lot of artifacts due to charge build up because of the size of the particles (Figure A.24 and A.25 in the Appendix). However, the size of the wax spheres does not influence the reactivity in photo-triggered grafting reactions.

SEM images of wax spheres covered with non-modified PGMA microspheres are depicted in Figure 4.16 on the opposite page together with images of a wax sphere cut with a scalpel.

Figure 4.16 shows that the microspheres are distributed evenly on the surface of the wax sphere which has a diameter of close to 1 mm. The microspheres are approximately covered with wax by half. The images of the wax sphere cut with a scalpel reveal that the microparticles cannot be found in the bulk of the wax but rather only on its surface (refer to Figure 4.16, parts c and d).

The photo-induced grafting of PDMAA onto the microspheres embedded in the wax is carried out in analogy to the grafting procedure described above, except that more polar methanol is employed as the solvent. Unpolar solvents can dissolve the wax or at least lead to an undesirable swelling of its surface so that the microparticles can leave the wax particle, which would lead to fully grafted spheres without Janus-morphology.^[211] The reaction mixture was deoxygenated and irradiated for 30 min. Subsequently, the wax was dissolved in chloroform and the now freed microparticles were filtered off, washed thoroughly, and dried. The Janus-spheres were analyzed via SEM and ATR FT-IR-microscopy. The SEM images show that there is no left over wax adhering to the particles and that the porous structure and spherical morphology of the particles is maintained (Figure A.26 - A.28 in the Appendix). IR imaging microscopy can be employed to illustrate the Janus-structure of the photo-grafted spheres. A comparison of the distribution of the amide signal and the ester signal clearly evidences that the entire sphere can be depicted via the ester vibration, whereas by mapping the amide signal only half of the sphere is visible (Figure 4.17 on page 80).

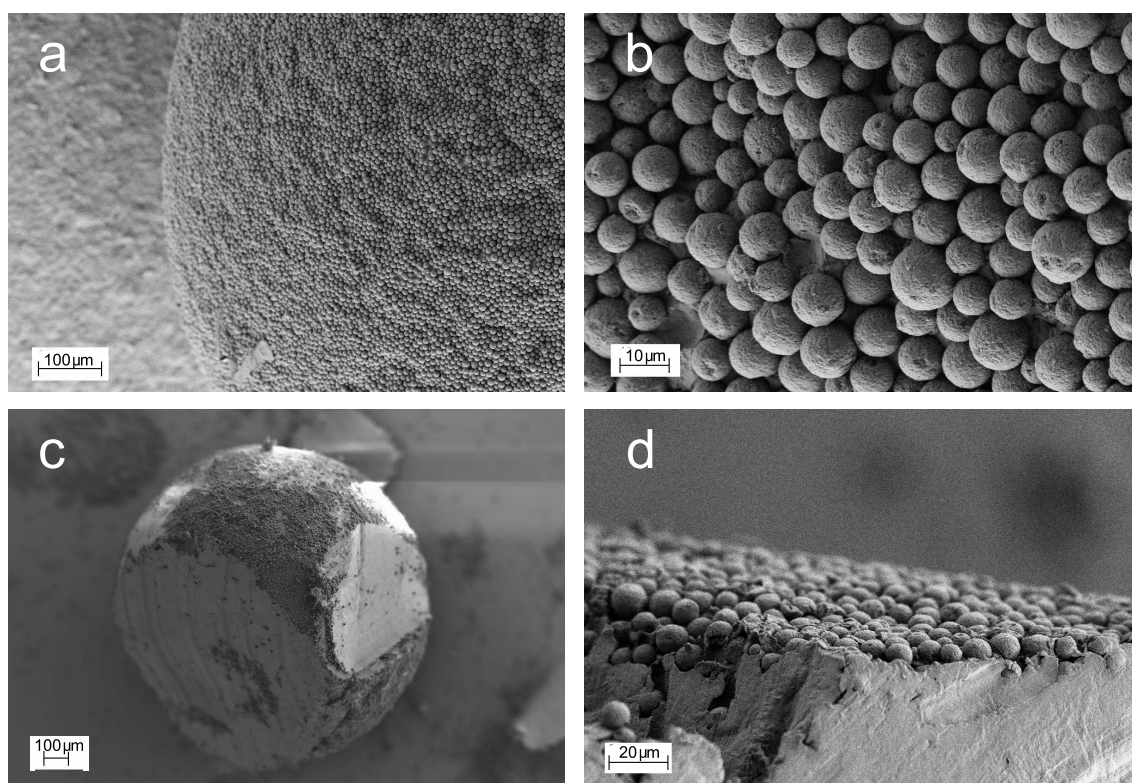


Figure 4.16: SEM images of wax spheres (diameter approximately 1 mm) covered with PGMA microspheres: (a) overview, (b) close up, (c) a sphere cut with a scalpel, and (d) close up of the surface of the cut sphere. The microspheres are evenly distributed on the surface of the wax sphere, not in the bulk of the wax, and are approximately covered with wax by half.

The Janus-structure is underpinned by an overlay of the spherical shape taken from mapping the ester vibration over the distribution of the amide band. Since the whole sphere exhibits ester bond, whereas the amide signal stems from a rather short polymeric chain grafted to half of the surface of the spheres, the mapping of the amide band is a little bit noisier. To illustrate this intensity difference, two exemplary IR spectra, one from the right half – with grafted-on PDMAA (black) – and one from the left half of the Janus-particle – without PDMAA (red) – are shown in Figure 4.18 on the following page.

These results underpin that the combination of photo-induced grafting reactions with RAFT-polymerization and a Pickering emulsion approach can successfully be employed to synthesize polymeric Janus-microparticles.

4. Photo-Sensitive RAFT-Agents for Advanced Microparticle Design

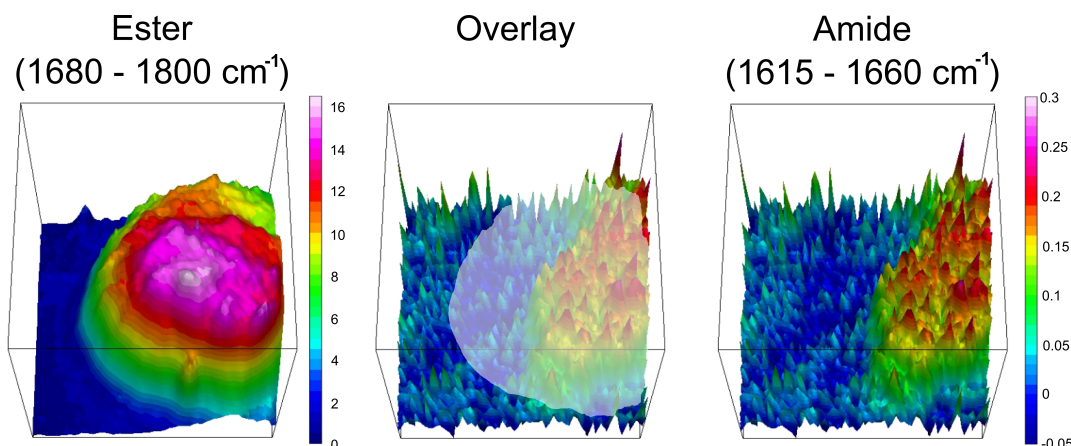


Figure 4.17: False color high resolution FT-IR-microscopy images (4 cm^{-1} spectral resolution with a pixel resolution of $0.25\text{ }\mu\text{m}^2$) of a maleimide-functionalized microsphere after photo-grafting of PDMAA on one-half of the sphere employing a Pickering emulsion approach. The measured area is $32\text{ }\mu\text{m} \times 32\text{ }\mu\text{m}$. Red color corresponds to a high degree of functionalization. In the left spectra, the intensity of bands corresponding to the O–C=O stretching vibration is visualized, in the right spectra the N–C=O bands. In the middle, the overlay of the spherical shape taken from the ester band on top of the amide band distribution indicates the Janus-type surface morphology of the particle.

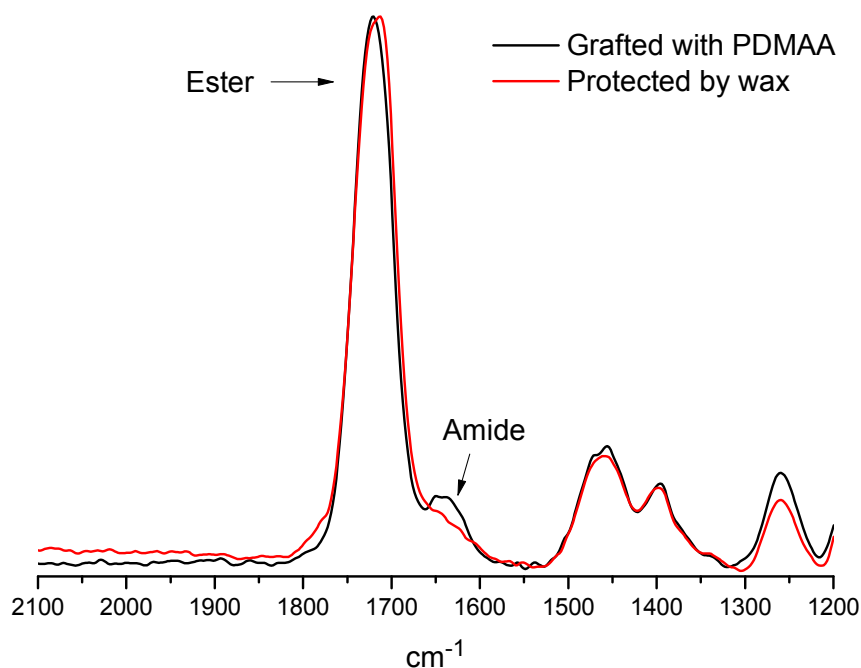


Figure 4.18: Comparison of IR spectra extracted from the mapping in Figure 4.17 to illustrate the difference generated by the spatial resolved photo-induced grafting of PDMAA onto microparticles partially protected by wax.

4.3 Conclusions

A novel RAFT-agent was synthesized which carries a photo-active group based on ortho-quinodimethane or photo-enol chemistry. The novel RAFT-agent controls the polymerization of a wide range of monomers, such as dimethylacrylamide, styrene, and a protected glycomonomer (AcManEA) with dispersities well below 1.2 and high degree of end group functionalization. The photo-enol group reacts with dienophiles without any catalyst and under mild irradiation at ambient conditions, so that the RAFT-group stays unaltered, to form block copolymers in a matter of minutes. Furthermore, the RAFT-polymers can also be photo-grafted onto porous polymeric microspheres, after a facile one-step prefunctionalization with maleimide moieties. The successful grafting is evidenced by EA, XPS, SEM, and high resolution ATR FT-IR-microscopy, which leads to qualitative as well as quantitative information. The grafting densities reach up to 0.12 molecules per nm². To demonstrate the benefit of employing a light-induced grafting reaction the synthesis of Janus-particles was conducted, employing a Pickering emulsion approach. The Janus-structure was illustrated via ATR FT-IR-microscopy.

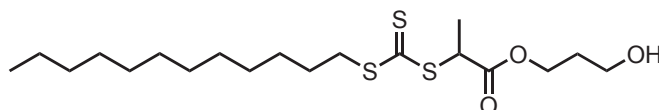
The current work underpins the robustness and versatility of the photo-enol approach as well as of the RAFT-polymerization technique. The combination of a mild light-triggered modular ligation reaction with an easy to use reversible deactivation radical polymerization method opens the door to an entirely new field of opportunities for the modification of microparticles and surfaces as well as the synthesis of challenging macromolecule architectures.

4.4 Experimental Part

4.4.1 Materials

Maleimide-functionalized poly(ethylene glycol) (PEG-Mal),^[179] 4-(2-hydroxyethyl)-10-oxa-4-azatricyclo-[5.2.1.0^{2,6}]dec-8-ene-3,5-dione,^[212] and methyl 4-((2-formyl-3-methylphenoxy)methyl)benzoic acid^[180] were synthesized according to the literature. 2,2'-Azobis(2-methylpropionitrile) (AIBN) was recrystallized twice from methanol and stored at -19 °C. Styrene and *N,N*-dimethylacrylamide (DMAA) were passed through a column of basic alumina to remove inhibitor and subsequently stored at -19 °C. Dichloromethane (DCM) was dried and stored over CaCl₂, *N,N*-dimethylformamide (DMF) was dried and stored over Na₂SO₄. Poly(glycidyl methacrylate) (PGMA) microspheres with a PGMA content of 80 % and pore size of 1000 Å were synthesized by Polymer Standards Service (PSS) GmbH as described in Section 3.4.3 on page 51. 2-((Dodecylsulfanyl)carbonothioyl)sulfanyl propanoic acid (DoPAT) was obtained from Orica Pty Ltd., Melbourne, Australia. All other chemicals were used as supplied by the manufacturers.

4.4.2 Synthesis of 1-((3-Hydroxypropoxy)Carbonyl)Ethyl Dodecyl Carbonotrithioate (DoPATOH)



DoPAT (6.00 g, 17.1 mmol, 1.00 equiv), 1,3-propanediol (3.75 mL, 3.92 g, 51.5 mmol, 3.00 equiv) and 4-dimethylaminopyridine (41.8 mg, 0.34 mmol, 0.02 equiv) were dissolved in 40 mL of dry THF. The solution was cooled to 0 °C in an ice bath and dicyclohexylcarbodiimide (4.44 g, 21.5 mmol, 1.26 equiv) dissolved in 8 mL dry THF was added dropwise. After one hour, the ice bath was removed and the reaction proceeded over night at ambient temperature. The solvent was removed under reduced pressure and the residue dissolved in diethyl ether. After filtration, the organic layer was washed with 5 % HCl, saturated NaHCO₃ solution and distilled water, dried over MgSO₄ and the solvent removed. The crude product was purified via column chromatography (silica gel, cyclohexane/ethyl acetate 2:1) to afford a yellow solid (6.30 g, 90 %). ¹H-NMR (CDCl₃, 400 MHz) δ/ppm: 4.81 (q, ³J=7.4 Hz, 1H, SCHCH₃), 4.29 (m, 2H, HOCH₂CH₂CH₂), 3.69 (t, ³J=6.0 Hz, 2H, HOCH₂CH₂CH₂), 3.34 (dt, ³J=7.4 Hz, ⁵J=1.3 Hz, 2H, SCH₂CH₂C₇H₁₄CH₂CH₂CH₃), 1.88 (quin, ³J=6.0 Hz, 2H, HOCH₂CH₂CH₂), 1.68 (quin, ³J=7.4 Hz, 2H, SCH₂CH₂C₇H₁₄CH₂CH₂CH₃), 1.59 (d,

4. Photo-Sensitive RAFT-Agents for Advanced Microparticle Design

$^3J=7.4$ Hz, 3H, SCHCH₃), 1.39 (m, 2H, SCH₂CH₂C₇H₁₄CH₂CH₂CH₃), 1.25 (s_{br}, 16H, SCH₂CH₂C₇H₁₄CH₂CH₂CH₃), 0.87 (t, $^3J=6.9$ Hz, 3H, SCH₂CH₂C₇H₁₄CH₂CH₂CH₃). $^{13}\text{C-NMR}$ (CDCl₃, 100 MHz) δ /ppm: 222.1 (SC(S)S), 171.5 (SCHCH₃C(O)O), 62.8 (HOCH₂CH₂CH₂), 59.2 (HOCH₂CH₂CH₂), 47.8 (SCHCH₃C(O)O), 37.3 (SCH₂CH₂C₇H₁₄CH₂CH₂CH₃), 31.9 (SCH₂CH₂C₇H₁₄CH₂CH₂CH₃), 31.5 (HOCH₂CH₂CH₂), 29.6 (2 \times), 29.5, 29.4, 29.3, 29.1, 28.9, 27.9 (8C, SCH₂CH₂C₇H₁₄CH₂CH₂CH₃), 22.7 (SCH₂CH₂C₇H₁₄CH₂CH₂CH₃), 16.8 (SCHCH₃C(O)O), 14.1 (SCH₂CH₂C₇H₁₄CH₂CH₂CH₃). **MS:** (ESI) m/z calculated for C₁₉H₃₆O₃S₃ [M+Na]⁺: 431.17; found 431.16.

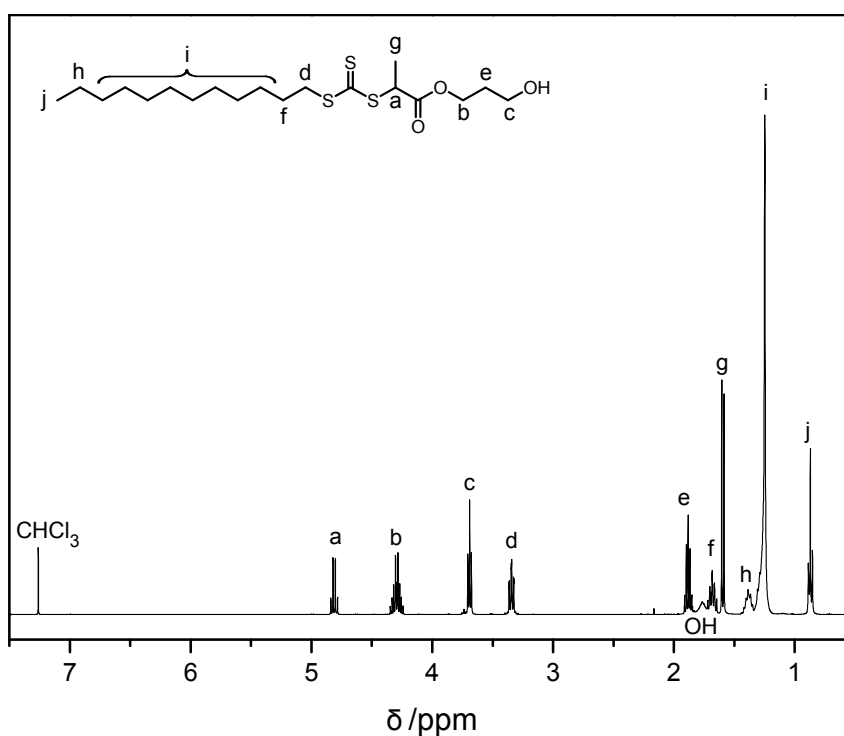


Figure 4.19: $^1\text{H-NMR}$ spectrum of 1-((3-hydroxypropoxy)carbonyl)ethyl dodecyl carbonotrithioate (DoPATO) in CDCl_3 at 400 MHz.

4. Photo-Sensitive RAFT-Agents for Advanced Microparticle Design

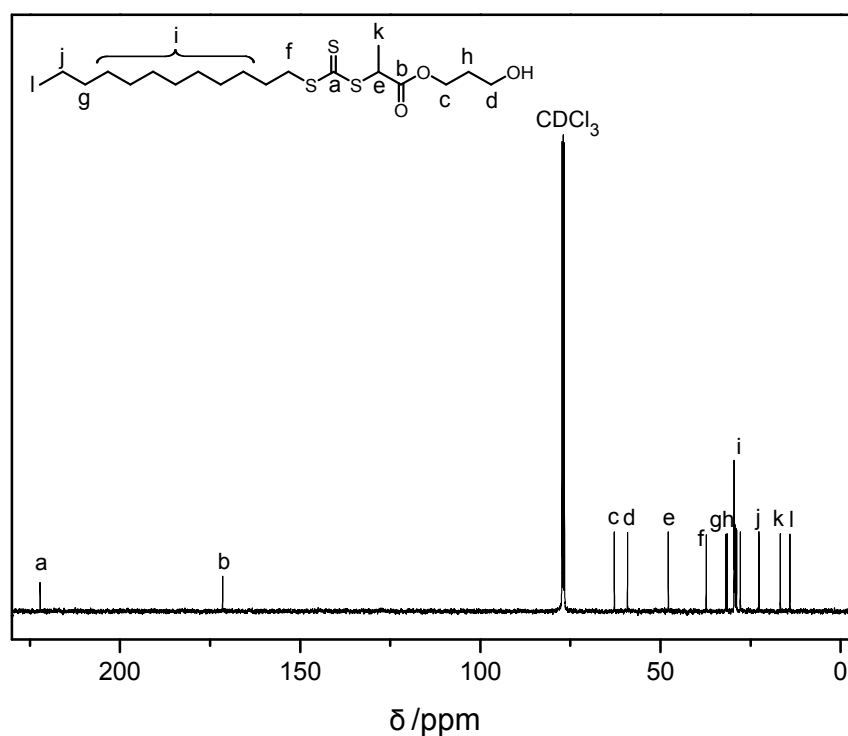
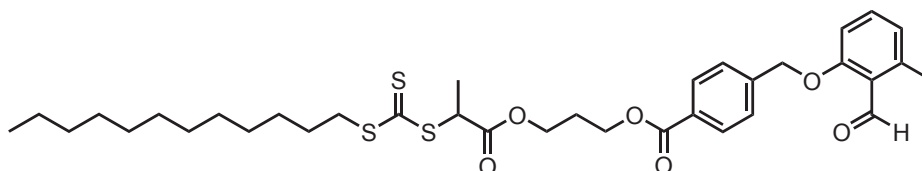


Figure 4.20: ^{13}C -NMR spectrum of 1-((3-hydroxypropoxy)carbonyl)ethyl dodecyl carbonotrithioate (DoPATOH) in CDCl_3 at 100 MHz.

4.4.3 Synthesis of DoPAT-Photo-Enol (DoPATPE)



DoPATOH (1.50 g, 3.67 mmol, 1.00 equiv), 4-((2-formyl-3-methylphenoxy)methyl)benzoic acid (1.14 g, 4.22 mmol, 1.15 equiv) and 4-dimethylaminopyridine (116 mg, 0.95 mmol, 0.26 equiv) were dissolved in dry DMF. Dicyclohexylcarbodiimide (1.16 g, 5.65 mmol, 1.35 equiv) dissolved in dry DMF was added dropwise. The reaction was covered with aluminum foil to protect it from ambient light. The reaction proceeded for 46 h at ambient temperature; subsequently, 100 mL DCM was added and the organic layer was washed with 5% HCl, saturated NaHCO_3 solution and distilled water, dried over Na_2SO_4 and the solvent removed. The crude product was purified via column chromatography (silica gel, cyclohexane/ethyl acetate 2:1) to give a yellow solid (1.48 g, 61%). ^1H -NMR (CDCl_3 , 300 MHz) δ /ppm: 10.75 (s, 1H, CHO), 8.06 (d, $^3J=8.3$ Hz, 2H, paraArH), 7.50 (d, $^3J=8.4$ Hz, 2H, paraArH), 7.36 (t, $^3J=8.0$ Hz, 2H, ArH), 6.85 (m, 2H, ArH), 5.24 (s, 2H, Ar CH_2O),

4. Photo-Sensitive RAFT-Agents for Advanced Microparticle Design

4.81 (q, $^3J=7.4$ Hz, 1H, SCHCH₃), 4.42 (t, $^3J=6.2$ Hz, 2H, ArC(O)OCH₂CH₂CH₂), 4.33 (m, 2H, ArC(O)OCH₂CH₂CH₂), 3.35 (dt, $^3J=7.4$ Hz, $^5J=1.0$ Hz, 2H, SCH₂CH₂C₇H₁₄CH₂CH₂CH₃), 2.61 (s, 3H, ArCH₃), 2.15 (quin, $^3J=6.2$ Hz, 2H, ArC(O)OCH₂CH₂CH₂), 1.68 (quin, $^3J=7.4$ Hz, 2H, SCH₂CH₂C₇H₁₄CH₂CH₂CH₃), 1.61 (d, $^3J=7.4$ Hz, 3H, SCHCH₃), 1.27 (s_{br}, 16H, SCH₂CH₂C₇H₁₄CH₂CH₂CH₃), 0.89 (t, $^3J=6.9$ Hz, 3H, SCH₂CH₂C₇H₁₄CH₂CH₂CH₃). ¹³C-NMR (CDCl₃, 75 MHz) δ/ppm: 222.0 (SC(S)S), 191.9 (CHO), 171.1 (ArC(O)OCH₂CH₂CH₂C(O)O), 165.9 (ArC(O)OCH₂CH₂CH₂C(O)O), 161.8 (Ar), 142.3 (paraAr), 141.4 (Ar), 134.4 (Ar) 130.0, 129.9, 126.8 (paraAr), 124.7, 123.6, 110.3 (Ar), 69.9 (ArCH₂O), 62.4 (ArC(O)OCH₂CH₂CH₂C(O)O), 61.4 (ArC(O)OCH₂CH₂CH₂C(O)O), 47.8 (SCHCH₃), 37.2 (SCH₂CH₂C₇H₁₄CH₂CH₂CH₃), 31.9 (SCH₂CH₂C₇H₁₄CH₂CH₂CH₃), 29.6 (2×), 29.5, 29.4, 29.3, 29.0, 28.9, 27.9, (8C, SCH₂CH₂C₇H₁₄CH₂CH₂CH₃), 27.8 (ArC(O)OCH₂CH₂CH₂C(O)O), 22.6 (SCH₂CH₂C₇H₁₄CH₂CH₂CH₃), 21.4 (ArCH₃), 16.7 (SCHCH₃C(O)O), 14.1 (SCH₂CH₂C₇H₁₄CH₂CH₂CH₃). MS: (ESI) *m/z* calculated for C₃₅H₄₈O₆S₃ [M+Na]⁺: 683.25; found 683.32.

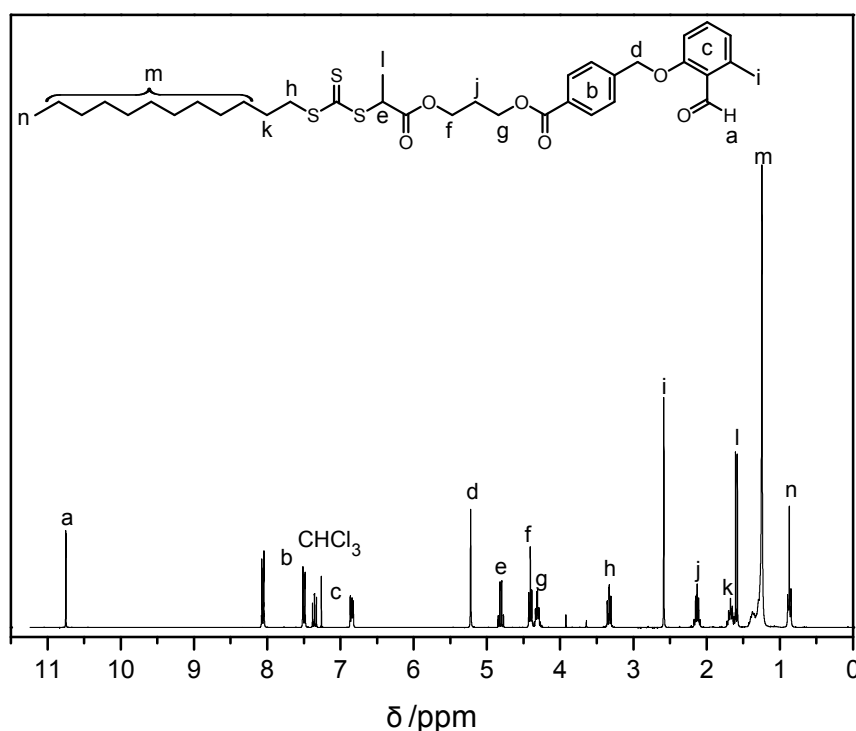


Figure 4.21: ¹H-NMR spectrum of DoPATPE in CDCl₃ at 300 MHz.

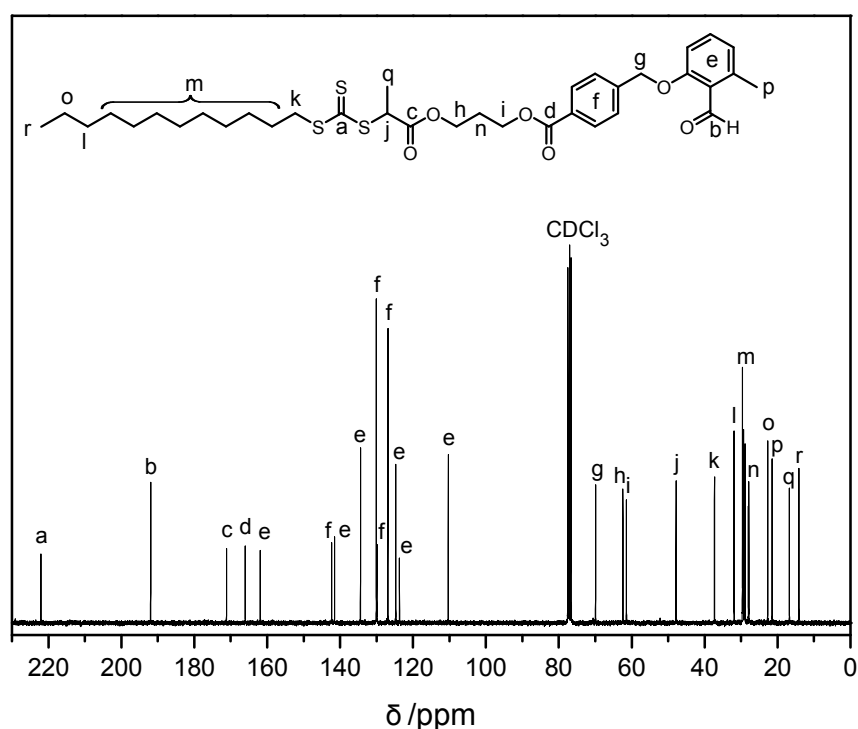
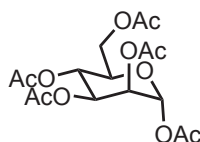


Figure 4.22: ^{13}C -NMR spectrum of DoPATPE in CDCl_3 at 75 MHz.

4.4.4 Synthesis of 2-(2',3',4',6'-Tetra-O-Acetyl- β -D-Mannosyloxy) Ethylacrylate (AcManEA)

Peracetylation of Mannose



Mannose (5.00 g, 27.7 mmol, 1.00 equiv) was suspended in acetic anhydride (26.2 mL, 28.3 g, 277 mmol, 10.0 equiv). The mixture was cooled to 0°C with an ice bath and two drops of sulfuric acid were added, which led to the formation of a clear solution. After 30 min, the ice bath was removed and the reaction proceeded at ambient temperature overnight. 100 mL of water was added and the solution was extracted three times with ethyl acetate. The organic phase was alternately washed with saturated NaHCO_3 solution and distilled water until the water was neutral after the washing procedure. The organic phase was dried over MgSO_4 and the solvent removed under reduced pressure to give a colorless waxy solid (8.89 g, 82 %). $^1\text{H-NMR}$ (CDCl_3 , 400 MHz) δ/ppm : 6.07 (s, 1H, anomeric C), 5.31, 4.17 (2 multiplets, each 3H, sugar moiety), 2.16, 2.15, 2.08, 2.04, 1.99 (5 s, each 3H, acetyl-groups). $^{13}\text{C-NMR}$ (CDCl_3 , 100 MHz) δ/ppm : 170.6, 170.0, 169.7, 169.5, 168.0 (5C, $\text{H}_3\text{C}\underline{\text{C}}(\text{O})\text{O}$), 90.5 (anomeric C), 70.5, 68.7, 68.3, 65.5, 62.1 (5C,

4. Photo-Sensitive RAFT-Agents for Advanced Microparticle Design

sugar moiety), 20.8, 20.7, 20.7 20.6, 20.6 (5C, H₃CC(O)O). MS: (ESI) *m/z* calculated for C₁₆H₂₂O₁₁ [M+Na]⁺: 413.11; found 413.12.

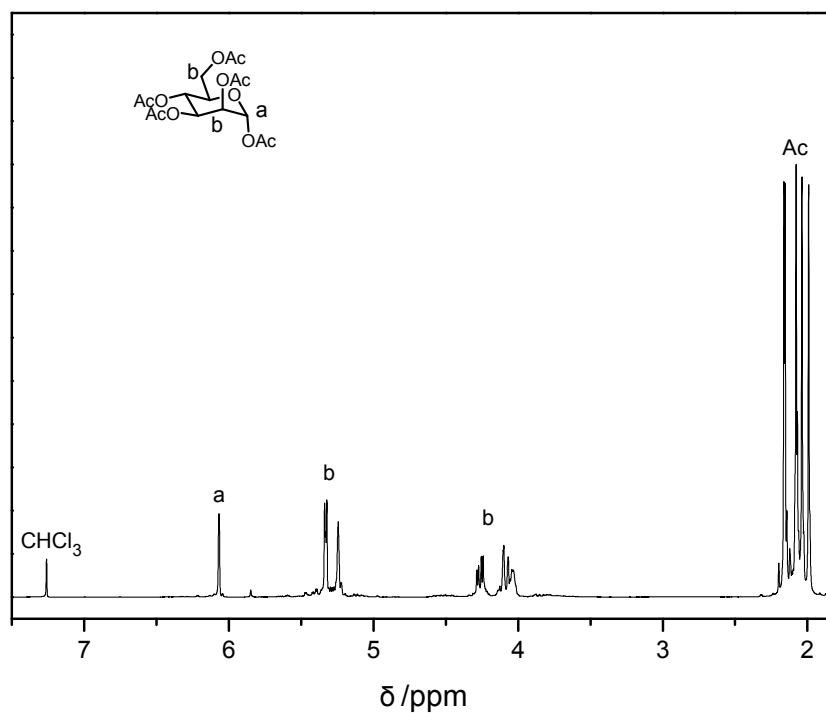


Figure 4.23: ¹H-NMR spectrum of β-D-mannose pentaacetate in CDCl₃ at 400 MHz.

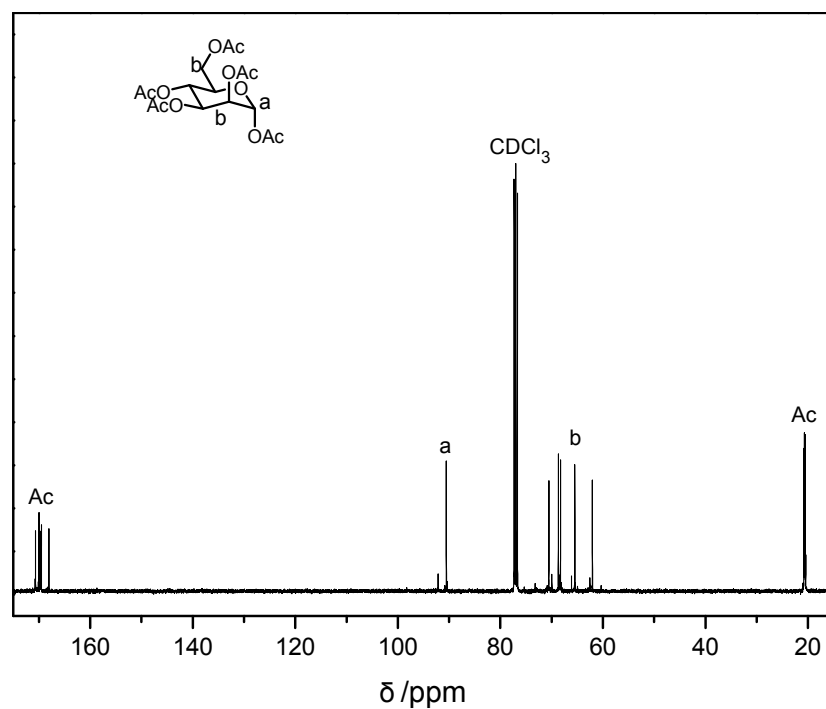
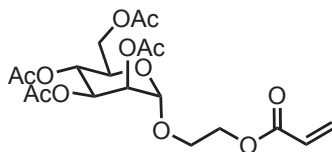


Figure 4.24: ¹³C-NMR spectrum of β-D-mannose pentaacetate in CDCl₃ at 100 MHz.

4. Photo-Sensitive RAFT-Agents for Advanced Microparticle Design

Acetalization with 2-Hydroxyethyl Acrylate



The synthesis was carried out based on a modified literature method.^[162] β -D-Mannose pentaacetate (1.98 g, 5.07 mmol, 1.00 equiv) was dissolved in dry DCM and 2-hydroxyethyl acrylate (700 μ L, 706 mg, 6.08 mmol, 1.20 equiv) was added. The mixture was cooled to $-10\text{ }^{\circ}\text{C}$ with an ice/salt-bath and $\text{BF}_3 \cdot \text{OEt}_2$ (3.60 g, 25.4 mmol, 5.00 equiv) was added dropwise. The reaction was allowed to reach ambient temperature and was stirred overnight. After addition of 10 mL of water, the mixture was extracted with DCM and the organic phase washed with water, saturated NaHCO_3 solution and again water. After drying over Na_2SO_4 , the solvent was removed under reduced pressure. The crude product was purified via column chromatography (silica gel, cyclohexane/ethyl acetate 1:3) to afford a colorless liquid (1.73 g, 76 %), which was stored at $-19\text{ }^{\circ}\text{C}$ and used rapidly to prevent autopolymerization. **$^1\text{H-NMR}$** (CDCl_3 , 400 MHz) δ /ppm: 6.43 (d, $^3\text{J}=17.3$ Hz, 1H, vinylic H), 6.13 (m, 1H, vinylic H), 5.86 (d, $^3\text{J}=10.4$ Hz, 1H, vinylic H), 5.28 (m, 3H, sugar moiety), 4.86 (s, 1H, sugar moiety), 4.14 (m, 6H, sugar and ethyl moiety), 3.83 (m, 2H, ethyl moiety), 2.14, 2.08, 2.03, 1.98 (4 s, each 3H, acetyl groups). **$^{13}\text{C-NMR}$** (CDCl_3 , 100 MHz) δ /ppm: 170.6, 170.0, 169.8, 169.7 (4C, $\text{H}_3\text{C}\underline{\text{C}}(\text{O})\text{O}$), 165.8 ($\text{H}_2\text{C}\underline{\text{C}}\text{H}\underline{\text{C}}(\text{O})\text{O}$), 131.3 ($\text{H}_2\underline{\text{C}}\text{C}\text{H}\underline{\text{C}}(\text{O})\text{O}$), 128.0 ($\text{H}_2\text{C}\underline{\text{C}}\text{H}\underline{\text{C}}(\text{O})\text{O}$), 97.6 (anomeric C), 69.4, 68.9, 68.6, 6.1, 66.0, 62.9, 62.4 (7C, sugar and ethyl moiety), 20.8, 20.7, 20.6, 20.6 (4C, $\text{H}_3\underline{\text{C}}\underline{\text{C}}(\text{O})\text{O}$). **MS:** (ESI) m/z calculated for $\text{C}_{19}\text{H}_{26}\text{O}_{12}$ $[\text{M}+\text{Na}]^+$: 469.13; found 469.20.

4. Photo-Sensitive RAFT-Agents for Advanced Microparticle Design

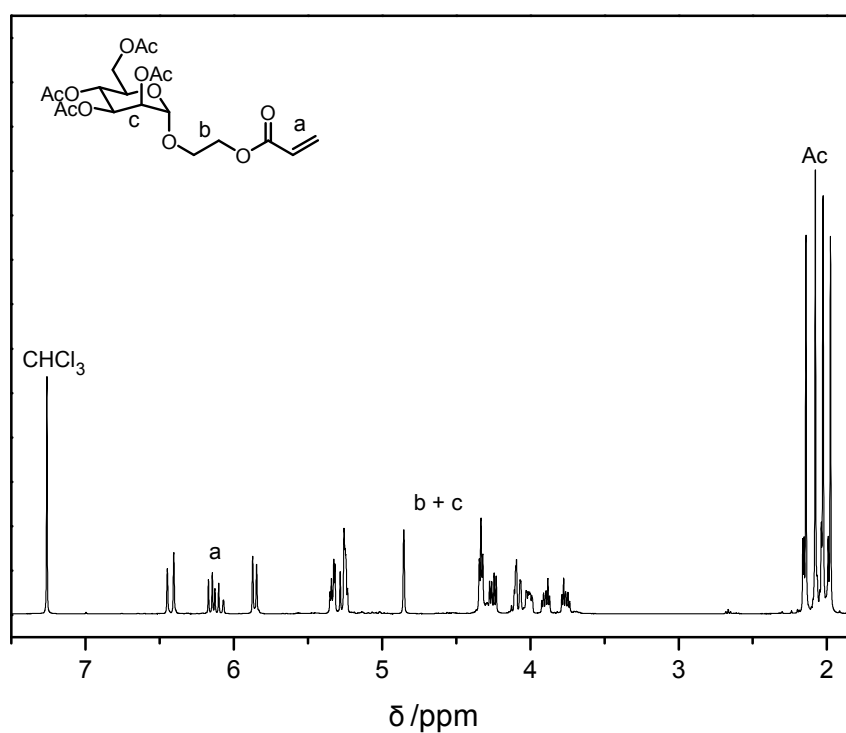


Figure 4.25: ¹H-NMR spectrum of 2-(2',3',4',6'-tetra-*O*-acetyl-β-D-mannosyloxy)ethylacrylate (AcManEA) in CDCl₃ at 400 MHz.

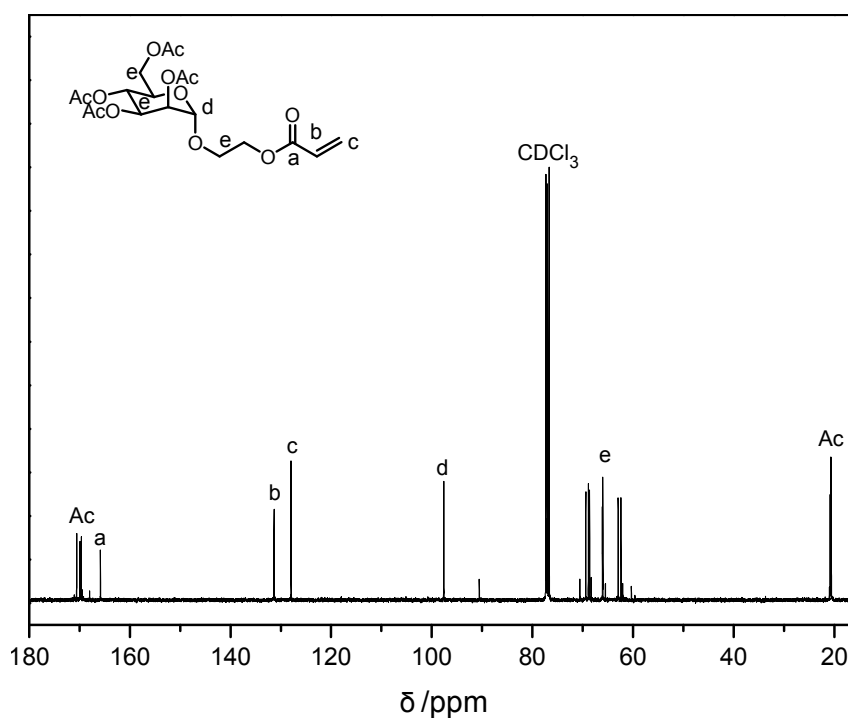
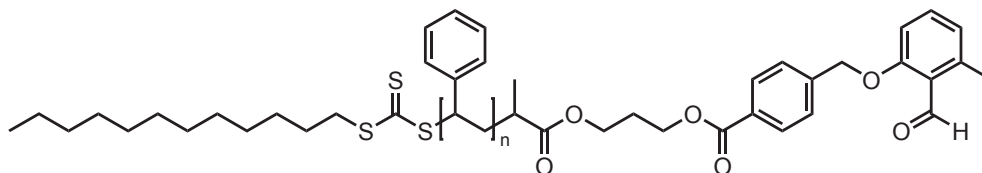


Figure 4.26: ¹³C-NMR spectrum of 2-(2',3',4',6'-tetra-*O*-acetyl-β-D-mannosyloxy)ethylacrylate (AcManEA) in CDCl₃ at 100 MHz.

4.4.5 RAFT-Polymerizations

Synthesis of Polystyrene (PS)



A solution of AIBN (3.8 mg, 0.023 mmol, 0.10 equiv) and DoPATPE (153 mg, 0.23 mmol, 1.00 equiv) in styrene (2.40 g, 23.0 mmol, 100 equiv) was deoxygenated with three consecutive freeze-pump-thaw cycles. The reaction was placed into a preheated oil-bath at 60 °C for 14 h. The reaction was stopped by cooling in an ice-bath and exposing the reaction mixture to oxygen. The polymer was isolated by 2-fold precipitation in cold methanol and subsequent drying under vacuum to afford 596 mg of a slightly yellow powder. $M_n = 3900 \text{ g} \cdot \text{mol}^{-1}$, $D = 1.07$ (GPC in THF, polystyrene calibration), $M_n = 3900 \text{ g} \cdot \text{mol}^{-1}$ (NMR).

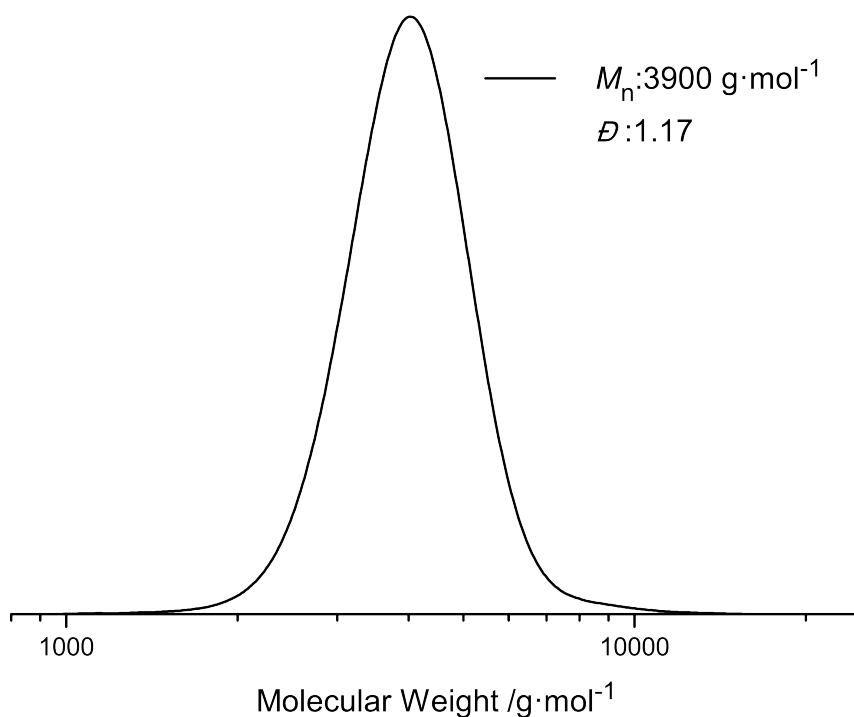


Figure 4.27: GPC trace in THF (PS calibration) of polystyrene polymerized with DoPATPE.

4. Photo-Sensitive RAFT-Agents for Advanced Microparticle Design

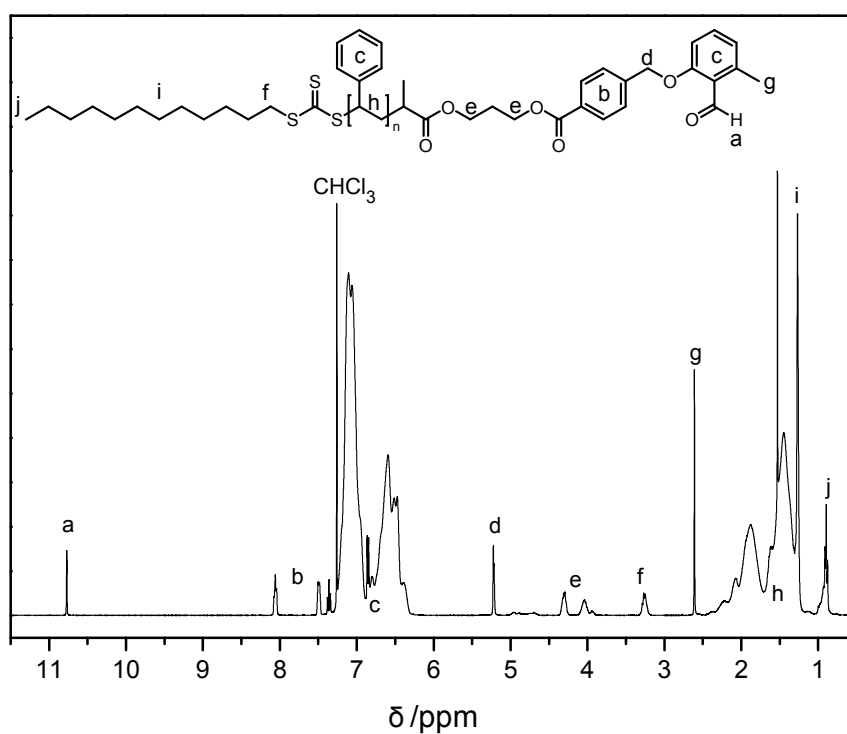


Figure 4.28: $^1\text{H-NMR}$ spectrum of polystyrene polymerized with DoPATPE in CDCl_3 at 400 MHz. Comparison of repetition unit resonance integrals (c, 7.25 - 6.25 ppm) to end group resonance integrals (b, 8.06 ppm) results in $M_n = 3900 \text{ g} \cdot \text{mol}^{-1}$.

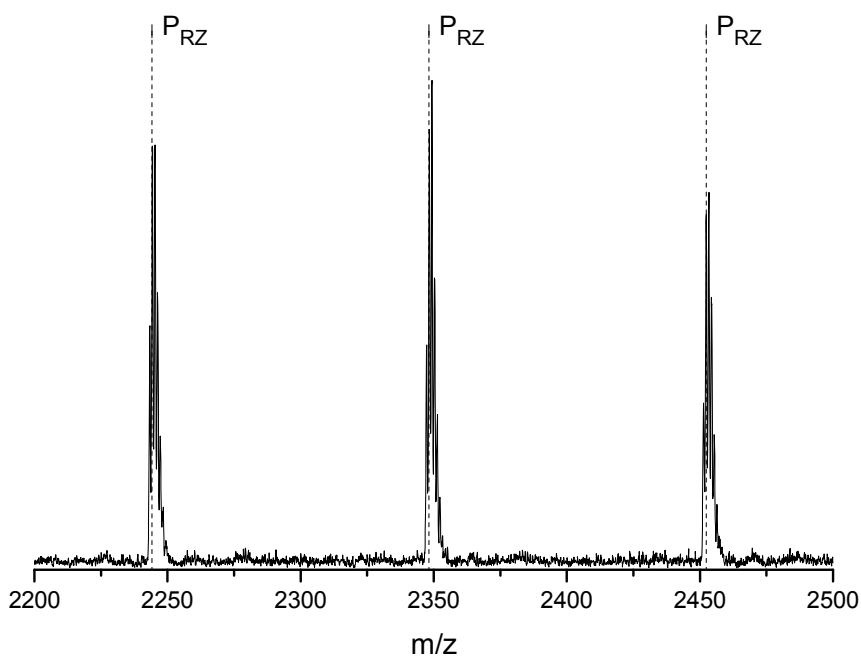
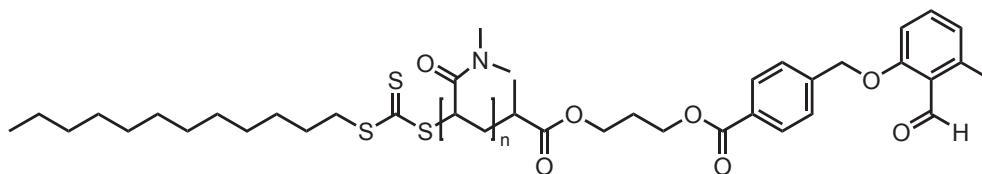


Figure 4.29: Zoom into the ESI-MS spectrum of polystyrene polymerized with DoPATPE. The label P_{RZ} indicates the theoretical mass of chains with the R- and Z-group of the RAFT-agent as end groups, ionized with Na^+ (stemming from added NaTfa).

4. Photo-Sensitive RAFT-Agents for Advanced Microparticle Design

Synthesis of Poly(*N,N*-dimethylacrylamide) (PDMAA)



A solution of AIBN (9.6 mg, 0.058 mmol, 0.2 equiv), DoPATPE (194.0 mg, 0.29 mmol, 1.00 equiv) and DMAA (1.46 g, 14.7 mmol, 50 equiv) in DMF (7.5 mL) was deoxygenated with three consecutive freeze-pump-thaw cycles. The reaction was placed into a pre-heated oil-bath at 60 °C for 3 h. The reaction was stopped by cooling in an ice-bath and exposing the reaction mixture to oxygen. The polymer was isolated by dialyzing the reaction mixture against distilled water (utilizing a SpectraPor3 membrane (MWCO = 1000 Da)) and subsequent freeze drying to give 597 mg of a yellow solid. $M_n = 3500 \text{ g} \cdot \text{mol}^{-1}$, $\mathcal{D} = 1.11$ (GPC in dimethylacetamide (DMAc), polystyrene calibration), $M_n = 2550 \text{ g} \cdot \text{mol}^{-1}$ (NMR).

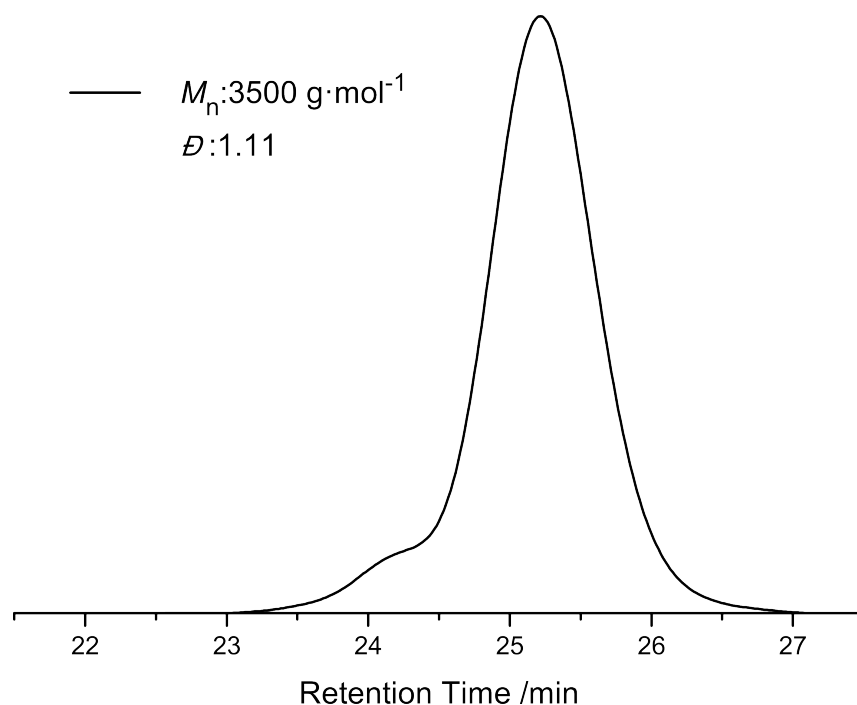


Figure 4.30: GPC trace (PS calibration) in DMAc of poly(*N,N*-dimethylacrylamide) polymerized with DoPATPE.

4. Photo-Sensitive RAFT-Agents for Advanced Microparticle Design

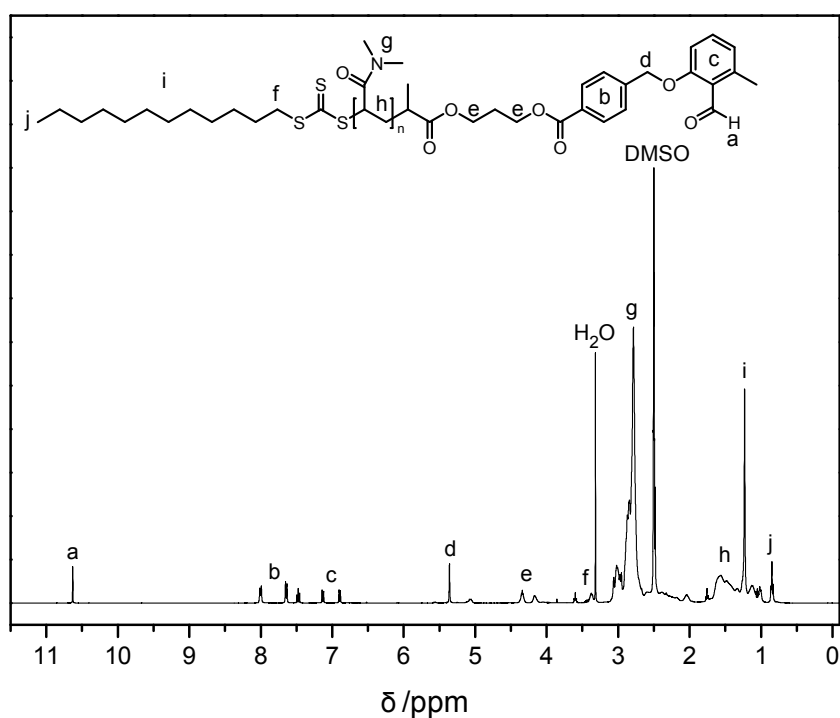


Figure 4.31: $^1\text{H-NMR}$ of poly(*N,N*-dimethylacrylamide) polymerized with DoPATPE in DMSO-d_6 at 400 MHz. Comparison of repetition unit resonance integrals (g, 3.15 - 2.60 ppm) to end group resonance integrals (c, 6.89 ppm) results in $M_n = 2550 \text{ g} \cdot \text{mol}^{-1}$.

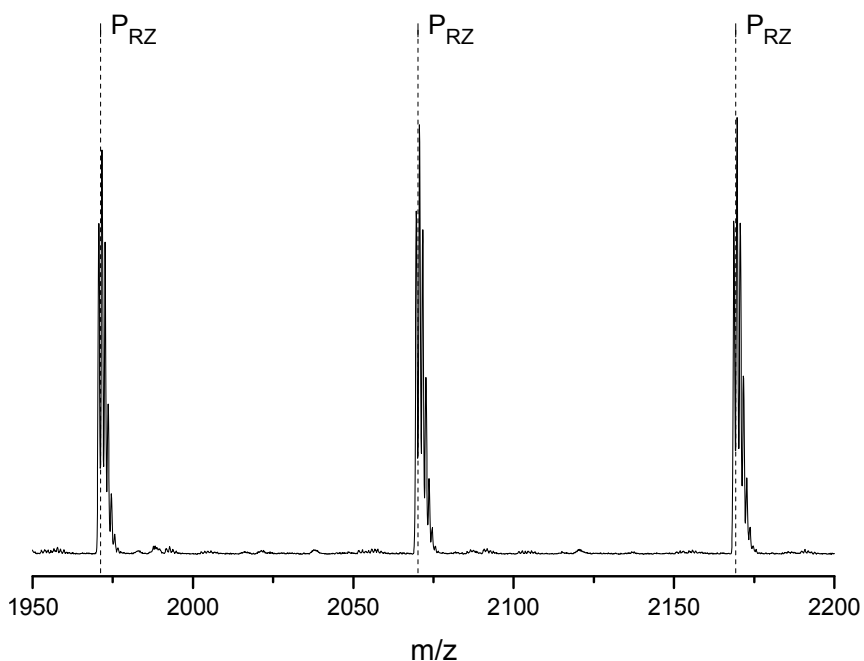


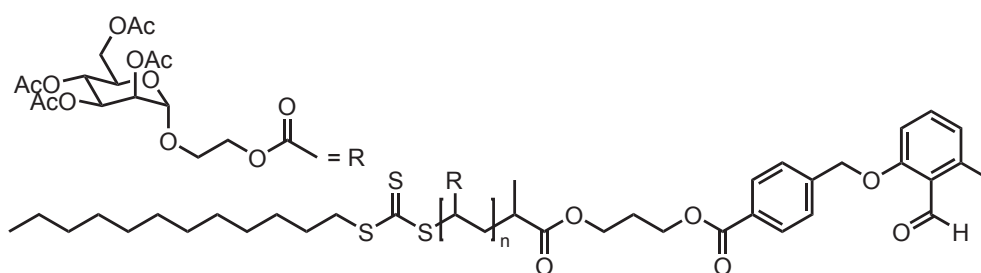
Figure 4.32: Zoom into the ESI-MS spectrum of poly(*N,N*-dimethylacrylamide) polymerized with DoPATPE. The label P_{RZ} indicates the theoretical mass of chains with the R- and Z-group of the RAFT-agent as end groups, ionized with Na^+ (stemming from added NaTfa).

4. Photo-Sensitive RAFT-Agents for Advanced Microparticle Design

Table 4.2: Experimental and theoretical m/z values for the labeled peaks in Figure 4.29 and Figure 4.32.

m/z_{exp}	assignment	formula	m/z_{theo}	$\Delta m/z$
2347.64	PS ₁₆	[C ₁₆₃ H ₁₇₆ O ₆ S ₃ Na] ⁺	2348.25	0.61
1971.00	PDMAA ₁₃	[C ₁₀₀ H ₁₆₅ N ₁₃ O ₁₉ S ₃ Na] ⁺	1971.14	0.14

Synthesis of Poly(2-(2',3',4',6'-tetra-*O*-acetyl- β -D-mannosyloxy)ethylacrylate) (PAcManEA)



A solution of AIBN (0.64 mg, 0.004 mmol, 0.10 equiv), DoPATPE (25.6 mg, 0.038 mmol, 1.00 equiv) and AcManEA (1.73 g, 3.88 mmol, 100 equiv) in DMAc (8.0 mL) was deoxygenated with three consecutive freeze-pump-thaw cycles. The reaction was placed into a preheated oil-bath at 60 °C for 3 h. The reaction was stopped by cooling in an ice-bath and exposing the reaction mixture to oxygen. The polymer was isolated by precipitation in cold diethyl ether and dried under vacuum to give 414 mg of a slightly yellow, waxy solid. $M_n = 5700 \text{ g} \cdot \text{mol}^{-1}$, $D = 1.17$ (GPC in THF, polystyrene calibration); $M_n = 10100 \text{ g} \cdot \text{mol}^{-1}$, $D = 1.14$ (GPC in DMAc, polystyrene calibration), $M_n = 17300 \text{ g} \cdot \text{mol}^{-1}$ (NMR). The block copolymer formation showed that the results from the GPC in DMAc are accurate, as for a successful reaction the stoichiometry has to be precise.

4. Photo-Sensitive RAFT-Agents for Advanced Microparticle Design

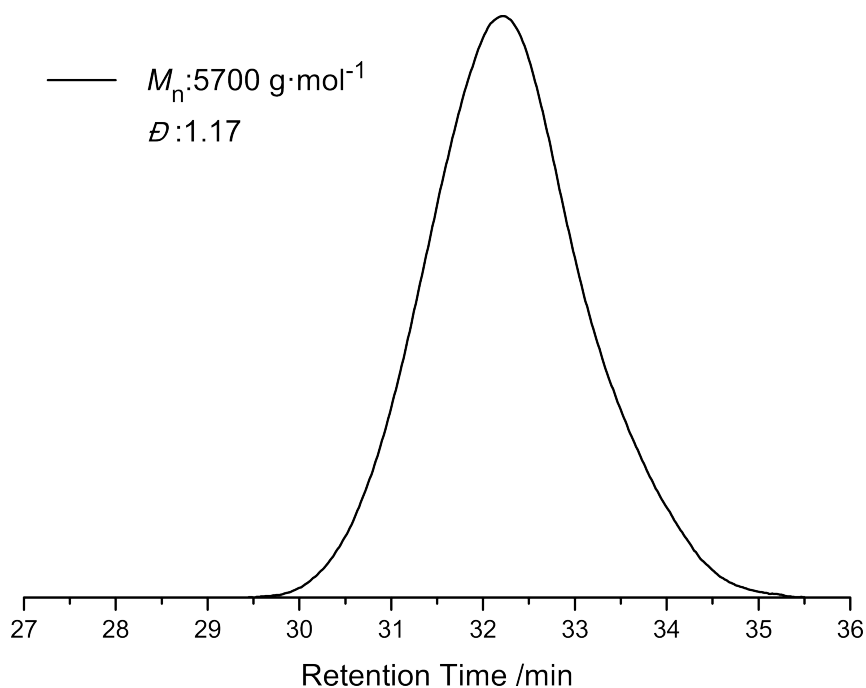


Figure 4.33: GPC trace (PS calibration) in THF of PAcManEA polymerized with DoPATPE.

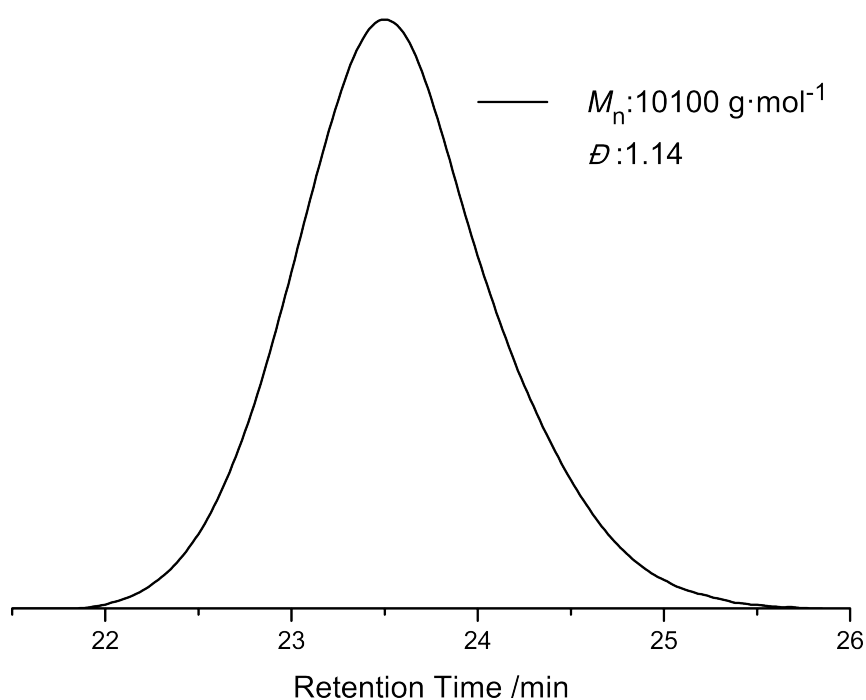


Figure 4.34: GPC trace (PS calibration) in DMAc of PAcManEA polymerized with DoPATPE.

4. Photo-Sensitive RAFT-Agents for Advanced Microparticle Design

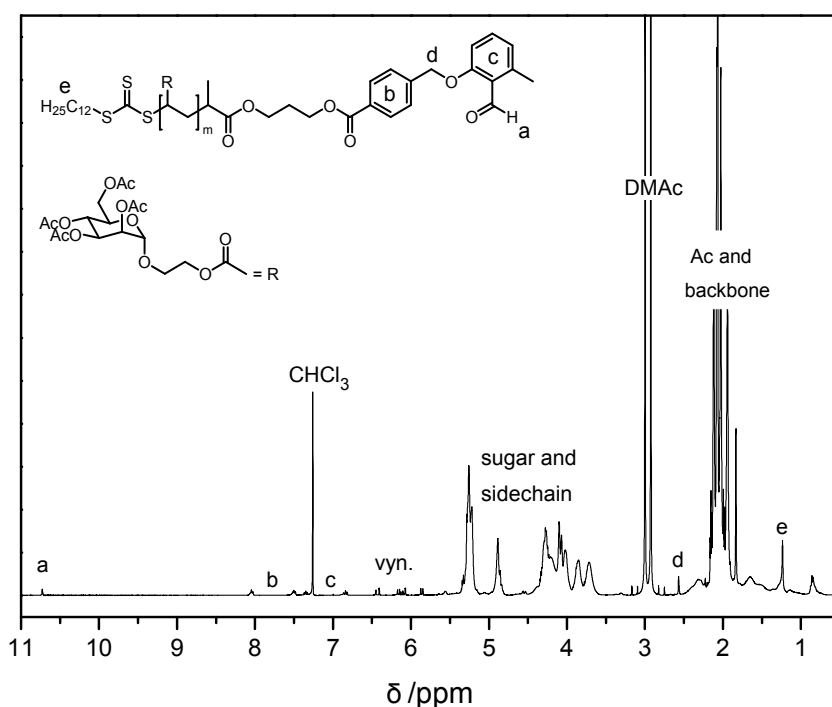
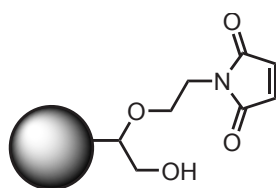


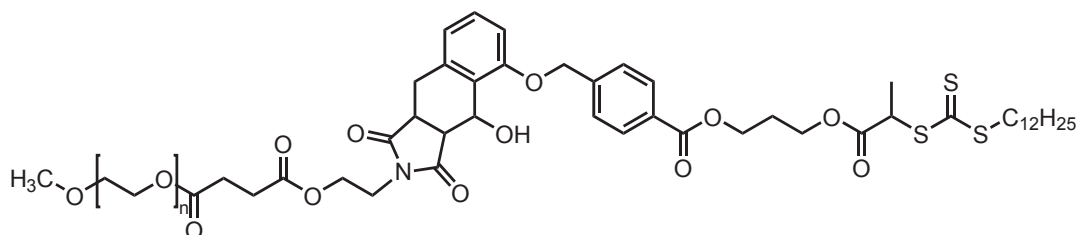
Figure 4.35: $^1\text{H-NMR}$ spectrum of PACmanEA polymerized with DoPATPE in CDCl_3 at 400 MHz. A comparison of repetition unit resonance integrals (5.40 - 3.60 ppm) to end group resonance integrals (c, 7.35 ppm) is challenging due to overlaps and small residues of monomer and results in $M_n = 17300 \text{ g} \cdot \text{mol}^{-1}$.

4.4.6 Maleimide-Functionalization of PGMA Microspheres



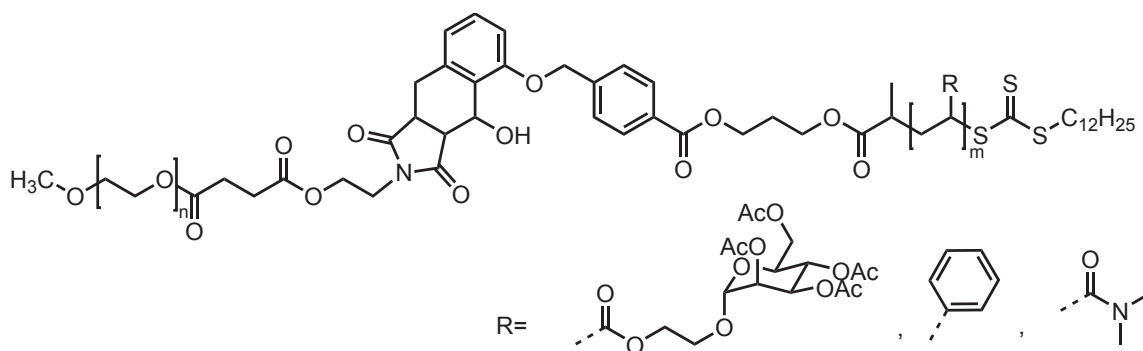
PGMA microspheres (1.24 g, 7.70 mmol, 1.00 equiv of epoxy groups) and 4-(2-hydroxyethyl)-10-oxa-4-azatricyclo-[5.2.1.0^{2,6}]dec-8-ene-3,5-dione (1.61 g, 7.70 mol, 1.00 equiv) were mixed in 1,4-dioxane (100 mL) and $\text{BF}_3 \cdot \text{OEt}_2$ (1.00 mL, 1.13 g, 7.96 mmol, 1.03 equiv) was added. The reaction was shaken at 60 °C over night to attach the protected maleimide to the microspheres and subsequently heated for 7 h to 95 °C for the deprotection of the maleimide. The microspheres were filtered off and washed with 100 mL of distilled water, acetone, THF, DCM and acetone and subsequently dried for two days at 50 °C under vacuum to afford 1.36 g of an off-white powder.

4.4.7 Model Photo-Reaction



PEG-maleimide (M_n approx. $1300 \text{ g} \cdot \text{mol}^{-1}$, 40.0 mg, 0.031 mmol, 1.00 equiv) and DoPATPE (22.6 mg, 0.034 mmol, 1.10 equiv) were dissolved in acetonitrile. Equal volumes of the solution were aliquoted into vials (Pyrex, diameter 20 mm), which were crimped airtight with styrene/butadiene rubber seals; each sample was deoxygenated by purging with nitrogen for 20 min. The vials were irradiated for a predetermined time by rotating around a compact low-pressure fluorescent lamp (Arimed B6, Cosmedico GmbH, Stuttgart, Germany, 36 W) emitting at $320 \text{ nm} \pm 30 \text{ nm}$ at a distance of 40-50 mm in a custom built photo-reactor (refer to Figure A.1 on page 162 for details). After irradiation, the solvent was removed under reduced pressure.

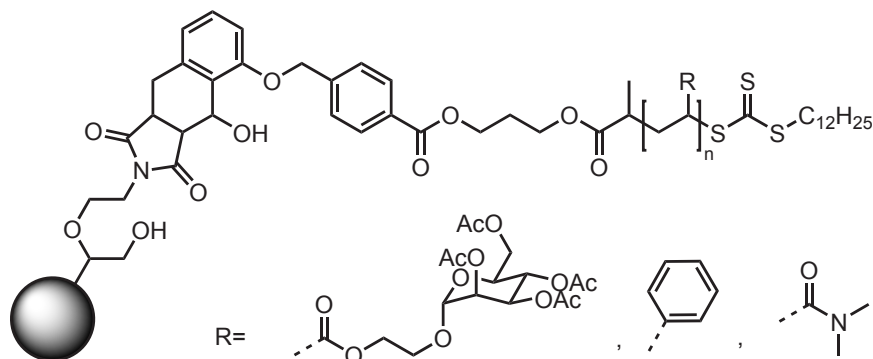
4.4.8 Photo-Induced Block Copolymer Formation



PEG-maleimide (M_n approx. $2300 \text{ g} \cdot \text{mol}^{-1}$) and the RAFT-based polymer (PDMAA, PAcManEA) were dissolved in 8 mL acetonitrile in the case of PDMAA or in 8 mL of a 1:1 mixture of acetonitrile and DCM in the case of PAcManEA, respectively. The mixture was deoxygenated via three consecutive freeze-pump-thaw cycles. In an argon glovebox, the solution was aliquoted into 8 vials (Pyrex, diameter 20 mm), which were crimped airtight with styrene/butadiene rubber seals. The vials were subsequently irradiated under the conditions described above. After irradiation, the solvent was removed under reduced pressure and the residue analyzed via GPC.

For the control reaction, the RAFT-polymer was treated analogous without any addition of PEG-maleimide.

4.4.9 Photo-Induced Grafting Reactions and Control Reaction on Microspheres



The microspheres and DoPATPE or RAFT-polymer, respectively, were mixed in equimolar amounts of their functional groups in DCM (4 mL in the case of DoPATPE, 5 mL in the case of the RAFT-polymers PS, PDMAA, PAcManEA) (refer to Table 4.3 for details). The mixture was deoxygenated with three consecutive freeze-pump-thaw cycles. The Schlenk-tubes were subsequently irradiated for 30 min under the conditions described above. The microspheres were filtered off and washed three times with DCM and dried for two days at 50 °C under vacuum prior to analysis.

Table 4.3: Details and weigh-ins of control and grafting reactions on microspheres employing DoPATPE

type of microspheres (amount)	grafted molecule (amount)
GMA (83.3 mg, 0.45 mmol epoxide)	DoPATPE (80.1 mg, 0.12 mmol photo-enol)
Mal (80.4 mg, 0.12 mmol maleimide)	DoPATPE (81.7 mg, 0.12 mmol photo-enol)
Mal (41.6 mg, 47 μ mol maleimide)	PS (190 mg, 49 μ mol photo-enol)
Mal (26.6 mg, 30 μ mol maleimide)	PAcManEA (190 mg, 19 μ mol photo-enol)
Mal (59.7 mg, 67 μ mol maleimide)	PDMAA (85.2 mg, 33.4 μ mol photo-enol)

4.4.10 Photo-Induced Synthesis of Janus-Particles

Pickering emulsion with paraffin wax

Paraffin wax (melting point 58-60 °C, 1.00 g) and maleimide-functionalized microspheres (100 mg) were heated in an oil bath to 75 °C until the wax was melted. Water (10 mL) was added and the emulsion vigorously stirred at that temperature for 1 h and subsequently

4. Photo-Sensitive RAFT-Agents for Advanced Microparticle Design

for 2 h without heating to reach ambient temperature. The wax spheres were filtered off, washed extensively with distilled water and dried under vacuum.

Photo-Grafting of PDMAA

Wax spheres (diameter approx. 5 μm) – with maleimide-functionalized microspheres embedded on their surface (approx. 7 μm , half covered by wax) (246 mg) – and PDMAA (36.5 mg) were mixed in methanol (5 mL) in a Schlenk-tube. The mixture was deoxygenated via three consecutive freeze-pump-thaw cycles. The Schlenk-tube was subsequently irradiated for 30 min under the conditions described above. The wax spheres were filtered off and subsequently dissolved in CHCl_3 . The microspheres were filtered off, washed with CHCl_3 , twice with DCM and methanol and dried under vacuum.

5

Functionalization of Microspheres with Photo-Reactive RAFT-Polymers Employing NITEC

A RAFT-agent containing a tetrazole was utilized to generate end-functional polystyrene and PDMAA. Under irradiation with UV-light ($\lambda_{\text{max}} = 254 \text{ nm}$) the end groups of the polymers expell molecular nitrogen and form a highly reactive nitrile imine, which can be employed for nitrile imine mediated tetrazole-ene coupling (NITEC).

Maleimide-functionalized porous polymeric microspheres were decorated with the RAFT-polymers employing the light-triggered reaction. As the cycloaddition generates a fluorescent moiety, fluorescent microscopy evidenced a successful reaction. However, other techniques – such as XPS, FT-IR microscopy and elemental analysis – indicated a rather low grafting density.

Further research to find suiting reaction conditions is required and ongoing in the group of the author.

5.1 Introduction

Nitrile imine mediated tetrazole-ene coupling (NITEC) is a very robust light-induced grafting reaction (Section 2.4.1). Of the photo-triggered grafting reactions mentioned in Section 2.4, such as the photo-enol approach, which was employed in the preceding chapter, only NITEC does not require the removal of oxygen. Although in the majority of cases UV-light is utilized to generate the nitrile imine,^[170] NITEC has been employed for many biological conjugations and applications.^[173] In our group the NITEC technique has been utilized to generate spatially resolved light-responsive surfaces^[175] and to pattern antifouling brushes onto PDA layers^[176] as well as polymer strands onto cellulose sheets.^[174] In combination with RDRP techniques, in particular RAFT-polymerization (refer to Section 2.2), NITEC has been applied to conjugate nitrile-butadiene rubber (NBR) chains via UV-light.^[172]

With the exception of the preceding chapter, where the photo-enol technique was applied and thiol-ene coupling employing UV-initiators, no light-induced grafting of RAFT-polymers onto polymeric microspheres has been reported in the literature. Thus, the application of NITEC technology would expand the 'tool-box' for ligations to microspheres with a second photo-triggered reaction.

The general reaction strategy of the current chapter is depicted in Figure 5.1.

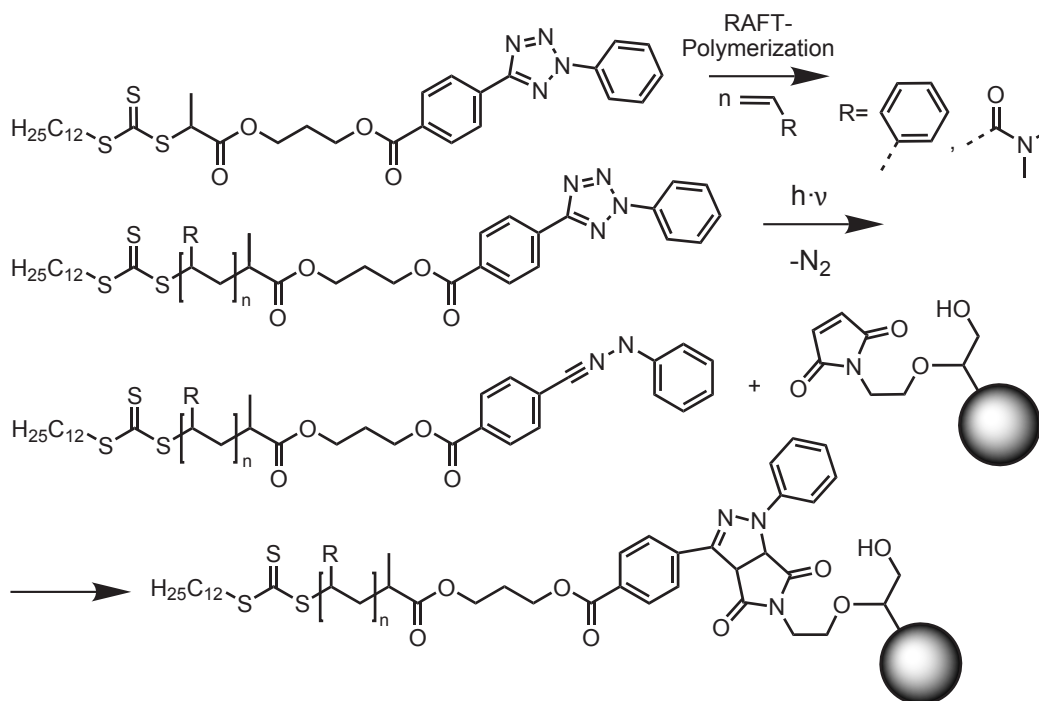


Figure 5.1: General reaction strategy to graft RAFT-polymers onto polymeric microspheres via NITEC.

5.2 Results and Discussion

5.2.1 RAFT-Polymerization

The RAFT-agent entailing a trithiocarbonate and a tetrazole moiety (DoPATTET) utilized in the present chapter has been employed earlier to mediate the polymerization of random copolymers consisting of acrylonitrile and butadiene, also known as nitrile-butadiene rubbers (NBR).^[213] DoPATTET is based on the well-known and widely used trithiocarbonate RAFT-agent 2-((dodecylsulfanyl)carbonothioyl)sulfanyl propanoic acid (DoPAT). In the present work DoPATTET proved its versatility by also polymerizing styrene and *N,N*-dimethylacrylamide in a controlled fashion. The resulting polymers were thoroughly analyzed via GPC, NMR and ESI-MS. The GPC analysis shows monomodal distributions with low polydispersities, well below 1.1 (refer to the Experimental Section 5.4.2 on page 114). NMR analysis reveals that all the resonances associated with the RAFT-agent can be detected, provided they are not covered by resonances associated with the polymeric backbone or its side-chain. In addition, integration and comparison of end group and main chain integrals allows for the determination of (number averaged) molecular weights. The molecular weights obtained from GPC and NMR analysis match very well for polystyrene, resulting in $3000 \text{ g} \cdot \text{mol}^{-1}$ and $2900 \text{ g} \cdot \text{mol}^{-1}$, respectively. In the case of PDMAA the obtained molecular weights differ substantially, i.e., $7000 \text{ g} \cdot \text{mol}^{-1}$ (GPC) and $4750 \text{ g} \cdot \text{mol}^{-1}$ (NMR). The discrepancy in the analytical results from GPC and NMR can readily be explained with the lack of MHKS parameters matching the applied conditions for the analysis of PDMAA, meaning that the PDMAA sample had to be analyzed as a polystyrene sample. An in-depth analysis via ESI-MS reveals that for both polymers only one set of signals can be detected, namely polymeric chains carrying both the R- and Z-group at the chain ends (the theoretical mass of the RAFT-polymer structure (including a sodium ion) is labeled P_{RZ} in Figure 5.12 and 5.15 in the Experimental Section 5.4.2 on page 114). According to Table 5.2 on page 118 the experimentally detected and theoretically expected m/z values match excellently. No other species of polymeric chains are detectable.

The combined analytical results lead to the conclusion that DoPATTET is able to mediate a reversible deactivation radical polymerization (RDRP) according to the RAFT-process resulting in polymers with low dispersities and a high degree of end group functionalization. In addition, the photo-active tetrazole group is not affected by the polymerization conditions.

5.2.2 Microsphere Modification

Microsphere Pre-Functionalization

Under UV-irradiation ($\lambda_{\text{max}} = 254 \text{ nm}$) the tetrazole moiety of the RAFT-agent DoPATTET forms in-situ a nitrile imine, which is an 1,3-dipole able to undergo cycloadditions with suitable dipolarophiles. An often used counterpart in NITEC reactions is the maleimide motif which has also been tethered on the surface of polymeric microspheres before to be used in light-induced reactions (refer to Chapter 4). In this chapter the identical starting material was employed (porous polymeric microparticles based on GMA, 1000 Å porosity) and functionalized with maleimide according to section 4.4.6 on page 96. The functionalized microspheres were analyzed via SEM, elemental analysis and XPS. SEM reveals that the morphology and porosity of the particles is not affected by the reaction (Figure A.29 - A.31 in the Appendix). Analysis of the XPS spectrum reveals an increase in nitrogen. For the non-modified spheres only traces of nitrogen can be found, arising from the radical initiator or stabilizer added during the synthesis of the particles. In contrast, for the functionalized spheres the signal associated with nitrogen shows a small but distinct increase to more than 0.8 at%. Quantifiable information can be obtained from the analysis of the elemental constitution after the functionalization, as elemental analysis – in contrast to XPS – analyzes the entire sample and not only a surface layer. The full EA results of all samples described in the current chapter can be found in Table 5.1 on the opposite page. Again, traces (0.19 wt%) of nitrogen are obtained for the non-modified PGMA-particles. For the maleimide-functionalized particles a clear increase in nitrogen to 0.80 wt% can be observed, which can be converted to a functionalization of around 16 % or one out of six epoxide groups, thus being in the same functionalization range than described in Chapter 4.

Light-Induced Modification of Microspheres

To investigate the ability of functionalizing microspheres with the NITEC technique – especially with the presence of a RAFT-group – a simple grafting reaction and a control reaction were conducted. For the test grafting reaction the maleimide functionalized spheres were suspended in DCM (the choice for the solvent being the similar density to the spheres, leading to an even distribution), DoPATTET was added and the mixture irradiated ($\lambda_{\text{max}} = 254 \text{ nm}$) for 1 h. The NITEC approach does not demand for a deoxygenation of the reaction mixture. For the control reaction, non-modified PGMA particles were utilized instead and subjected to the same reaction conditions (Figure 5.2 on the opposite page).

5. Functionalization of Microspheres with RAFT-Polymers Employing NITEC

Table 5.1: Collected data from the elemental analysis of all samples described in Chapter 5.

Sample	N [wt%] ¹	C [wt%]	H [wt%]	S [wt%] ²	O [wt%] ³	mass balance [wt%]
PGMA	0.19	55.77	6.88	0.00	32.84	95.69
±	0.012	0.260	0.035	0.000	0.259	
Mal	0.80	55.57	7.11	0.00	32.94	98.72
±	0.037	0.591	0.039	0.000	0.208	
DoPATTET	0.75	54.82	7.01	0.11	32.32	97.02
±	0.016	0.060	0.035	0.006	0.599	
Control	0.40	57.88	7.29	0.11	33.04	95.01
±	0.007	0.516	0.142	0.004	0.096	
PS	0.76	55.53	7.03	0.14	32.38	95.84
±	0.020	0.521	0.108	0.003	0.098	
PDMAA	0.82	55.26	7.01	0.17	32.49	95.75
±	0.002	0.519	0.078	0.005	0.458	

¹ The nitrogen found in the untreated microspheres and the control sample can be explained by fragments from the nitrogen containing initiator, stabilizer or gaseous nitrogen trapped in the porous surface morphology of the microspheres.

² Content measured independently, employing a water-trap.

³ Content measured independently.

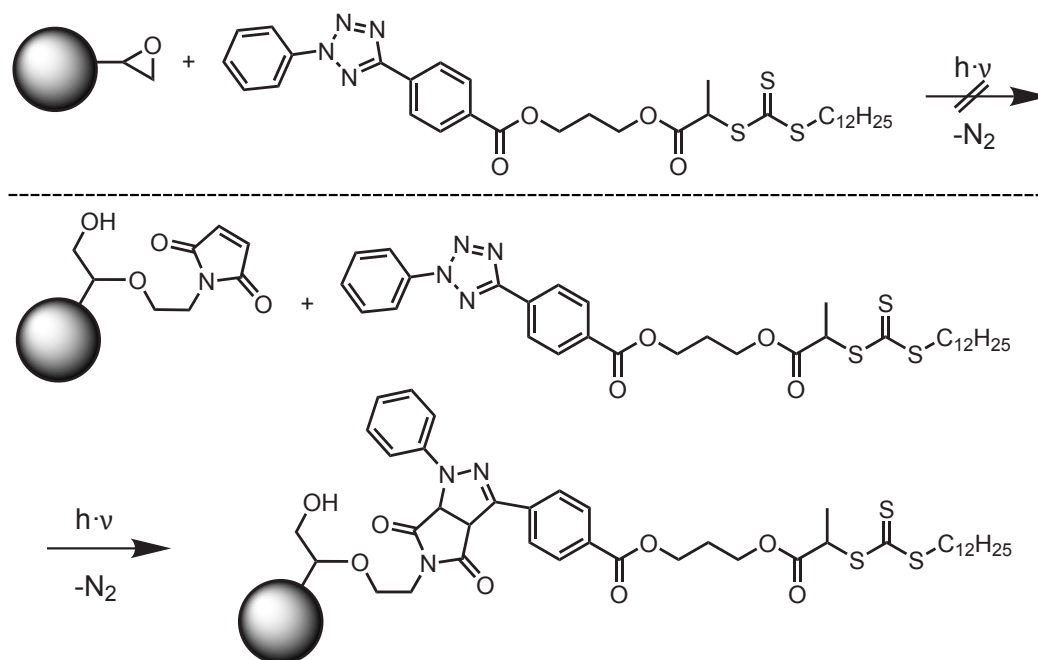


Figure 5.2: Test and control reaction for the UV-induced grafting on microspheres employing DoPATTET.

5. Functionalization of Microspheres with RAFT-Polymers Employing NITEC

The microparticles were filtered off, washed thoroughly and dried prior to analysis. Analysis consisted of SEM, EA, XPS and fluorescence microscopy. The scanning electron microscopy was conducted to confirm the unaltered morphology and porosity of the samples, which can be observed in Figure A.32 - A.34 in the Appendix. SEM imaging proves that although a much harsher light source is needed for NITEC ($\lambda_{\text{max}} = 254 \text{ nm}$), than e.g., for the photo-enol approach ($\lambda_{\text{max}} = 320 \text{ nm}$; refer to Chapter 4), the higher energy of the light does not lead to degradation of the spheres.

The elemental analysis of the test and control reaction are not unambiguous to interpret. The values of interest are the nitrogen and sulfur content after the reaction. Before the reaction the sulfur content in both starting materials was 0.00 wt% and the nitrogen content 0.19 wt% for the non-modified particles and 0.80 wt% for the maleimide-functionalized spheres, respectively. Via a successful grafting sulfur (3 atoms per molecule) as well as nitrogen (2 atoms per molecule) are introduced onto the microspheres. Sulfur can be detected for the test as well as the control sample, even with the same amount: 0.11 wt%. For the control reaction the nitrogen value also increases to 0.40 wt%. In contrast, for the grafting onto the maleimide-functionalized spheres there is no detectable increase in the nitrogen content. In conclusion, the EA results do not show results expected for a successful grafting. The detected change in sulfur and nitrogen value might be associated with a successful reaction, yet they are not sufficiently clear to rule out artifacts or impurities.

The XPS results lead to the same conclusion as elemental analysis. Both samples yield only noise in the region of the spectra where sulfur would give a signal. The spectrum of the control reaction also does not indicate any nitrogen on the sample. For the maleimide-functionalized particles reacted with DoPATTET, there is a signal associated with nitrogen, yet the intensity (0.9 at%) is close to the one obtained from the maleimide-functionalized particles before the light-induced reaction (0.8 at%). Nevertheless, these results can not rule out, that any reaction took place, as the sensitivity of XPS is too low to show positive results for very low reaction conversions.

The microspheres were also analyzed via confocal fluorescence microscopy, as the tetrazole is a profluorescent structure. Profluorescence means that only after the successful reaction the newly formed substituted pyrazoline is fluorescent. Thus, fluorescence is a clear indication for a successful reaction between the nitril imine and the maleimide on the microparticles. Figure 5.3 on the opposite page shows the fluorescence as well as the optical images of the light-induced reaction between DoPATTET and the maleimide-functionalized particles (top) and the control reaction (bottom).

Only the previously functionalized microspheres show fluorescence after the light-induced reaction, although a minority of the particles do not fluoresce. For the non-modified spheres no fluorescence associated with the grafted molecule can be

Light-Induced Reaction with DoPATTET

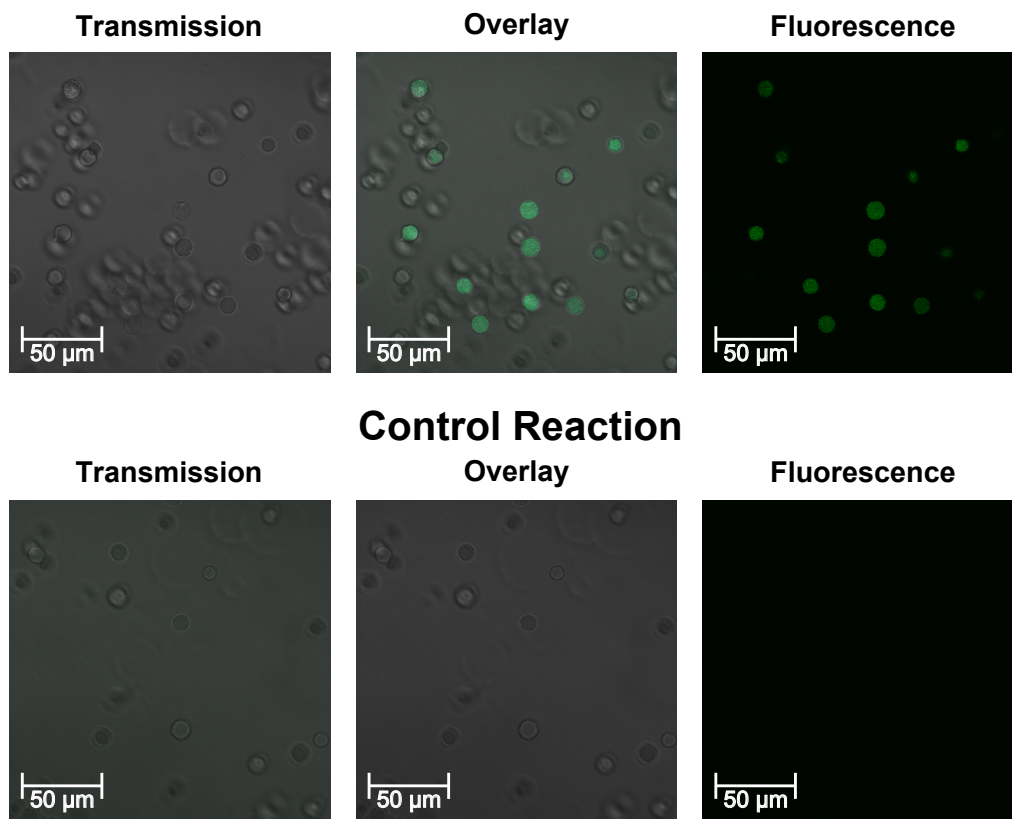


Figure 5.3: Fluorescence microscopy images of the test reaction of the UV-induced grafting on maleimide-functionalized microspheres employing DoPATTET (top) and the control reaction between DoPATTET and non-modified PGMA microspheres (bottom).

detected. The blurry circular structures that can be observed in the optical images as well are microspheres that are out of the focal plane of the microscope and thereby also not hit by the exciting laser beam. Since they are not excited by the laser, they do not show fluorescence even for the test reaction, where for most excited particles fluorescence can be observed. In fact, the results of fluorescence microscopy do indicate a successful NITEC reaction, which is only occurring between the photo-activated nitril imine and the maleimide moieties on the surface of the particles.

In summary, the analytical results lead to the conclusion that the reaction was successful, especially because of the occurring fluorescence. The other analytical techniques – such as XPS and EA – on the other hand, indicate that the reaction occurs only to a minor extent, compared to the photo-enol approach discussed in Chapter 4.

5. Functionalization of Microspheres with RAFT-Polymers Employing NITEC

Light-Induced Grafting of RAFT-Polymers onto Microspheres

The light-induced grafting of RAFT-polymers (PS and PDMAA) onto the maleimide-functionalized microspheres was conducted analogously as the test reaction described above. The microspheres and the RAFT-polymers were mixed in DCM and the reaction mixture irradiated for 1 h at $\lambda_{\text{max}} = 254$ nm without prior deoxygenation (Figure 5.4). After the reaction the microparticles were filtered off, washed thoroughly and dried prior to analysis.

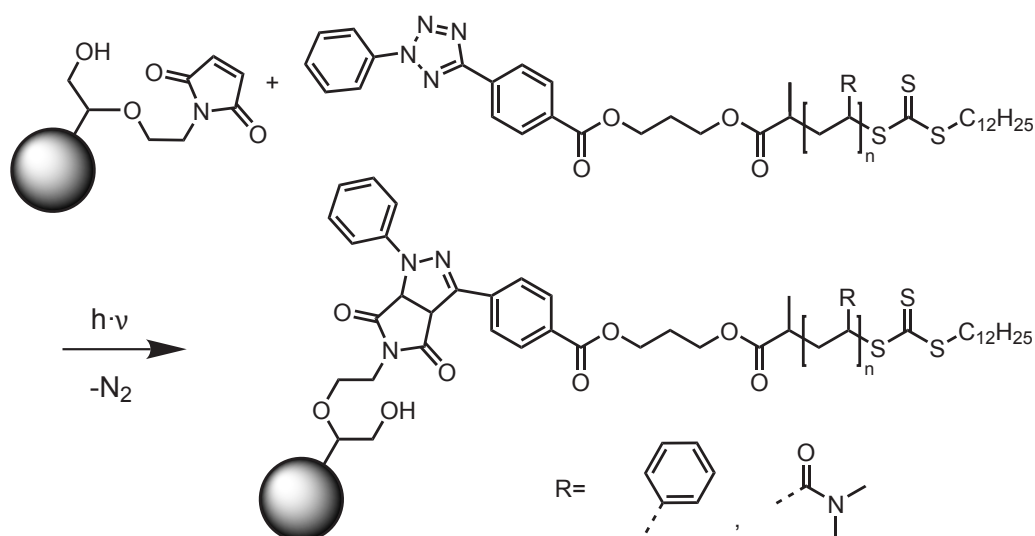


Figure 5.4: Light-induced grafting of RAFT-polymers onto maleimide-functionalized microspheres employing NITEC.

The analysis consisted of SEM, XPS, EA, confocal fluorescence microscopy and – in the case of grafted-on PDMAA – ATR IR-microscopy. The SEM analysis is primarily conducted to verify that the spherical morphology and porosity are not altered by the reaction, since no chemical information can be gained by SEM imaging. Figure A.35 to A.40 in the Appendix show that the morphology as well as the porosity are not altered. XP spectroscopy gives chemical information about the samples. For spheres grafted with polymer each sample gives a signal that can be associated with nitrogen (Figure 5.5 on the opposite page).

For grafted-on polystyrene integration of the signal yields 0.7 at%, which is approximately the same value as after the maleimide-functionalization, although a successful grafting leads to an incorporation of two nitrogen atoms per chain. For the reaction with PDMAA a slight increase in the nitrogen content to 1.1 at% can be detected. With nitrogen present in the repeating unit of the polymer as well as in the chain end, a more distinct increase is expected to take place, and has been detected in the photo-grafting of PDMAA onto microparticles before (Chapter 4).

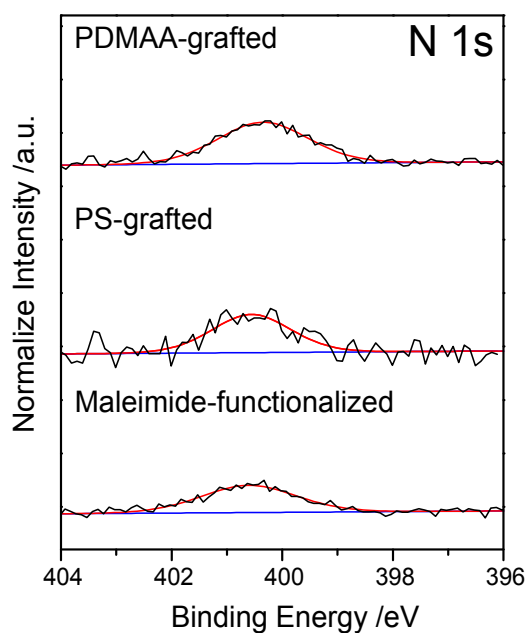


Figure 5.5: N 1s XPS spectra of maleimide functionalized PGMA particles (bottom) and microspheres photo-grafted with PS (middle) and PDMAA (top). The nitrogen content does not increase significantly due to the photo-grafting.

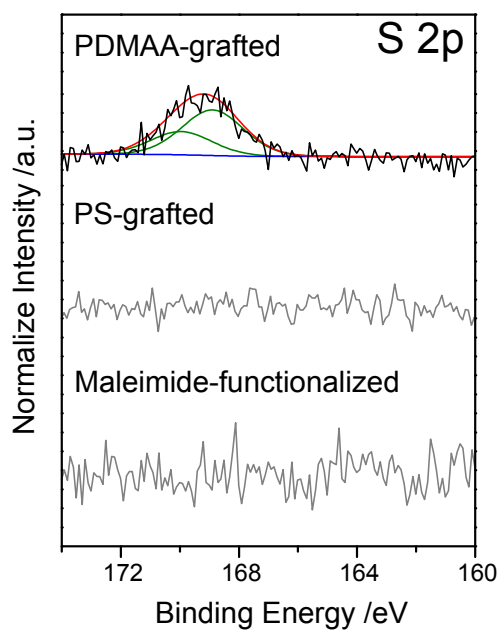


Figure 5.6: S 2p XPS spectra of maleimide functionalized PGMA particles (bottom) and microspheres photo-grafted with PS (middle) and PDMAA (top). Traces of sulfur can only be detected for the particles grafted with PDMAA.

5. Functionalization of Microspheres with RAFT-Polymers Employing NITEC

In the case of grafted-on PS, the spectra only gives noise in the area associated with sulfur (Figure 5.6 on the previous page). On the other hand, for the sample with grafted-on PDMAA traces of sulfur can be detected (0.3 at%), showing an oxidized sulfur species that have been observed via XPS analysis of grafted RAFT-polymers before.^[144]

The C 1s peak could be deconvoluted to several signals stemming from chemically different carbon species – differentiated by amount of bonds and kind of atoms they are bound to – to give insight if a grafting reaction was succesful (refer to Chapter 4). In the present study, this approach does not lead to any further insights as the changes are within the error margin of the analytical method and do not show any trend that would be expected by the grafting of polymeric chains.

The analysis of the elemental constitution of the samples after the grafting of the polymers gives no further insights. The nitrogen content is nearly unaltered for the PS sample (0.76 wt%) and the increase for grafted-on PDMAA (with nitrogen contained in the repeating unit) is neglectible (0.82 wt%). Sulfur can be found for both samples, reaching 0.14 wt% for grafted PS and 0.14 wt% for PDMAA, respectively. Since the EA results are inconclusive, no determination of loading capacities or grafting densities was conducted employing the EA data. Further analysis of the the EA results, such as investigating the ratio of oxygen to carbon, does not show a trend that would match the expectations for the conducted grafting reactions.

With a succesful grafting of PDMAA amide moities are introduced onto the particles. Since these amide groups have a vibration that can be distinguished from the ester vibration inherent by the PGMA the particles consist of, FT-IR-microscopy can be employed to visualize the success, spatial distribution and intensity of the grafting (Chapter 4). The ATR FT-IR-microscopy results for the UV-induced grafting of PDMAA onto microparticles employing NITEC is shown in Figure 5.7 on the opposite page. By mapping the ester stretching vibration the shape of the microsphere can be depicted, with the highest degree of functionalization in the middle of the particle. The mapping off the amide band on the other hand only results in noise for the maleimide-funtionalized sphere as well as for the one reacted with PDMAA. In the present study ATR IR-microscopy can not show that PDMAA was grafted onto the spheres, at least not to an extent detectable with this kind of analytical setup and data processing.

5. Functionalization of Microspheres with RAFT-Polymers Employing NITEC

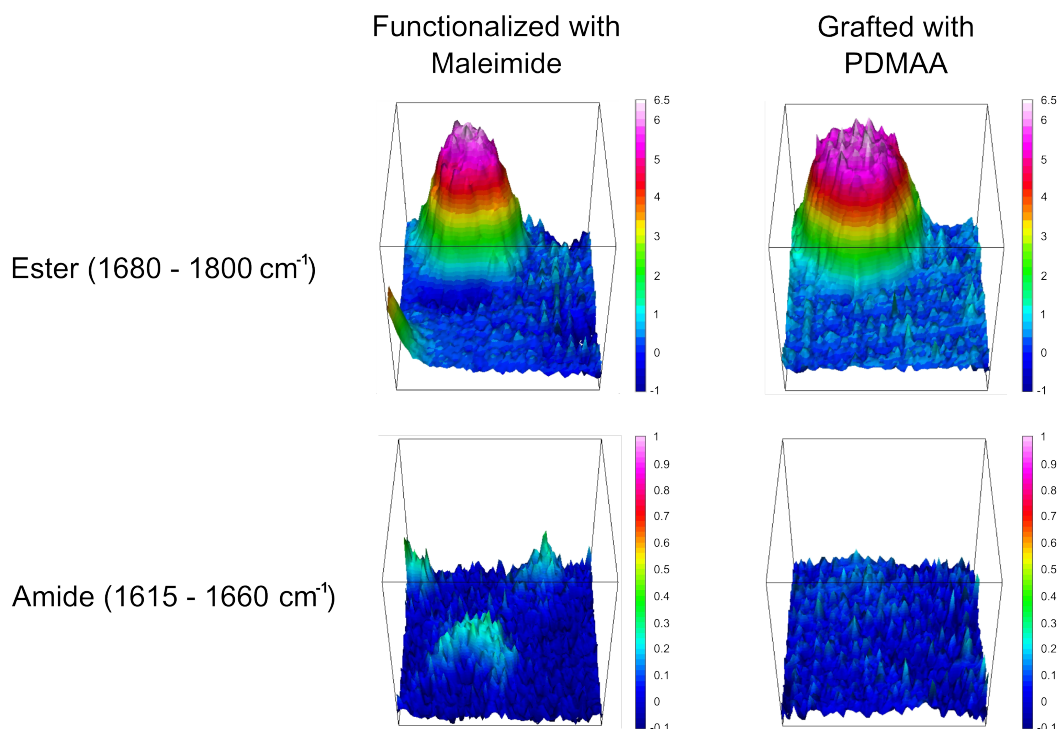
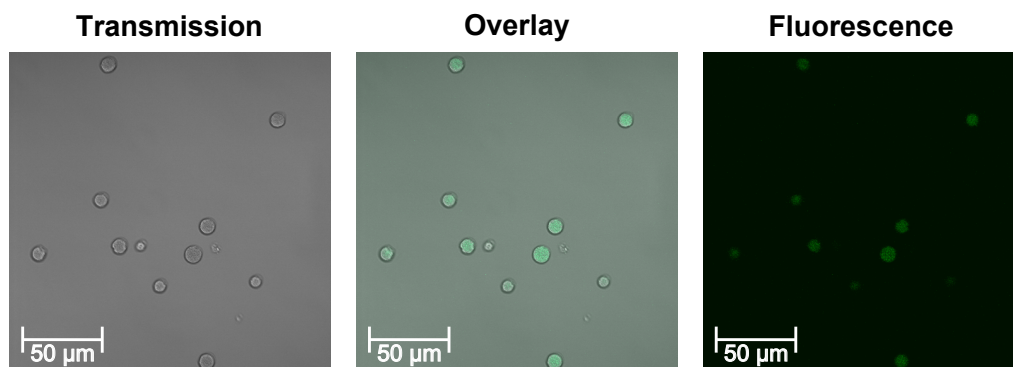


Figure 5.7: False color high resolution FT-IR-microscopy images (4 cm^{-1} spectral resolution with a pixel resolution of $0.25\text{ }\mu\text{m}^2$) of a GMA microsphere functionalized with maleimide and after UV-grafting of PDMAA. The measured area is $32\text{ }\mu\text{m} \times 32\text{ }\mu\text{m}$. Red color corresponds to a high degree of functionalization. In the top row, the intensity of bands corresponding to the O–C=O stretching vibration is visualized, in the bottom row the N–C=O bands.

In contrast to the above mentioned results, fluorescence microscopy gives a positive result for the grafting reactions. For both grafted polymers fluorescence can be detected on the microspheres after the UV-induced grafting reaction (Figure 5.8 on the next page), which can only be explained with fluorescent pyrazoline being formed by the grafting.

Compared to the test reaction, where DoPATTET was grafted onto the spheres, almost no particles do not show any fluorescence. Similar to the above described test and control reaction, fluorescence microscopy delivers the only clear indication of a successful grafting reaction. Since fluorescence microscopy exhibits – of the employed analysis techniques – the highest sensitivity it is likely that with the applied reaction conditions the conversion of the reaction is too low to be detected with the other analytical techniques. Degradation of the polymeric chains, which could also explain some of the results, can be ruled out. PDMAA, which was recovered after the UV-induced grafting reaction, was analyzed via ESI-MS. The spectra of the PDMAA before and after the reaction look identical and no new signals that could be associated with degradation or other side reactions can be detected (Figure 5.9 on page 113).

Light-Induced Grafting of PS



Light-Induced Grafting of PDMAA

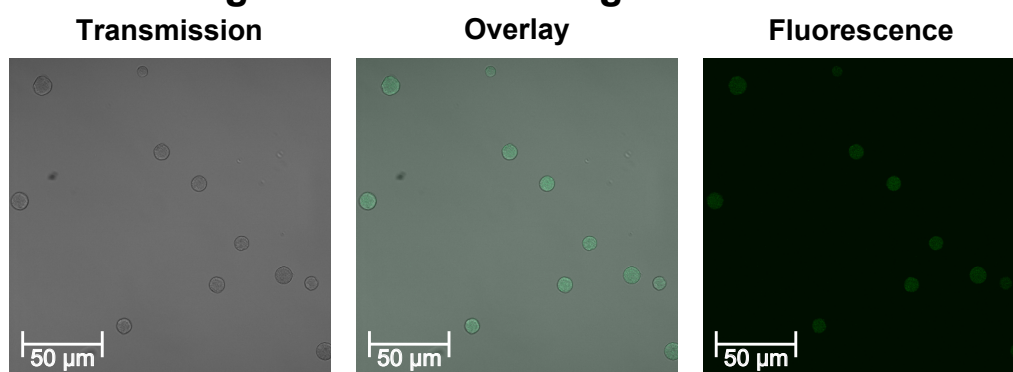


Figure 5.8: Fluorescence microscopy images of the UV-induced grafting of PS (top) and PDMAA (bottom) on maleimide-functionalized microspheres employing NITEC.

NITEC has proven before to be an easy to use and versatile tool to modify various surfaces, such as silicone wafers,^[175] cellulose,^[174] and poly(dopamine) interfaces.^[176] The main difference in the present work is that – in contrast to the aforementioned examples – the tetrazole was not placed on the surfaces, yet on the to-be grafted molecules. The author is optimistic that with the current approach NITEC can also be employed to graft RAFT-polymers onto microparticles with better yields as soon as the correct reaction conditions concerning reaction time, intensity and wavelength of the light source as well as concentrations are identified.

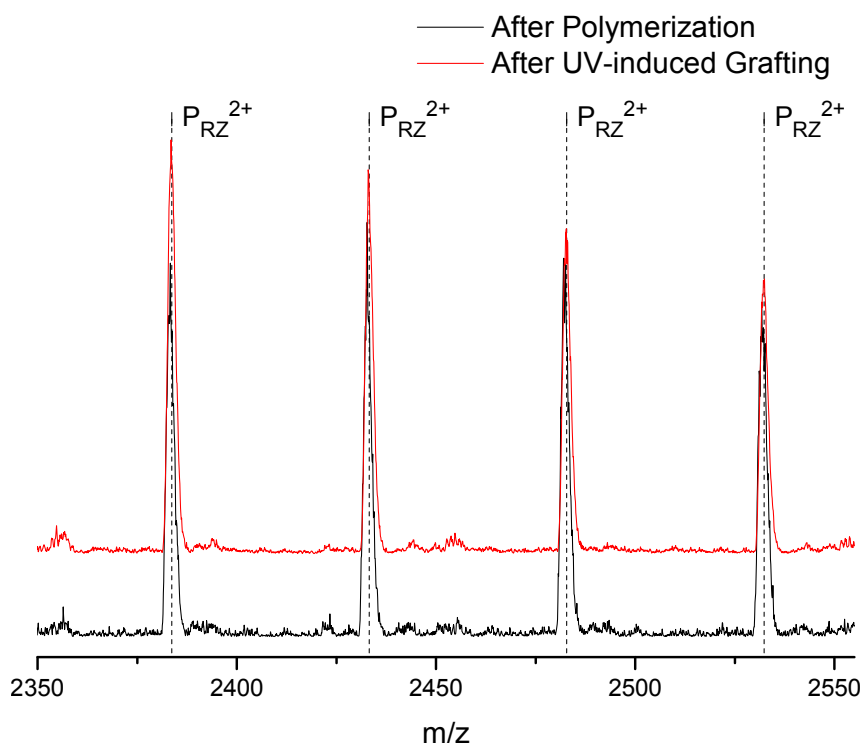


Figure 5.9: Comparison of the spectra of poly(*N,N*-dimethylacrylamide) polymerized with DoPATTET before and after the UV-induced grafting reaction. The label P_{RZ}^{2+} indicates the theoretical average mass to charge ratio of chains with the R- and Z-group of the RAFT-agent as end groups, ionized with two Na^+ (stemming from added NaTfa). No change is observable.

5.3 Conclusions

In the present chapter it was demonstrated that the UV-active RAFT-agent DoPATTET is able to promote the controlled polymerization of styrene and *N,N*-dimethylacrylamide with low polydispersities ($D < 1.1$) and a high end group fidelity. Polymeric microspheres were successfully equipped with an dipolarophilic counterpart for an UV-induced NITEC ligation (maleimide moieties), which could be proven via XPS as well as EA. As an profluorescent motif is grafted onto the spheres, confocal fluorescence microscopy demonstrates that the grafting reactions were successful. Other analytical results – such as XPS, IR-microscopy, and elemental analysis – indicate that the achieved grafting is unexpectedly low. Further investigations leading to better reaction conditions are expected to generate microparticles with a higher degree of grafting.

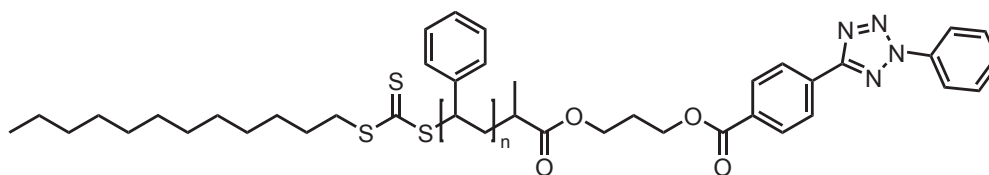
5.4 Experimental Part

5.4.1 Materials

Tetrazole-functional RAFT-agent (DoPATTET)^[213] was synthesized according to the literature. 2,2'-Azobis(2-methylpropionitrile) (AIBN) was recrystallized twice from methanol and stored at -19 °C. Styrene and *N,N*-dimethylacrylamide (DMAA) were passed through a column of basic alumina to remove inhibitor and subsequently stored at -19 °C. Dichloromethane (DCM) was dried and stored over CaCl₂. Poly(glycidyl methacrylate) (PGMA) microspheres with a PGMA content of 80 % and pore size of 1000 Å were synthesized by Polymer Standards Service (PSS) GmbH and functionalized with maleimide moieties as described in Section 4.4.6 on page 96 or Reference [214]. All other chemicals were used as supplied by the manufacturers.

5.4.2 RAFT-Polymerizations

Synthesis of Polystyrene (PS)



A solution of AIBN (4.0 mg, 0.026 mmol, 0.09 equiv) and DoPATTET (171.8 mg, 0.26 mmol, 1.00 equiv) in styrene (2.98 g, 28.5 mmol, 109 equiv) was deoxygenated with four consecutive freeze-pump-thaw cycles. The reaction was placed into a preheated oil-bath at 60 °C for 14 h. The reaction was stopped by cooling in an ice-bath and exposing the reaction mixture to oxygen. The remaining styrene was removed via evaporation at ambient conditions and the polymer isolated via precipitation in cold methanol and subsequent drying under vacuum to afford 674 mg of a slightly yellow powder. Conversion = 31 % (gravimetry); $M_n = 3000 \text{ g} \cdot \text{mol}^{-1}$, $D = 1.08$ (GPC in THF, polystyrene calibration); $M_n = 2900 \text{ g} \cdot \text{mol}^{-1}$ (NMR, comparison of the integrals between 8.40 - 8.10 ppm and 7.30 - 6.25 ppm).

5. Functionalization of Microspheres with RAFT-Polymers Employing NITEC

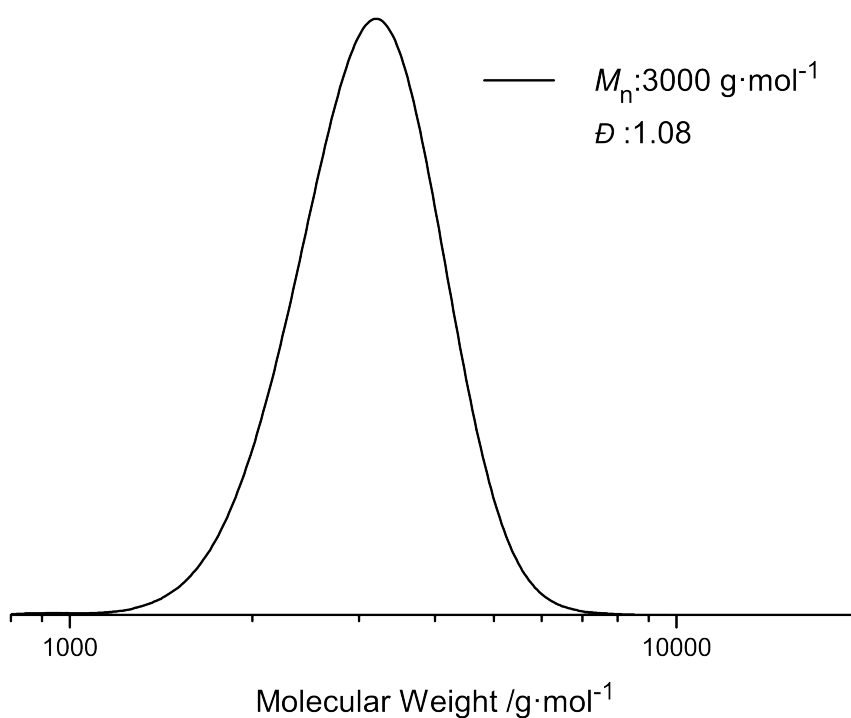


Figure 5.10: GPC trace in THF (PS calibration) of polystyrene polymerized with DoPAT-TET.

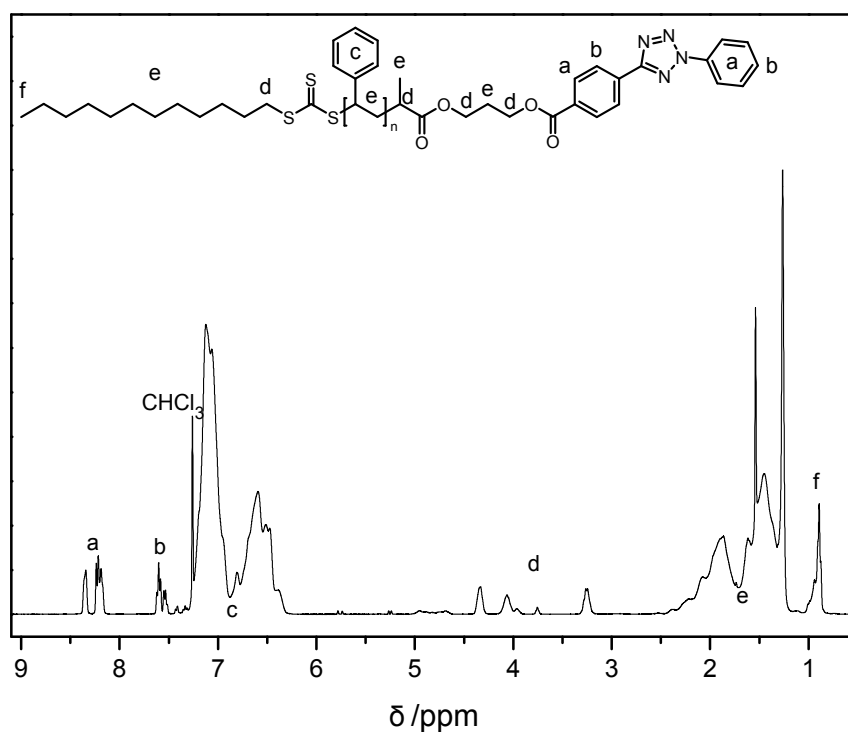


Figure 5.11: ^1H -NMR spectrum of polystyrene polymerized with DoPAT-TET in CDCl_3 at 400 MHz. Comparison of repetition unit resonance integrals (c, 7.30 - 6.25 ppm) to end group resonance integrals (a, 8.40 - 8.10 ppm) results in $M_n = 2900 \text{ g} \cdot \text{mol}^{-1}$.

5. Functionalization of Microspheres with RAFT-Polymers Employing NITEC

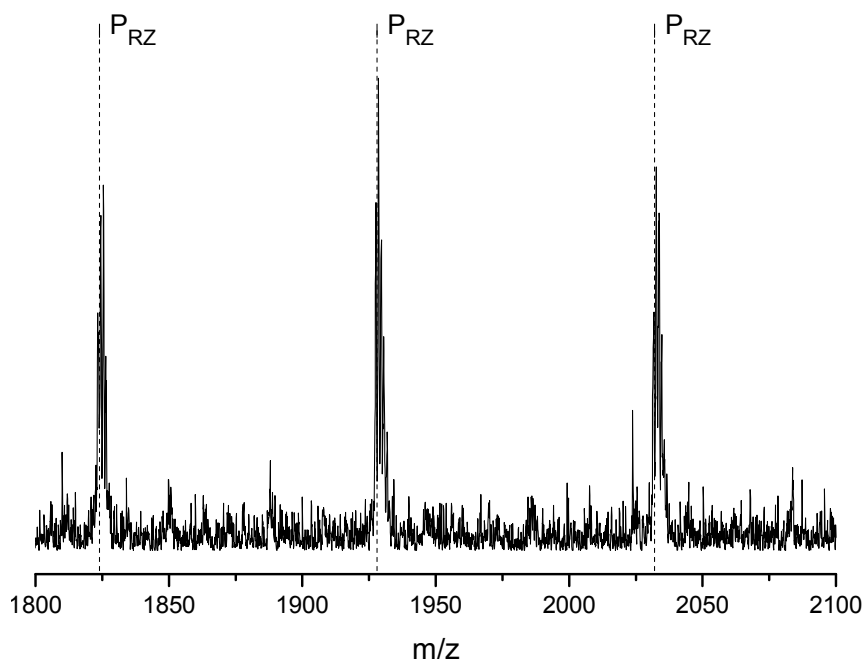
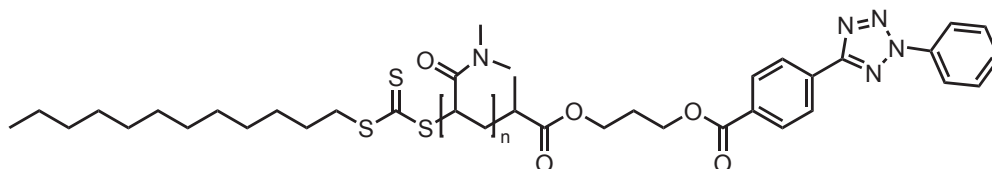


Figure 5.12: Zoom into the ESI-MS spectrum of polystyrene polymerized with DoPAT-TET. The label P_{RZ} indicates the theoretical mass of chains with the R- and Z-group of the RAFT-agent as end groups, ionized with Na^+ (stemming from added NaTfa).

Synthesis of Poly(*N,N*-dimethylacrylamide) (PDMAA)



A solution of AIBN (9.7 mg, 0.060 mmol, 0.20 equiv), DoPATPAS (194,8 mg, 0.30 mmol, 1.00 equiv) and DMAA (1.47 g, 14.8 mmol, 50 equiv) in DMF (7.5 mL) was deoxygenated with four consecutive freeze-pump-thaw cycles. The reaction was placed into a preheated oil-bath at 60 °C for 3 h. The reaction was stopped by cooling in an ice-bath and exposing the reaction mixture to oxygen. The polymer was isolated by dialyzing the reaction mixture against distilled water (utilizing a SpectraPor3 membrane (MWCO = 500 Da)) and subsequent freeze drying to afford 787 mg of a yellow solid. $M_n = 7000 \text{ g} \cdot \text{mol}^{-1}$, $D = 1.06$ (GPC in dimethylacetamide (DMAc), polystyrene calibration); $M_n = 4750 \text{ g} \cdot \text{mol}^{-1}$ (NMR, comparison of the integrals between 8.30 - 8.10 ppm and 3.15 - 2.60 ppm).

5. Functionalization of Microspheres with RAFT-Polymers Employing NITEC

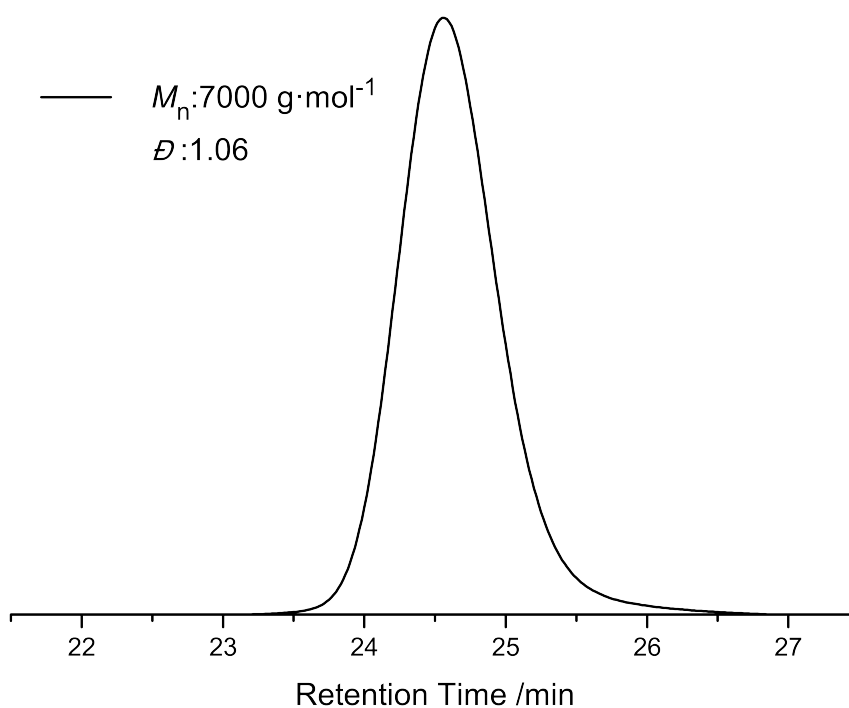


Figure 5.13: GPC trace (PS calibration) in DMAc of poly(*N,N*-dimethylacrylamide) polymerized with DoPATTET.

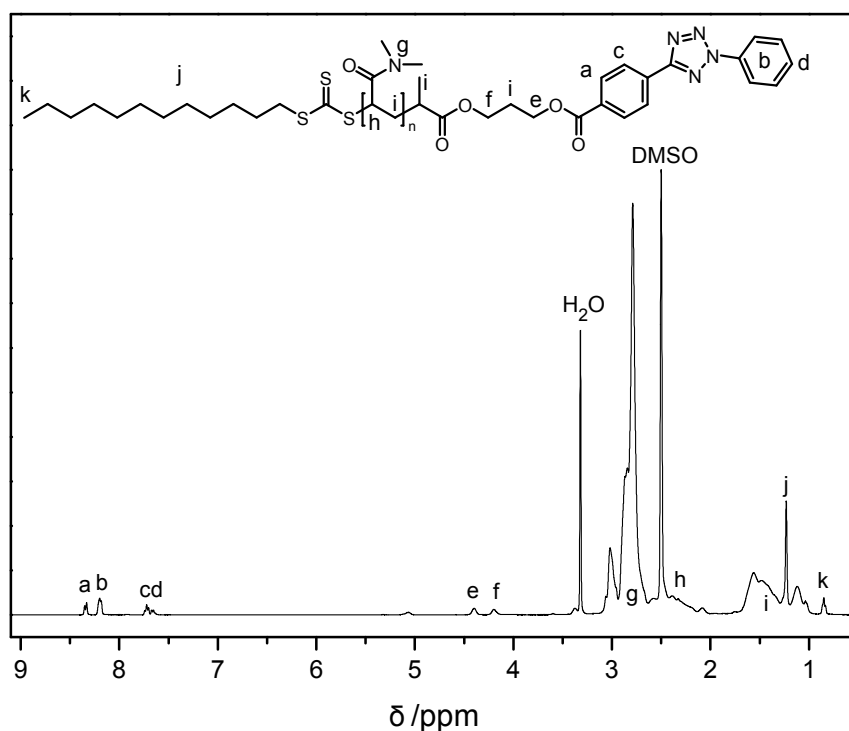


Figure 5.14: ^1H -NMR spectrum of poly(*N,N*-dimethylacrylamide) polymerized with DoPATTET in $\text{DMSO}-d_6$ at 400 MHz. Comparison of repetition unit resonance integrals (g, 3.15 - 2.60 ppm) to end group resonance integrals (b, 8.30 - 8.10 ppm) results in $M_n = 4750 \text{ g}\cdot\text{mol}^{-1}$.

5. Functionalization of Microspheres with RAFT-Polymers Employing NITEC

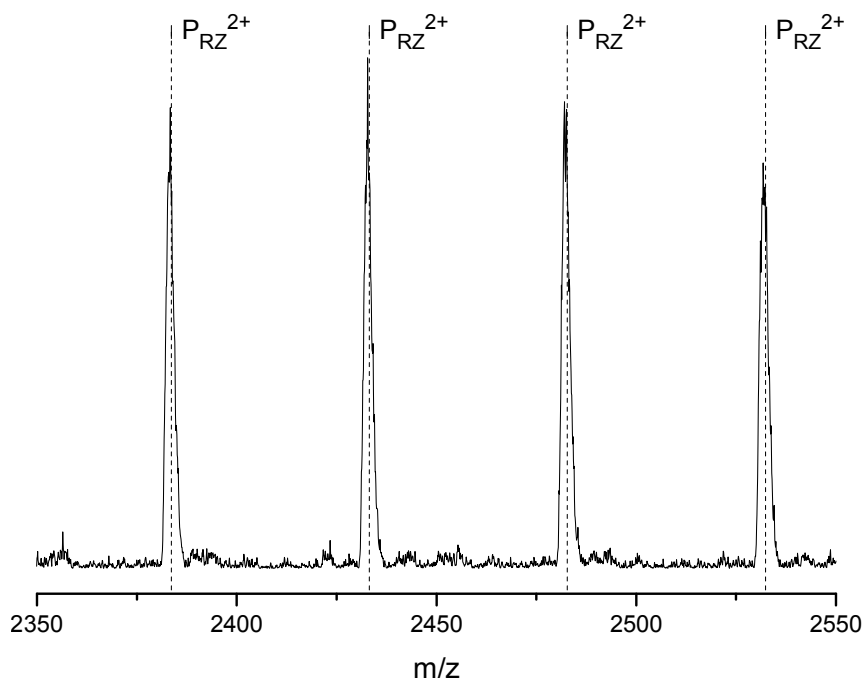


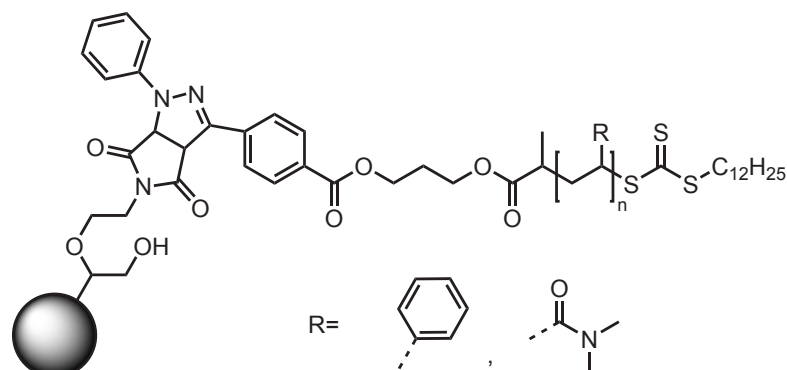
Figure 5.15: Zoom into the ESI-MS spectrum of poly(*N,N*-dimethylacrylamide) polymerized with DoPATTET. The label P_{RZ}^{2+} indicates the theoretical average mass to charge ratio of chains with the R- and Z-group of the RAFT-agent as end groups, ionized with two Na^+ (stemming from added NaTfa).

Table 5.2: Experimental and theoretical m/z values for the labeled peaks in Figure 5.12 and Figure 5.15. For the single charged ions the base peak was analyzed. For the double charged peaks the averaged molecular weight was employed, since the resolution is too low to show single isotopic peaks in this mass region.

m/z_{exp}	assignment	formula	m/z_{theo}	$\Delta m/z$
1928.00	PS ₁₂	$[C_{129}H_{140}N_4O_4S_3Na]^+$	1927.99	0.01
2433.1	PDMAA ₄₂	$[C_{243}H_{422}N_{46}O_{46}S_3Na_2]^{2+}$	2433.2	0.1

5.4.3 Photo-Reactions

Grafting Reactions and Control Reaction on Microspheres



The microspheres and DoPATTET or RAFT-polymer, respectively, were mixed in DCM (5 mL) in glass vials (Pyrex, diameter 20 mm), which were crimped with styrene/butadiene rubber seals (refer to Table 5.3 for details). The vials were subsequently irradiated for 60 minutes by rotating around a compact low-pressure fluorescent lamp (Osram Puritec HNS, $\lambda_{\max} = 254$ nm) at a distance of 40-50 mm in a custom built photo-reactor (refer to Figure A.1 on page 162 for details). The microspheres were filtered off and washed three times with DCM and dried for four days at 50 °C under vacuum prior to analysis.

Table 5.3: Details and weigh-ins of control and grafting reactions on microspheres employing DoPATTET

type of microspheres (amount)	grafted molecule (amount)
GMA (100.4 mg, 0.54 mmol epoxide)	DoPATTET (101.6 mg, 155 μ mol tetrazole)
Mal (99.9 mg, 157 μ mol maleimide)	DoPATTET (101.6 mg, 155 μ mol tetrazole)
Mal (80.1 mg, 126 μ mol maleimide)	PS (365.9 mg, 126 μ mol tetrazole)
Mal (60.0 mg, 95 μ mol maleimide)	PDMAA (444.9 mg, 95 μ mol tetrazole)

6

Photo-Induced Functionalization of Spherical and Planar Surfaces via Caged Thioaldehyde End-Functional Polymers

A novel RAFT-agent containing a photo-caged thioaldehyde was synthesized and employed for the controlled generation of various end-functional RAFT-polymers, including a glycopolymer, which was evidenced via SEC, NMR and ESI-MS. Porous, polymeric, and cyclopentadiene-functionalized microspheres were grafted with the aforementioned polymers utilizing the light-induced cycloaddition ($\lambda_{max} = 355 \text{ nm}$). The successful tethering of the polymeric chains was evidenced via SEM, XPS and IR-microscopy as well as quantitatively analyzed via elemental analysis. Grafting densities up to $0.10 \text{ molecules} \cdot \text{nm}^{-2}$ were reached.

Thioaldehydes are able to react with nucleophiles as well, thus surfaces coated with poly(dopamine) – which contains nucleophilic amine groups – were decorated in a spatially controlled manner with polymer chains via a two-dimensional direct laser writing process. The successful patterning was imaged via ToF-SIMS.

Parts of this chapter were reproduced from M. Kaupp, A. S. Quick, C. Rodriguez-Emmenegger, A. Welle, V. Trouillet, O. Pop-Georgievski, M. Wegener, C. Barner-Kowollik, *Adv. Funct. Mater.* **2014**, DOI: 10.1002/adfm.201400609 with permission from John Wiley & Sons.

6.1 Introduction

Photo-generated thioaldehyde ligation (Section 2.4.3) is the third and last light-induced grafting reaction employed in the current thesis. Compared to the two aforementioned reactions, i.e., photo-enol ligation (Chapter 4) and NITEC (Chapter 5), thioaldehydes can be generated with the least energetic light ($\lambda_{max} = 355 \text{ nm}$) and are the most versatile functional group as they can undergo [4+2] cycloadditions with dienes^[19] as well as react with nucleophiles.^[184] Both reaction paths have been applied in our group to photo-pattern a (phenacylthio)acetic acid-functionalized silicon wafer employing a shadow mask. Furthermore, the thioaldehyde-precursor (phenacylthio)acetic acid can readily be synthesized from commercially available, low cost materials (2-chloroacetophenone and mercaptoacetic acid) via a nucleophilic reaction in just one facile step.^[183] The combination of the previously described properties and the ubiquity of nucleophilic groups makes the thioaldehyde-approach the most versatile light-induced ligation chemistry.

Thioaldehyde-ligation has not been combined with RDRP techniques, e.g., RAFT-polymerization (Section 2.2), before. Such a combination would allow a vast variety of polymer classes – including glycopolymers (Section 2.3) – to be generated and subsequently grafted onto various surfaces. Possible substrates for grafting include (porous) polymeric microspheres (Section 2.1), which would generate functional core-shell particles.

Moreover, poly(dopamine) (PDA) coated surfaces are highly interesting substrates. PDA films are inspired by mussel adhesives and can adhere to virtually any surface^[215] after formation via spontaneous polymerization of dopamine in aqueous solution.^[216,217] PDA has been employed as a linking layer for antifouling polymer brushes prepared by 'grafting-from'^[176,217] and 'grafting-to' techniques.^[215,218,219] In addition, surfaces coated with PDA are remarkable substrates for the adhesion of cells.^[220,221] PDA exhibits amine groups that can be utilized for functionalization with moieties allowing for thermally-induced^[222] as well as light-triggered^[176,181] ligation reactions for polymers prior or subsequent to the surface coating.

Direct laser writing (DLW) is a versatile two-photon lithographic technique for the fabrication of structures and devices on the micrometer scale by utilizing a precisely moveable sample holder and a tightly focused laser beam.^[223–226] The main focus and strength of DLW is the generation of three-dimensional objects, however the experimental setup also enables photo-induced modification and patterning of device surfaces, e.g., via the photo-enol technique.^[227] By applying light as a reaction trigger, various photo-chemical processes (Section 2.4) can be employed for the spatially controlled modification and patterning of surfaces with sub-micrometer resolution. In addition, the number of potential

6. Photo-Induced Functionalization of Surfaces via Caged Thioaldehyde Polymers

photochemical systems is highly increased by the opportunity to tune the wavelength of the laser beam.

The study in the current chapter combines – for the first time – the photo-triggered thioaldehyde ligation reaction with RAFT-polymerization, thus allowing for the light-triggered tethering of any polymer, which is polymerizable in combination with the novel RAFT agent, onto surfaces carrying a diene or nucleophilic moiety, such as porous polymeric microspheres functionalized with cyclopentadiene and surfaces coated with PDA. Moreover, by combination with a DLW setup any two-dimensional pattern can be grafted onto PDA coated surfaces with submicrometer resolution. In summary, the combination of RAFT-polymerization, light-triggered thioaldehyde ligation, and DLW opens the door for immobilizing a wide variety of polymeric structures in any micrometer resolved pattern to virtually every surface.

6.2 Results and Discussion

6.2.1 Photo-RAFT-Agent Design

The design and synthesis of the novel photo-reactive RAFT-agent containing a phenacyl sulfide follows a similar synthetic rationale than previously selected for the synthesis of a RAFT-agent that carries a photo-enol moiety (Section 4.4.3 and reference [214]). It is based on 2-((dodecylsulfanyl)carbonothioyl)sulfanyl propanoic acid (DoPAT), a commonly used trithiocarbonate, which can be readily equipped with a small spacer containing an alcohol function. The alcohol moiety can subsequently be used in a simple Steglich-esterification^[202] to attach a phenacyl sulfide (Figure 6.1).

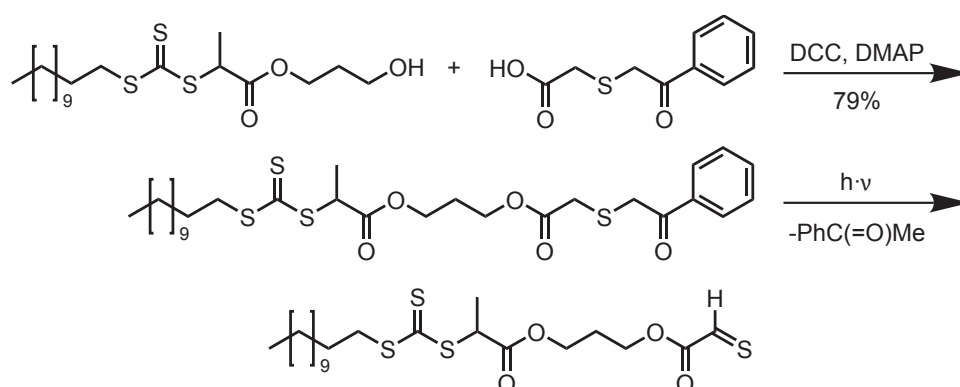


Figure 6.1: Synthesis and reactivity of the novel photo-reactive RAFT-agent DoPATPAS.

Under UV-irradiation ($\lambda_{max} = 355$ nm) the phenacyl sulfide undergoes photolysis and forms acetophenone and a thioaldehyde which can react with nucleophiles and dienes

6. Photo-Induced Functionalization of Surfaces via Caged Thioaldehyde Polymers

(for the UV-Vis spectra of DoPATPAS refer to Figure 6.16 in the Experimental Section 6.4.2 .^[19,183,184]

The trithiocarbonate group should be stable under the applied irradiation conditions.^[203,204] Nevertheless to prevent any side reaction leading to degrafting of the photo-ligated chains, the photo-reactive group is attached to R-group of the RAFT-agent. Thus, if any degradation of the Z-group (trithiocarbonate) occurs, the thioaldehyde is still attached to the polymeric chain. The attachment of the photo-reactive group to the R-group renders the novel photo-reactive RAFT-agent thus also suitable for applications demanding harsher reaction conditions, such as intensive UV-light, amines or high temperatures.

6.2.2 RAFT-Polymerization

In order to evidence that the attachment of the phenacyl sulfide does not influence the ability of the RAFT-agent to mediate a radical polymerization process, several RAFT-polymerizations were conducted utilizing the aforementioned RAFT-agent. The versatility and robustness of the approach is demonstrated by choosing rather different and partially challenging (functional) monomers: styrene, dimethylacrylamide and a protected glycomonomer 2-(2',3',4',6'-tetra-*O*-acetyl- β -D-mannosyloxy) ethylacrylate (AcManEA). The polymerizations were carried out in bulk as well as in solution and were thoroughly analyzed via NMR, GPC and ESI-MS. The NMR analysis reveals that the resulting polymers still carry both of the RAFT-end groups and can be fully isolated from non-reacted monomer (Figure 6.18, 6.21, and 6.24 in the Experimental Section 6.4.3). The GPC traces (Figure 6.17, 6.20, and 6.23 in the Experimental Section 6.4.3) show a monomodal distribution and low dispersities (below 1.1 for polystyrene and PDMAA, 1.2 for PAcManEA, which was polymerized to a higher conversion to achieve a molecular weight that results in a polymer that can be isolated via precipitation). The small shoulder at higher retention times in the case of PAcManEA indicates some termination or transfer side products, which are probably due to the higher conversion which is required to prepare longer chains.

The number average molecular weights derived from GPC and NMR analysis match in the case of polystyrene, yet differ for PDMAA and PAcManEA, where the NMR-analysis results in higher molecular weights. The difference can be readily explained, as all samples were analyzed with the MHKS parameters for styrene (direct calibration), since there are no parameters listed in the literature for the other polymers at the employed conditions.

The analysis via ESI-MS further underlines the controlled behavior of the polymerization as the spectra show almost exclusively signals which belong to polymeric chains carrying

6. Photo-Induced Functionalization of Surfaces via Caged Thioaldehyde Polymers

the Z- as well as the R-group of the RAFT-agent (Figure 6.19 and 6.22 in the Experimental Section 6.4.3). The structure is indicated by the label P_{RZ} in the spectra, which shows the theoretical mass of a chain containing the intact RAFT-agent ionized with a Na^+ -ion (lightest isotope for PS, average molecular weight for PDMAA, since for double charged ions the resolution is too low to show single isotopic peaks in this mass region). The theoretical and experimental m/z values match excellently (refer to Table 6.2). Since there is a potential bias of the ionization towards higher molecular weights, no information regarding the average molecular weight of the polymer can or should be obtained from mass spectrometric measurements. The relatively high molecular weight of the PAcManEA ($M_n = 15000 \text{ g} \cdot \text{mol}^{-1}$, derived from NMR) did not allow for an ESI-MS analysis, yet the NMR results (Figure 6.24) and the low polydispersity also indicate a high end group functionality.

6.2.3 Functionalization of Microspheres

Pre-Functionalization, Test and Control Reaction

Although the photo-generated thioaldehyde can also undergo reactions with a wide range of nucleophiles,^[183,184] the PGMA microspheres were functionalized with cyclopentadiene moieties, thus employing the released (thioformyl)formate species as a dienophile in a [4+2] cycloaddition. The cyclopentadiene is introduced by employing sodium cyclopentadienide in a single step via a procedure described in Section 3.4.3 or reference [228] (see the top line of Figure 6.2 on the following page). Since the photo-generated thioaldehyde is very reactive, a test experiment was conducted in order to evidence that the introduction of the cyclopentadiene strongly increases the rate of the grafting reaction. Thus, two reactions were performed: A grafting reaction between the RAFT-agent DoPATPAS and the cyclopentadiene functionalized microspheres (test reaction) and a grafting reaction between the RAFT-agent and the unaltered PGMA microspheres (control reaction) (Figure 6.2 on the next page).

The amount of microspheres and RAFT-agent was identical in both cases. The reaction was conducted in DCM as due to the similar density of DCM and the spheres these are evenly dispersed in the solution, leading to an even irradiation of the entire reaction mixture. Subsequently, the suspension was percolated with nitrogen for 20 minutes and irradiated with a 36 W compact fluorescent lamp ($\lambda_{max} = 355 \text{ nm}$) for 60 minutes. After thorough filtering, washing and drying, the spheres were analyzed via SEM, XPS and elemental analysis.

SEM analysis cannot provide any information regarding the chemical changes of the particles, yet it is of critical importance to check if the porosity and spherical shape of the

6. Photo-Induced Functionalization of Surfaces via Caged Thioaldehyde Polymers

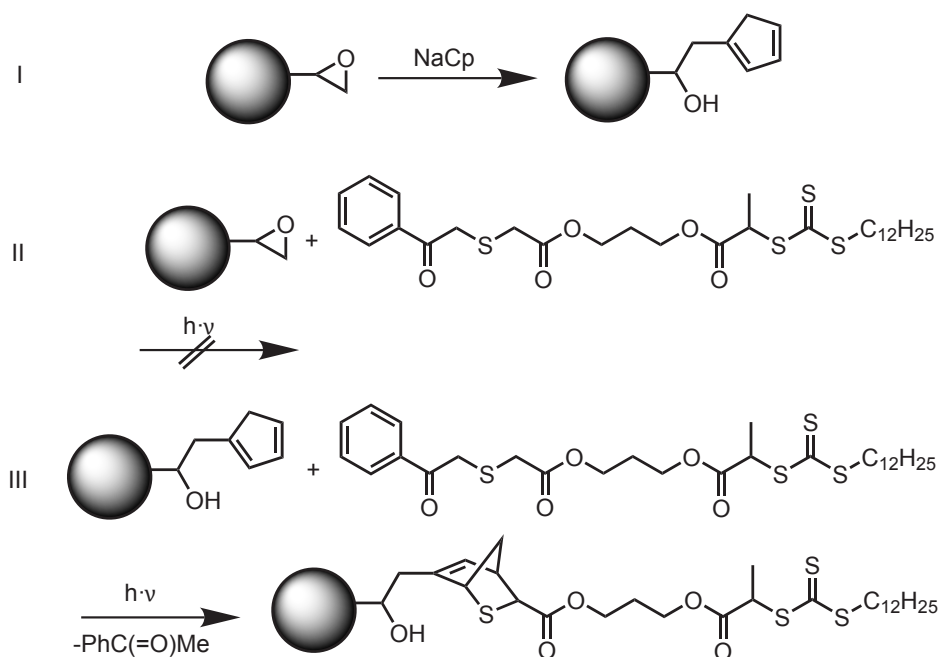


Figure 6.2: Top: Cp-functionalization of PGMA microspheres employing sodium cyclopentadienide; middle: Control reaction between PGMA spheres and DoPATPAS; bottom: Test reaction between Cp-functional spheres and DoPATPAS.

particles is not altered by the reaction. In the current case, the microspheres have maintained their shape and structural integrity (refer to Figure A.41 to A.43 in the Appendix). In-depth chemical information can be gained via the elemental analysis and XPS. Although XPS is a surface analysis technique and EA gives information about the entire sample, both techniques essentially provide proof for the successful grafting experiment utilizing DoPATPAS. Only the XPS data on the test reaction revealed the presence of sulfur (1.6 at%) after the successful grafting. The sulfur peak (Figure 6.3 on the opposite page), can be deconvoluted into two doublets, one S $2p_{3/2}$ at 163.5 eV and one with S $2p_{3/2}$ at 164.9 eV (associated to the trithiocarbonate).^[229] As expected, the control reaction shows only noise in the sulfur signal region, just as the unaltered GMA spheres and Cp-functionalized spheres.

The elemental analysis of the reactions shows sulfur in both experiments (the full results of the elemental analysis can be found in Table 6.1 on page 128). For the test reaction a sulfur content of 0.53 wt% is observed, which is a clear and distinct increase. However, for the control reaction the sulfur content is merely 0.13 wt%, which is only slightly higher than for the Cp-functionalized spheres (0.10 wt%). Such values for the sulfur content are within the error margin of the technique, and it is unknown if they are just artifacts or stemming from cross contamination, side reactions or impurities.

6. Photo-Induced Functionalization of Surfaces via Caged Thioaldehyde Polymers

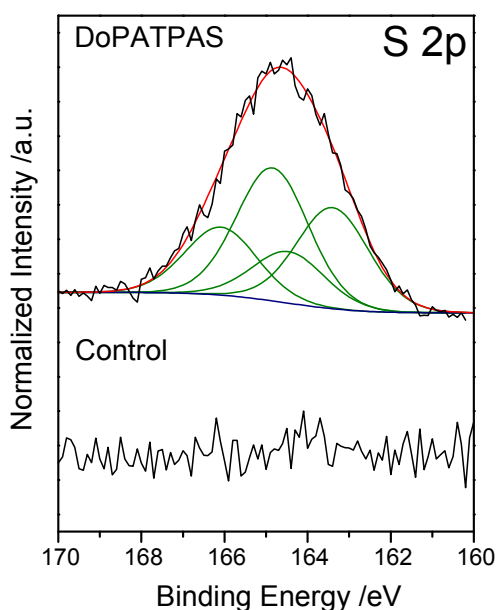


Figure 6.3: S 2p XP spectra of Cp-microspheres photo-grafted with DoPATPAS (top) and of PGMA spheres subjected to the same reaction conditions (bottom). Only for the previously Cp-functionalized spheres sulfur can be detected.

The sulfur content can be employed to calculate a loading capacity via Equation 3.1 on page 42, which is repeated here for clarity:

$$LC = \frac{W(S)}{n(S) \cdot M(S)} \quad (6.1)$$

where LC is the loading capacity (in $\text{mol} \cdot \text{g}^{-1}$), $W(S)$ is the weight of sulfur per 1 g of microspheres obtained via EA $n(S)$ is the number of sulfur atoms per grafted molecule (here 4) and $M(S)$ is the molecular weight of sulfur. Employing Equation 6.1 leads to a loading capacity of $44.5 \mu\text{mol} \cdot \text{g}^{-1}$. A loading capacity of $44.5 \mu\text{mol} \cdot \text{g}^{-1}$ is in excellent agreement with values obtained by grafting RAFT-polymers via the also photo-triggered photo-enol approach employing similar maleimide-functionalized porous microspheres ($41.6 \mu\text{mol} \cdot \text{g}^{-1}$, refer to Chapter 4). Furthermore, the value is only slightly smaller than the loading capacities obtained by the thermal induced grafting reaction employing the RAFT-HDA approach (more than $150 \mu\text{mol} \cdot \text{g}^{-1}$ for reaction times of up to 5 days) on microspheres that were also Cp-functionalized (refer to Chapter 3).

Via inverse size exclusion chromatography the relative surface area of the (non-functionalized) PGMA starting material was determined to be close to $225.4 \text{m}^2 \cdot \text{cm}^{-3}$. The density of the spheres has been measured to be close to $1.39 \text{g} \cdot \text{cm}^{-3}$ (refer to Section 3.2.4). Thus, the surface area of the spheres is $1.62 \cdot 10^{20} \text{nm}^2 \cdot \text{g}^{-1}$. By employing

6. Photo-Induced Functionalization of Surfaces via Caged Thioaldehyde Polymers

Table 6.1: Collected data from the elemental analysis of all samples described in Chapter 6.

Sample	N [wt%] ¹	C [wt%]	H [wt%]	S [wt%] ²	O [wt%] ³	mass balance [wt%]
PGMA	0.19	55.77	6.88	0.00	32.84	95.69
±	0.012	0.260	0.035	0.000	0.259	
Cp	0.39	58.05	7.16	0.10	31.32	95.83
±	0.012	0.115	0.011	0.000	0.663	
DoPATPAS	0.37	57.90	7.08	0.57	30.92	94.99
±	0.021	0.213	0.079	0.001	0.086	
Control	0.37	58.06	7.09	0.13	32.92	98.78
±	0.004	0.021	0.003	0.001	0.130	
PS	0.39	58.19	6.94	0.24	29.24	96.52
±	0.003	0.363	0.059	0.003	0.039	
PAcManEA	0.48	58.24	7.13	0.16	33.51	99.52
±	0.019	0.109	0.027	0.006	0.294	
PDMAA	1.54	57.75	7.16	0.33	29.75	98.57
±	0.066	0.047	0.019	0.006	0.274	

¹ The nitrogen found in the untreated microspheres and the control sample can be explained by fragments from the nitrogen containing initiator, stabilizer or gaseous nitrogen trapped in the porous surface morphology of the microspheres.

² Content measured independently, employing a water-trap.

³ Content measured independently.

the measured surface area the grafting density can be determined via Equation 3.2 on page 48, which is also repeated here for clarity:

$$GD = \frac{W(S) \cdot N_A}{n(S) \cdot M(S) \cdot A} \quad (6.2)$$

where GD is the grafting density in chains per unit area; $W(S)$ is the weight of sulfur in 1 g of microspheres obtained via elemental analysis, N_A is the Avogadro's number, $n(S)$ is the number of sulfur atoms per polymer chain, $M(S)$ is the molecular weight of sulfur and A is the surface area of the microspheres. Via the light-induced phenacyl sulfide based reaction a grafting density of close to 0.17 molecules per nm^2 is reached. The grafting density might even be higher as there is the possibility of a degradation of the trithiocarbonate group, although earlier results suggest that it is stable under the applied or similar conditions. [203,204,214]

In summary, it can be stated that the photo-generated thioaldehyde reacts in cycloaddition-

6. Photo-Induced Functionalization of Surfaces via Caged Thioaldehyde Polymers

reactions with Cp-functionalized microspheres, which is underpinned via XPS and EA data. The grafting density and loading capacity calculated from the elemental constitution are in the same dimension as values obtained for similar (thermal and light-triggered) grafting reactions performed on functional porous microspheres.

Photo-Triggered Grafting of RAFT-Polymers

In a similar fashion as for the test reaction, RAFT-polymers (PS, PDMAA and PAcManEA) can be grafted onto the microspheres. The Cp-functional microspheres and the RAFT-polymer are mixed in DCM, the suspension is percolated with nitrogen and subsequently irradiated for 60 minutes (Figure 6.4).

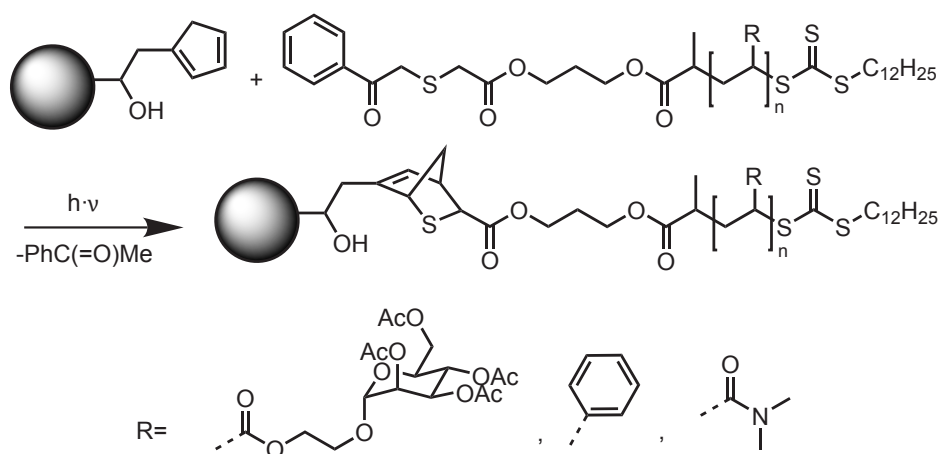


Figure 6.4: Photo-triggered grafting reactions of RAFT-polymers onto Cp-functionalized microspheres.

After intensive washing and drying (refer to the Experimental Part 6.4.5 for details on the washing procedure), the particles are analyzed via SEM, XPS, EA and - in the case of grafted PDMAA - FT-IR-microscopy.

As noted above, the SEM analysis cannot prove a chemical transformation, yet it is important to demonstrate that no change in the shape and porosity of the spheres has occurred: For all grafted-on polymers no change can be observed (refer to the Figure A.44 to A.52 in the Appendix).

Analysis of the XP spectra provides chemical information regarding the surface of the particles. No sulfur can be detected for the Cp-functionalized microspheres (Figure 6.5 on the next page). For all grafted polymers there is a clear signal for sulfur (between 0.4 at% (PAcManEA) and 0.8 at% (PDMAA)), indicating a successful grafting reaction. Sulfur can be found in the newly formed thiopyran ring as well as in the trithiocarbonate (S 2p_{3/2} at 163.4 eV and S 2p_{3/2} at 164.9 eV). In the cases of grafted-on PDMAA and PAcManEA, a third sulfur signal associated with oxidized sulfur (S 2p_{3/2} at 169.2 eV)

6. Photo-Induced Functionalization of Surfaces via Caged Thioaldehyde Polymers

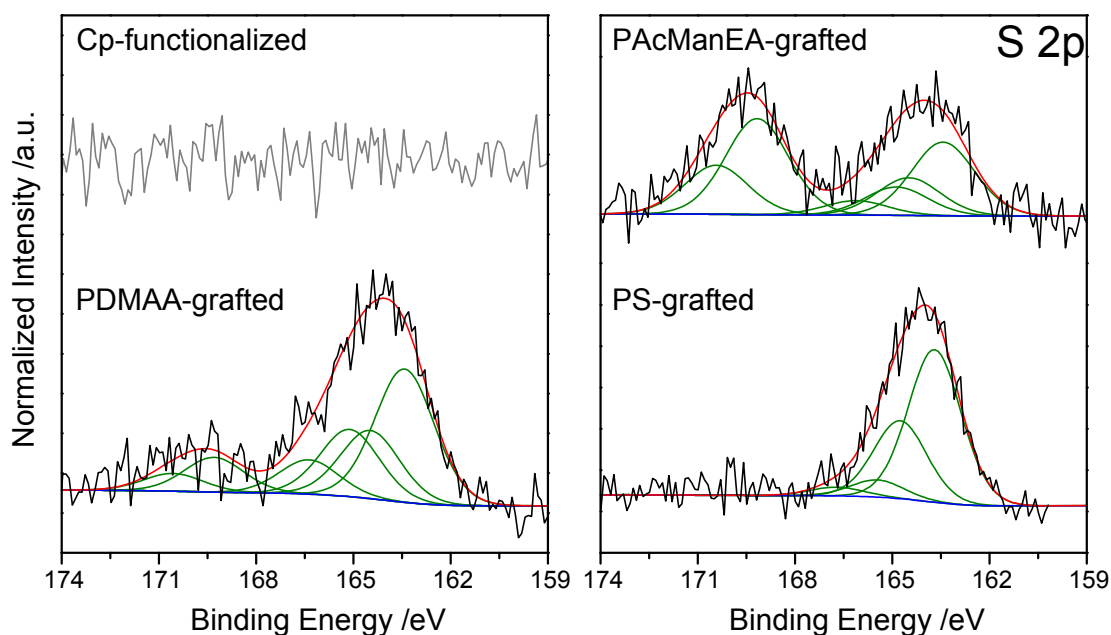


Figure 6.5: S 2p XP spectra of Cp-microspheres (top left) photo-grafted with PACManEA (top left), PDMAA (bottom left) and PS (bottom right). Sulfur can be detected in all samples after the photo-grafting.

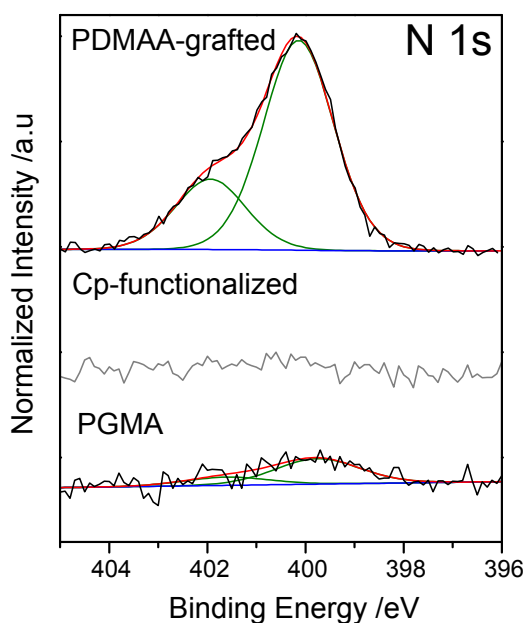


Figure 6.6: N 1s XP spectra of non-modified PGMA particles (bottom), Cp-functionalized microspheres (middle) and microspheres photo-grafted with PDMAA (top). Only traces of nitrogen can be detected for non-modified particle, none can be found after Cp-functionalization and - as expected - a distinct nitrogen peak can be observed after the grafting. The increase of the nitrogen signal evidences the successful macromolecular grafting.

6. Photo-Induced Functionalization of Surfaces via Caged Thioaldehyde Polymers

can be identified. Such a signal has been found in the XP spectra of RAFT-polymers before.^[144]

For the non-modified PGMA microspheres only traces of nitrogen can be found in the XPS (0.4 at%; refer to Figure 6.6 on the opposite page). The nitrogen most likely originates from the radical initiator or the stabilizer added during the particle synthesis. After the Cp-functionalization the signal vanishes and only noise can be found in the area of the spectra associated with nitrogen. For microspheres grafted with PDMAA a clear and distinct nitrogen signal can be detected stemming from the amide in the repeating unit (5.9 at%), further underpinning the successful grafting of the polymer. Two species can be distinguished: one at 400.1 eV, which is attributed to the amide^[230] and one at 401.8 eV, which represents a protonated nitrogen.

The successful photo-grafting of PS and PAcManEA can additionally be evidenced by a closer inspection of the C 1s signal in the XP spectra. The C 1s peak can be deconvoluted into several signals attributable to carbon atoms in different chemical environment (Figure 6.7 on the next page).

The signal at 285.0 eV is assigned to carbon bound to carbon or hydrogen (C–C, C–H) and the signal at 286.7 eV to carbon bound to oxygen (C–O). The third signal at 289.0 eV is associated with esters (O–C=O). For the grafted PDMAA a fourth signal at 287.9 eV can be detected, which is associated with the amide functionality in the lateral polymer chain.^[231] The peak attributed to (C–O, C–N) also shifts to a slightly smaller binding energy (286.4 eV) because of the amount of C–N bonds present in PDMAA.

The ratio of the different carbon species in the C 1s peak are correlated to the chemical changes occurring in the reaction sequence and can thus now be employed to visualize the functionalization and grafting reactions. Especially the ratio of the peaks belonging to carbon bound to oxygen or nitrogen (C–O, C–N) and carbon bound to carbon or hydrogen (C–C, C–H) effectively visualizes the functionality change on the microspheres (Figure 6.8 on page 133).

The addition of small molecules, such as cyclopentadiene or the RAFT-agent DoPATPAS should not change the ratio of these signals significantly, yet the addition of cyclopentadiene (only consisting of carbon and hydrogen) leads to a slight decrease of the ratio. The introduction of PDMAA, which has similar ratios of the concerned carbons in its repeating unit as PGMA, should also not significantly affect the ratio of the considered signals. In contrast, via the introduction of polystyrene (repeating unit only contains carbon and hydrogen) and PAcManEA (expressing many carbons bound to oxygen) onto the microspheres surface, the ratio should change significantly. Inspection of Figure 6.8 indicates that the change of the ratios exactly matches the theoretical expectation, again proving a successful light-induced grafting reaction employing the photo-reactive RAFT-polymers.

6. Photo-Induced Functionalization of Surfaces via Caged Thioaldehyde Polymers

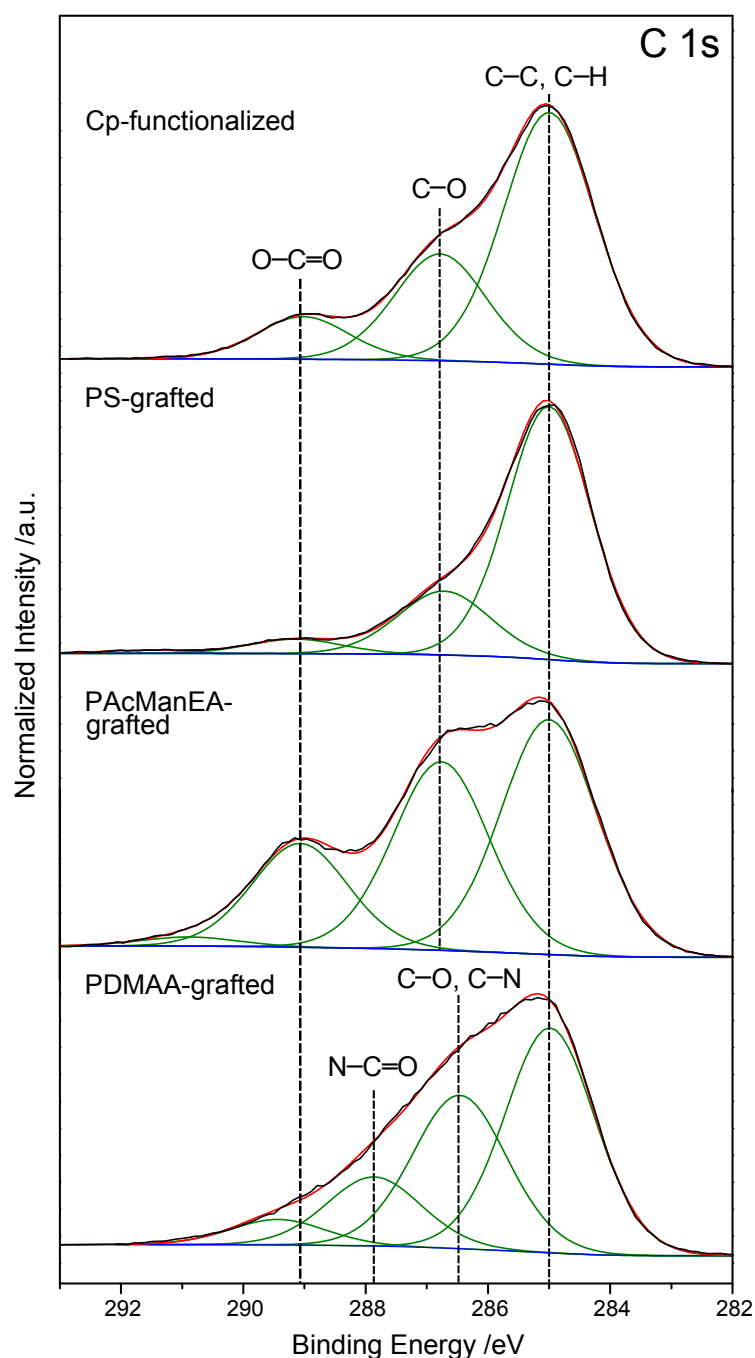


Figure 6.7: C 1s XP spectra of Cp-functionalized microspheres (top) and microspheres photo-grafted with PS (2nd row), PAcManEA (3rd row), and PDMAA (bottom). The peaks are deconvoluted into signals stemming from chemically different carbon species.

For the error margins an estimated error of 10 % was employed, which is associated with the accuracy of XPS analysis.

High resolution FT-IR-microscopy can be employed to determine the spatial distribution as well as the amount of IR-active groups on microspheres (Chapter 3 and 4) and on flat substrates.^[198] Since PDMAA contains an amide exhibiting an IR-band that can readily be

6. Photo-Induced Functionalization of Surfaces via Caged Thioaldehyde Polymers

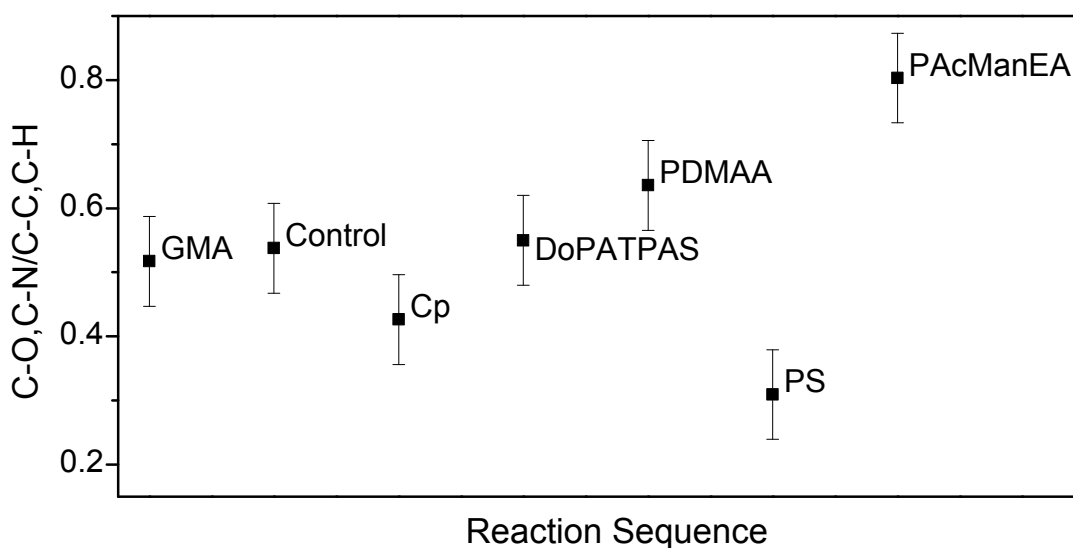


Figure 6.8: Comparison of the amount of carbon bound to oxygen or nitrogen and carbon bound to carbon or hydrogen based on the deconvolution of the carbon peak in the XP spectra (see also Figure 6.7 and Figure A.10). The values are in agreement with the theoretically expected changes for grafted-on polymers.

distinguished from the ester vibration of the PGMA spheres, IR-microscopy is an elegant tool to show the successful and evenly distributed grafting of PDMAA onto microspheres as evidenced in Figure 6.9 on the next page.

By mapping the ester vibration close to 1750 cm^{-1} the microsphere can be imaged, showing its circular shape and the highest intensity in the middle of the sphere for the Cp-functionalized spheres as well as for the ones grafted with PDMAA. Imaging of the amide vibration at approximately 1650 cm^{-1} only returns noise for the Cp functionalized sphere, whereas the same shape as well as intensity distribution can be found for the particle with PDMAA, again confirming the successful grafting.

Quantitative information regarding the grafting onto microspheres can be obtained via elemental analysis. To quantify the grafting efficiency the sulfur content is employed, as sulfur is an element which is only introduced into the particles via a successful grafting reaction. Furthermore, sulfur is only present in the chain end groups thereby eliminating any errors of the loading capacity or grafting density associated with inaccuracies in the chain length of the grafted polymers. For grafted PS a sulfur content of 0.24 wt% is observed, for PDMAA 0.33 wt%, and for PAcManEA 0.16 wt%. Applying the above noted Equation 6.1 and Equation 6.2 leads to loading capacities and grafting densities of $18.7\text{ }\mu\text{mol}\cdot\text{g}^{-1}$ and $0.07\text{ molecules}\cdot\text{nm}^{-2}$ for grafted PS, $25.7\text{ }\mu\text{mol}\cdot\text{g}^{-1}$ and $0.10\text{ molecules}\cdot\text{nm}^{-2}$ for grafted PDMAA, and $10.1\text{ }\mu\text{mol}\cdot\text{g}^{-1}$ and $0.05\text{ molecules}\cdot\text{nm}^{-2}$ for PAcManEA, respectively. Inspection of these numbers indicates a significant decrease of the grafting density with the chain length of the grafted

6. Photo-Induced Functionalization of Surfaces via Caged Thioaldehyde Polymers

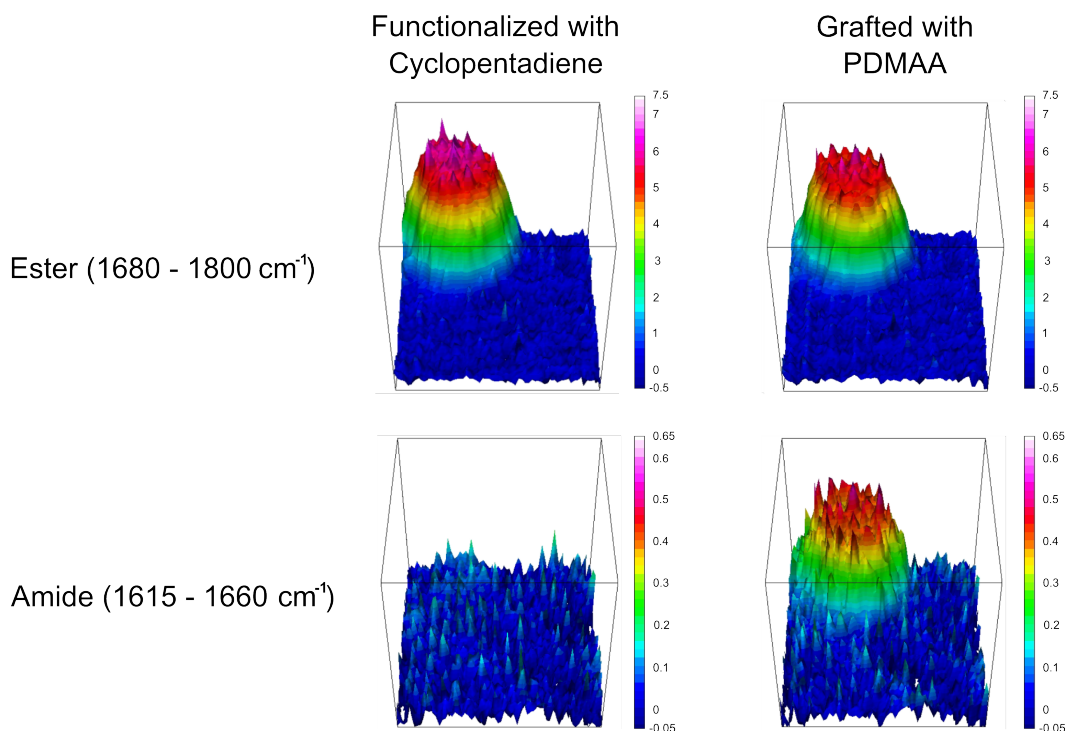


Figure 6.9: False color high resolution FT-IR-microscopy images (4 cm^{-1} spectral resolution with a pixel resolution of $0.25\text{ }\mu\text{m}^2$) of a cyclopentadiene functionalized PGMA microsphere before and after photo-grafting of PDMAA. The measured area is $32\text{ }\mu\text{m} \times 32\text{ }\mu\text{m}$. Red color corresponds to a high degree of functionalization. In the top row, the intensity of bands corresponding to the O–C=O stretching vibration is visualized, in the bottom row the N–C=O bands.

glycopolymers, suggesting that steric hindrance is limiting the achievable grafting density. The grafting densities obtained using the current phenacyl sulfide photo-grafting approach are in excellent agreement with the values obtained by the different photo-triggered grafting reaction – the photo-enol approach – leading to grafting densities around $0.1\text{ molecules} \cdot \text{nm}^{-2}$ with polymers similar in structure and chain length (Chapter 4).

By combining the data from the elemental analysis and XPS measurements a complete picture of the photo-induced grafting can be constructed. Although XPS is mainly a surface analysis tool with penetration depths in the range of five to ten nanometers and elemental analysis gives information about the entire sample, they both lead to the same conclusions. Figure 6.10 on the opposite page shows a comparison of the nitrogen contents derived from EA and XPS (for the error margins in the EA the standard deviation of the measurements was employed, for XPS an error of 10 % was estimated).

XPS shows only noise for all samples, with the exception of the spheres photo-grafted with PDMAA. Via elemental analysis some nitrogen traces can be found in every sample, as it can stem from the radical initiator, stabilizer, porogen, impurities or even trapped

6. Photo-Induced Functionalization of Surfaces via Caged Thioaldehyde Polymers

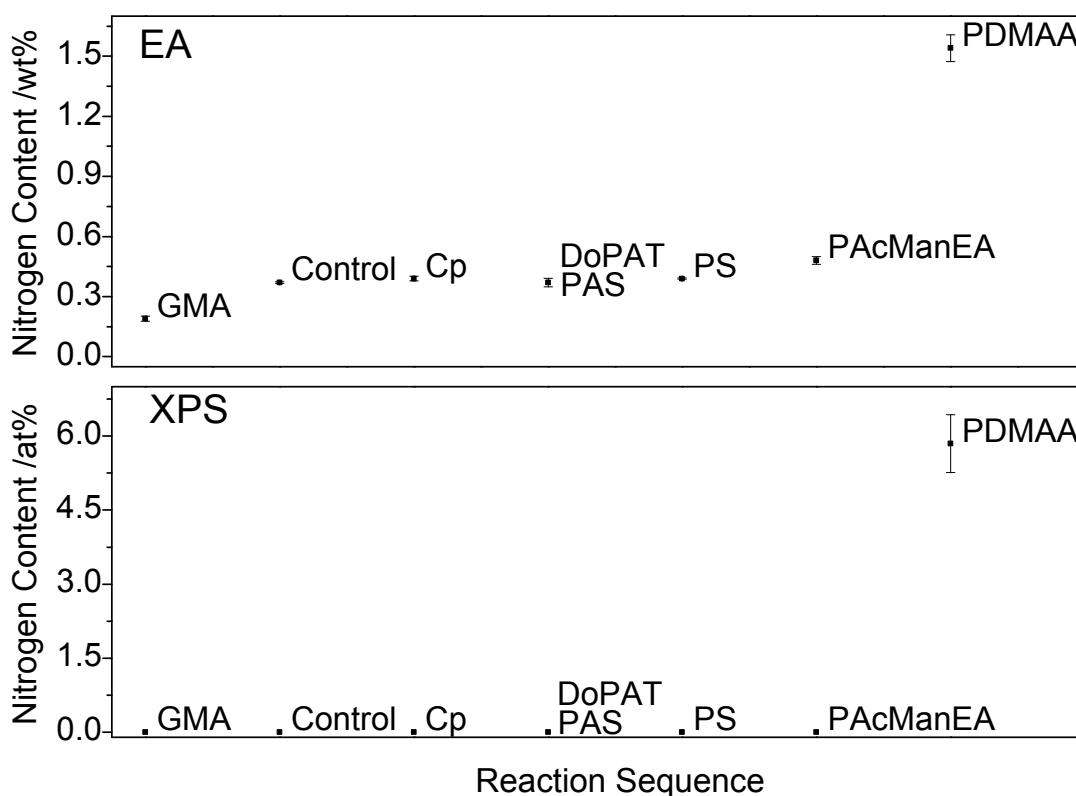


Figure 6.10: Comparison of the nitrogen contents derived from elemental (EA, top) and XPS (bottom) analysis of all microsphere samples.

atmospheric nitrogen. Nevertheless, a distinct and unambiguous increase in the nitrogen content can be seen for grafted PDMAA. An identical result is obtained for the sulfur content when comparing XPS and EA as illustrated in Figure 6.11 on the next page.

The highest sulfur content is found in the test reaction, where the novel photo-reactive RAFT-agent DoPATPAS was grafted onto Cp-functionalized microspheres. The untreated spheres show no sulfur content in both techniques. The Cp-functionalized spheres as well as the test reaction employing unfunctionalized PGMA spheres show no sulfur content via XPS and only low quantities in the elemental analysis. For all the grafted-on polymers, sulfur can be detected with the highest amount found for PDMAA and the lowest for PAcManEA, which had the highest molecular weight and therefore also the largest steric hindrance impeding the grafting of the chains.

In summary, the photo-induced grafting of RAFT-polymers onto Cp-functionalized porous microspheres employing thioaldehyde ligation was successful utilizing a single-photon irradiation process, as evidenced via XPS, FT-IR microscopy and elemental analysis. Determined grafting densities are comparable to previously reported values obtained via light-induced immobilization techniques on polymeric particles (Chapter 4).

To illustrate the universality of thioaldehyde ligation, the photo-functional RAFT-

6. Photo-Induced Functionalization of Surfaces via Caged Thioaldehyde Polymers

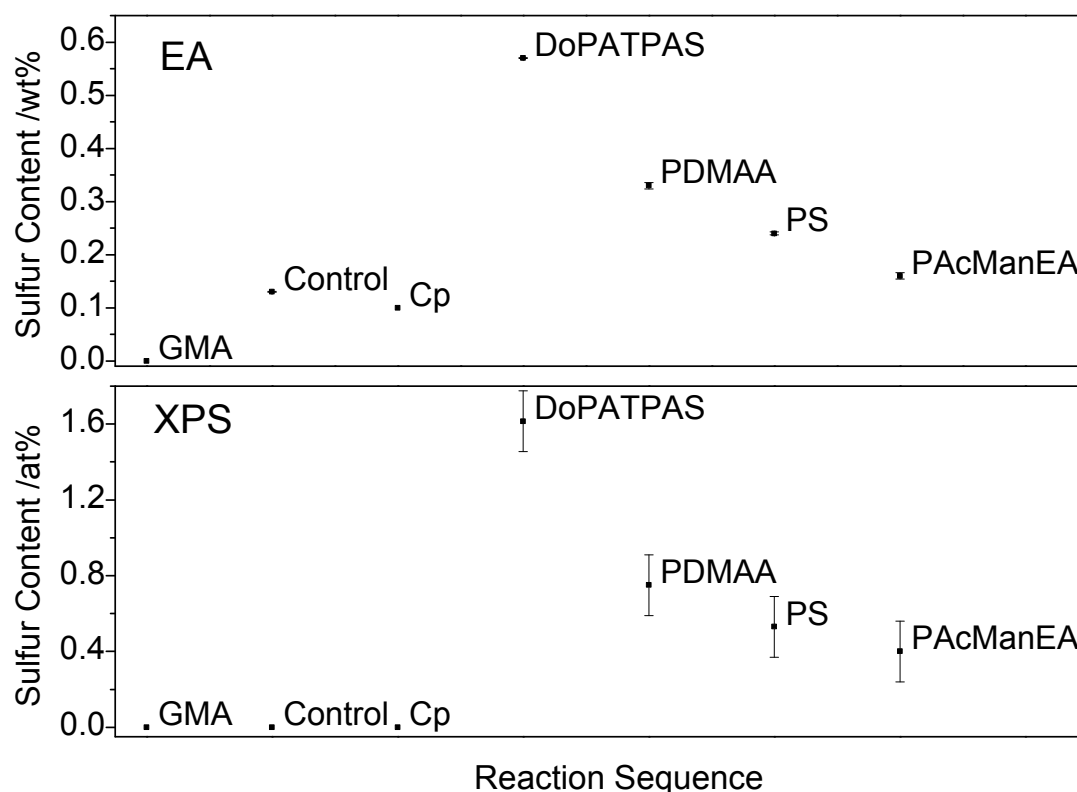


Figure 6.11: Comparison of the sulfur contents derived from elemental (EA, top) and XPS (bottom) analysis of all microsphere samples.

polymers were also tethered to nucleophilic planar surfaces in a spatially resolved fashion applying a two-photon direct laser writing (DLW) process.

6.2.4 Spatially Resolved Grafting via Direct Laser Writing

Coating with PDA

PDA was deposited from a $2 \text{ mg} \cdot \text{mL}^{-1}$ solution prepared by dissolution of dopamine hydrochloride in an air-saturated 10 mM Tris-HCl (pH 8.5) buffer.^[216] Glass slides and silicon wafers were coated by the autopolymerization of dopamine in aqueous solution in the presence of the respective substrate. The thickness of the PDA layer is $16.8 \pm 2.1 \text{ nm}$, determined via spectroscopic ellipsometry. Since dopamine contains an amine group, the surface exhibits a significant amount of nucleophilic^[232,233] groups that can be employed for further grafting reactions in particular with phenacyl sulfides (Figure 6.12 on the opposite page).

6. Photo-Induced Functionalization of Surfaces via Caged Thioaldehyde Polymers

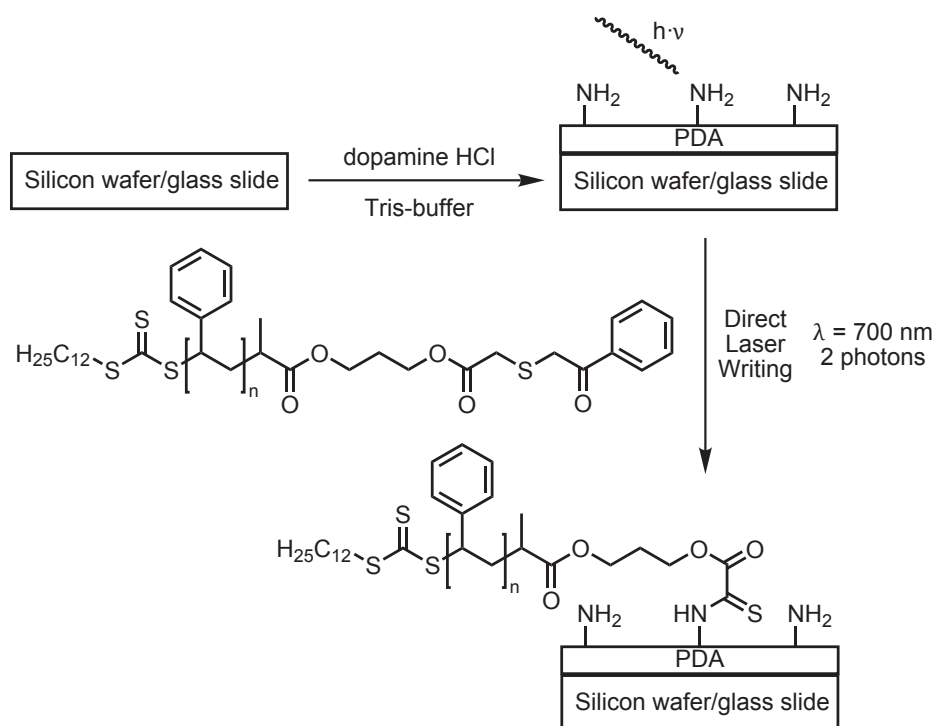


Figure 6.12: Synthetic route for the photo-patterning of PDA-interfaces.

Spatially Resolved Surface Patterning of RAFT-Polymers onto PDA Interfaces

For the direct surface patterning, a droplet of polystyrene containing thioaldehyde precursor in ϵ -caprolactone is placed onto a PDA-functionalized glass slide or silicon wafer. The functionalized side of the substrate is then covered with another glass slide. Thus, the droplet is located between the cover glass slide and the substrate. Subsequently, the sample was inserted into the direct laser writing (DLW) setup and surface patterning was performed by focusing the laser beam through the glass slide and the reaction mixture directly onto the PDA-functionalized surface. With this technique, surface patterning of non-transparent substrates (such as silicon wafers) is possible. Light induced surface modification was performed utilizing different patterns, such as squares ($40 \times 40\ \mu\text{m}$ with an interval of $10\ \mu\text{m}$) or the logo of the KIT ($20 \times 50\ \mu\text{m}$), were written with the DLW setup, as described in the Experimental Section 6.4.5 on page 150.

The surfaces grafted with the RAFT-polymer were analyzed by Time-of-Flight Secondary Ion Mass Spectrometry (ToF-SIMS), allowing for the imaging of the surface functionalization on the micrometer scale. The successful local grafting of the polystyrene chains was proven by imaging the lateral distribution of the tropylium cation, together with other characteristic PS derived ions (Figure 6.13 on the following page).

The DLW technology provides small patterns with high fidelity yielding sharp structures as depicted in Figure 6.13 left and center. The C_7H_7^+ intensity profile across a patterned

6. Photo-Induced Functionalization of Surfaces via Caged Thioaldehyde Polymers

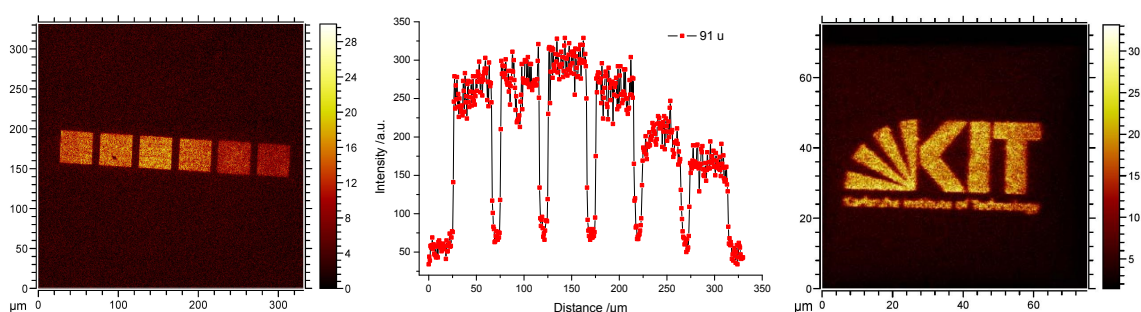


Figure 6.13: ToF-SIMS imaging of the $C_7H_7^+$ ion from PS grafted onto a PDA-functionalized silicon wafer (left). Imaging of the sum of $C_7H_7^+$, $C_8H_9^+$, $C_9H_7^+$, and $C_9H_9^+$ signals from PS grafted onto a PDA-functionalized glass slide by DLW (right). The diagram in the center depicts the 'intensity profile' for the $C_7H_7^+$ signal across the squares of the DLW patterned structure shown left visualizing the lateral resolution of the obtained structures.

line obtained from the analysis shown in Figure 6.13 right demonstrates a lateral resolution better than $1\ \mu\text{m}$ based on the (80/20) definition (Figure A.11 in the Appendix). Notably, virtually any two-dimensional structure can be written onto a PDA-coated surface employing the here described procedure. As an example the logo of the KIT was chosen (Figure 6.13 right). The high spatial resolution that was achieved is an indication for a very fast grafting process. The possibility to functionalize PDA surfaces in a spatially resolved fashion is particularly interesting, as PDA can be applied to a vast range of surfaces, enabling precise grafting of a range of polymers via DLW. Furthermore, the phenacyl sulfide reaction is not restricted to macromolecules providing the possibility to graft small molecules such as orthogonal functional groups or even ligands to the PDA surface.

6.3 Conclusions

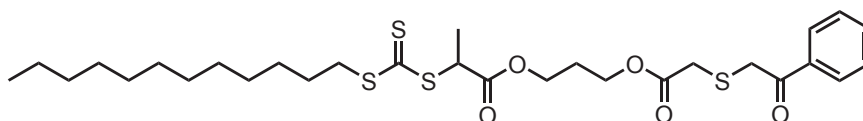
The synthesis and application of a novel RAFT-agent carrying a phenacylsulfide, which forms a thioaldehyde when irradiated with light ($\lambda_{max} = 355 \text{ nm}$) is introduced. RAFT-polymerization of styrene and dimethylacrylamide was conducted, reaching dispersities below 1.1 for M_n of 3600 and 4800 $\text{g} \cdot \text{mol}^{-1}$. In addition, a protected glycopolymer was synthesized with $\bar{D} = 1.2$ ($M_n = 15000 \text{ g} \cdot \text{mol}^{-1}$). All polymers show high end group fidelity. The photo-generated thioaldehyde on the chain ends can undergo hetero Diels-Alder reactions with dienes as well as reactions with nucleophiles. Subsequently, the RAFT-polymers were photo-ligated to porous polymeric microspheres, previously functionalized with cyclopentadiene moieties. The grafted particles were thoroughly characterized via SEM, elemental analysis, XPS, and high resolution FT-IR-microscopy, leading to qualitative as well as quantitative information about the reaction efficiency. Grafting densities up to 0.10 molecules $\cdot \text{nm}^{-2}$ were reached. The versatility of the thioaldehyde ligation is further evidenced by the spatially resolved grafting of polystyrene onto poly(dopamine) coated glass slides and silicon wafers via two-photon direct laser writing (DLW). The polydopamine layers, which exhibit a significant amount of nucleophilic amine groups, can be applied on any surface. The DLW approach allows for the generation of virtually any (two-dimensional) polymer pattern to be grafted. In summary, the combination of thioaldehyde ligation, RAFT-polymerization, PDA coated surfaces and DLW allows for the spatially resolved grafting of a vast range of polymers onto various substrates in any desired pattern.

6.4 Experimental Part

6.4.1 Materials

1-((3-Hydroxypropoxy)carbonyl)ethyl dodecyl carbonotrithioate (DoPATOH) and 2-(2',3',4',6'-tetra-*O*-acetyl- β -D-mannosyloxy) ethylacrylate (AcManEA) were synthesized as described in Chapter 4 and (phenacylthio)acetic acid,^[183] according to the literature. 2,2'-Azobis(2-methylpropionitrile) (AIBN) was recrystallized twice from methanol and stored at -19 °C. Styrene and *N,N*-dimethylacrylamide (DMAA) were passed through a column of basic alumina to remove inhibitor and subsequently stored at -19 °C. Dichloromethane (DCM) was dried and stored over CaCl₂. Poly(glycidyl methacrylate) (PGMA) microspheres with a PGMA content of 80 % and pore size of 1000 Å were synthesized by Polymer Standards Service (PSS) GmbH and functionalized with cyclopentadiene moieties as described in Section 3.4.3 on page 51 or Reference [228]. All other chemicals were used as supplied by the manufacturers.

6.4.2 Synthesis of DoPAT-Phenacylsulfid (DoPATPAS)



DoPATOH (1.537 g, 3.76 mmol, 1.00 equiv), (phenacylthio)acetic acid (872 mg, 4.15 mmol, 1.10 equiv) and 4-dimethylaminopyridine (9.1 mg, 0.075 mmol, 0.02 equiv) were dissolved in 10 mL dry DCM (dried over CaCl₂). The solution was cooled to 0 °C in an ice bath and dicyclohexylcarbodiimide (990 mg, 4.80 mmol, 1.28 equiv) dissolved in 4 mL dry DCM was added dropwise. The reaction was covered with aluminum foil to protect it from ambient light. After one hour, the ice bath was removed and the reaction proceeded over night at ambient temperature. After filtration, the organic layer was washed with 5% HCl, saturated NaHCO₃ solution and distilled water, dried over Na₂SO₄ and the solvent removed. The crude product was purified via column chromatography (silica gel, cyclohexane/ethyl acetate 4:1) to afford a yellow oil (1.792 g, 79 %). ¹H-NMR (CDCl₃, 400 MHz) δ /ppm: 7.96 (d, ³J=7.3 Hz, 2H, orthoAr), 7.59 (t, ³J=7.3 Hz, 1H, paraAr), 7.48 (t, ³J=7.5 Hz, 2H, metaAr), 4.80 (q, ³J=7.4 Hz, 1H, SCHCH₃), 4.21 (m, 4H, C(O)OCH₂CH₂CH₂OC(O)), 4.02 (s, 2H, ArC(O)CH₂SCH₂), 3.33 (m, 4H, ArC(O)CH₂SCH₂ and SCH₂CH₂C₇H₁₄CH₂CH₂CH₃), 1.99 (quin, ³J=6.0 Hz, 2H, C(O)OCH₂CH₂CH₂OC(O)), 1.68 (quin, ³J=7.4 Hz, 2H, SCH₂CH₂C₇H₁₄CH₂CH₂CH₃), 1.59 (d, ³J=7.4 Hz, 3H, SCHCH₃), 1.38 (m, 2H, SCH₂CH₂C₇H₁₄CH₂CH₂CH₃), 1.25 (s_{br}, 16H, SCH₂CH₂C₇H₁₄CH₂CH₂CH₃), 0.87

6. Photo-Induced Functionalization of Surfaces via Caged Thioaldehyde Polymers

(t, $^3J=6.8$ Hz, 3H, $\text{SCH}_2\text{CH}_2\text{C}_7\text{H}_{14}\text{CH}_2\text{CH}_2\text{CH}_3$). $^{13}\text{C-NMR}$ (CDCl_3 , 100 MHz) δ/ppm : 222.0 ($\text{SC}(\text{S})\text{S}$), 193.9 ($\text{ArC}(\text{O})\text{CH}_2\text{SCH}_2$), 171.0 ($\text{SCH}(\text{CH}_3)\text{C}(\text{O})\text{O}$), 169.7 ($\text{SCH}_2\text{C}(\text{O})\text{O}$), 135.3 (substituted Ar), 133.5 (paraAr), 128.7 (orthoAr), 128.6 (metaAr), 62.1 ($\text{SCH}(\text{CH}_3)\text{C}(\text{O})\text{OCH}_2$), 61.8 ($\text{SCH}_2\text{C}(\text{O})\text{OCH}_2$), 47.8 (SCHCH_3), 37.7 ($\text{SCH}_2\text{C}(\text{O})\text{O}$), 37.3 ($\text{SCH}_2\text{CH}_2\text{C}_7\text{H}_{14}\text{CH}_2\text{CH}_2\text{CH}_3$), 33.3 ($\text{ArC}(\text{O})\text{OCH}_2$), 31.9 ($\text{SCH}_2\text{CH}_2\text{C}_7\text{H}_{14}\text{CH}_2\text{CH}_2\text{CH}_3$), 29.6, 29.5 (2x), 29.4, 29.3, 29.0, 28.9, 27.8, (8C, $\text{SCH}_2\text{CH}_2\text{C}_7\text{H}_{14}\text{CH}_2\text{CH}_2\text{CH}_3$), 27.7 ($\text{C}(\text{O})\text{OCH}_2\text{CH}_2\text{CH}_2\text{C}(\text{O})\text{O}$), 22.7 ($\text{SCH}_2\text{CH}_2\text{C}_7\text{H}_{14}\text{CH}_2\text{CH}_2\text{CH}_3$), 16.7 ($\text{SCHCH}_3\text{C}(\text{O})\text{O}$), 14.1 ($\text{SCH}_2\text{CH}_2\text{C}_7\text{H}_{14}\text{CH}_2\text{CH}_2\text{CH}_3$). **UV-Vis:** (acetonitrile) $\lambda_{\text{max}} = 307, 240$ nm **MS:** (ESI) m/z calculated for $\text{C}_{29}\text{H}_{44}\text{O}_5\text{S}_4$ $[\text{M}+\text{Na}]^+$: 623.19, found 623.24.

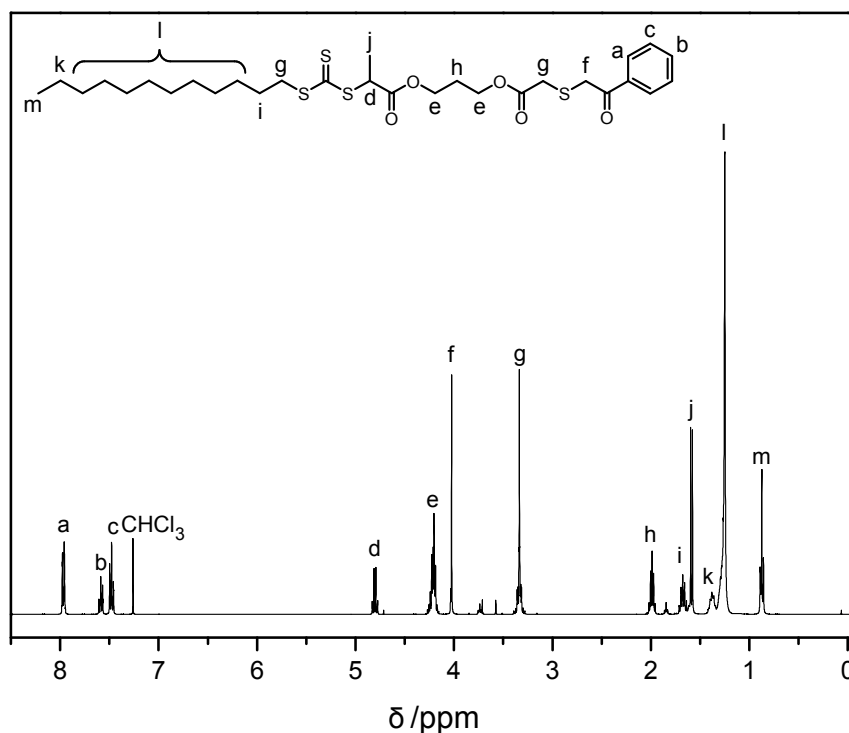


Figure 6.14: $^1\text{H-NMR}$ spectrum of DoPATPAS in CDCl_3 at 400 MHz.

6. Photo-Induced Functionalization of Surfaces via Caged Thioaldehyde Polymers

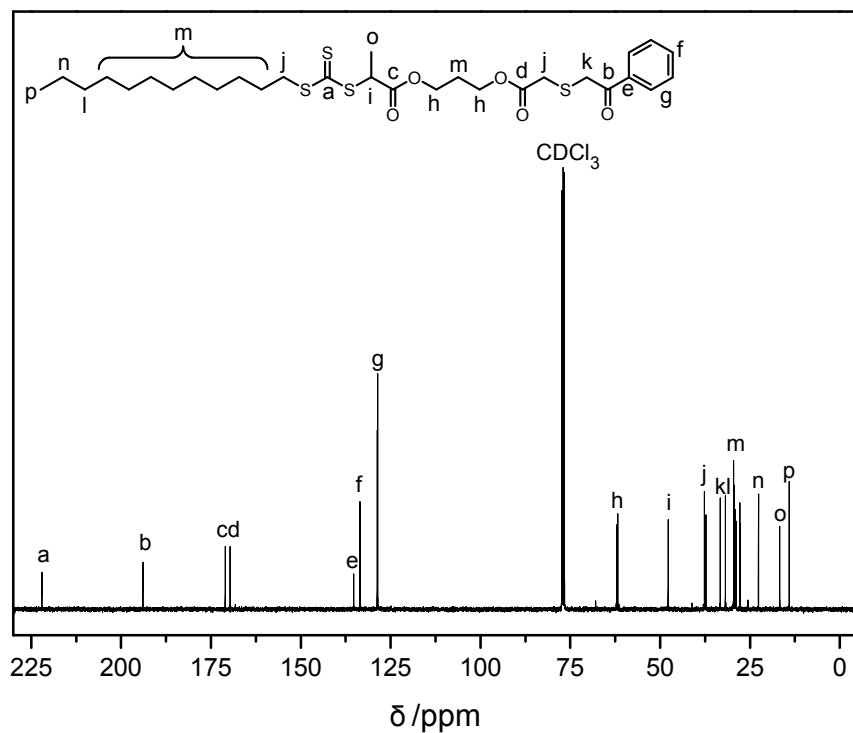


Figure 6.15: ^{13}C -NMR spectrum of DoPATPAS in CDCl_3 at 100 MHz.

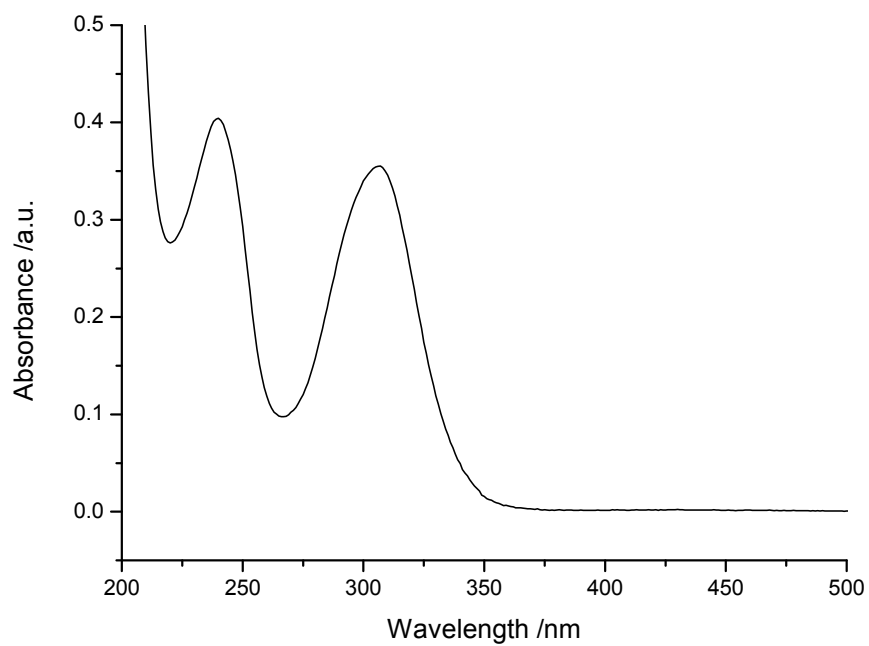
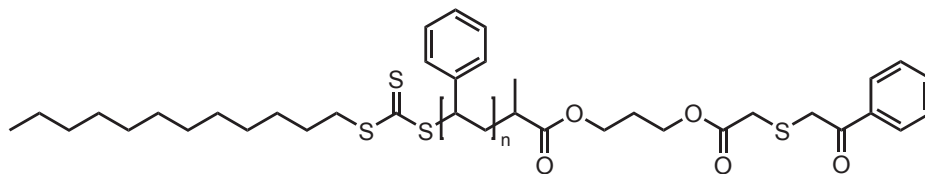


Figure 6.16: UV-Vis spectrum of DoPATPAS in acetonitrile ($0.019 \text{ g} \cdot \text{L}^{-1}$).

6. Photo-Induced Functionalization of Surfaces via Caged Thioaldehyde Polymers

6.4.3 RAFT-Polymerizations

Synthesis of Polystyrene (PS)



A solution of AIBN (4.2 mg, 0.026 mmol, 0.10 equiv) and DoPATPAS (156.1 mg, 0.26 mmol, 1.00 equiv) in styrene (2.98 g, 28.5 mmol, 110 equiv) was deoxygenated with four consecutive freeze-pump-thaw cycles. The reaction was placed into a preheated oil-bath at 60 °C for 14.5 h. The reaction was stopped by cooling in an ice-bath and exposing the reaction mixture to oxygen. The remaining styrene was removed via evaporation at ambient conditions and the polymer isolated via precipitation in cold methanol and subsequent drying under vacuum to afford 774 mg of a slightly yellow powder. Conversion = 33 % (gravimetry); $M_n = 3600 \text{ g} \cdot \text{mol}^{-1}$, $\mathcal{D} = 1.08$ (GPC in THF, polystyrene calibration); $M_n = 3650 \text{ g} \cdot \text{mol}^{-1}$ (NMR, comparison of the integrals between 8.05 - 7.90 ppm and 7.36 - 6.25 ppm).

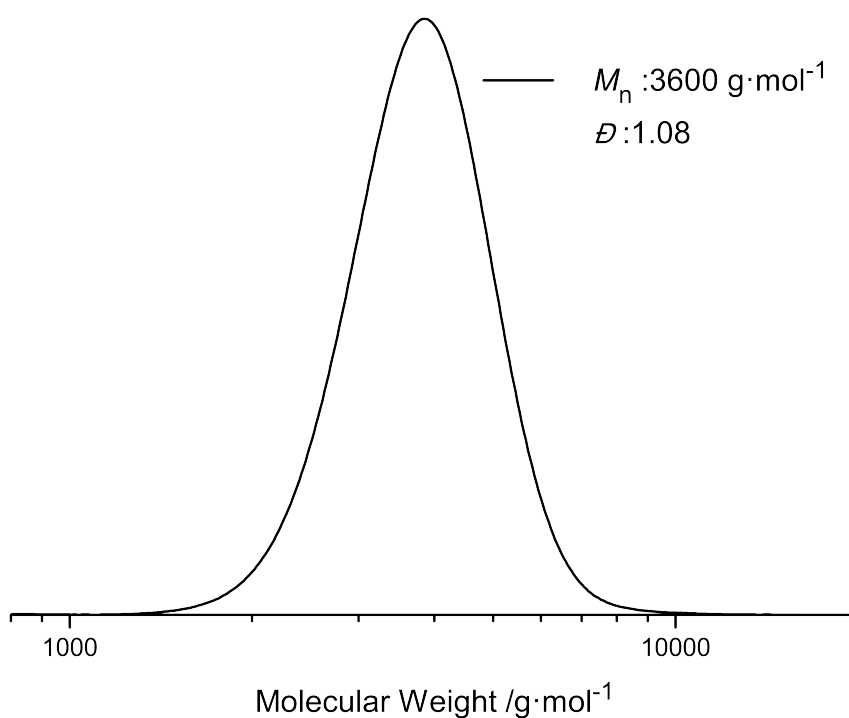


Figure 6.17: GPC trace in THF (PS calibration) of polystyrene polymerized with DoPATPAS.

6. Photo-Induced Functionalization of Surfaces via Caged Thioaldehyde Polymers

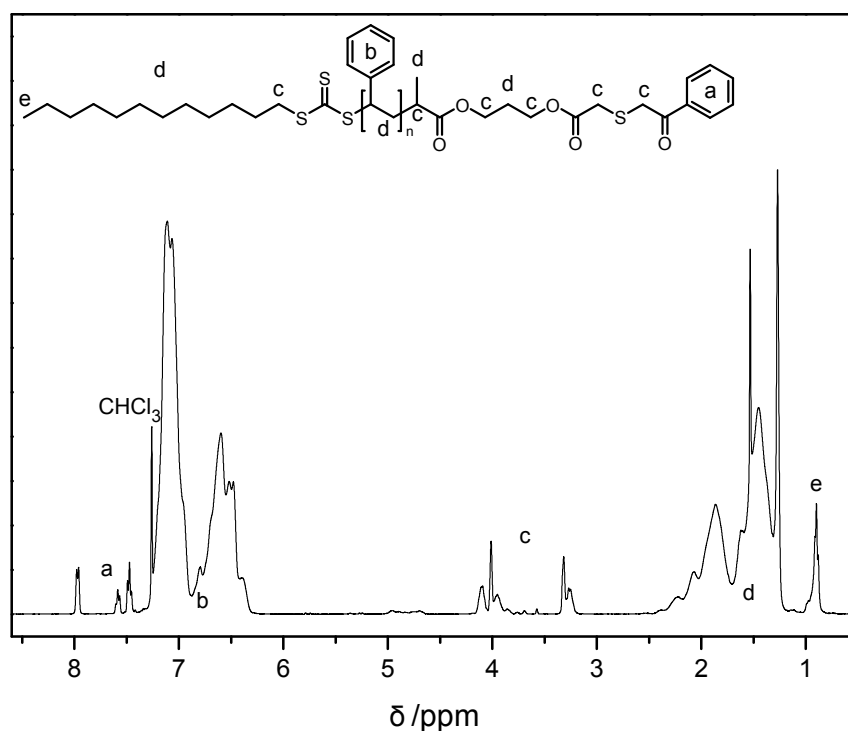


Figure 6.18: $^1\text{H-NMR}$ spectrum of polystyrene polymerized with DoPATPE in CDCl_3 at 400 MHz. Comparison of repetition unit resonance integrals (b, 7.36 - 6.25 ppm) to end group resonance integrals (a, 8.05 - 7.90 ppm) results in $M_n = 3650 \text{ g} \cdot \text{mol}^{-1}$.

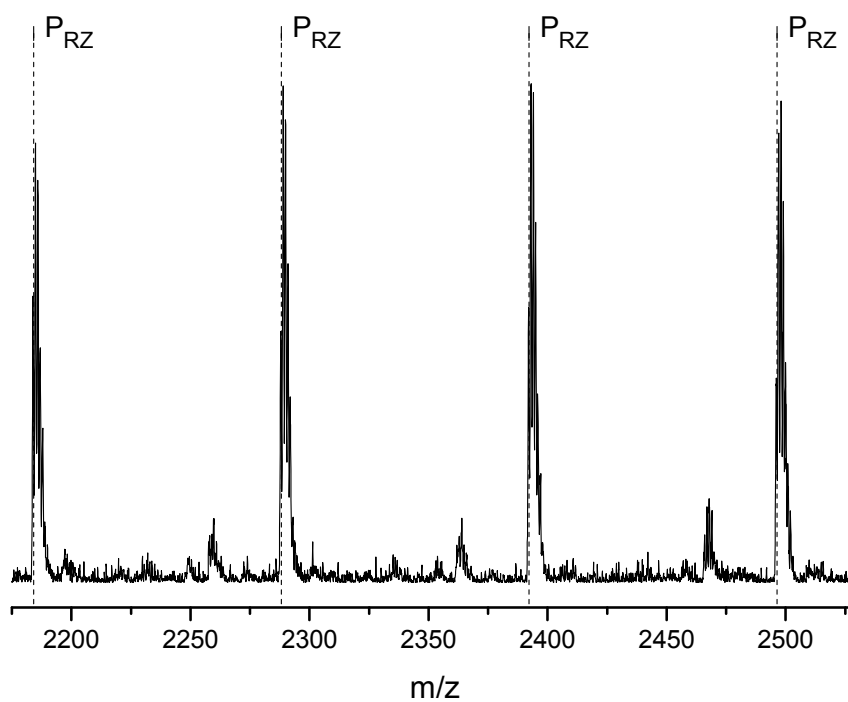
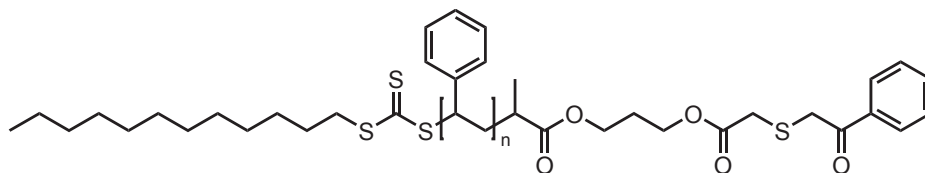


Figure 6.19: Zoom into the ESI-MS spectrum of polystyrene polymerized with DoPATPAS. The label P_{RZ} indicates the theoretical mass of chains with the R- and Z-group of the RAFT-agent as end groups, ionized with Na^+ (stemming from added NaTfa).

6. Photo-Induced Functionalization of Surfaces via Caged Thioaldehyde Polymers

Synthesis of Poly(*N,N*-dimethylacrylamide) (PDMAA)



A solution of AIBN (9.4 mg, 0.057 mmol, 0.20 equiv), DoPATPAS (174.1 mg, 0.29 mmol, 1.00 equiv) and DMAA (1.47 g, 14.8 mmol, 51 equiv) in DMF (7.5 mL) was deoxygenated with four consecutive freeze-pump-thaw cycles. The reaction was placed into a preheated oil-bath at 60 °C for 3 h. The reaction was stopped by cooling in an ice-bath and exposing the reaction mixture to oxygen. The polymer was isolated by dialyzing the reaction mixture against distilled water (utilizing a SpectraPor3 membrane (MWCO = 500 Da)) and subsequent freeze drying to give 1.10 g of a yellow solid. $M_n = 7200 \text{ g} \cdot \text{mol}^{-1}$, $D = 1.07$ (GPC in dimethylacetamide (DMAc), polystyrene calibration); $M_n = 4800 \text{ g} \cdot \text{mol}^{-1}$ (NMR, comparison of the integrals between 8.05 - 7.90 ppm and 3.15 - 2.60 ppm).

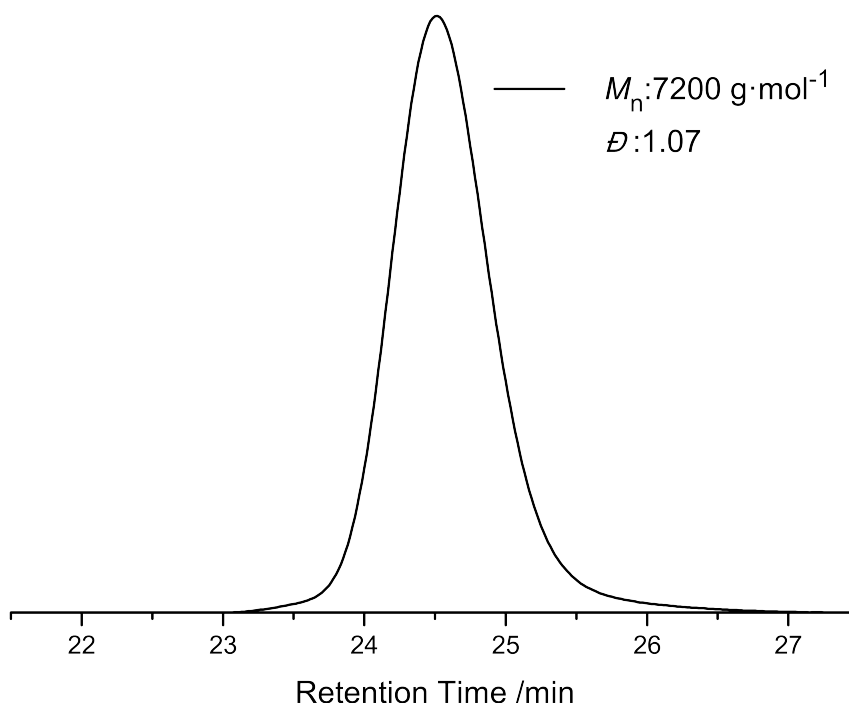


Figure 6.20: GPC trace (PS calibration) in DMAc of poly(*N,N*-dimethylacrylamide) polymerized with DoPATPAS.

6. Photo-Induced Functionalization of Surfaces via Caged Thioaldehyde Polymers

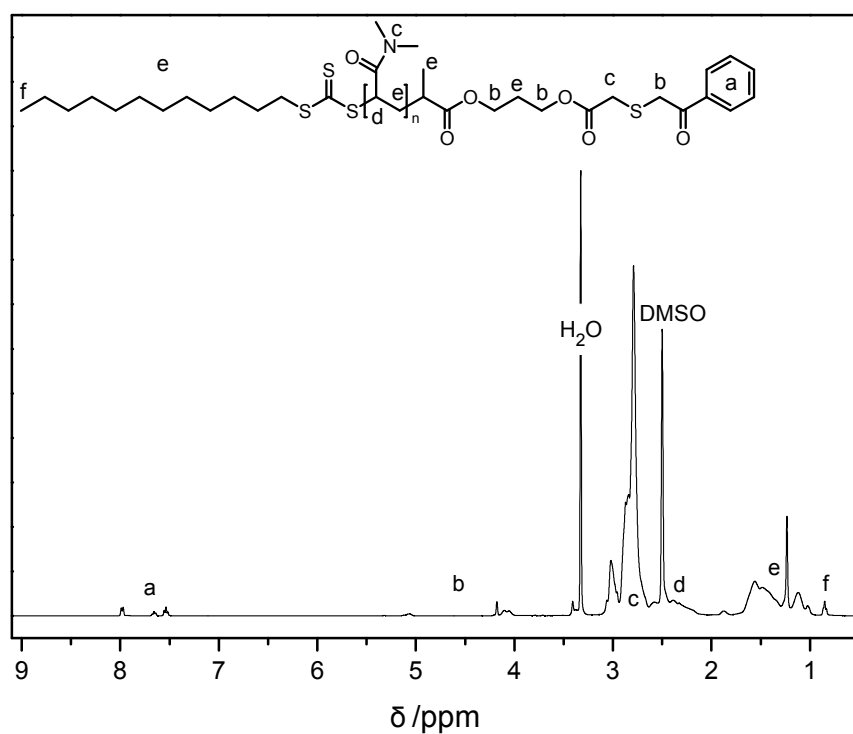


Figure 6.21: ¹H-NMR spectrum of poly(*N,N*-dimethylacrylamide) polymerized with DoPATPE in DMSO-*d*₆ at 400 MHz. Comparison of repetition unit resonance integrals (c, 3.15 - 2.60 ppm) to end group resonance integrals (a, 8.05 - 7.90 ppm) results in $M_n = 4800 \text{ g} \cdot \text{mol}^{-1}$.

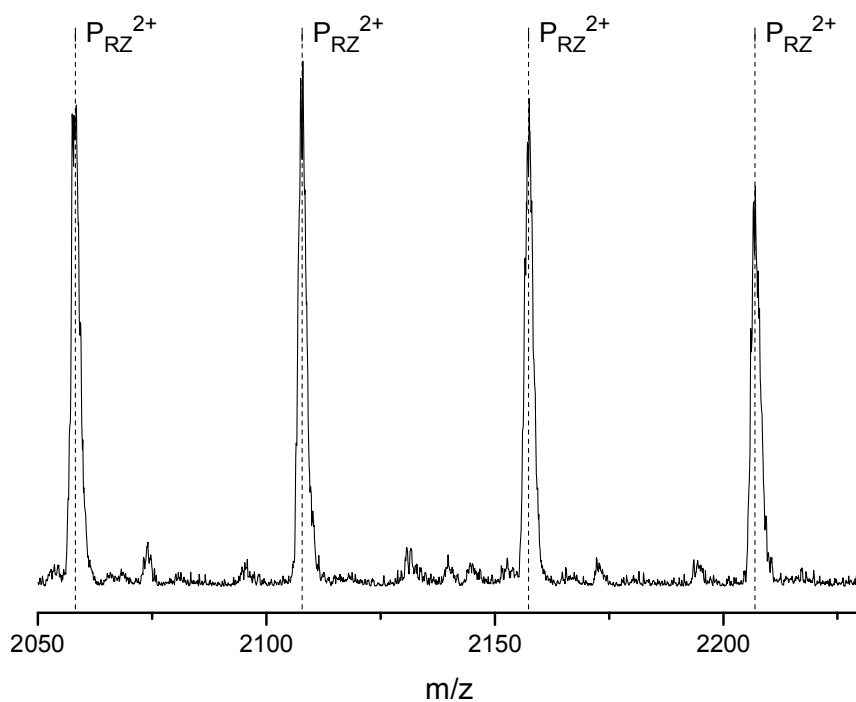


Figure 6.22: Zoom into the ESI-MS spectrum of poly(*N,N*-dimethylacrylamide) polymerized with DoPATPAs. The label P_{RZ}²⁺ indicates the theoretical average mass to charge ratio of chains with the R- and Z-group of the RAFT-agent as end groups, ionized with two Na⁺ (stemming from added NaTfa).

6. Photo-Induced Functionalization of Surfaces via Caged Thioaldehyde Polymers

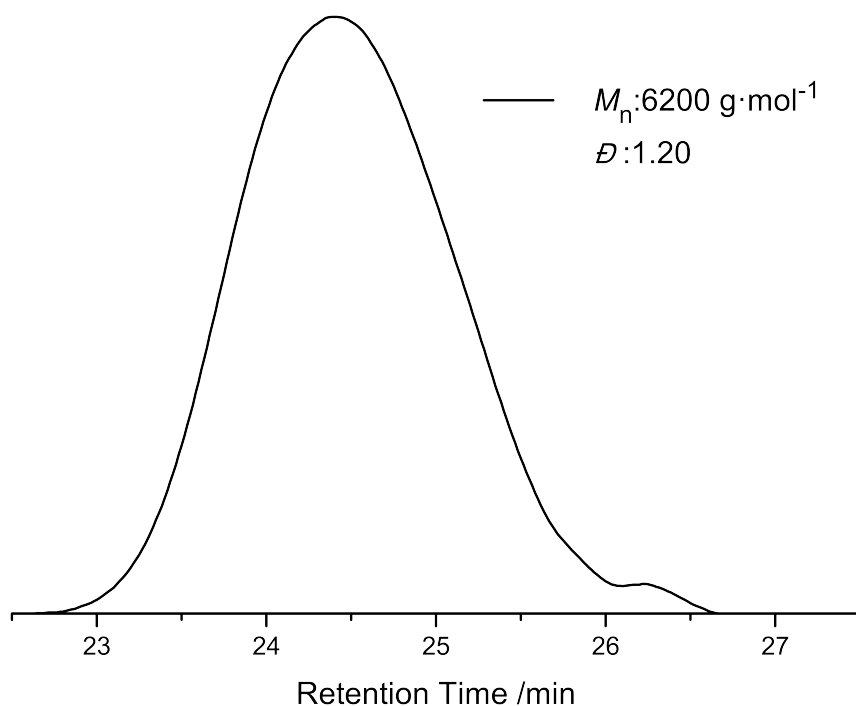


Figure 6.23: GPC trace (PS calibration) in DMAc of PAcManEA polymerized with DoPATPAS.

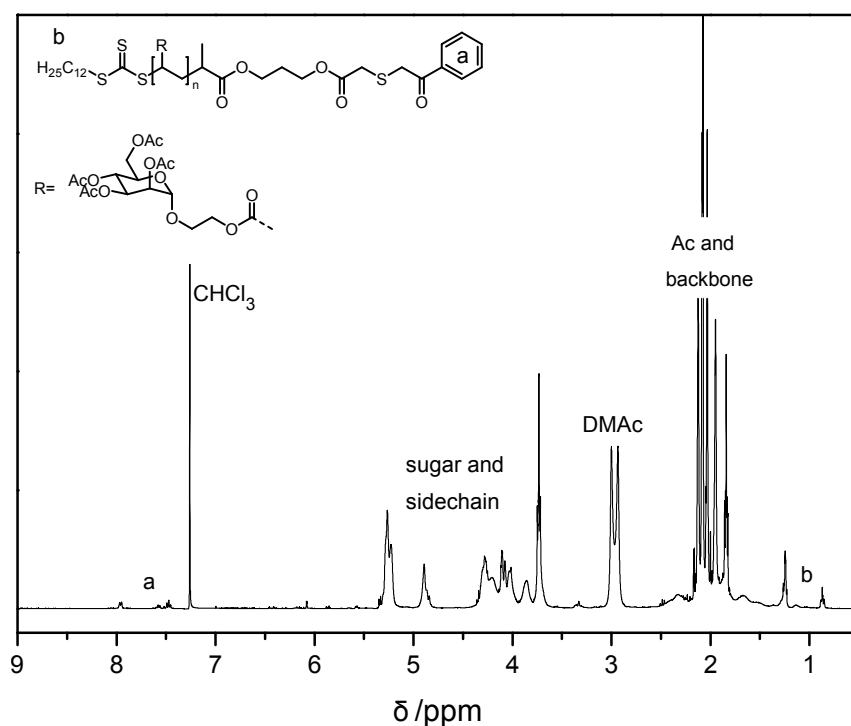


Figure 6.24: ¹H-NMR spectrum of PAcManEA polymerized with DoPATPE in CDCl₃ at 400 MHz. Comparison of repetition unit resonance integrals (5.40 - 3.60 ppm) to end group resonance integrals (a, 8.05 - 7.90 ppm) results in $M_n = 15000$ g·mol⁻¹.

6. Photo-Induced Functionalization of Surfaces via Caged Thioaldehyde Polymers

6.4.4 Functionalization of Silicon Wafers and Glass Slides with Polydopamin (PDA)*

Substrate Preparation

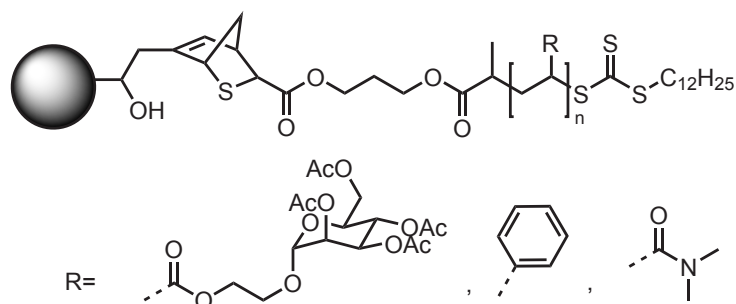
One side polished silicon wafers with a 50 nm thermal silicon dioxide (SiO_2) over-layer and BK-7 glass slides were sonicated in methanol and deionized water (Milli Q system, Millipore) for 15 min, immersed in a mixture of 25 % ammonia, 30 % hydrogen peroxide and water (1:1:5 v/v/v) heated at 70 °C for 10 min and finally thoroughly rinsed with water. Dry samples were exposed to air plasma (25 W) for 5 min just before PDA deposition.

Polydopamine (PDA) Coating

PDA was deposited from a $2 \text{ mg} \cdot \text{mL}^{-1}$ solution prepared by dissolution of dopamine hydrochloride in an air-saturated 10 mM tris(hydroxymethyl)aminomethane-HCl (pH 8.5) buffer.^[216] The deposition of PDA on the Si-substrates was performed in open glass dishes and under controlled stirring that provided a continuous supply of oxygen through the air/solution interface. In addition, the flat substrates were kept vertical to suppress microparticle sedimentation.^[215,218,232] The coated surfaces were finally rinsed with water, sonicated in water for 15 min and dried in a stream of nitrogen.

6.4.5 Photo-Reactions

Grafting Reactions and Control Reaction on Microspheres



The microspheres and DoPATPAS or RAFT-polymer, respectively, were mixed in DCM (5 mL) in glass vials (Pyrex, diameter 20 mm), which were crimped airtight with styrene/butadiene rubber seals (refer to Table 6.3 for details). The mixture was deoxygenated via purging with nitrogen for 20 min. The vials were subsequently irradiated for 60 minutes by rotating around a compact low-pressure fluorescent lamp (Philips CLEO

*Functionalization was performed by Dr. Ognen Pop-Georgievski, Institute of Macromolecular Chemistry, Academy of Sciences of the Czech Republic v.v.i., Prague, Czech.

6. Photo-Induced Functionalization of Surfaces via Caged Thioaldehyde Polymers

Compact PL-L, $\lambda_{\max} = 355$ nm) at a distance of 40-50 mm in a custom built photo-reactor (refer to Figure A.1 on page 162 for details). The microspheres were filtered off and washed three times with DCM and dried for four days at 50 °C under vacuum prior to analysis.

Table 6.3: Details and weigh-ins of control and grafting reactions on microspheres employing DoPATPAS

type of microspheres (amount)	grafted molecule (amount)
GMA (100.6 mg)	DoPATPAS (60.7 mg)
Cp (100.4 mg)	DoPATPAS (61.0 mg)
Cp (100.1 mg)	PS (360.5 mg)
Cp (100.8 mg)	PACManEA (629.3 mg)
Cp (99.9 mg)	PDMAA (470.2 mg)

Direct Laser Writing (DLW)[†]

Direct laser writing experiments were conducted using a home-built setup that has been previously described in detail.^[234] The setup is based on a Chameleon Ultra II, Coherent. The pulses were focused to a diffraction-limited spot by a 100x oil-immersion microscope lens (Leica HCX PL APO 100/1.4-0.7 CS Oil) with numerical aperture $NA = 1.4$. To write patterns, the samples were scanned with respect to the fixed focus by means of piezoelectric actuators. The pulse-picker described in the reference has been removed resulting in a repetition rate of 80 MHz and the laser has been tuned to 700 nm center wavelength. Patterning experiments were conducted using laser powers ranging from 8 mW to 3 mW and a writing speed of $100 \mu\text{m} \cdot \text{s}^{-1}$. For the patterns depicted in Figure 6.13 the squares (left) were functionalized (left to right) employing laser powers ranging from 8 mW to 3 mW in 1 mW steps. For the KIT logo (right) a laser power of 6 mW was employed.

[†]DLW was conducted by Alexander Quick, Institut für Technische Chemie und Polymerchemie, Karlsruhe Institute of Technology (KIT).

7

Concluding Remarks and Outlook

Polymeric microspheres are established as versatile substrates for a wide range of applications, notably in chromatographic systems and as carrier materials. Current research focuses not only on the synthesis of novel microparticles, yet in particular on the effective and versatile modification of existing and facile to synthesize spheres, thereby intensifying present or introducing novel properties.

The current thesis describes several techniques for the modular modification of porous polymeric microspheres as well as further possibilities of the developed grafting techniques. All the tethering strategies have in common that the grafted polymers were generated by RAFT-polymerization, underpinning its status as the most versatile controlled RDRP technique. The excellent control over the molecular weight distribution was evidenced via GPC evaluation and the high end group fidelity – a requirement for successful grafting – confirmed by NMR and ESI-MS analysis.

The second commonality of the employed approaches is the utilization of 'grafting-to' techniques, permitting the thorough examination of the polymer chains preceding the immobilization reaction. Steric hindrance tends to limit the achievable grafting densities, yet modular 'grafting-to' techniques separate the polymerization from the immobilization reaction, thereby increasing the amount of operational conjugation reactions and introducable functional groups.

The primary substrates employed in every chapter of the current work are porous

polymeric microparticles based on glycidyl methacrylate. The motif required for the subsequent ligation could be introduced to the spheres in one facile modification step. The conjugation of the polymer chains onto the particle was followed by a thorough investigation utilizing diverse instrumentations such as SEM, XPS, inverse SEC, elemental analysis, fluorescence microscopy, and high resolution attenuated total reflectance FT-IR-microscopy providing qualitative as well as quantitative insights into the modified particles and the achieved grafting densities.

The first ligation strategy applied RAFT-HDA, a thermally-induced cycloaddition utilizing electron deficient thiocarbonyls originating from RAFT-agents, which were before employed for the controlled polymerization of a glycopolymer. A comprehensive study of the achievable loading capacities on Cp-functionalized microspheres – with pore sizes ranging over several orders of magnitude – was carried out. Moreover, the first grafting of a glycopolymer onto microparticles via mild cycloaddition chemistry was performed and a grafting density of $0.16 \text{ chains} \cdot \text{nm}^{-2}$ was obtained.

The remaining chapters describe the precise ligation of polymers onto microspheres via photo-induced conjugation reactions, an unexplored concept for the modification of microparticles. Two novel light-sensitive RAFT-agents were developed in the course of the thesis, containing functional motifs previously unknown in the structures of RAFT-mediators. The novel RAFT-agents can be utilized to generate a wide range of different polymers, including glycopolymers, in a controlled fashion.

The primary RAFT-agent contains an ortho-quinodimethane or photo-enol precursor, which forms an a highly reactive diene for Diels-Alder reactions upon irradiation ($\lambda_{\text{max}} = 320 \text{ nm}$). The end-functional polymers are capable of generating block copolymers in minutes and can be photo-grafted onto previously maleimide-functionalized particles. Furthermore, the light-triggered reaction allows for the generation of Janus-microspheres, featuring two different hemispheres, utilizing a Pickering emulsion approach, which can be depicted via high resolution ATR FT-IR microscopy. The second novel RAFT-agent gives rise to a thioaldehyde upon irradiation ($\lambda_{\text{max}} = 355 \text{ nm}$), which can react with dienes as well as nucleophiles. Cp-functional microparticles can be photo-grafted with RAFT-polymers generated with the aforementioned RAFT-mediator. The two light-induced ligation techniques lead to grafting densities of up to $0.12 \text{ chains} \cdot \text{nm}^{-2}$ (photo-enol) and $0.10 \text{ chains} \cdot \text{nm}^{-2}$ (thioaldehyde-ligation), respectively. In combination with a direct laser writing setup the latter RAFT-agent can further be utilized to generate patterns of polymers on nucleophilic surfaces, such as PDA interfaces, with submicrometer resolution, which can be imaged via ToF-SIMS.

7. Concluding Remarks and Outlook

The candidate envisions further research for the modification of microspheres aiming for an even milder conjugation technique employing visible and ambient (sun-)light, although the herein described approaches already open a wide range of possibilities for the grafting of macromolecular entities. More challenging (bio-)substrates such as proteins and DNA should be grafted with the described or similar techniques to prove and underpin the mild nature of the light-induced reactions. The versatility of light-induced reactions should be further exploited by examining more strategies to generate Janus-microspheres and micro- or nanostructured spherical objects, with distinguishable segments and patterns. The combination of patterned or segmented tethering and immobilization of biosubstrates paves the way to binary, even ternary microspheres expressing various bioactive entities, thus augmenting possible application fields. The generation and examination of modified substrates for actual chromatographic, medical or biological system is a wide research area with many opportunities for exciting results and might pave the way for commercial applications of modified polymeric microspheres.

8

Characterization Methods

8.1 Scanning Electron Microscopy (SEM)*

The morphology of the microspheres was studied on a Zeiss Supra 55. The samples were sputter-coated with 30 nm of gold before the measurement.

8.2 Gel Permeation Chromatography (GPC)

GPC measurements were performed on a Polymer Laboratories PL-GPC 50 Plus Integrated System, comprising an autosampler, a PLgel 5 mm bead-size guard column (50 × 7.5 mm) followed by three PLgel 5 mm MixedC columns (300 × 7.5 mm) and a differential refractive index detector using THF at 35 °C or *N,N*-dimethylacetamide (DMAc) containing 0.3 % LiBr at 50 °C as the eluent with a flow rate of 1 mL · min⁻¹. The GPC system was calibrated using linear polystyrene standards ranging from 160 to 6 · 10⁶ g · mol⁻¹. All GPC calculations were carried out relative to a polystyrene calibration (Mark-Houwink parameters $K = 14.1 \cdot 10^{-5} \text{ dL} \cdot \text{g}^{-1}$, $\alpha = 0.70$).^[235]

*SEM preparations and measurements were conducted by Udo Geckle, Institute for Applied Materials (IAM-ESS), Karlsruhe Institute of Technology (KIT).

8.3 Electrospray Ionization – Mass Spectrometry (ESI–MS)

Spectra were recorded on an LXQ mass spectrometer (Thermo Fisher Scientific, San Jose, CA) equipped with an atmospheric pressure ionization source operating in the nebulizer assisted electrospray mode. The instrument was calibrated in the m/z range 195–1822 using a standard containing caffeine, Met-Arg-Phe-Ala acetate (MRFA) and a mixture of fluorinated phosphazenes (Ultramark 1621) (all from Aldrich). A constant spray voltage of 6 kV was used and nitrogen at a dimensionless sweep gas flow rate of 2 (approximately $3 \text{ L} \cdot \text{min}^{-1}$) and a dimensionless sheath gas flow rate of 5 (approximately $0.5 \text{ L} \cdot \text{min}^{-1}$) were applied. The capillary voltage, the tube lens offset voltage and the capillary temperature were set to 10 V, 70 V and 300°C , respectively. The samples were dissolved with a concentration of $0.1 \text{ mg} \cdot \text{mL}^{-1}$ in a mixture of THF and MeOH (3:2) containing $100 \mu\text{mol}$ of sodium triflate and infused with a flow of $10 \mu\text{L} \cdot \text{min}^{-1}$.

8.4 Density Measurements

The density of the microspheres was measured on an Anton Paar DMA 5000 M according to a procedure described by Barner and coworkers.^[49]

8.5 Nuclear Magnetic Resonance (NMR) Spectroscopy

NMR measurements were carried out on a Bruker AM400 (Chapter 3), a Bruker Ascend 400 or a Bruker Avance III spectrometer at 400 MHz or 300 MHz, respectively, for hydrogen nuclei. Samples were dissolved in CDCl_3 or $\text{DMSO}-d_6$ using residual solvent peaks for shift correction.

8.6 Inverse Size Exclusion Chromatography (iSEC)[†]

The total surface area of the microspheres was determined via iSEC, by the method described by Gorbunov^[236,237] and has been employed for similar systems before.^[197] The measurement was conducted on a PSSecurity 1200 HPLC-system equipped with an autosampler, pump, degasser and RI detector. The software used for data processing was PoroCheck (PSS GmbH, Mainz) and the system was calibrated with polymer standard reference kits of pullulan and polystyrene.

[†]iSEC measurements were conducted by Polymer Standards Service GmbH, Mainz.

8.7 Gel Permeation Chromatography – Electrospray Ionization – Mass Spectrometry (GPC–ESI–MS)

Spectra were recorded on an LXQ mass spectrometer as described above. The LXQ was coupled to a Series 1200 HPLC-system (Agilent, Santa Clara, CA, USA) consisting of a solvent degasser (G1322A), a binary pump (G1312A), a high-performance autosampler (G1367B), followed by a thermostated column compartment (G1316A). Separation was performed on two mixed bed size exclusion chromatography columns (Polymer Laboratories, Mesopore 250 × 4.6 mm, particle diameter 3 μm) with precolumn (Mesopore 50 × 4.6 mm) operating at 30 °C. THF at a flow rate of 0.30 mL · min⁻¹ was used as eluent. The mass spectrometer was coupled to the column in parallel to an RI-detector (G1362A with SS420xA/D) in a setup described earlier.^[238] 0.27 mL · min⁻¹ of the eluent were directed through the RI-detector and 30 μL · min⁻¹ infused into the electrospray source after postcolumn addition of a 100 μM solution of sodium iodide in methanol at 20 μL · min⁻¹ by a micro-flow HPLC syringe pump (Teledyne ISCO, Model 100DM). A 20 μL aliquot of a polymer solution with a concentration of 3 mg · mL⁻¹ was injected onto the HPLC system.

8.8 X-Ray Photoelectron Spectroscopy (XPS)[‡]

XPS investigations were performed on a K-Alpha spectrometer (Thermo Fisher Scientific, East Grinstead, UK) using a micro-focused, monochromated Al K-α X-ray source (400 μm spot size). The kinetic energy of the electrons was measured by a 180° hemispherical energy analyzer operated in the constant analyzer energy mode (CAE) at 50 eV pass energy for elemental spectra. The photoelectrons were detected at an emission angle of 0° with respect to the normal of the sample surface. The K-Alpha charge compensation system was employed during analysis, using electrons of 8 eV energy and low-energy argon ions to prevent any localized charge build-up. Data acquisition and processing using the Thermo Avantage software is described elsewhere.^[239] The spectra were fitted with one or more Voigt profiles (BE uncertainty: ±0.2 eV). The analyzer transmission function, Scofield^[240] sensitivity factors, and effective attenuation lengths (EALs) for photoelectrons were applied for quantification. EALs were calculated using the standard TPP-2 M formalism.^[241] All spectra were referenced to the C 1s peak of hydrocarbon at 285.0 eV binding energy, controlled by means of the well-known photoelectron peaks of metallic Cu, Ag, and Au, respectively.

[‡]XPS measurements and raw data analysis were performed by Vanessa Trouillet, Institute for Applied Materials (IAM-ESS), Karlsruhe Institute of Technology (KIT).

8.9 High Resolution Attenuated Total Reflectance (ATR) FT-IR-Microscopy Imaging[§]

Infrared measurements were performed using a Bruker FT-IR-microscope HYPERION 3000 coupled to a research spectrometer VERTEX 80. The HYPERION 3000 microscope is equipped with two types of detectors: a single element MCT-detector (Mercury Cadmium Telluride) for the conventional mapping approach and a multi-element FPA-detector (focal plane array) for imaging. The FPA-detector was used for the laterally resolved measurements. The multielement FPA-detector consists of 64×64 elements, allowing for the simultaneous acquisition of 4096 spectra covering a sample area of $32 \times 32 \mu\text{m}$ (for ATR detection). With the FPA-detector in combination with the $20\times$ Germanium ATR-lens, a lateral pixel resolution of $0.25 \mu\text{m}^2$ is achieved, with the optical resolution depending on the employed wavelength (1000 cm^{-1} to $\sim 1 \mu\text{m}$ lateral resolution). For postprocessing baseline correction and atmospheric compensation were employed.

8.10 Ultraviolet-Visible (UV-Vis) Spectroscopy

UV-Vis spectra were recorded on a Varian Cary 300 Bio spectrophotometer. Spectra were recorded in acetonitrile in a 10 mm path length cell. Spectra were collected between 200 and 800 nm. Samples were baseline corrected with respect to the pure solvent.

8.11 Confocal Fluorescence Microscopy[¶]

The confocal laser scanning microscope LSM 510 Meta (Carl Zeiss Microscope Systems, Jena, Germany) was used for imaging microspheres embedded in mounting media (Mowiol[®], Merck, Darmstadt, Germany). The fluorescence molecules were excited with an Argon-Laser (405 nm). The optical magnification was achieved by a Plan-Apochromat $20\times/0.8$ suitable for DIC or a LCI Plan NEOFLUAR $63\times/1.3$ DIC ImKorr objective, respectively. The images were acquired with the Zeiss LSM510 operating software (V 4.2 SP1).

[§]Imaging in Chapter 4 was conducted by Thomas Tischer, Institut für Technische Chemie und Polymerchemie, Karlsruhe Institute of Technology (KIT).

[¶]Fluorescence imaging was conducted by Dr. Alexandra M. Greiner from the Zoological Institute, Cell- and Neurobiology and Centre for Functional Nanostructures (CFN), Karlsruhe Institute of Technology (KIT).

8.12 Elemental Analysis (EA)^{||}

The elemental composition of the microsphere samples was analyzed using an automatic elemental analyzer Flash EA1112 from Thermo Scientific, which was equipped with a MAS 200R auto sampler. More details can be found in the supporting information of ref. [86].

8.13 Time-of-Flight Secondary Ion Mass Spectrometry (ToF-SIMS)^{**}

ToF-SIMS was performed on a TOF.SIMS5 instrument (ION-TOF, Münster, Germany) equipped with a Bi cluster liquid metal primary ion source and a nonlinear time-of-flight analyzer. The Bi source was operated in the "bunched" mode, providing 0.7 ns Bi⁺ ion pulses at 25 keV energy and a lateral resolution of ~4 μm . The short pulse length allowed for high mass resolution to analyze the complex mass spectra of the immobilized organic layers. Images larger than the maximum deflection range of the primary ion gun of $500 \times 500 \mu\text{m}^2$ were obtained using the manipulator stage scan mode. Negative polarity spectra were calibrated on the C⁻, C²⁻, C³⁻, and Br⁻ or F⁻ peaks. Positive polarity spectra were calibrated on the C⁺, CH⁺, CH₂⁺ and CH₃⁺ peaks. Primary ion doses were kept below 10^{11} ions \cdot cm⁻² (static SIMS limit).

8.14 Spectroscopic Ellipsometry^{††}

The thickness of the films in the dry state was determined by ellipsometry using a Variable Angle Spectroscopic Imaging Auto-Nulling Ellipsometer EP3-SE (Nanofilm Technologies GmbH, Germany) in the wavelength range of $\lambda = 399\text{-}811$ nm (source Xe-arc lamp, wavelength step ~ 10 nm) at an angle of incidence AOI = 70° in air at room temperature. The optical constants of the PDA layers and SiO₂/Si substrates were taken from elsewhere.^[215,242]

^{||}Elemental analyses were conducted by the Fraunhofer-Institut für Chemische Technologie (ICT) in Pfinztal.

^{**}ToF-SIMS measurements were performed by Dr. Alexander Welle from the Institut für Biologische Grenzflächen (IBG), Karlsruhe Institute of Technology (KIT).

^{††}Spectroscopic ellipsometry was conducted by Dr. Ognen Pop-Georgievski at the Institute of Macromolecular Chemistry, Academy of Sciences of the Czech Republic v.v.i., Prague, Czech.

A

Appendix

Table A.1: Collected data from the inverse size exclusion chromatography of the non-modified microspheres employed in the current thesis under the assumption of cylindrical pores by the method described by Gorbunov.^[236,237]

Sample	Average pore dimension [nm]	Width of pore size distribution [nm]	Surface area [m²/cm³]
PGMA 30 Å	3.33 ± 0.06	11.9 ± 0.1	601.3 ± 11.4
PGMA 100 Å	6.29 ± 0.09	8.5 ± 0.1	318.0 ± 4.5
PGMA 1000 Å	8.87 ± 1.27	29.8 ± 1.5	225.4 ± 34.6
PGMA 3000 Å	24.37 ± 2.06	57.9 ± 2.6	82.1 ± 7.4
PGMA 10000 Å	15.13 ± 1.42	67.7 ± 2.4	132.2 ± 13.1
PGMA 30000 Å	8.55 ± 0.76	108.4 ± 3.0	234.0 ± 21.8

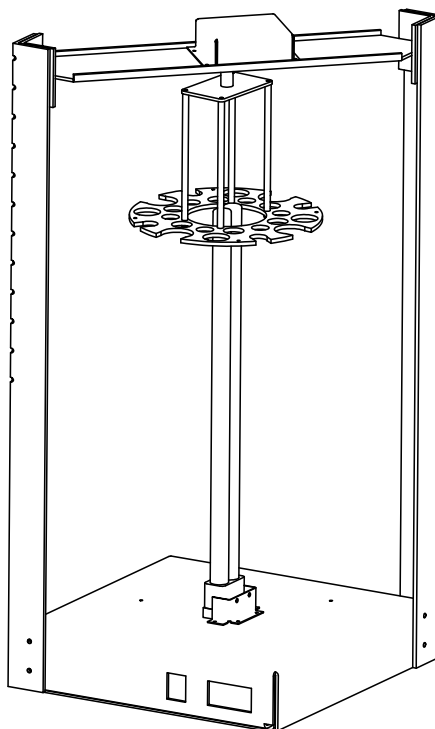


Figure A.1: Illustration of the employed photo-reactor.

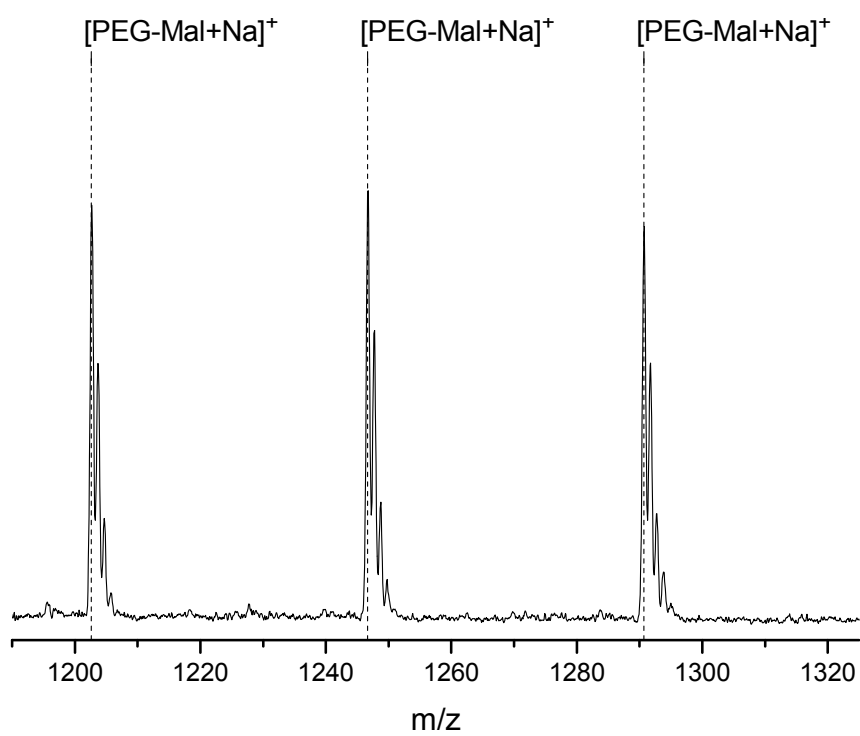


Figure A.2: Zoom into the ESI-MS spectrum of PEG-Mal. The label indicates the theoretical mass of chains ionized with Na^+ (stemming from added NaTfa).

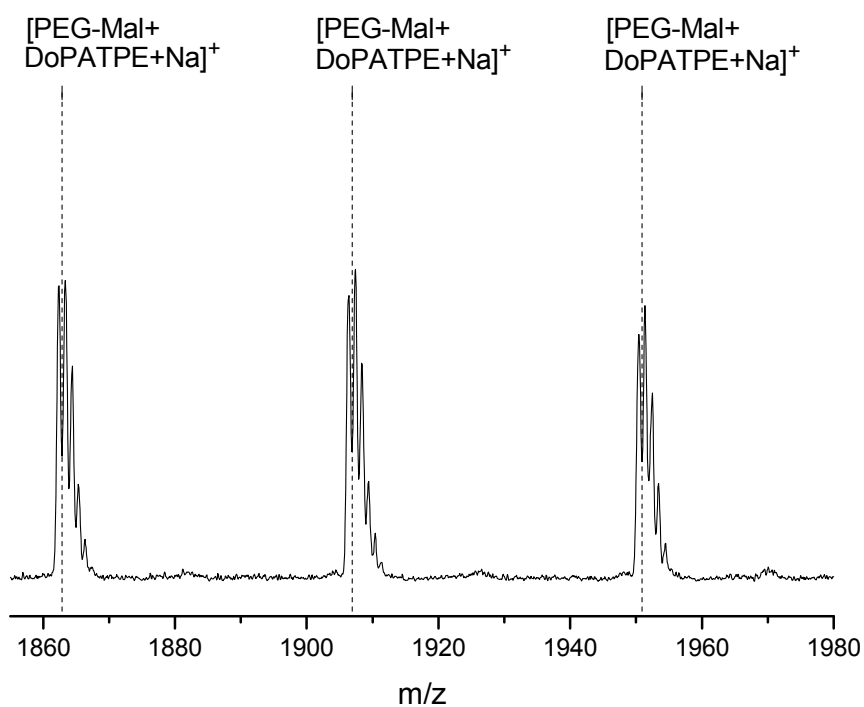


Figure A.3: Zoom into the ESI-MS spectrum of the photo-adduct between PEG-Mal and DoPATPE after 60 min irradiation. The label indicates the theoretical mass of chains ionized with Na^+ (stemming from added NaTfa).

Table A.2: Experimental and theoretical m/z values for the labeled peaks of Figure A.2 and Figure A.3.

m/z_{exp}	assignment	formula	m/z_{theo}	$\Delta m/z$
1246.67	PEG-Mal+Na	$[\text{C}_{55}\text{H}_{101}\text{NO}_{28}\text{Na}]^+$	1246.64	0.03
1906.75	PEG-Mal+ DoPATPE+Na	$[\text{C}_{90}\text{H}_{149}\text{NO}_{34}\text{S}_3\text{Na}]^+$	1906.90	0.15

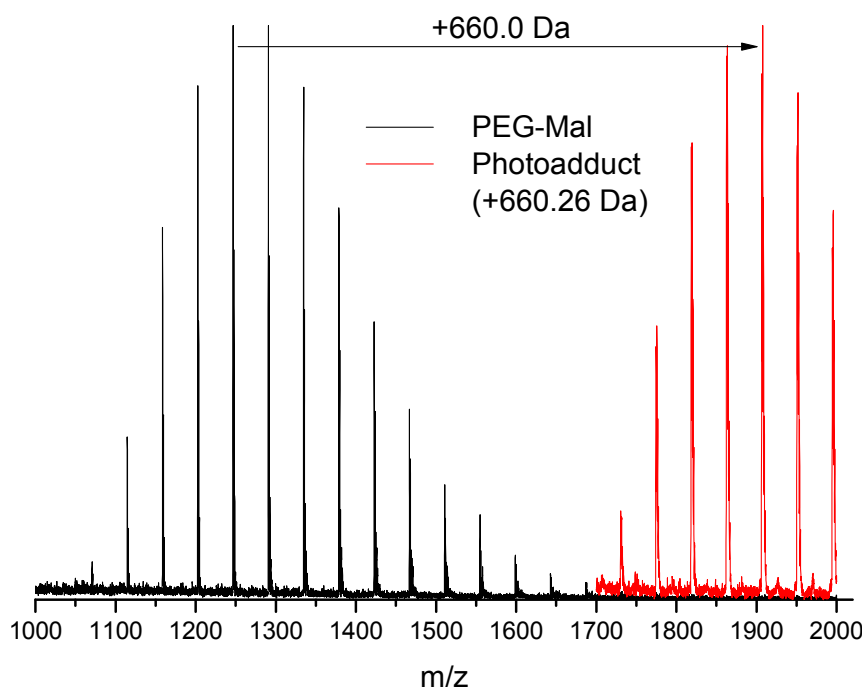


Figure A.4: Zoom into the single charged region of the ESI-MS spectrum of the model reaction between DoPATPE and PEG-Mal. The red spectrum shows the photo-adduct after 60 min irradiation. The shift of the peaks matches the mass of DoPATPE. No other signals are observed, underlining full conversion and stability of the photo-adduct.



Figure A.5: Picture of the suspension of maleimide-functionalized microspheres in a solution of RAFT-polymer (here PDMAA) in DCM prior to irradiation.

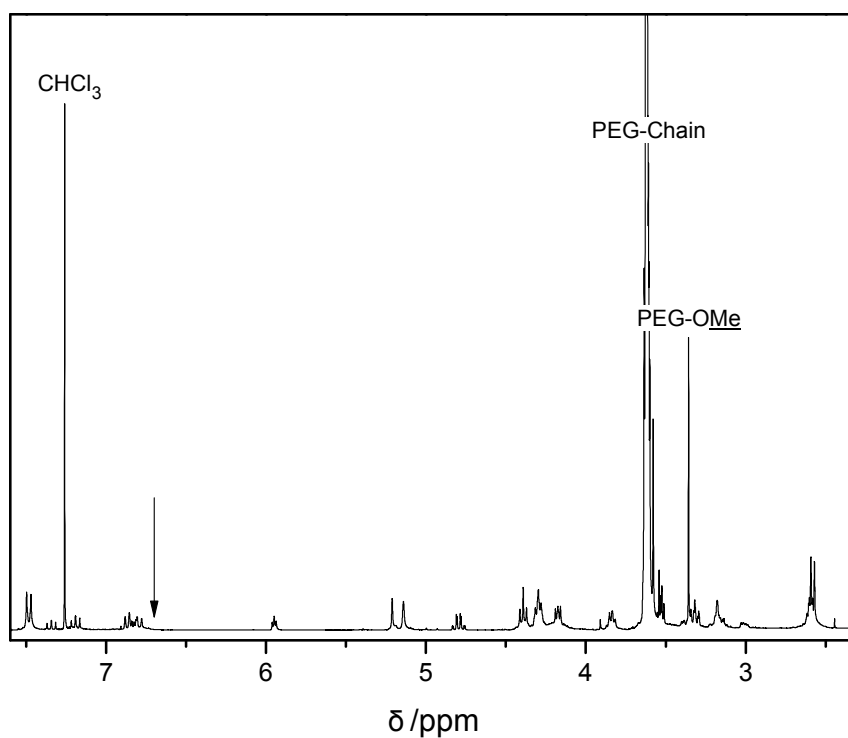


Figure A.6: Excerpt of the ¹H-NMR spectrum of the photo-addition of DoPATPE to PEG-Mal in CDCl₃ at 400 MHz. The arrow depicts the position, where the signal of the maleimide vanished (6.71 ppm, compare to resonance a in Figure A.7).

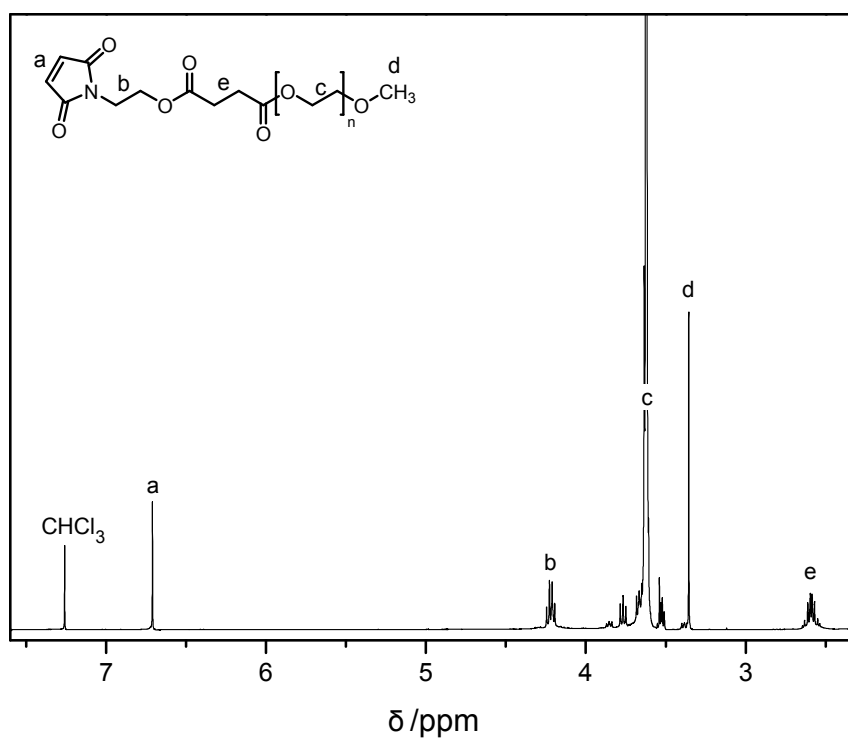


Figure A.7: ¹H-NMR spectrum of PEG-Mal in CDCl₃ at 300 MHz.

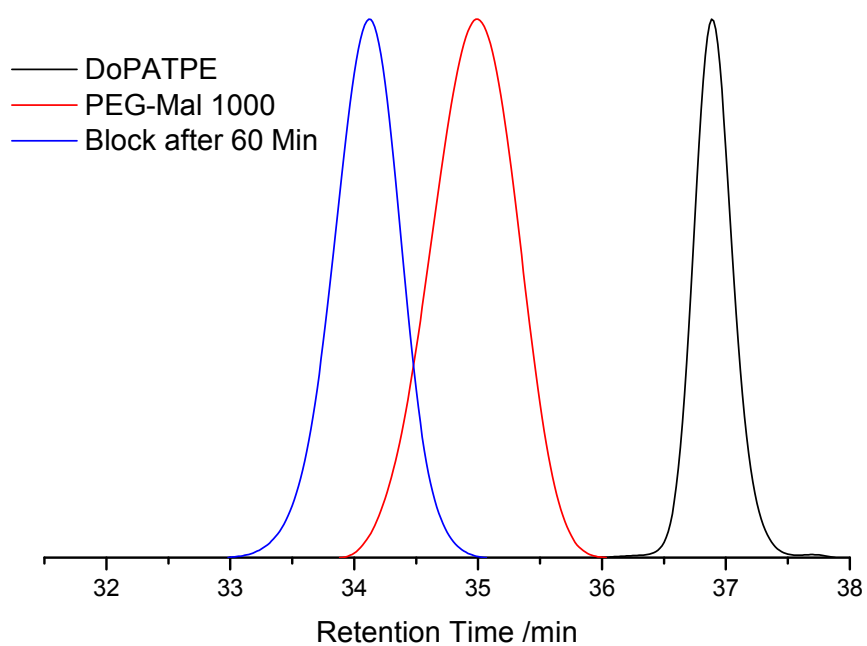


Figure A.8: Overlay of GPC traces in THF showing the formation of the photo-adduct between PEG-Mal and DoPATPE.



Figure A.9: Image of the wax sphere decorated with maleimide-functionalized microspheres.

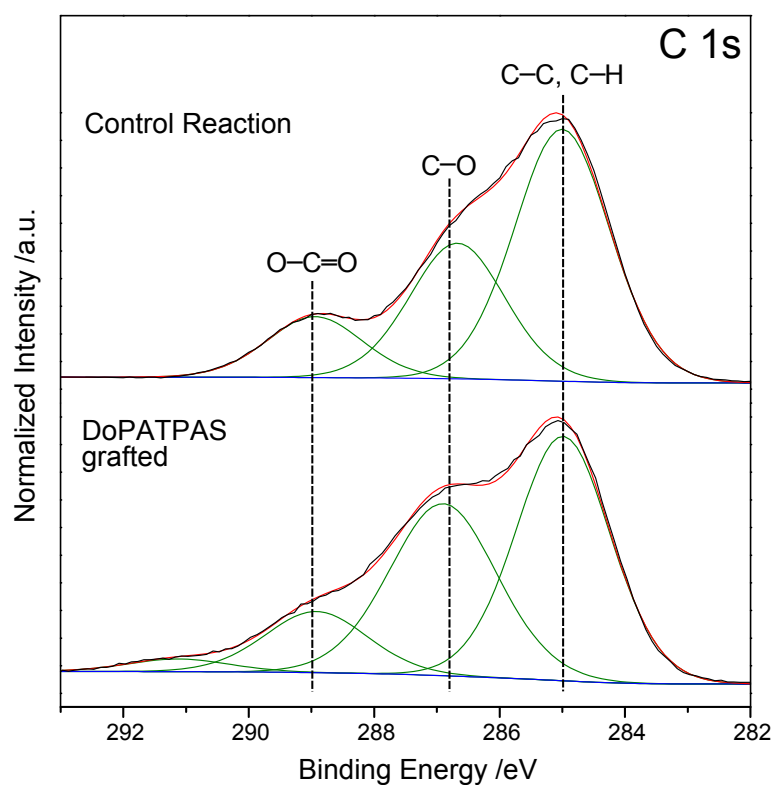


Figure A.10: C 1s XP spectrum of Cp-functionalized microspheres photo-grafted with DoPATPAS (bottom) and the control reaction of PGMA spheres applied to the same reaction conditions (top).

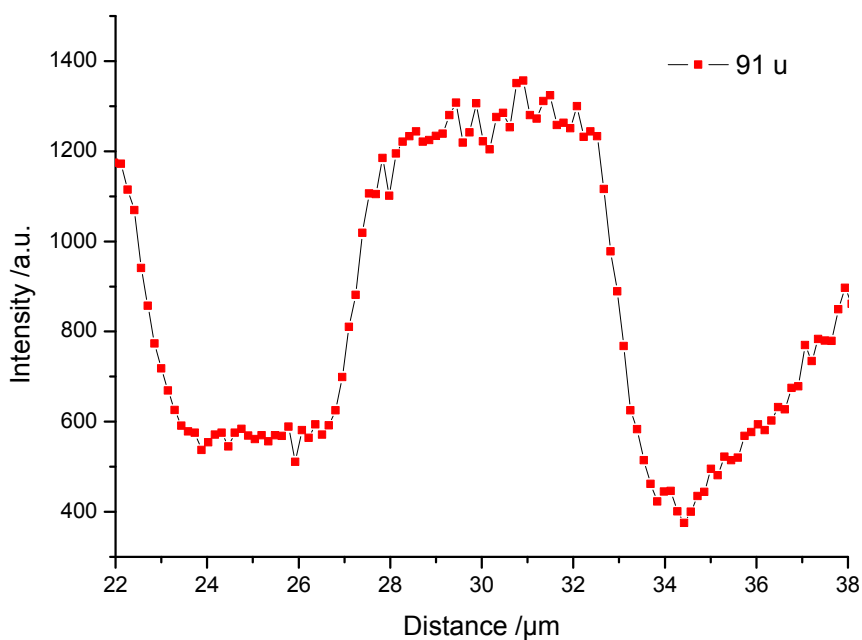


Figure A.11: 'Intensity profile' for the $C_7H_7^+$ signal across an edge of the DLW patterned structure shown in Figure 6.13 right.

A.1 Additional SEM Images from Chapter 4

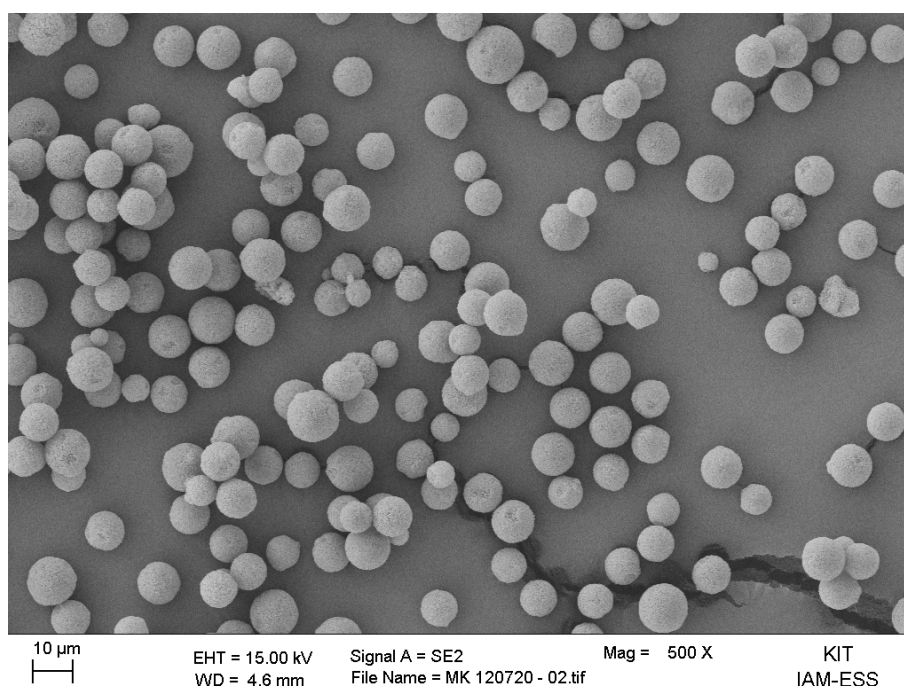


Figure A.12: SEM image of the maleimide-functionalized microspheres. Overview image.

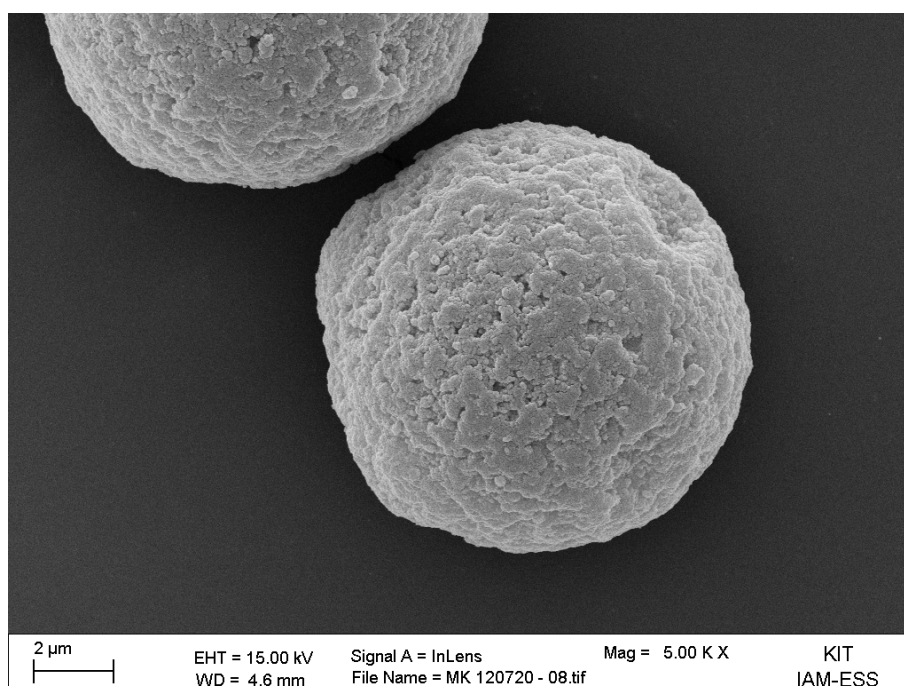


Figure A.13: SEM image of the maleimide-functionalized microspheres. Zoom image.

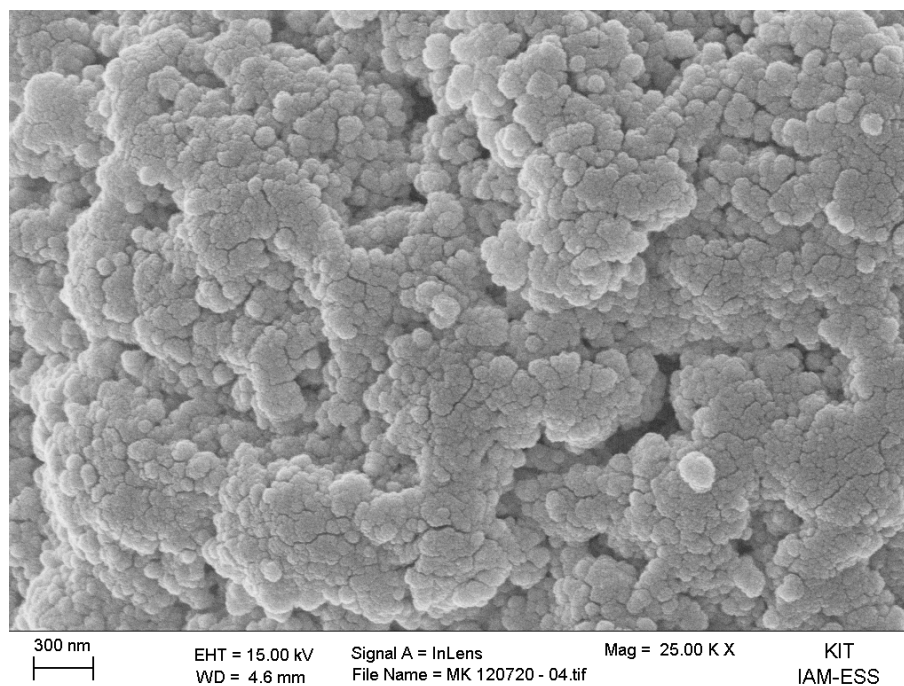


Figure A.14: SEM image of the maleimide-functionalized microspheres. Surface morphology image.

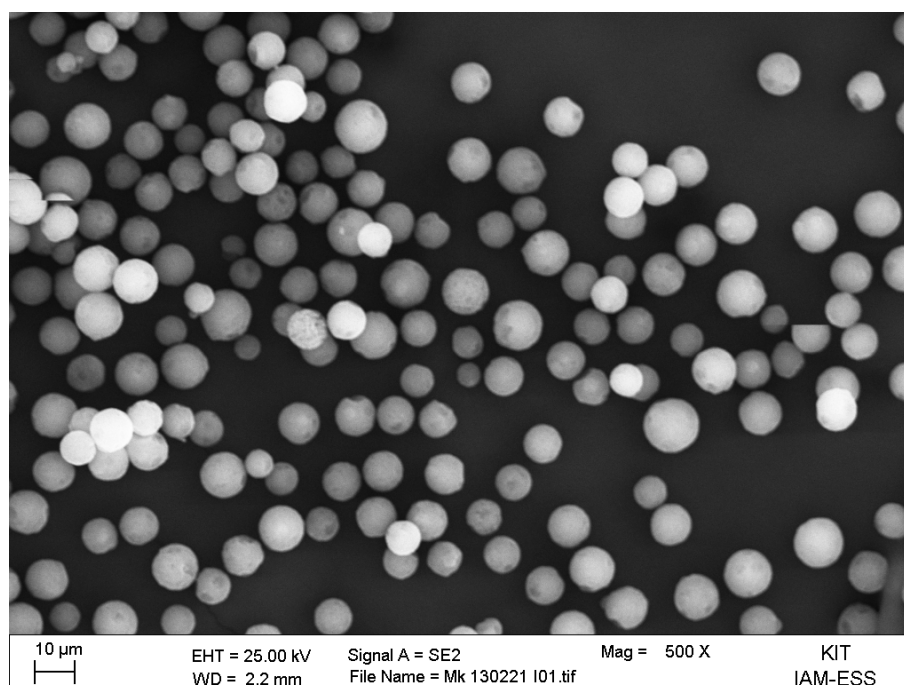


Figure A.15: SEM image of the maleimide-functionalized microspheres grafted with PS. Overview image.

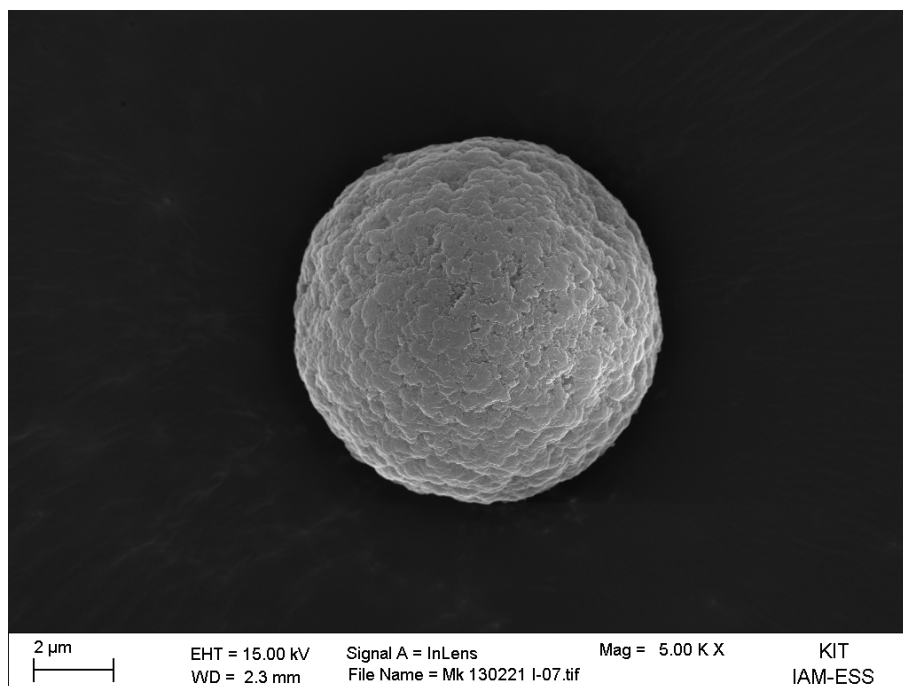


Figure A.16: SEM image of the maleimide-functionalized microspheres grafted with PS. Zoom image.

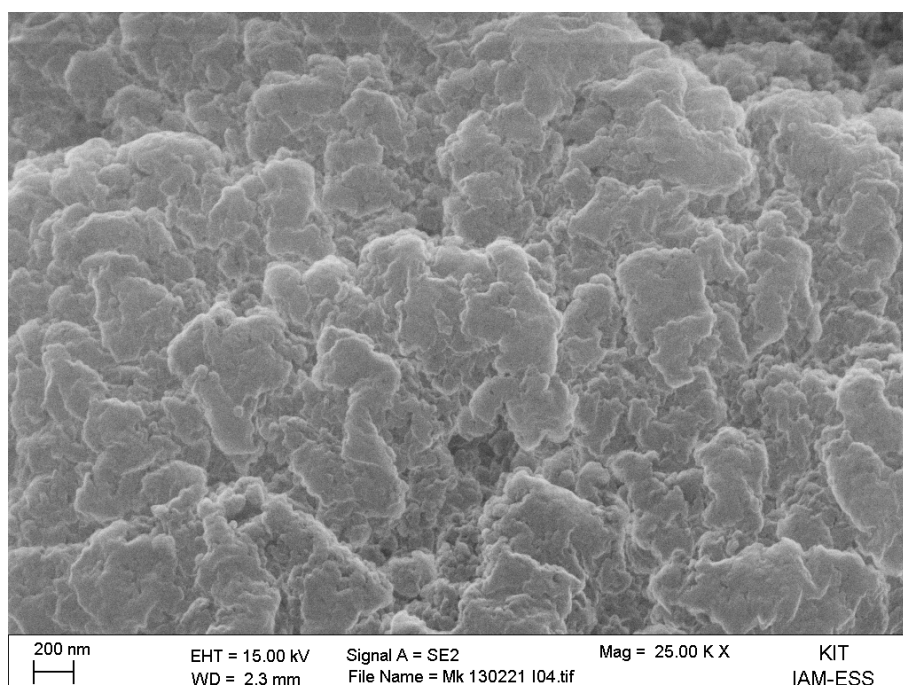


Figure A.17: SEM image of the maleimide-functionalized microspheres grafted with PS. Surface morphology image.

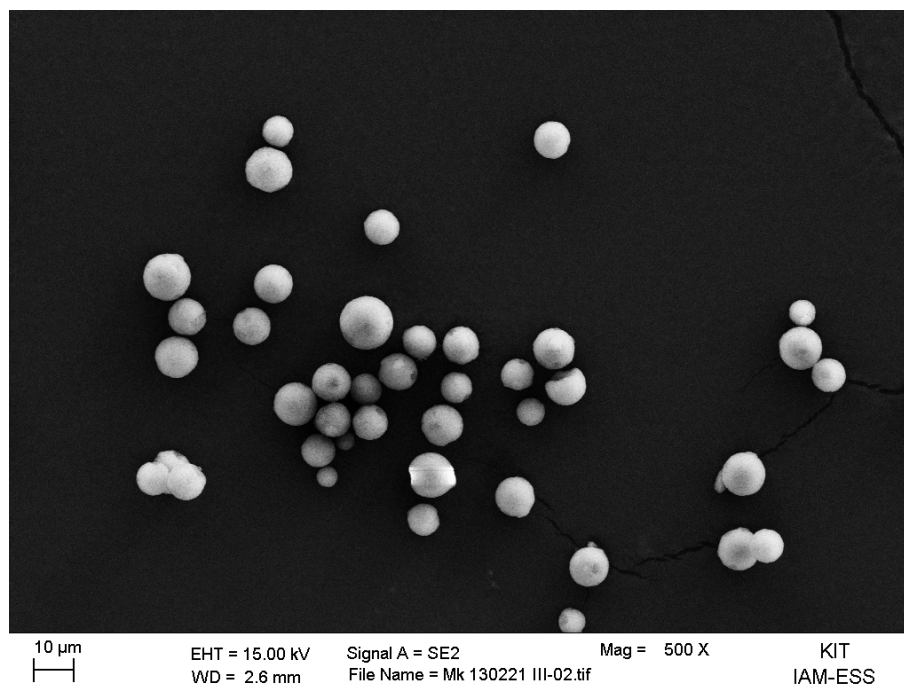


Figure A.18: SEM image of the maleimide-functionalized microspheres grafted with PAcManEA. Overview image.

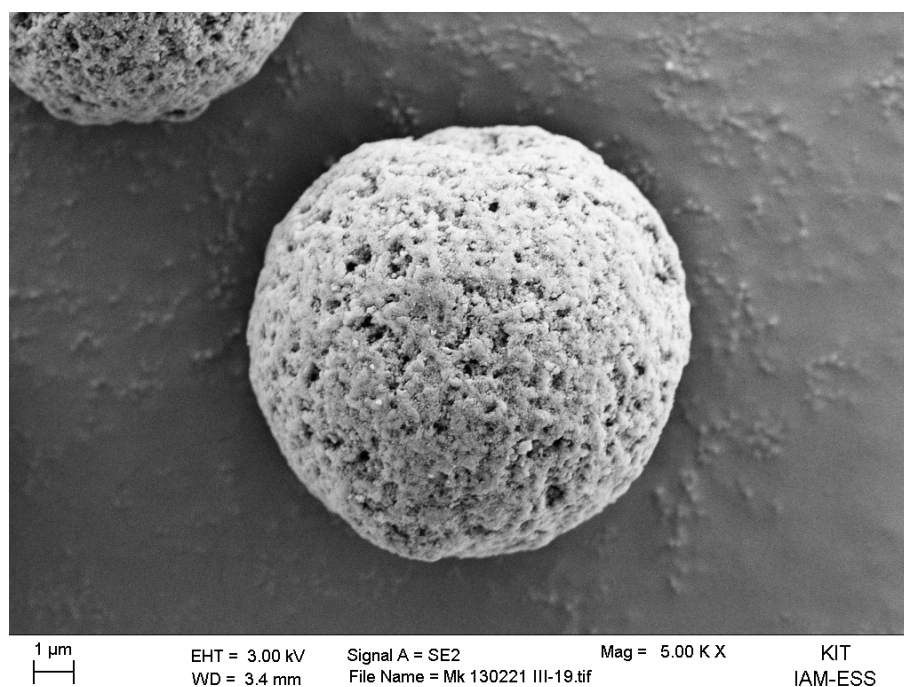


Figure A.19: SEM image of the maleimide-functionalized microspheres grafted with PAcManEA. Zoom image.

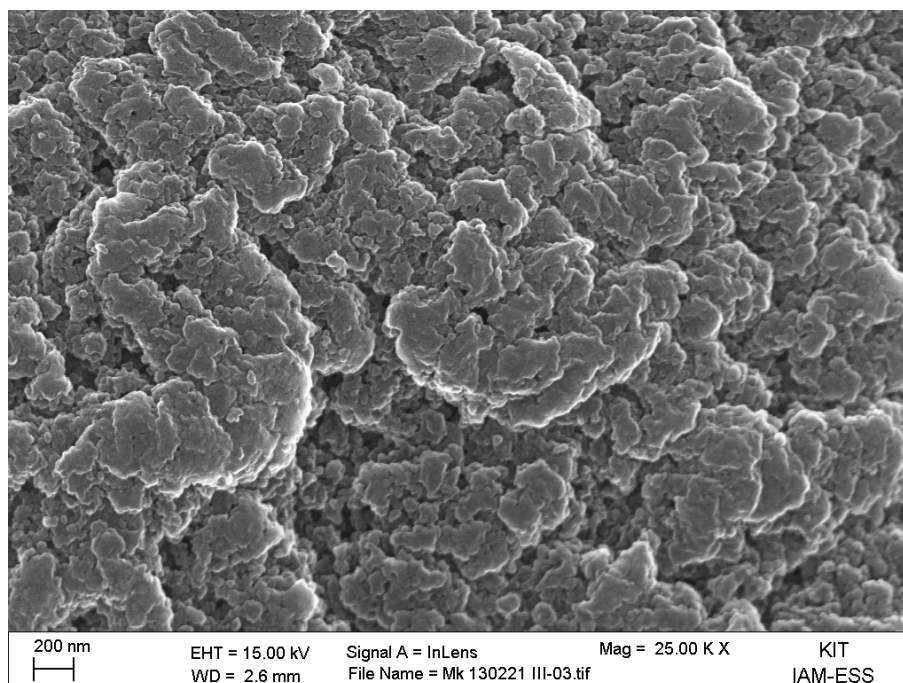


Figure A.20: SEM image of the maleimide-functionalized microspheres grafted with PAcManEA. Surface morphology image.

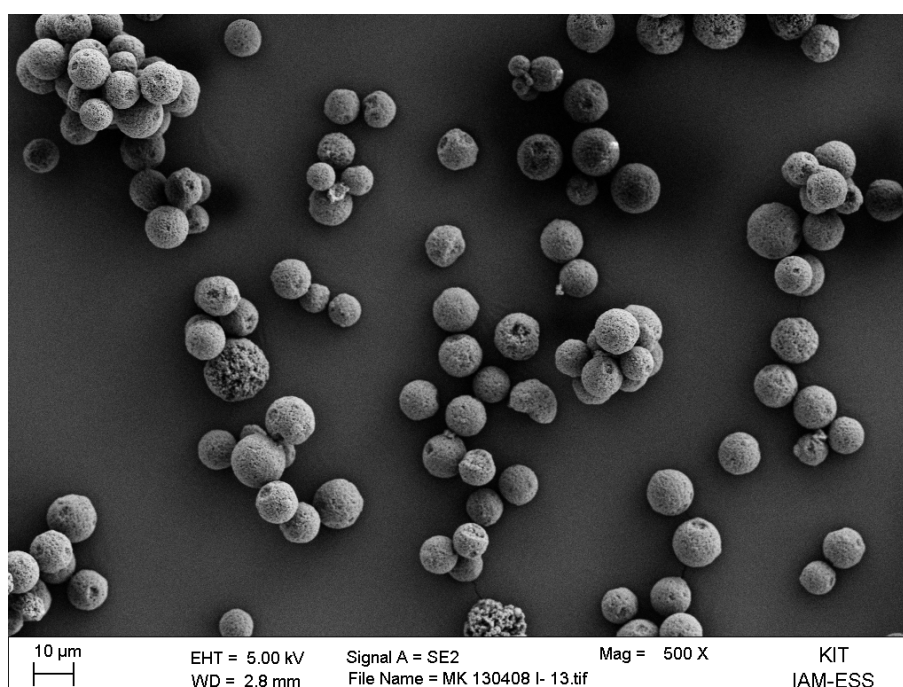


Figure A.21: SEM image of the maleimide-functionalized microspheres grafted with PDMAA. Overview image.

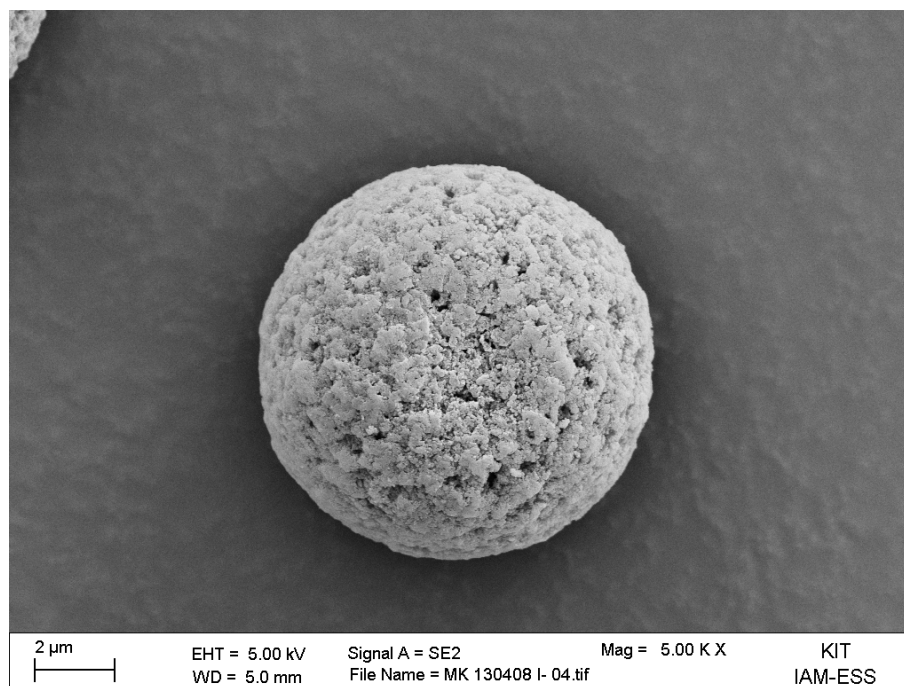


Figure A.22: SEM image of the maleimide-functionalized microspheres grafted with PDMAA. Zoom image.

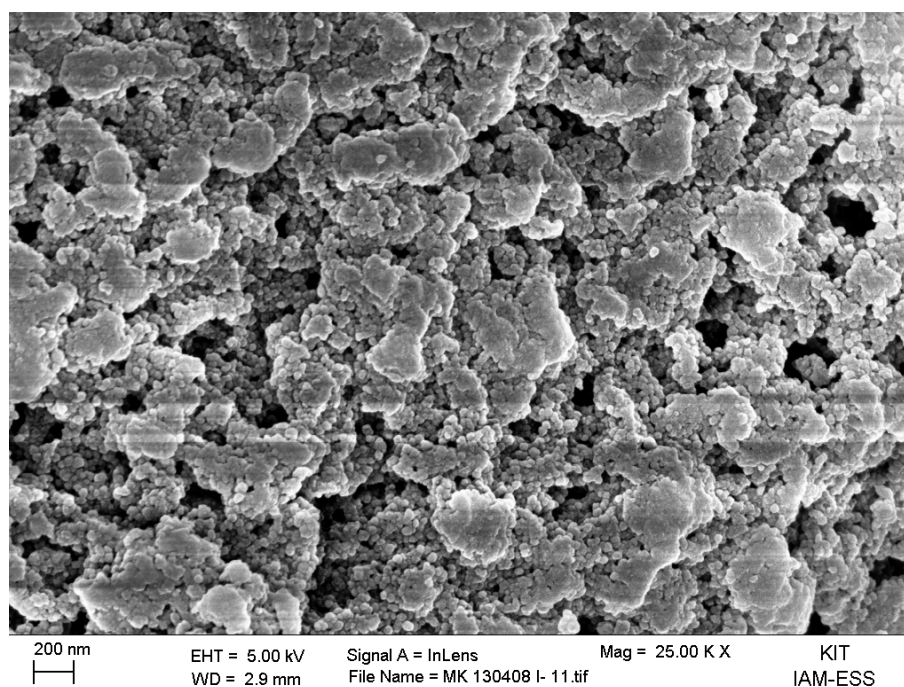


Figure A.23: SEM image of the maleimide-functionalized microspheres grafted with PDMAA. Surface morphology image.

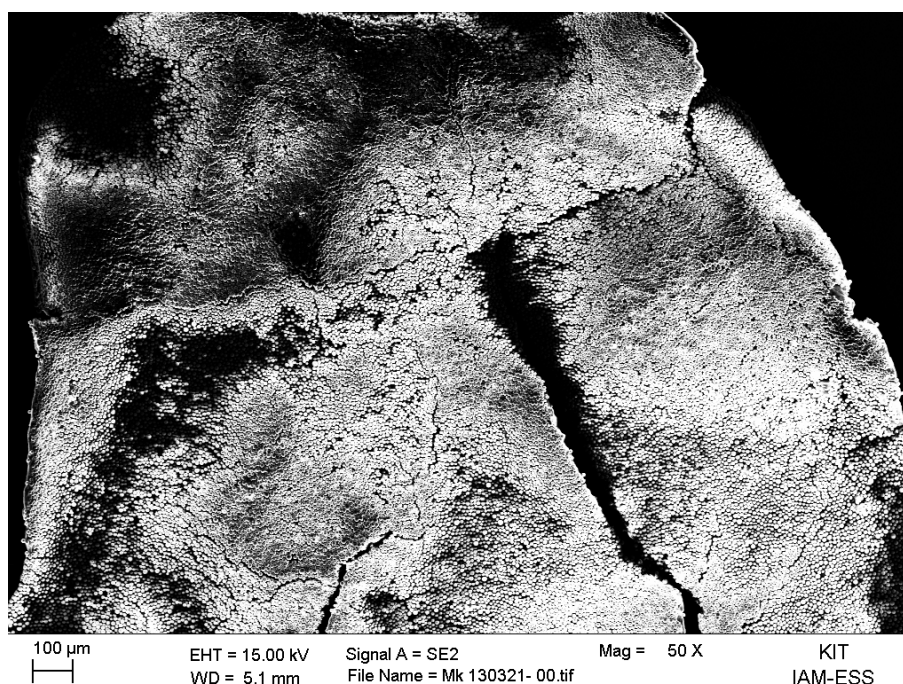


Figure A.24: SEM image of a wax sphere (diameter approx. 5 mm) covered with maleimide-functionalized microspheres. The microspheres are evenly distributed on the surface of the wax sphere.

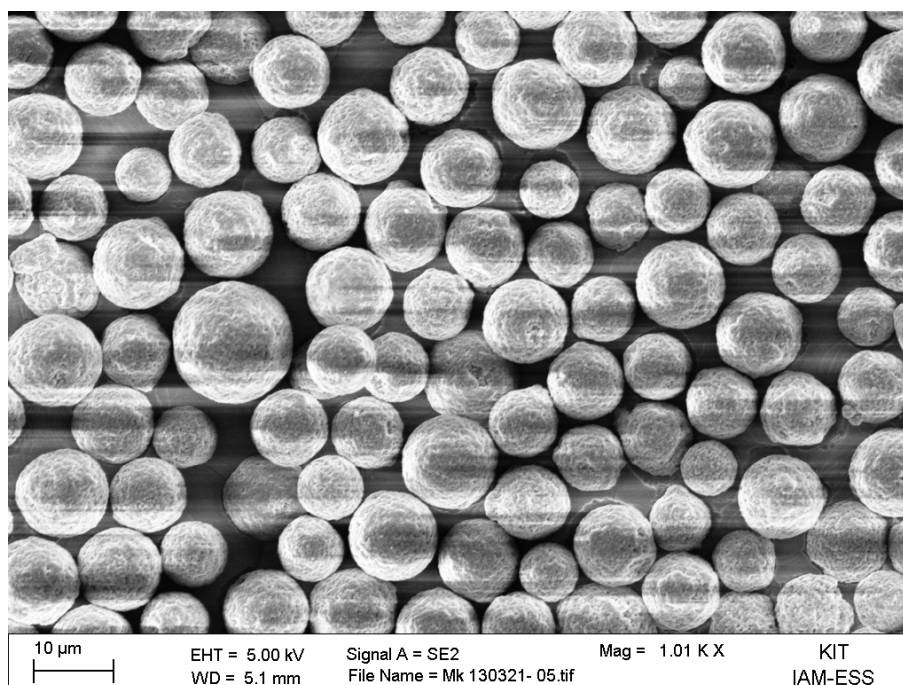


Figure A.25: SEM image of the surface of a wax sphere covered with maleimide-functionalized microspheres. The microspheres are evenly distributed on the surface of the wax sphere. The artifacts stem from charge build up due to the size of the wax sphere (diameter approx. 5 mm).

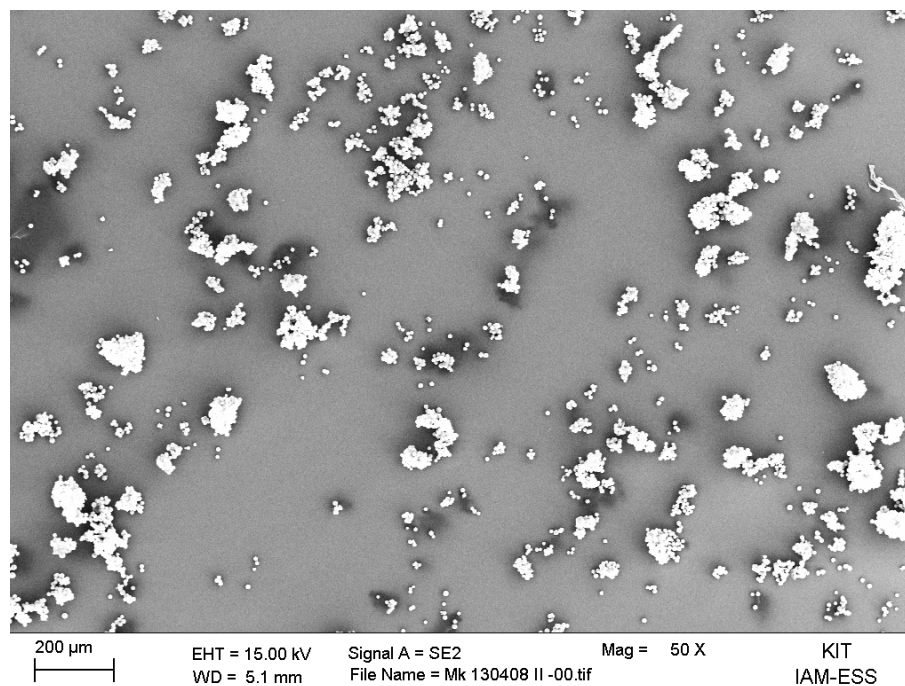


Figure A.26: SEM image of the maleimide-functionalized microspheres half grafted with PDMAA. Overview image.

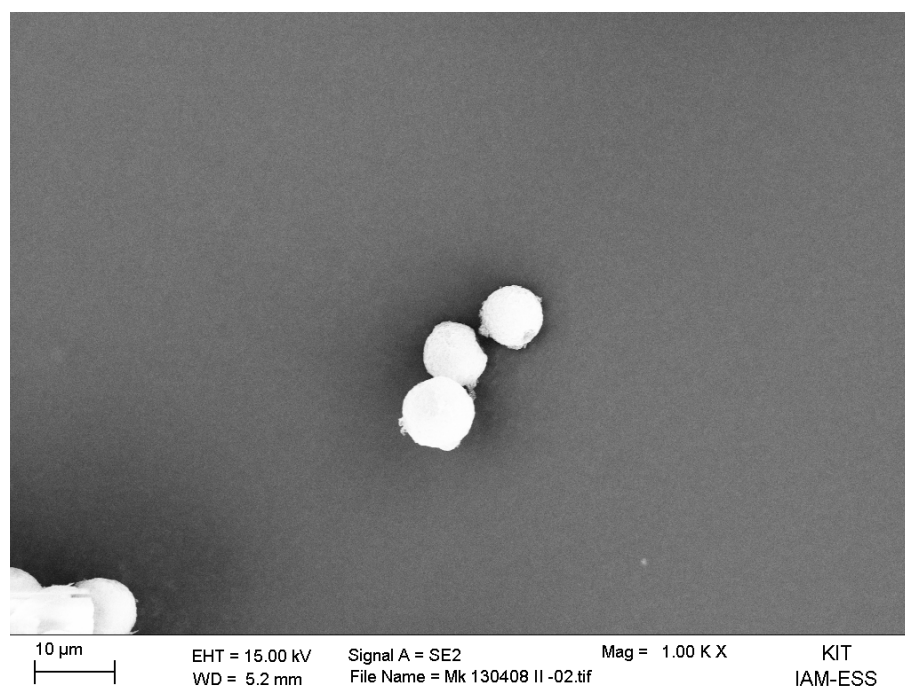


Figure A.27: SEM image of the maleimide-functionalized microspheres half grafted with PDMAA. Zoom image.

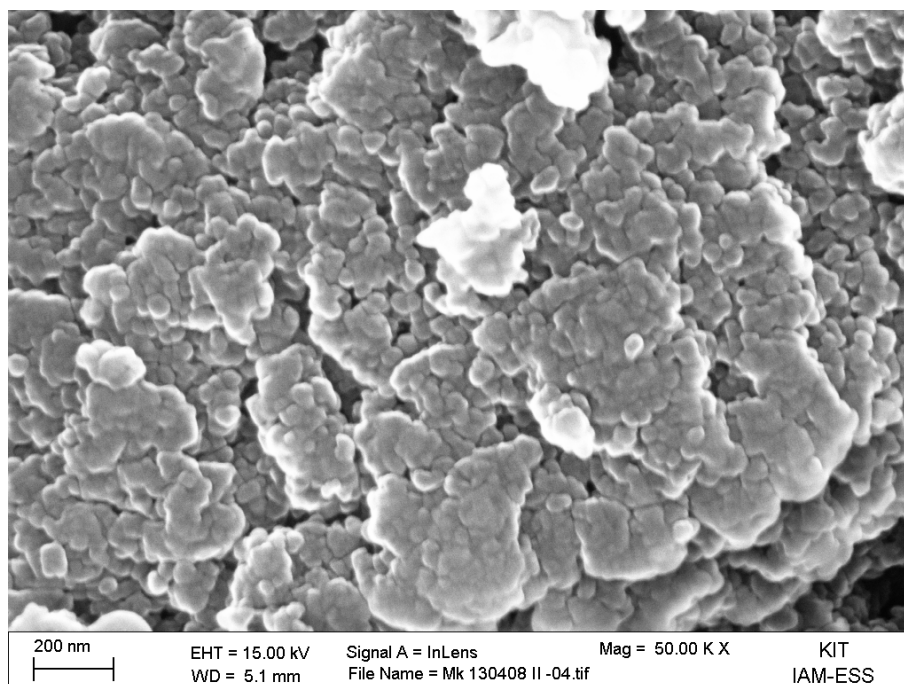


Figure A.28: SEM image of the maleimide-functionalized microspheres half grafted with PDMAA. Surface morphology image.

A.2 SEM Images from Chapter 5

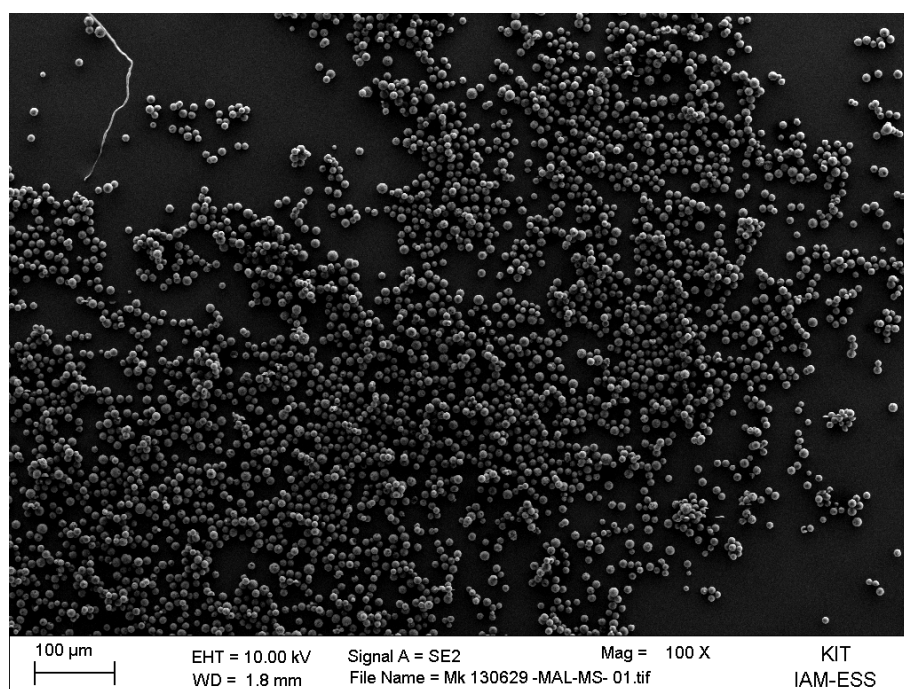


Figure A.29: SEM image of the maleimide-functionalized microspheres. Overview image.

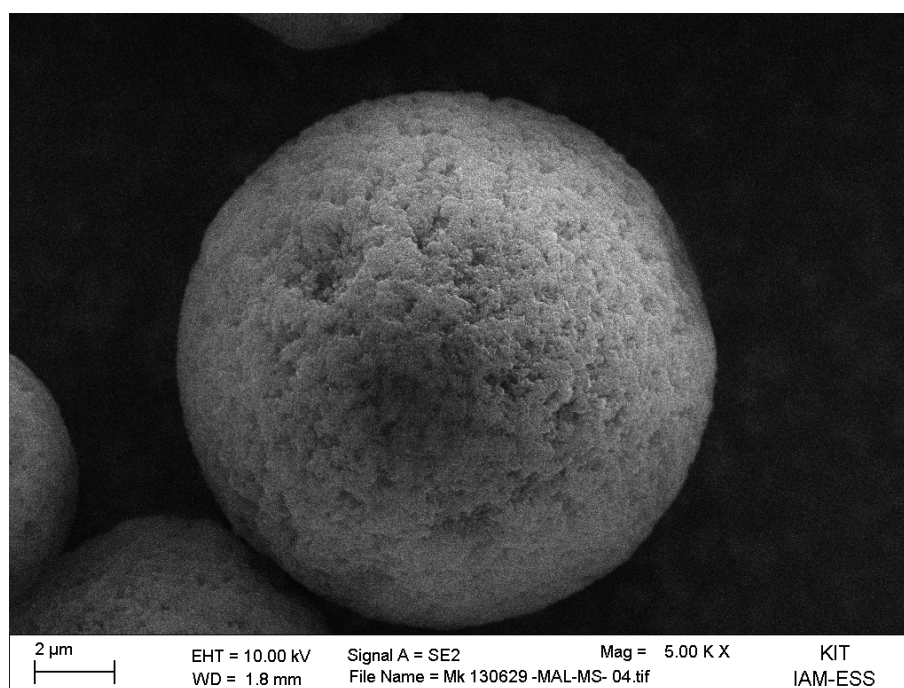


Figure A.30: SEM image of the maleimide-functionalized microspheres. Zoom image.

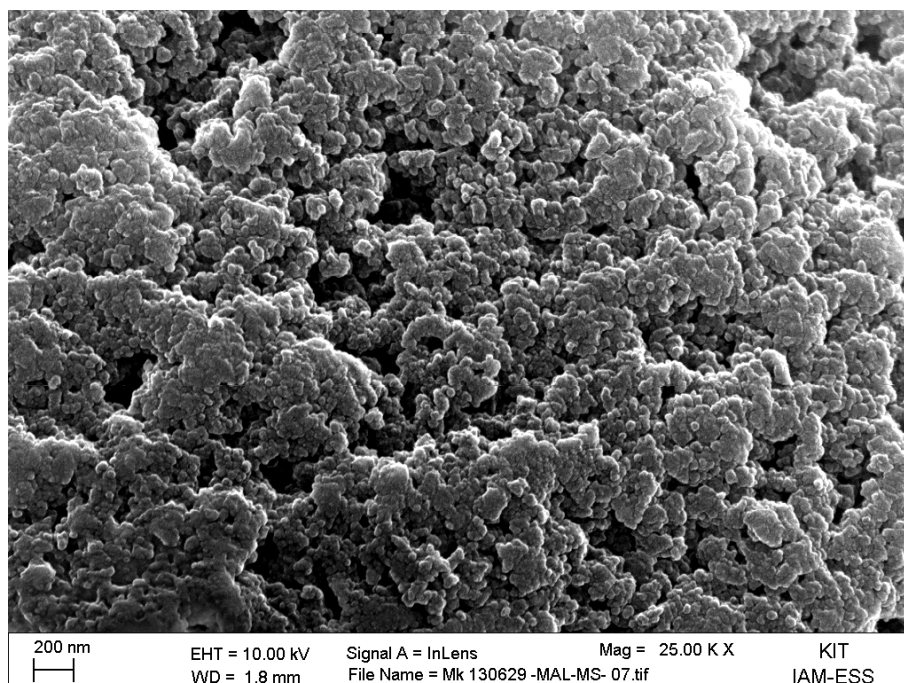


Figure A.31: SEM image of the maleimide-functionalized microspheres. Surface morphology image.

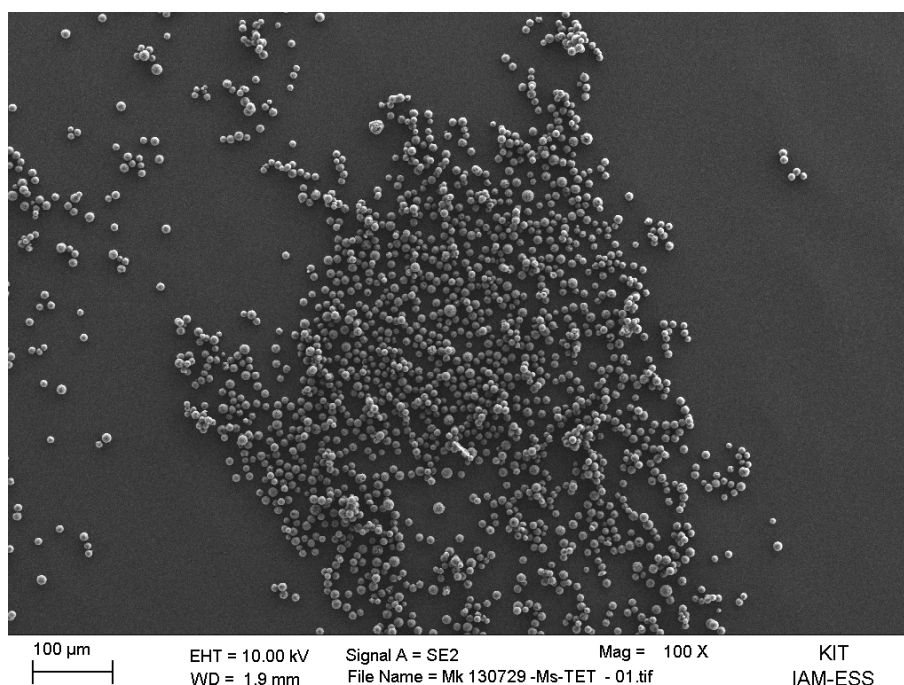


Figure A.32: SEM image of the maleimide-functionalized microspheres grafted with DoPATTET. Overview image.

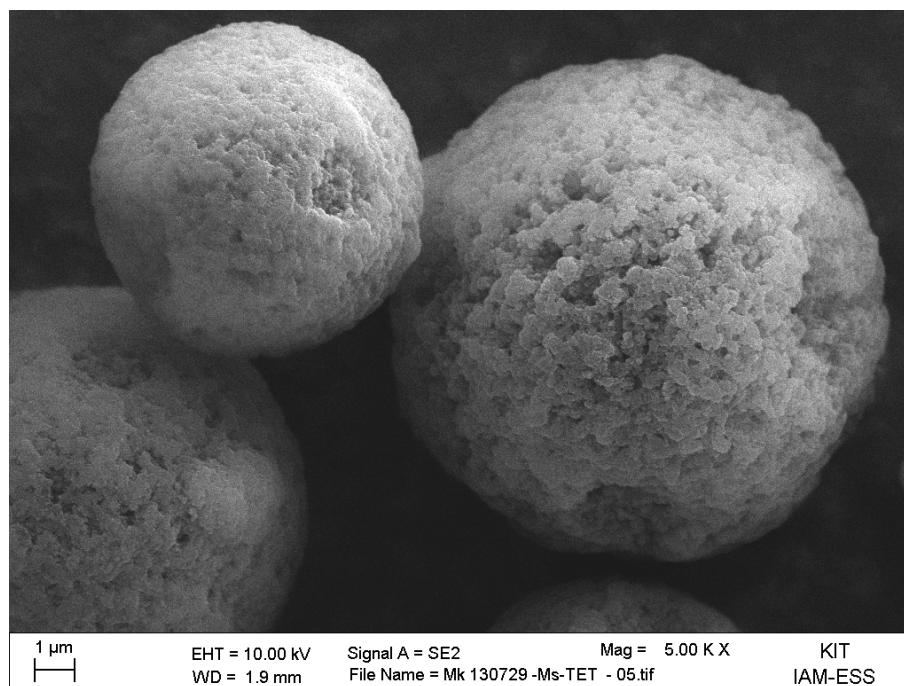


Figure A.33: SEM image of the maleimide-functionalized microspheres grafted with DoPATET. Zoom image.

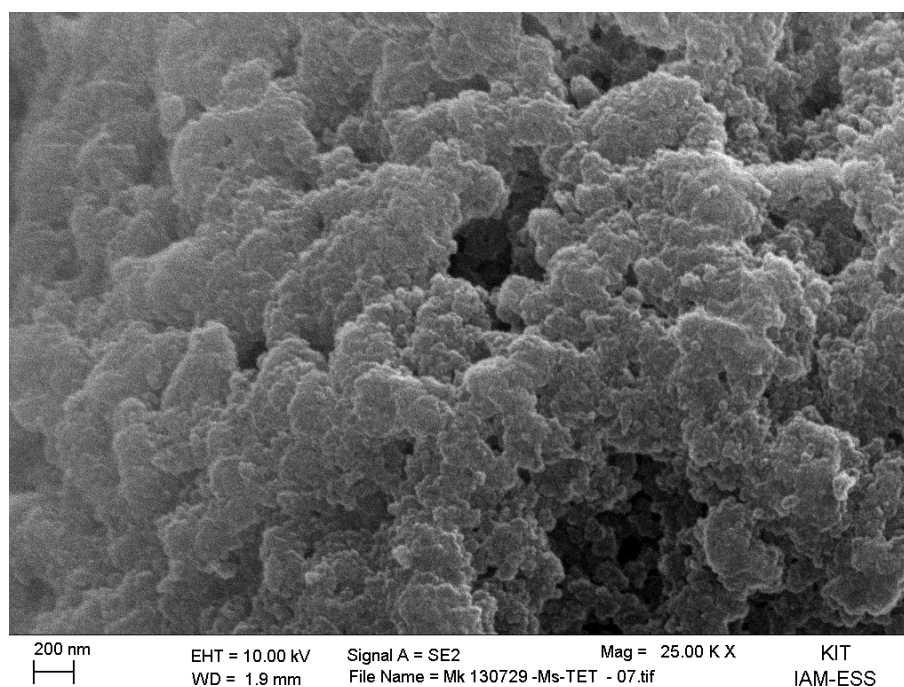


Figure A.34: SEM image of the maleimide-functionalized microspheres grafted with DoPATET. Surface morphology image.

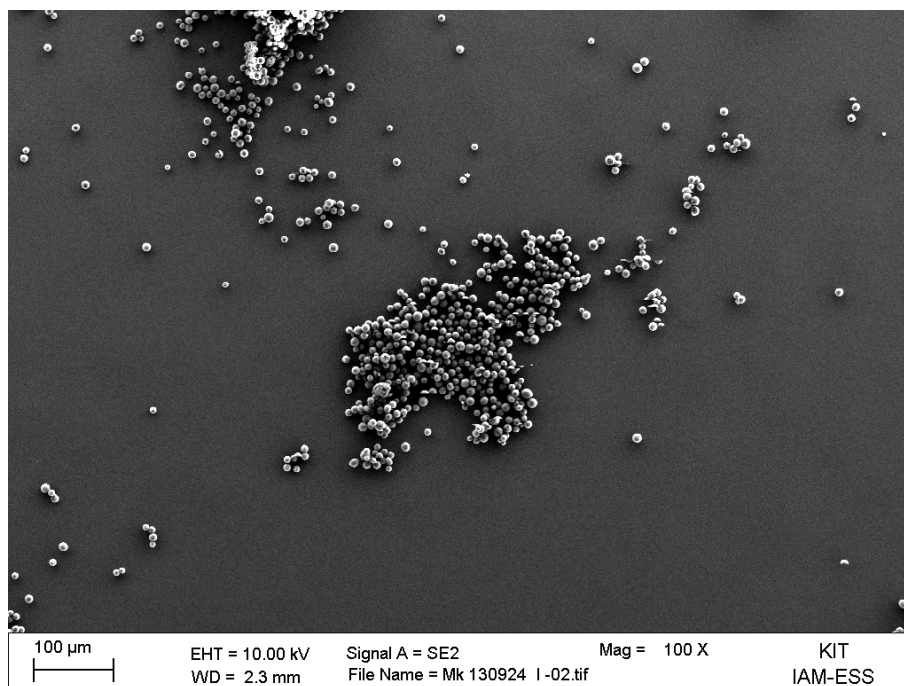


Figure A.35: SEM image of the maleimide-functionalized microspheres grafted with PS. Overview image.

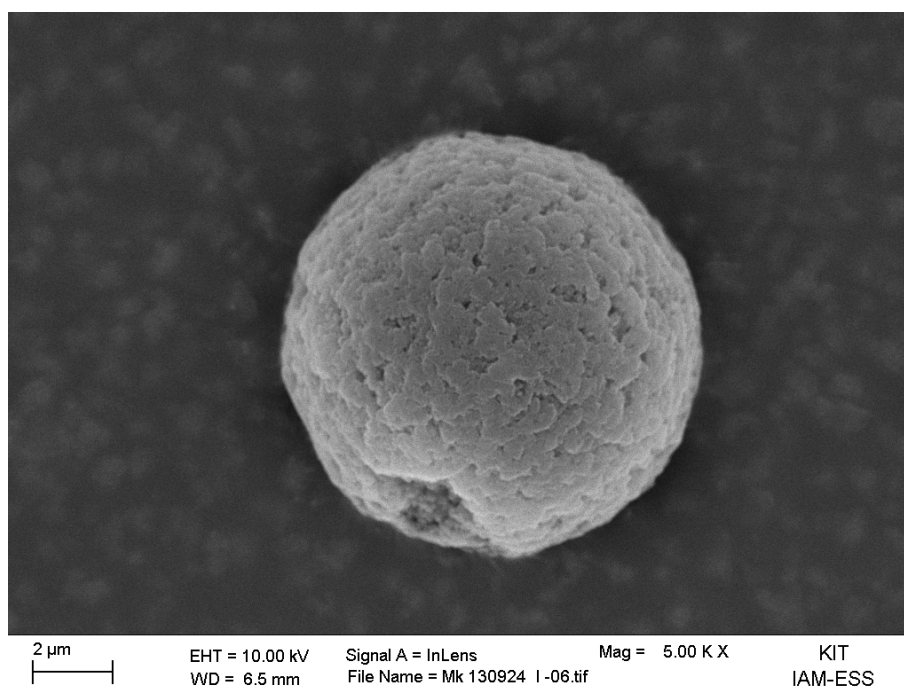


Figure A.36: SEM image of the maleimide-functionalized microspheres grafted with PS. Zoom image.

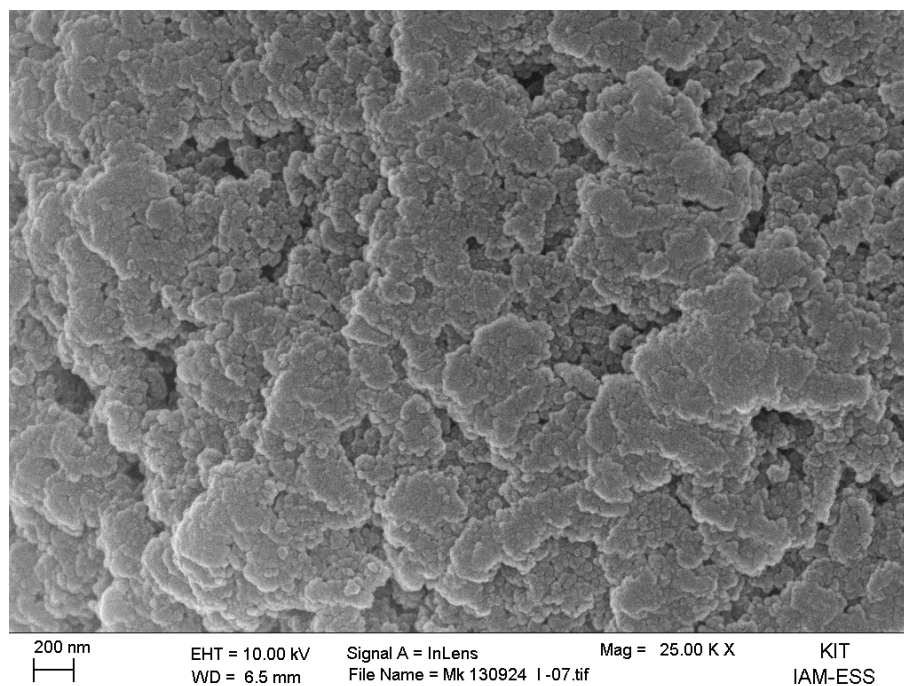


Figure A.37: SEM image of the maleimide-functionalized microspheres grafted with PS. Surface morphology image.

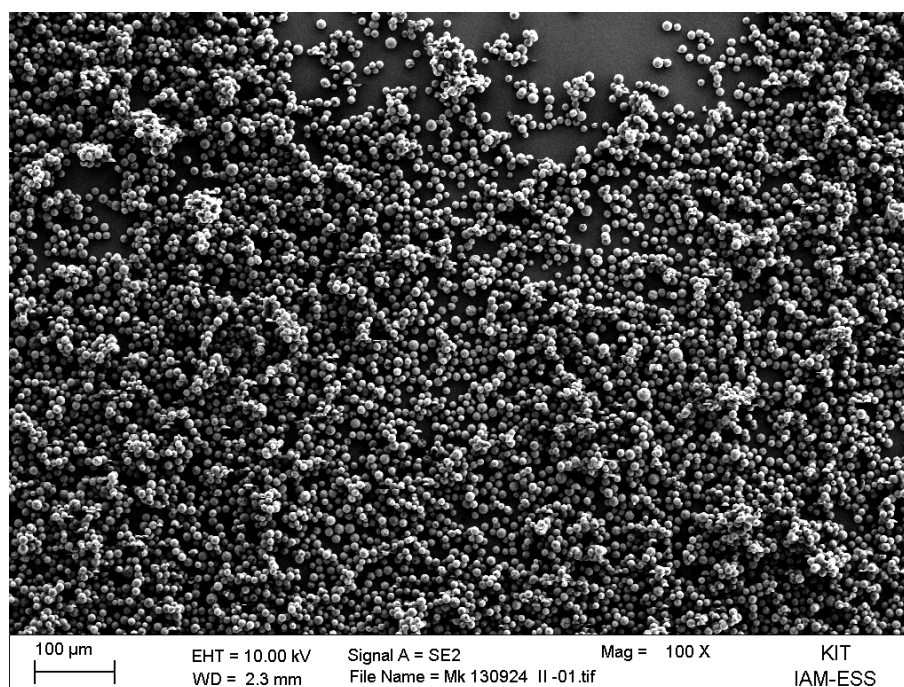


Figure A.38: SEM image of the maleimide-functionalized microspheres grafted with PDMAA. Overview image.

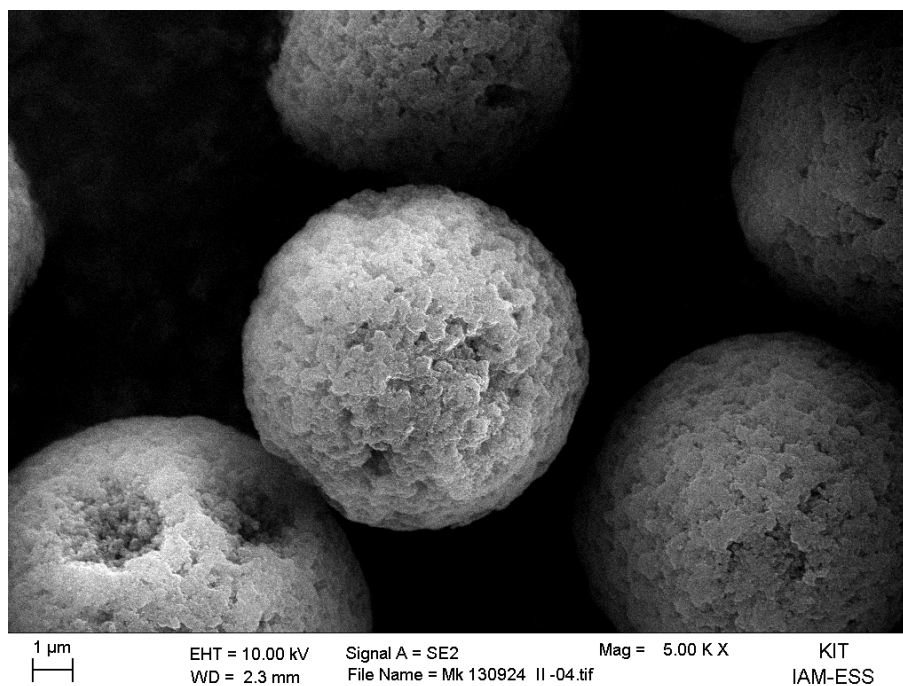


Figure A.39: SEM image of the maleimide-functionalized microspheres grafted with PDMAA. Zoom image.

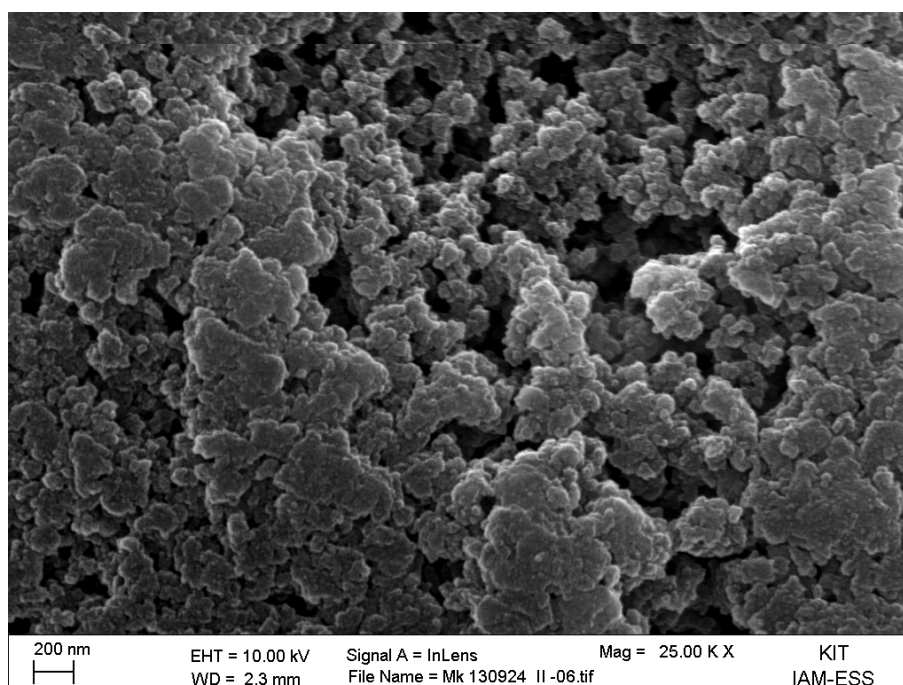


Figure A.40: SEM image of the maleimide-functionalized microspheres grafted with PDMAA. Surface morphology image.

A.3 SEM Images from Chapter 6

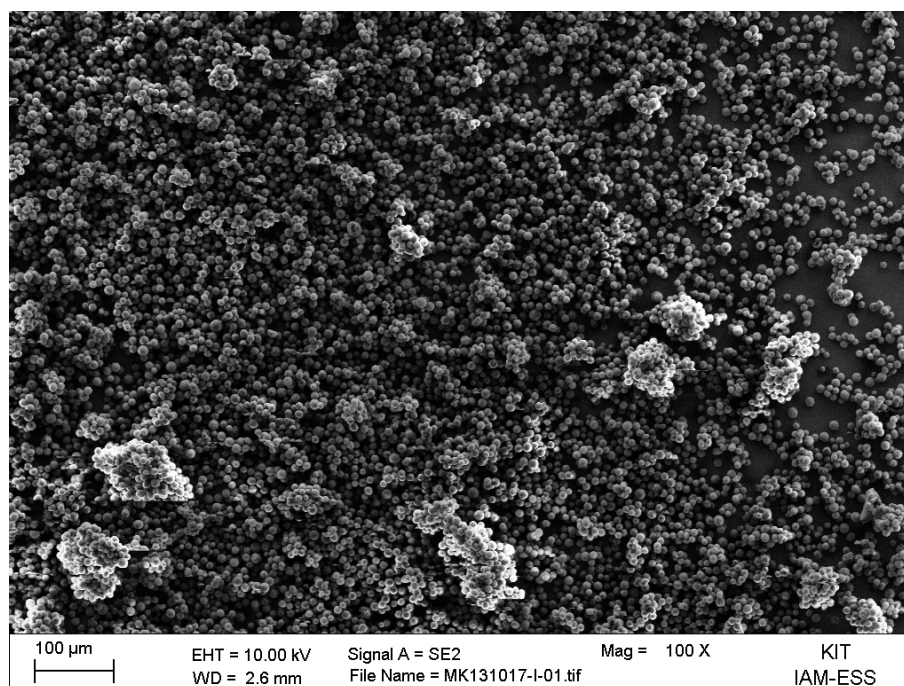


Figure A.41: SEM image of the Cp-functionalized microspheres photo-grafted with DoPATPAS. Overview image.

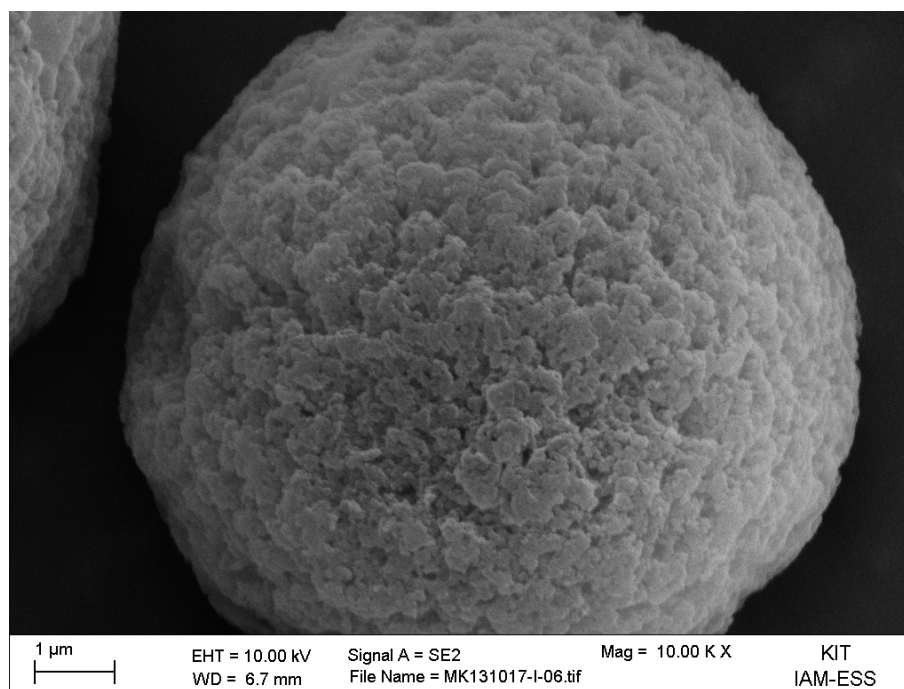


Figure A.42: SEM image of the Cp-functionalized microspheres photo-grafted with DoPATPAS. Zoom image.

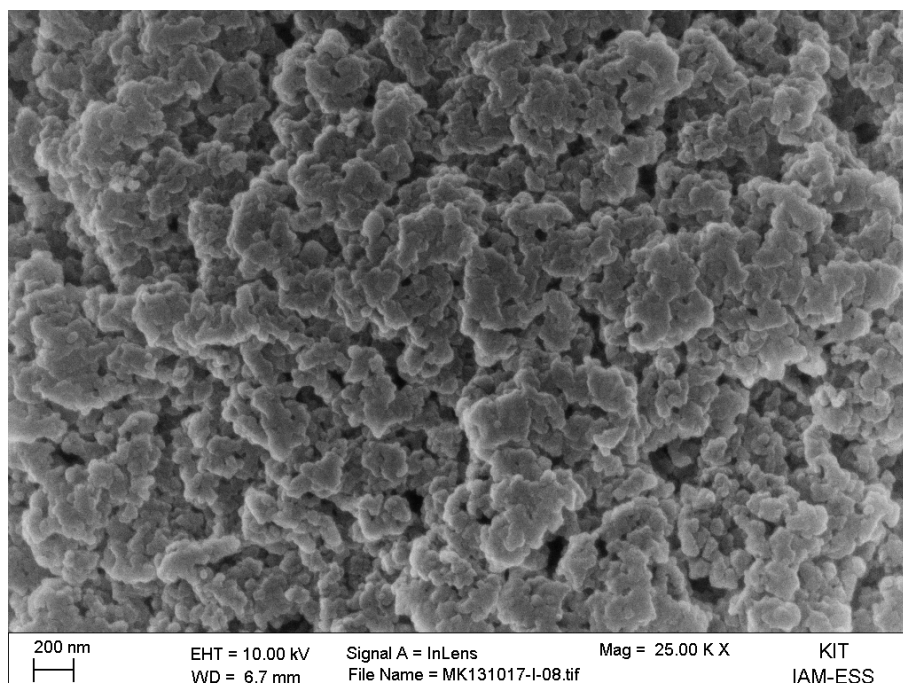


Figure A.43: SEM image of the Cp-functionalized microspheres photo-grafted with DoPATPAS. Surface morphology image.

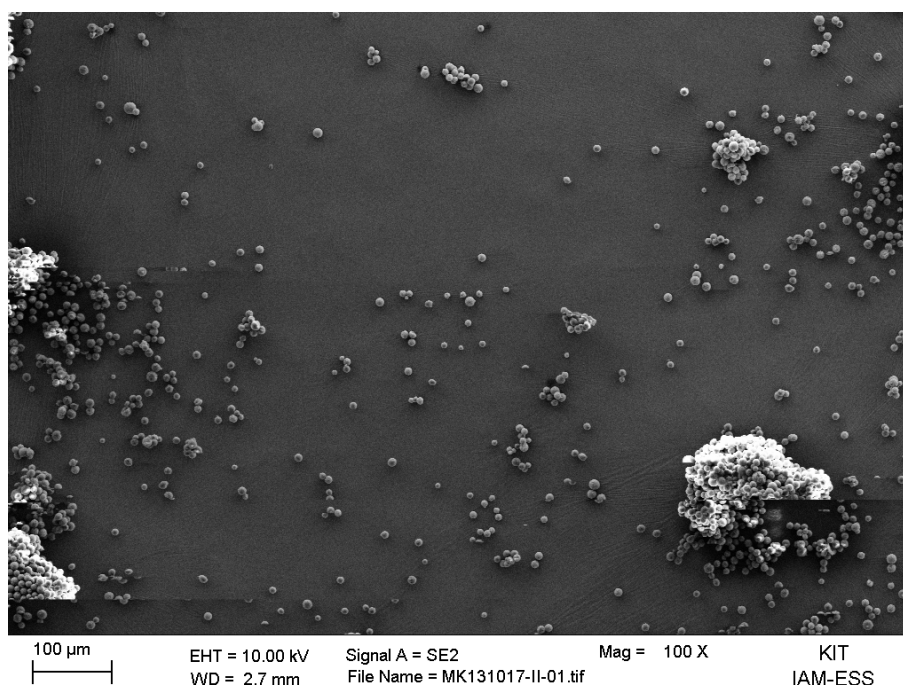


Figure A.44: SEM image of the Cp-functionalized microspheres photo-grafted with PS. Overview image.

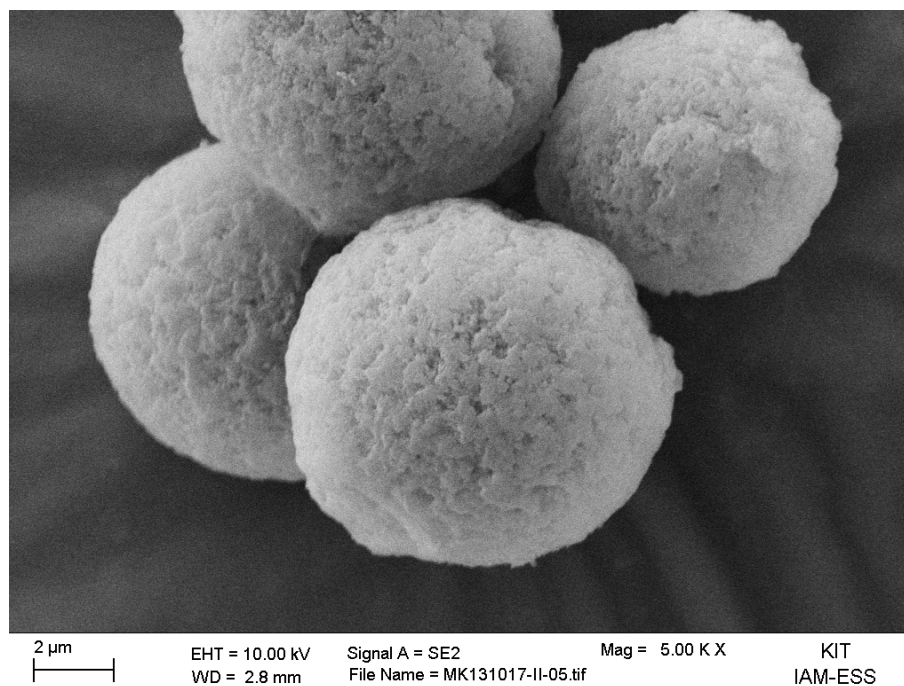


Figure A.45: SEM image of the Cp-functionalized microspheres photo-grafted with PS. Zoom image.

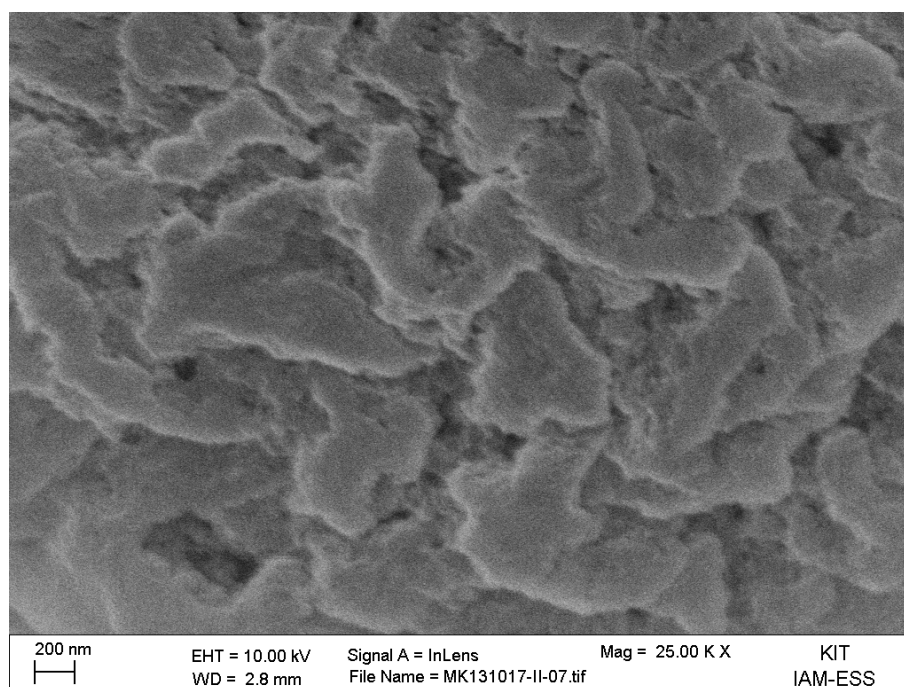


Figure A.46: SEM image of the Cp-functionalized microspheres photo-grafted with PS. Surface morphology image.

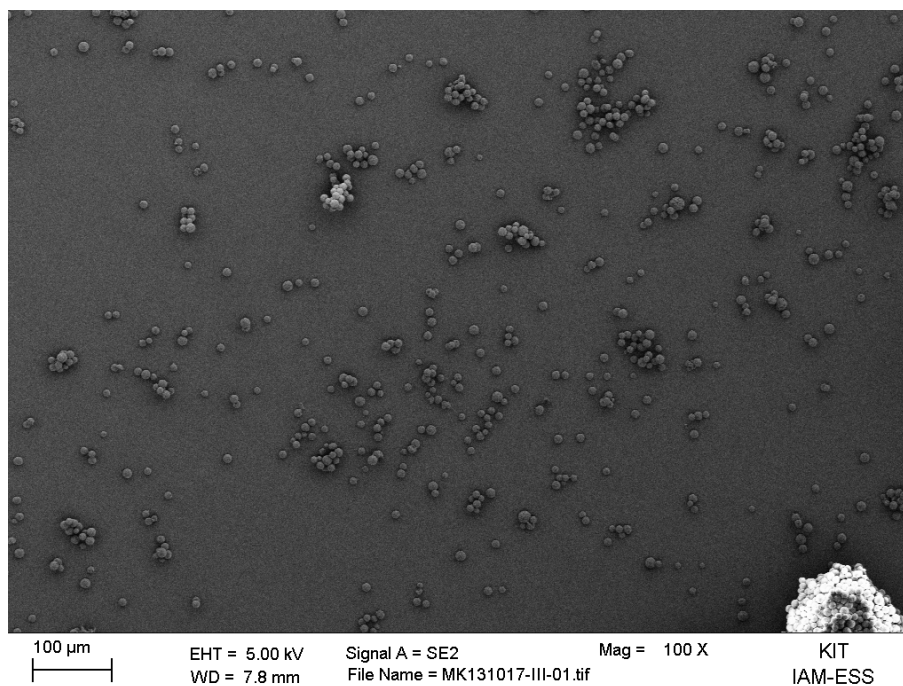


Figure A.47: SEM image of the Cp-functionalized microspheres photo-grafted with PDMAA. Overview image.

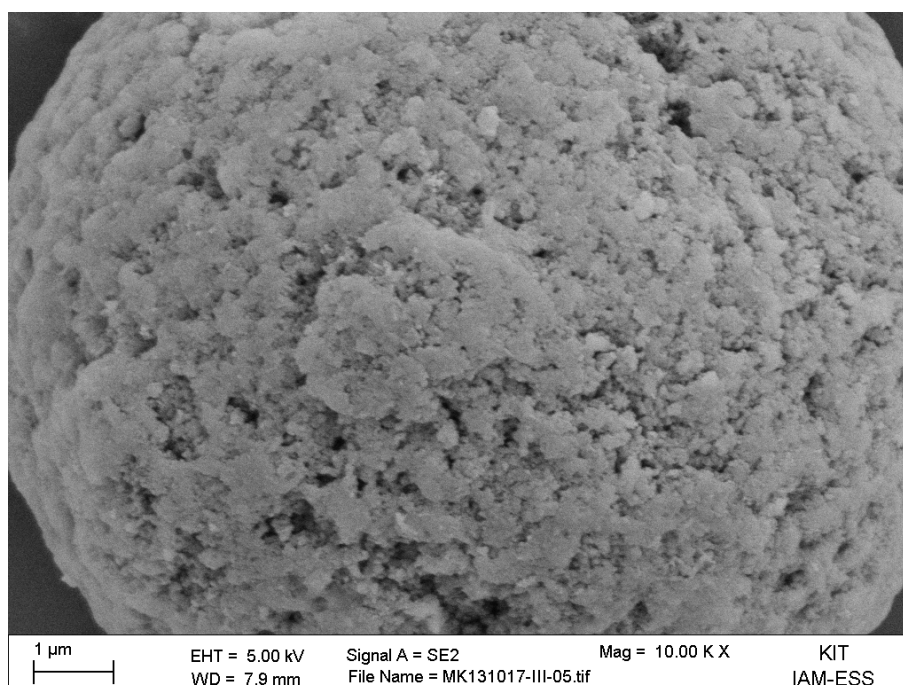


Figure A.48: SEM image of the Cp-functionalized microspheres photo-grafted with PDMAA. Zoom image.

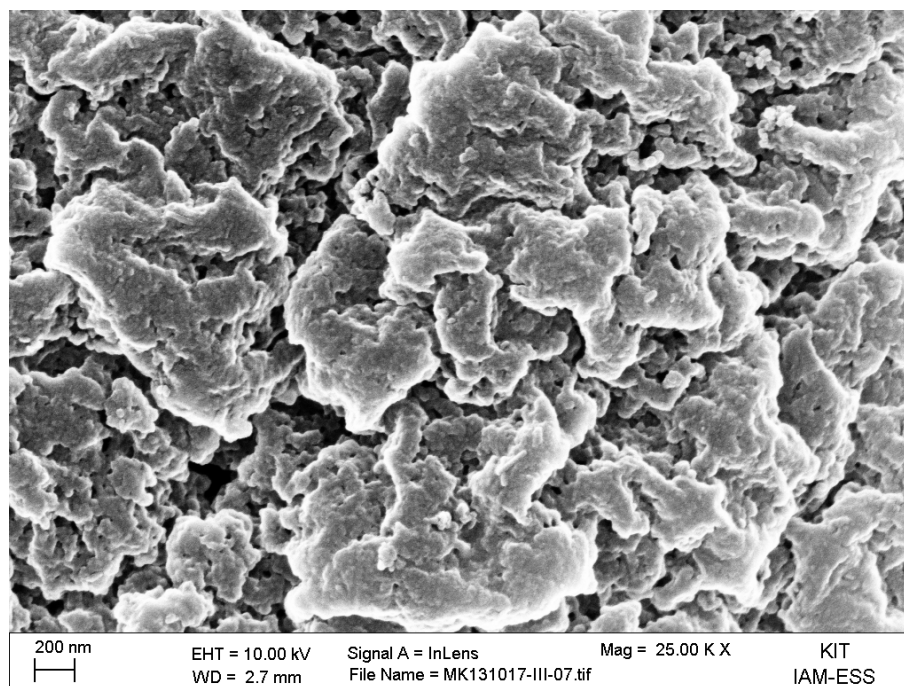


Figure A.49: SEM image of the Cp-functionalized microspheres photo-grafted with PDMAA. Surface morphology image.

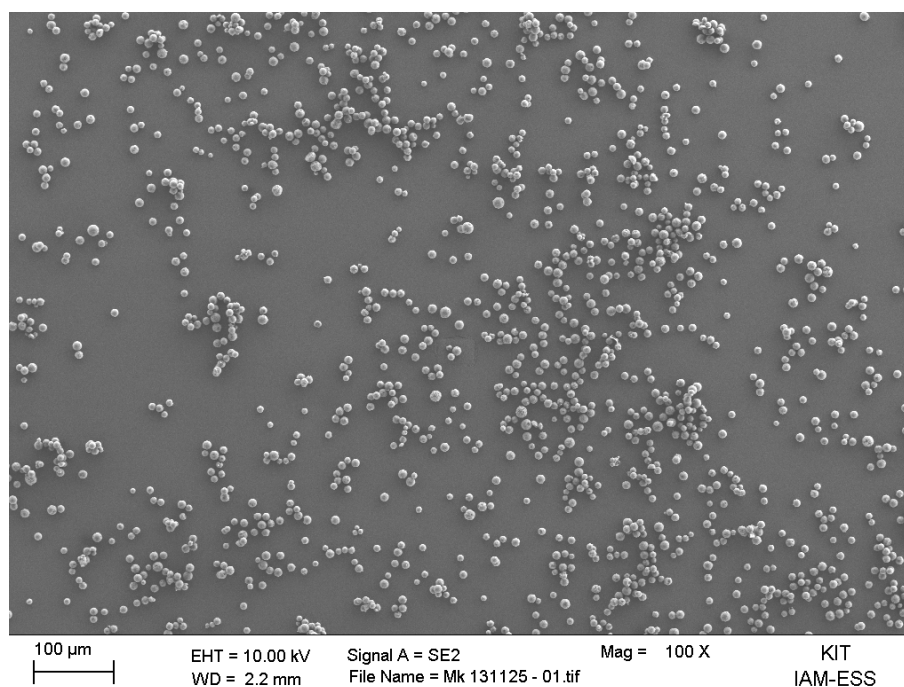


Figure A.50: SEM image of the Cp-functionalized microspheres photo-grafted with PAcManEA. Overview image.

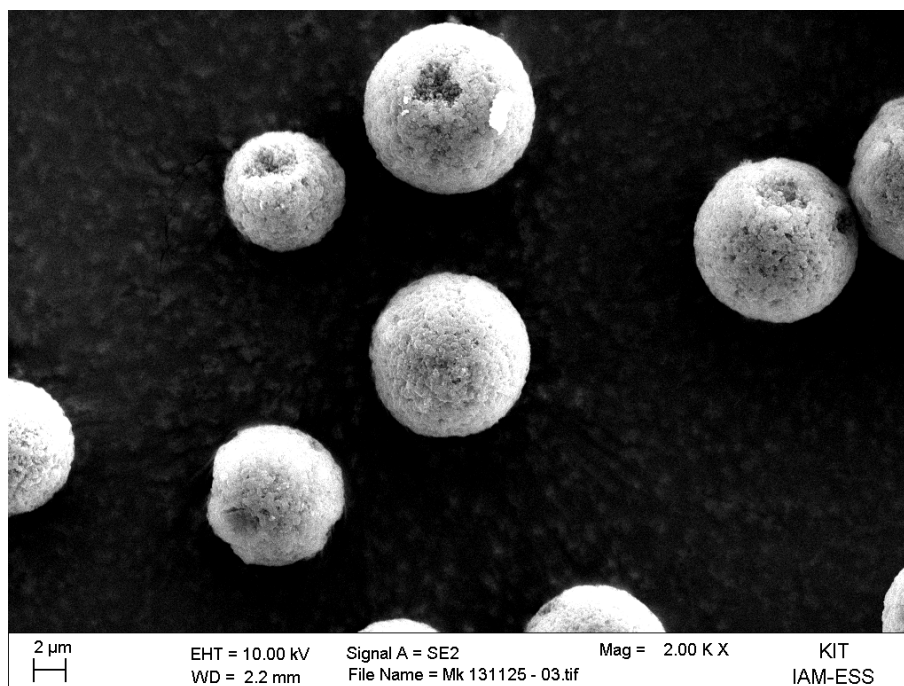


Figure A.51: SEM image of the Cp-functionalized microspheres photo-grafted with PAcManEA. Zoom image.

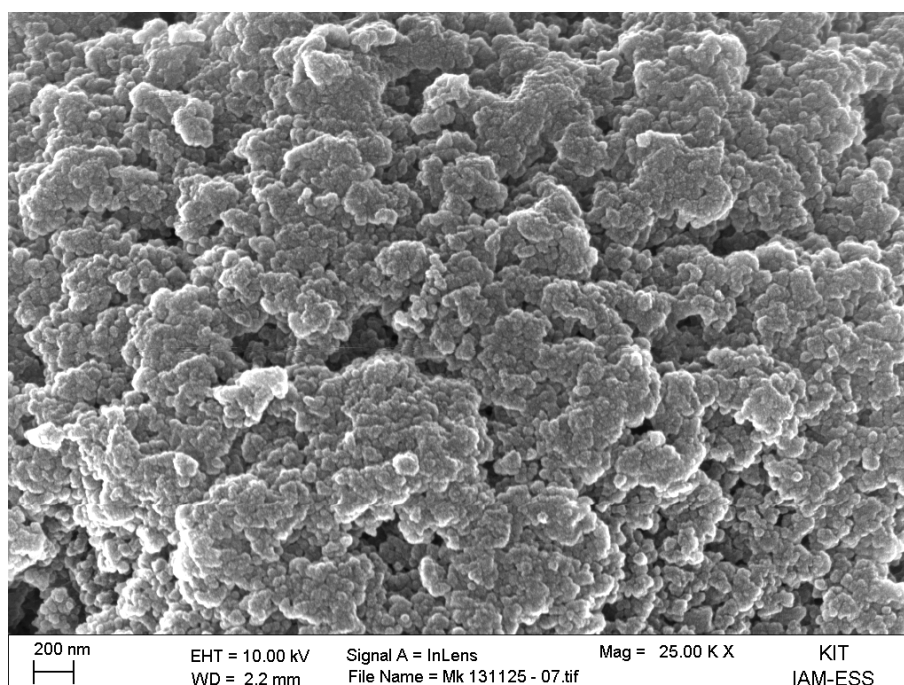


Figure A.52: SEM image of the Cp-functionalized microspheres photo-grafted with PAcManEA. Surface morphology image.

Bibliography

- [1] J. Lu, P. H. Toy, *Chem. Rev.* **2009**, *109*, 815–838.
- [2] M. Benaglia, A. Puglisi, F. Cozzi, *Chem. Rev.* **2003**, *103*, 3401–3430.
- [3] M. Orzáez, P. Mora, L. Mondragón, E. Pérez-Payá, M. Vicent, *Int. J. Pept. Res. Ther.* **2007**, *13*, 281–293.
- [4] A. R. Vaino, K. D. Janda, *J. Comb. Chem.* **2000**, *2*, 579–596.
- [5] W.-H. Li, H. D. H. Stöver, *J. Polym. Sci., Part A: Polym. Chem.* **1998**, *36*, 1543–1551.
- [6] M. Slater, M. Snauko, F. Svec, J. M. J. Fréchet, *Anal. Chem.* **2006**, *78*, 4969–4975.
- [7] M. T. Gokmen, F. E. D. Prez, *Prog. Polym. Sci.* **2012**, *37*, 365–405.
- [8] Q. Liu, C. Huang, S. Luo, Z. Liu, B. Liu, *Polymer* **2007**, *48*, 1567–1572.
- [9] C. Yang, Y. Guan, J. Xing, J. Liu, G. Shan, Z. An, H. Liu, *AIChE J.* **2005**, *51*, 2011–2015.
- [10] A. S. Goldmann, L. Barner, M. Kaupp, A. P. Vogt, C. Barner-Kowollik, *Prog. Polym. Sci.* **2012**, *37*, 975–984.
- [11] C. Barner-Kowollik, *Handbook of RAFT Polymerization*, Wiley-VCH, Weinheim, **2008**.
- [12] G. Moad, E. Rizzardo, S. H. Thang, *Aust. J. Chem.* **2012**, *65*, 985–1076.
- [13] G. Moad, E. Rizzardo, S. H. Thang, *Aust. J. Chem.* **2009**, *62*, 1402–1472.
- [14] G. Moad, E. Rizzardo, S. H. Thang, *Aust. J. Chem.* **2006**, *59*, 669–692.
- [15] G. Moad, E. Rizzardo, S. H. Thang, *Aust. J. Chem.* **2005**, *58*, 379–410.

- [16] A. J. Inglis, S. Sinnwell, T. P. Davis, C. Barner-Kowollik, M. H. Stenzel, *Macromolecules* **2008**, *41*, 4120–4126.
- [17] J. S. Clovis, A. Eckell, R. Huisgen, R. Sustmann, *Chem. Ber.* **1967**, *100*, 60–70.
- [18] T. Gruending, K. K. Oehlenschlaeger, E. Frick, M. Glassner, C. Schmid, C. Barner-Kowollik, *Macromol. Rapid Commun.* **2011**, *32*, 807–812.
- [19] M. Glassner, K. K. Oehlenschlaeger, A. Welle, M. Bruns, C. Barner-Kowollik, *Chem. Commun.* **2013**, *49*, 633–635.
- [20] S. Bhaskar, K. M. Pollock, M. Yoshida, J. Lahann, *Small* **2010**, *6*, 404–411.
- [21] J. A. Champion, Y. K. Katare, S. Mitragotri, *Proc. Natl. Acad. Sci. USA* **2007**, *104*, 11901–11904.
- [22] R. Arshady, *J. Microencapsulation* **1988**, *5*, 101–114.
- [23] H. Kawaguchi, *Prog. Polym. Sci.* **2000**, *25*, 1171–1210.
- [24] A. P. Vogt, T. Tischer, U. Geckle, A. M. Greiner, V. Trouillet, M. Kaupp, L. Barner, T. Hofe, C. Barner-Kowollik, *Macromol. Rapid Commun.* **2013**, *34*, 916–921.
- [25] J. Crevecoeur, L. Nelissen, P. Lemstra, *Polymer* **1999**, *40*, 3685–3689.
- [26] K. Li, H. D. H. Stöver, *J. Polym. Sci., Part A: Polym. Chem.* **1993**, *31*, 3257–3263.
- [27] F. Bai, X. Yang, W. Huang, *Macromolecules* **2004**, *37*, 9746–9752.
- [28] J.-S. Song, F. Tronc, M. A. Winnik, *J. Am. Chem. Soc.* **2004**, *126*, 6562–6563.
- [29] H. B. Yamak, „Emulsion Polymerization: Effects of Polymerization Variables on the Properties of Vinyl Acetate Based Emulsion Polymers“ in *Polymer Science* (Ed.: F. Yilmaz), InTech, **2013**, pp. 35–72.
- [30] K. Landfester, *Annu. Rev. Mater. Res.* **2006**, *36*, 231–279.
- [31] M. Ballauff, Y. Lu, *Polymer* **2007**, *48*, 1815–1823.
- [32] S. C. Thickett, R. G. Gilbert, *Polymer* **2007**, *48*, 6965–6991.
- [33] V. Mittal, *Polymer Latex Technology*, CRC Press, Boca Raton (FL), **2010**.
- [34] Z. Nie, S. Xu, M. Seo, P. C. Lewis, E. Kumacheva, *J. Am. Chem. Soc.* **2005**, *127*, 8058–8063.

- [35] D. Dendukuri, K. Tsoi, T. A. Hatton, P. S. Doyle, *Langmuir* **2005**, *21*, 2113–2116.
- [36] T. Nisisako, T. Torii, T. Higuchi, *Chem. Eng. J.* **2004**, *101*, 23–29.
- [37] Z. Nie, W. Li, M. Seo, S. Xu, E. Kumacheva, *J. Am. Chem. Soc.* **2006**, *128*, 9408–9412.
- [38] J. Ugelstad, K. H. Kaggerud, F. K. Hansen, A. Berge, *Makromol. Chem.* **1979**, *180*, 737–744.
- [39] Y.-S. Cho, S.-H. Kim, G.-R. Yi, S.-M. Yang, *Colloids Surf., A* **2009**, *345*, 237–245.
- [40] L. Jiang, Y. Zhao, J. Zhai, *Angew. Chem. Int. Ed.* **2004**, *43*, 4338–4341.
- [41] K.-H. Roh, D. C. Martin, J. Lahann, *Nat. Mater.* **2005**, *4*, 759–763.
- [42] L. Barner, *Adv. Mater.* **2009**, *21*, 2547–2553.
- [43] N. Hadjichristidis, H. Iatrou, M. Pitsikalis, J. Mays, *Prog. Polym. Sci.* **2006**, *31*, 1068–1132.
- [44] A. G. Mayes, K. Mosbach, *Anal. Chem.* **1996**, *68*, 3769–3774.
- [45] L. Ye, R. Weiss, K. Mosbach, *Macromolecules* **2000**, *33*, 8239–8245.
- [46] J. Haginaka, *J. Chromatogr. B* **2008**, *866*, 3–13.
- [47] J. Wang, P. A. G. Cormack, D. C. Sherrington, E. Khoshdel, *Angew. Chem. Int. Ed.* **2003**, *42*, 5336–5338.
- [48] G. Zheng, H. D. H. Stöver, *Macromolecules* **2003**, *36*, 7439–7445.
- [49] R. Joso, S. Reinicke, A. Walther, H. Schmalz, A. H. E. Müller, L. Barner, *Macromol. Rapid Commun.* **2009**, *30*, 1009–1014.
- [50] L. Barner, C. Li, X. Hao, M. H. Stenzel, C. Barner-Kowollik, T. P. Davis, *J. Polym. Sci., Part A: Polym. Chem.* **2004**, *42*, 5067–5076.
- [51] R. Joso, M. H. Stenzel, T. P. Davis, C. Barner-Kowollik, L. Barner, *Aust. J. Chem.* **2005**, *58*, 468–471.
- [52] N. T. L. Uyen, F. Brooke, T. P. Davis, C. Barner-Kowollik, M. H. Stenzel, *J. Polym. Sci., Part A: Polym. Chem.* **2007**, *45*, 3256–3272.
- [53] A. Pfaff, L. Barner, A. H. Müller, A. M. Granville, *Eur. Polym. J.* **2011**, *47*, 805–815.

- [54] G. Zheng, H. D. H. Stöver, *Macromolecules* **2002**, *35*, 6828–6834.
- [55] G. Zheng, H. D. H. Stöver, *Macromolecules* **2002**, *35*, 7612–7619.
- [56] E. Unsal, B. Elmas, B. Caglayan, M. Tuncel, S. Patir, A. Tuncel, *Anal. Chem.* **2006**, *78*, 5868–5875.
- [57] A. M. Granville, W. J. Brittain, „Recent Advances in Polymer Brush Synthesis“ in *Polymer Brushes*, Wiley-VCH, Weinheim, **2005**, pp. 33–50.
- [58] H. C. Kolb, M. G. Finn, K. B. Sharpless, *Angew. Chem. Int. Ed.* **2001**, *40*, 2004–2021.
- [59] C. Barner-Kowollik, F. E. Du Prez, P. Espeel, C. J. Hawker, T. Junkers, H. Schlaad, W. Van Camp, *Angew. Chem. Int. Ed.* **2011**, *50*, 60–62.
- [60] R. Huisgen, *Angew. Chem.* **1963**, *75*, 604–637.
- [61] C. W. Tornøe, C. Christensen, M. Meldal, *J. Org. Chem.* **2002**, *67*, 3057–3064.
- [62] V. V. Rostovtsev, L. G. Green, V. V. Fokin, K. B. Sharpless, *Angew. Chem. Int. Ed.* **2002**, *41*, 2596–2599.
- [63] G. Chen, L. Tao, G. Mantovani, J. Geng, D. Nyström, D. M. Haddleton, *Macromolecules* **2007**, *40*, 7513–7520.
- [64] Y. Han, Q. Shi, J. Hu, Q. Du, X. Chen, X. Jing, *Macromol. Biosci.* **2008**, *8*, 638–644.
- [65] A. S. Goldmann, A. Walther, L. Nebhani, R. Joso, D. Ernst, K. Loos, C. Barner-Kowollik, L. Barner, A. H. E. Müller, *Macromolecules* **2009**, *42*, 3707–3714.
- [66] D. R. Breed, R. Thibault, F. Xie, Q. Wang, C. J. Hawker, D. J. Pine, *Langmuir* **2009**, *25*, 4370–4376.
- [67] G. Chen, L. Tao, G. Mantovani, V. Ladmiral, D. P. Burt, J. V. Macpherson, D. M. Haddleton, *Soft Matter* **2007**, *3*, 732–739.
- [68] Y. Y. Durmaz, B. Karagoz, N. Bicak, D. O. Demirkol, E. E. Yalcinkaya, S. Timur, Y. Yagci, *Macromol. Biosci.* **2011**, *11*, 141–150.
- [69] C. Diehl, H. Schlaad, *Chem. Eur. J.* **2009**, *15*, 11469–11472.
- [70] W. Gu, G. Chen, M. H. Stenzel, *J. Polym. Sci., Part A: Polym. Chem.* **2009**, *47*, 5550–5556.

- [71] M. Álvarez Paino, A. Muñoz Bonilla, G. Marcelo, J. Rodríguez-Hernández, M. Fernández-García, *Polym. Chem.* **2012**, *3*, 3282–3288.
- [72] R. A. Prasath, M. T. Gokmen, P. Espeel, F. E. Du Prez, *Polym. Chem.* **2010**, *1*, 685–692.
- [73] M. T. Gokmen, J. Brassinne, R. A. Prasath, F. E. Du Prez, *Chem. Commun.* **2011**, *47*, 4652–4654.
- [74] B. Falk, J. V. Crivello, *J. Appl. Polym. Sci.* **2005**, *97*, 1574–1585.
- [75] A. P. Vogt, V. Trouillet, A. M. Greiner, M. Kaupp, U. Geckle, L. Barner, T. Hofe, C. Barner-Kowollik, *Macromol. Rapid Commun.* **2012**, *33*, 1108–1113.
- [76] R. Wang, Y. Zhang, G. Ma, Z. Su, *Colloids Surf., B* **2006**, *51*, 93–99.
- [77] M. Yakup Arica, E. Yalcin, G. Bayramoglu, *Polym. Int.* **2005**, *54*, 153–160.
- [78] Z. Ma, Y. Guan, X. Liu, H. Liu, *Polym. Adv. Technol.* **2005**, *16*, 554–558.
- [79] W. Wang, L. Deng, Z. H. Peng, X. Xiao, *Enzyme Microb. Technol.* **2007**, *40*, 255–261.
- [80] M.-Y. Ren, S. Bai, D.-H. Zhang, Y. Sun, *J. Agric. Food Chem.* **2008**, *56*, 2388–2391.
- [81] Y. Yong, Y.-X. Bai, Y.-F. Li, L. Lin, Y.-J. Cui, C.-G. Xia, *Process. Biochem.* **2008**, *43*, 1179–1185.
- [82] A. Nordborg, F. Limé, A. Shchukarev, K. Irgum, *J. Sep. Sci.* **2008**, *31*, 2143–2150.
- [83] T. Kaufmann, M. T. Gokmen, C. Wendeln, M. Schneiders, S. Rinnen, H. F. Arlinghaus, S. A. F. Bon, F. E. Du Prez, B. J. Ravoo, *Adv. Mater.* **2011**, *23*, 79–83.
- [84] T. Kaufmann, M. T. Gokmen, S. Rinnen, H. F. Arlinghaus, F. Du Prez, B. J. Ravoo, *J. Mater. Chem.* **2012**, 23–27.
- [85] L. Nebhani, S. Sinnwell, A. J. Inglis, M. H. Stenzel, C. Barner-Kowollik, L. Barner, *Macromol. Rapid Commun.* **2008**, *29*, 1431–1437.
- [86] L. Nebhani, D. Schmiedl, L. Barner, C. Barner-Kowollik, *Adv. Funct. Mater.* **2010**, *20*, 2010–2020.
- [87] M. J. Beneš, D. Horák, F. Svec, *J. Sep. Science* **2005**, *28*, 1855–1875.

- [88] T. Tennikova, D. Horák, F. Švec, M. Tennikov, E. Kever, B. Belenkii, *J. Chromatogr. A* **1989**, 475, 187–194.
- [89] V. Davankov, M. Tsyurupa, N. Alexienko, *J. Chromatogr. A* **2005**, 1100, 32–39.
- [90] F. H. Ling, V. Lu, F. Svec, J. M. J. Fréchet, *J. Org. Chem.* **2002**, 67, 1993–2002.
- [91] F. Ling, E. Brahmachary, M. Xu, F. Svec, J. M. J. Fréchet, *J. Sep. Science* **2003**, 26, 1337–1346.
- [92] J. Wang, P. A. G. Cormack, D. C. Sherrington, E. Khoshdel, *Angew. Chem. Int. Ed.* **2003**, 42, 5336–5338.
- [93] P. Šmidl, J. Plicka, I. Kleinmann, *J. Chromatogr. A* **1992**, 598, 15–21.
- [94] S. V. Ley, I. R. Baxendale, R. N. Bream, P. S. Jackson, A. G. Leach, D. A. Longbottom, M. Nesi, J. S. Scott, R. I. Storer, S. J. Taylor, *J. Chem. Soc., Perkin Trans. 1* **2000**, 3815–4195.
- [95] R. B. Merrifield, *J. Am. Chem. Soc.* **1963**, 85, 2149–2154.
- [96] A. Poschalko, T. Rohr, H. Gruber, A. Bianco, G. Guichard, J.-P. Briand, V. Weber, D. Falkenhagen, *J. Am. Chem. Soc.* **2003**, 125, 13415–13426.
- [97] R. Haag, S. Roller, „Polymeric Supports for the Immobilisation of Catalysts“ in *Topics in Current Chemistry, Vol. 242* (Ed.: A. Kirschning), Springer, Berlin/Heidelberg, **2004**, pp. 1–42.
- [98] M. R. Buchmeiser, *Chem. Rev.* **2008**, 109, 303–321.
- [99] N. Miletić, Z. Vuković, A. Nastasović, K. Loos, *J. Mol. Catal. B: Enzym.* **2009**, 56, 196–201.
- [100] D. C. Sherrington, *J. Polym. Sci., Part A: Polym. Chem.* **2001**, 39, 2364–2377.
- [101] P. Barbaro, F. Liguori, *Chem. Rev.* **2008**, 109, 515–529.
- [102] J. Hradil, F. Švec, A. Aratskova, L. Beljakova, V. Orlov, Y. Yashin, *J. Chromatogr. A* **1989**, 475, 209–217.
- [103] L. Leeb, P. Gmeiner, S. Löber, *QSAR Comb. Sci.* **2007**, 26, 1145–1150.
- [104] J. Eames, M. Watkinson, *Eur. J. Org. Chem.* **2001**, 2001, 1213–1224.

- [105] N. Fontanals, R. M. Marcé, P. A. Cormack, D. C. Sherrington, F. Borrull, *J. Chromatogr. A* **2008**, *1191*, 118–124.
- [106] Z. Xu, Q. Zhang, H. H. P. Fang, *Crit. Rev. Environ. Sci. Technol.* **2003**, *33*, 363–389.
- [107] D. L. Elbert, *Acta Biomater.* **2011**, *7*, 31–56.
- [108] U. Eberle, M. Felderhoff, F. Schüth, *Angew. Chem. Int. Ed.* **2009**, *48*, 6608–6630.
- [109] M. I. J. Stich, M. Schaeferling, O. S. Wolfbeis, *Adv. Mater.* **2009**, *21*, 2216–2220.
- [110] A. Salinas-Castillo, M. Camprubi-Robles, R. Mallavia, *Chem. Commun.* **2010**, *46*, 1263–1265.
- [111] M. Szwarc, *Nature* **1956**, *178*, 1168 – 1169.
- [112] D. H. Solomon, E. Rizzardo, P. Cacioli, *U.S. Patent 4581429* **1986**.
- [113] G. Moad, E. Rizzardo, *Macromolecules* **1995**, *28*, 8722–8728.
- [114] M. Kato, M. Kamigaito, M. Sawamoto, T. Higashimura, *Macromolecules* **1995**, *28*, 1721–1723.
- [115] J.-S. Wang, K. Matyjaszewski, *J. Am. Chem. Soc.* **1995**, *117*, 5614–5615.
- [116] J. Chiefari, Y. K. Chong, F. Ercole, J. Krstina, J. Jeffery, T. Le, R. Mayadunne, G. Meijs, C. Moad, G. Moad, E. Rizzardo, S. H. Thang, *Macromolecules* **1998**, *31*, 5559–5562.
- [117] W. Braunecker, K. Matyjaszewski, *Prog. Polym. Sci.* **2007**, *32*, 93–146.
- [118] C. Barner-Kowollik, M. Buback, B. Charleux, M. L. Coote, M. Drache, T. Fukuda, A. Goto, B. Klumperman, A. B. Lowe, J. B. Mcleary, G. Moad, M. J. Monteiro, R. D. Sanderson, M. P. Tonge, P. Vana, *J. Polym. Sci., Part A: Polym. Chem.* **2006**, *44*, 5809–5831.
- [119] A. Theis, A. Feldermann, N. Charton, M. H. Stenzel, T. P. Davis, C. Barner-Kowollik, *Macromolecules* **2005**, *38*, 2595–2605.
- [120] K. Matyjaszewski, J. Xia, *Chem. Rev.* **2001**, *101*, 2921–2990.
- [121] M. Georges, R. Veregin, P. Kazmaier, G. Hamer, *Macromolecules* **1993**, *26*, 2987–2988.

- [122] C. J. Hawker, *J. Am. Chem. Soc.* **1994**, *116*, 11185–11186.
- [123] C. J. Hawker, A. W. Bosman, E. Harth, *Chem. Rev.* **2001**, *101*, 3661–3688.
- [124] F. di Lena, K. Matyjaszewski, *Prog. Polym. Sci.* **2010**, *35*, 959–1021.
- [125] V. Coessens, T. Pintauer, K. Matyjaszewski, *Prog. Polym. Sci.* **2001**, *26*, 337–377.
- [126] D. J. Keddie, G. Moad, E. Rizzardo, S. H. Thang, *Macromolecules* **2012**, *45*, 5321–5342.
- [127] M. Benaglia, J. Chiefari, Y. K. Chong, G. Moad, E. Rizzardo, S. H. Thang, *J. Am. Chem. Soc.* **2009**, *131*, 6914–6915.
- [128] G. Moad, E. Rizzardo, S. H. Thang, *Polym. Int.* **2011**, *60*, 9–25.
- [129] C. Schmid, S. Weidner, J. Falkenhagen, C. Barner-Kowollik, *Macromolecules* **2011**, *45*, 87–99.
- [130] A. B. Lowe, B. S. Sumerlin, C. L. McCormick, *Polymer* **2003**, *44*, 6761–6765.
- [131] Y. K. Chong, T. P. T. Le, G. Moad, E. Rizzardo, S. H. Thang, *Macromolecules* **1999**, *32*, 2071–2074.
- [132] R. T. A. Mayadunne, J. Jeffery, G. Moad, E. Rizzardo, *Macromolecules* **2003**, *36*, 1505–1513.
- [133] J. F. Quinn, R. P. Chaplin, T. P. Davis, *J. Polym. Sci., Part A: Polym. Chem.* **2002**, *40*, 2956–2966.
- [134] A. Gregory, M. H. Stenzel, *Prog. Polym. Sci.* **2011**, *37*, 38–105.
- [135] Y. Tsujii, M. Ejaz, K. Sato, A. Goto, T. Fukuda, *Macromolecules* **2001**, *34*, 8872–8878.
- [136] M. Semsarilar, V. Ladmiral, S. Perrier, *J. Polym. Sci., Part A: Polym. Chem.* **2010**, *48*, 4361–4365.
- [137] B. Zhang, Y. Chen, L. Xu, L. Zeng, Y. He, E.-T. Kang, J. Zhang, *J. Polym. Sci., Part A: Polym. Chem.* **2011**, *49*, 2043–2050.
- [138] S. Sinnwell, A. J. Inglis, T. P. Davis, M. H. Stenzel, C. Barner-Kowollik, *Chem. Commun.* **2008**, 2052–2054.
- [139] A. J. Inglis, C. Barner-Kowollik, *Macromol. Rapid Commun.* **2010**, *31*, 1247–1266.

- [140] A. J. Inglis, M. H. Stenzel, C. Barner-Kowollik, *Macromol. Rapid Commun.* **2009**, *30*, 1792–1798.
- [141] S. Sinnwell, A. J. Inglis, M. H. Stenzel, C. Barner-Kowollik, *Macromol. Rapid Commun.* **2008**, *29*, 1090–1096.
- [142] N. Zydziak, C. M. Preuss, V. Winkler, M. Bruns, C. Hübner, C. Barner-Kowollik, *Macromol. Rapid Commun.* **2013**, *34*, 672–680.
- [143] M. Glassner, G. Delaittre, M. Kaupp, J. P. Blinco, C. Barner-Kowollik, *J. Am. Chem. Soc.* **2012**, *134*, 7274–7277.
- [144] A. S. Goldmann, T. Tischer, L. Barner, M. Bruns, C. Barner-Kowollik, *Biomacromolecules* **2011**, *12*, 1137–1145.
- [145] M. Okada, *Prog. Polym. Sci.* **2001**, *26*, 67–104.
- [146] V. Ladmiral, E. Melia, D. M. Haddleton, *Eur. Polym. J.* **2004**, *40*, 431–449.
- [147] S. G. Spain, M. I. Gibson, N. R. Cameron, *J. Polym. Sci., Part A: Polym. Chem.* **2007**, *45*, 2059–2072.
- [148] A. Ghadban, L. Albertin, *Polymers* **2013**, *5*, 431–526.
- [149] L. Albertin, C. Kohlert, M. Stenzel, L. J. R. Foster, T. P. Davis, *Biomacromolecules* **2004**, *5*, 255–260.
- [150] L. Albertin, M. Stenzel, C. Barner-Kowollik, L. J. R. Foster, T. P. Davis, *Macromolecules* **2004**, 7530–7537.
- [151] V. Hořeší, P. Smolek, J. Kocourek, *Biochim. Biophys. Acta* **1978**, *538*, 293–298.
- [152] N. Sharon, H. Lis, *Science* **1989**, *246*, 227–234.
- [153] J. Li, S. Zacharek, X. Chen, J. Wang, W. Zhang, A. Janczuk, P. G. Wang, *Bioorg. Med. Chem.* **1999**, *7*, 1549–1558.
- [154] E. J. Gordon, L. E. Strong, L. L. Kiessling, *Bioorg. Med. Chem.* **1998**, *6*, 1293–1299.
- [155] T. Taguchi, A. Kishida, N. Sakamoto, M. Akashi, *J. Biomed. Mater. Res.* **1998**, *41*, 386–391.
- [156] S. J. Novick, J. S. Dordick, *Chem. Mater.* **1998**, *10*, 955–958.

- [157] M. Ambrosi, N. R. Cameron, B. G. Davis, S. Stolnik, *Org. Biomol. Chem.* **2005**, *3*, 1476–1480.
- [158] O. León, V. Bordegé, A. Muñoz Bonilla, M. Sánchez-Chaves, M. Fernández-García, *J. Polym. Sci., Part A: Polym. Chem.* **2010**, *48*, 3623–3631.
- [159] V. Bordegé, A. Muñoz Bonilla, O. León, R. Cuervo-Rodríguez, M. Sánchez-Chaves, M. Fernández-García, *Macromol. Chem. Phys.* **2011**, *212*, 1294–1304.
- [160] V. Bordegé, A. Muñoz Bonilla, O. León, M. Sánchez-Chaves, R. Cuervo-Rodríguez, M. Fernández-García, *React. Funct. Polym.* **2011**, *71*, 1–10.
- [161] A. Muñoz Bonilla, E. Ibarboure, V. Bordegé, M. Fernández-García, J. Rodríguez-Hernández, *Langmuir* **2010**, *26*, 8552–8558.
- [162] P. Escalé, S. R. S. Ting, A. Khoukh, L. Rubatat, M. Save, M. H. Stenzel, L. Billon, *Macromolecules* **2011**, *44*, 5911–5919.
- [163] S. R. S. Ting, A. M. Gregory, M. H. Stenzel, *Biomacromolecules* **2009**, *10*, 342–352.
- [164] J. Bernard, X. Hao, T. P. Davis, C. Barner-Kowollik, M. H. Stenzel, *Biomacromolecules* **2006**, *7*, 232–238.
- [165] L. Zhang, M. H. Stenzel, *Aust. J. Chem.* **2009**, *62*, 813–822.
- [166] A. Pfaff, A. H. E. Müller, *Macromolecules* **2011**, *44*, 1266–1272.
- [167] Q. Yang, M. Ulbricht, *Macromolecules* **2011**, *44*, 1303–1310.
- [168] C. Gao, S. Muthukrishnan, W. Li, J. Yuan, Y. Xu, A. H. E. Müller, *Macromolecules* **2007**, *40*, 1803–1815.
- [169] A. Pfaff, A. Schallon, T. M. Ruhland, A. P. Majewski, H. Schmalz, R. Freitag, A. H. E. Müller, *Biomacromolecules* **2011**, *12*, 3805–3811.
- [170] J. S. Clovis, A. Eckell, R. Huisgen, R. Sustmann, *Chem. Ber.* **1967**, *100*, 60–70.
- [171] R. Darkow, M. Yoshikawa, T. Kitao, G. Tomaschewski, J. Schellenberg, *J. Polym. Sci., Part A: Polym. Chem.* **1994**, *32*, 1657–1664.
- [172] C. J. Dürr, P. Lederhose, L. Hlalele, D. Abt, A. Kaiser, S. Brandau, C. Barner-Kowollik, *Macromolecules* **2013**, *46*, 5915–5923.
- [173] R. K. V. Lim, Q. Lin, *Acc. Chem. Res.* **2011**, *44*, 828–839.

- [174] M. Dietrich, G. Delaittre, J. P. Blinco, A. J. Inglis, M. Bruns, C. Barner-Kowollik, *Adv. Funct. Mater.* **2012**, *22*, 304–312.
- [175] E. Blasco, M. Piñol, L. Oriol, B. V. K. J. Schmidt, A. Welle, V. Trouillet, M. Bruns, C. Barner-Kowollik, *Adv. Funct. Mater.* **2013**, *23*, 4011–4019.
- [176] C. Rodriguez-Emmenegger, C. M. Preuss, B. Yameen, O. Pop-Georgievski, M. Bachmann, J. O. Mueller, M. Bruns, A. S. Goldmann, M. Bastmeyer, C. Barner-Kowollik, *Adv. Mater.* **2013**, *25*, 6123–6127.
- [177] K. K. Oehlenschlaeger, J. O. Mueller, N. B. Heine, M. Glassner, N. K. Guimard, G. Delaittre, F. G. Schmidt, C. Barner-Kowollik, *Angew. Chem. Int. Ed.* **2013**, *52*, 762–766.
- [178] M. Winkler, J. O. Mueller, K. K. Oehlenschlaeger, L. Montero de Espinosa, M. A. R. Meier, C. Barner-Kowollik, *Macromolecules* **2012**, *45*, 5012–5019.
- [179] M. Glassner, K. K. Oehlenschlaeger, T. Gruending, C. Barner-Kowollik, *Macromolecules* **2011**, *44*, 4681–4689.
- [180] T. Pauloehrl, G. Delaittre, V. Winkler, A. Welle, M. Bruns, H. G. Börner, A. M. Greiner, M. Bastmeyer, C. Barner-Kowollik, *Angew. Chem. Int. Ed.* **2012**, *51*, 1071–1074.
- [181] C. M. Preuss, T. Tischer, C. Rodriguez-Emmenegger, M. M. Zieger, M. Bruns, A. S. Goldmann, C. Barner-Kowollik, *J. Mater. Chem. B* **2014**, *2*, 36–40.
- [182] T. Tischer, T. K. Claus, M. Bruns, V. Trouillet, K. Linkert, C. Rodriguez-Emmenegger, A. S. Goldmann, S. Perrier, H. G. Börner, C. Barner-Kowollik, *Biomacromolecules* **2013**, *14*, 4340–4350.
- [183] E. Vedejs, T. H. Eberlein, R. G. Wilde, *J. Org. Chem.* **1988**, *53*, 2220–2226.
- [184] T. Pauloehrl, A. Welle, K. K. Oehlenschlaeger, C. Barner-Kowollik, *Chem. Sci.* **2013**, *4*, 3503–3507.
- [185] T. Pauloehrl, G. Delaittre, M. Bruns, M. Meißer, H. G. Börner, M. Bastmeyer, C. Barner-Kowollik, *Angew. Chem. Int. Ed.* **2012**, *51*, 9181–9184.
- [186] T. Pauloehrl, A. Welle, M. Bruns, K. Linkert, H. G. Börner, M. Bastmeyer, G. Delaittre, C. Barner-Kowollik, *Angew. Chem. Int. Ed.* **2013**, *52*, 9714–9718.
- [187] S. Arumugam, V. V. Popik, *J. Am. Chem. Soc.* **2009**, *131*, 11892–11899.

- [188] S. Arumugam, V. V. Popik, *J. Am. Chem. Soc.* **2011**, *133*, 5573–5579.
- [189] S. Arumugam, V. V. Popik, *J. Am. Chem. Soc.* **2011**, *133*, 15730–15736.
- [190] S. Arumugam, S. V. Orski, J. Locklin, V. V. Popik, *J. Am. Chem. Soc.* **2011**, *134*, 179–182.
- [191] S. Arumugam, V. V. Popik, *J. Am. Chem. Soc.* **2012**, *134*, 8408–8411.
- [192] M. A. Tasdelen, Y. Yagci, *Angew. Chem. Int. Ed.* **2013**, *52*, 5930–5938.
- [193] A. J. Inglis, T. Paulöhr, C. Barner-Kowollik, *Macromolecules* **2010**, *43*, 33–36.
- [194] A. J. Inglis, L. Nebhani, O. Altintas, F. G. Schmidt, C. Barner-Kowollik, *Macromolecules* **2010**, *43*, 5515–5520.
- [195] L. Nebhani, S. Sinnwell, C. Y. Lin, M. L. Coote, M. H. Stenzel, C. Barner-Kowollik, *J. Polym. Sci., Part A: Polym. Chem.* **2009**, *47*, 6053–6071.
- [196] K. Ohno, Y. Izu, S. Yamamoto, T. Miyamoto, T. Fukuda, *Macromol. Chem. Phys.* **1999**, *200*, 1619–1625.
- [197] P. DePhillips, A. M. Lenhoff, *J. Chromatogr. A* **2000**, *883*, 39–54.
- [198] S. Hansson, T. Tischer, A. S. Goldmann, A. Carlmark, C. Barner-Kowollik, E. Malmström, *Polym. Chem.* **2012**, *3*, 307–309.
- [199] Y. Joseph, I. Besnard, M. Rosenberger, B. Guse, H. Nothofer, J. Wessels, U. Wild, A. Knop-Gericke, D. Su, R. Schlögl, A. Yasuda, T. Vossmeier, *J. Phys. Chem. B* **2003**, *107*, 7406–7413.
- [200] M. Ejaz, K. Ohno, Y. Tsujii, T. Fukuda, *Macromolecules* **2000**, *33*, 2870–2874.
- [201] I. Abrunhosa, M. Gulea, S. Masson, *Synthesis* **2004**, *6*, 928–934.
- [202] B. Neises, W. Steglich, *Angew. Chem. Int. Ed.* **1978**, *17*, 522–524.
- [203] T. Gruending, M. Kaupp, J. P. Blinco, C. Barner-Kowollik, *Macromolecules* **2011**, *44*, 166–174.
- [204] M. Buback, T. Junkers, P. Vana, *Macromol. Rapid Commun.* **2005**, *26*, 796–802.
- [205] C. Barner-Kowollik, *Macromol. Rapid Commun.* **2009**, *30*, 1625–1631.
- [206] C. M. Preuss, C. Barner-Kowollik, *Macromol. Theory Simul.* **2011**, *20*, 700–708.

- [207] S. Hansson, V. Trouillet, T. Tischer, A. S. Goldmann, A. Carlmark, C. Barner-Kowollik, E. Malmström, *Biomacromolecules* **2013**, *14*, 64–74.
- [208] S. U. Pickering, *J. Chem. Soc., Trans.* **1907**, *91*, 2001–2021.
- [209] B. P. Binks, *Curr. Opin. Colloid Interface Sci.* **2002**, *7*, 21–41.
- [210] C. Kaewsaneha, P. Tangboriboonrat, D. Polpanich, M. Eissa, A. Elaissari, *Colloids Surf., A* **2013**, *439*, 35–42.
- [211] L. Hong, S. Jiang, S. Granick, *Langmuir* **2006**, *22*, 9495–9499.
- [212] G. Mantovani, F. Lecolley, L. Tao, D. M. Haddleton, J. Clerx, J. J. L. M. Cornelissen, K. Velonia, *J. Am. Chem. Soc.* **2005**, *127*, 2966–2973.
- [213] C. J. Dürr, P. Lederhose, L. Hlalele, D. Abt, A. Kaiser, S. Brandau, C. Barner-Kowollik, *Macromolecules* **2013**, *46*, 5915–5923.
- [214] M. Kaupp, T. Tischer, A. F. Hirschbiel, A. P. Vogt, U. Geckle, V. Trouillet, T. Hofe, M. H. Stenzel, C. Barner-Kowollik, *Macromolecules* **2013**, *46*, 6858–6872.
- [215] O. Pop-Georgievski, S. Popelka, M. Houska, D. Chvostová, V. Proks, F. Rypáček, *Biomacromolecules* **2011**, *12*, 3232–3242.
- [216] H. Lee, S. M. Dellatore, W. M. Miller, P. B. Messersmith, *Science* **2007**, *318*, 426–430.
- [217] O. Pop-Georgievski, C. Rodriguez-Emmenegger, A. de los Santos Pereira, V. Proks, E. Brynda, F. Rypáček, *J. Mater. Chem. B* **2013**, *1*, 2859–2867.
- [218] O. Pop-Georgievski, D. Verreault, M.-O. Diesner, V. Proks, S. Heissler, F. Rypáček, P. Koelsch, *Langmuir* **2012**, *28*, 14273–14283.
- [219] V. Proks, J. Jaroš, O. Pop-Georgievski, J. Kučka, v. Popelka, P. Dvořák, A. Hampl, F. Rypáček, *Macromol. Biosci.* **2012**, *12*, 1232–1242.
- [220] S. H. Ku, C. B. Park, *Biomaterials* **2010**, *31*, 9431–9437.
- [221] J.-L. Wang, K.-F. Ren, H. Chang, F. Jia, B.-C. Li, Y. Ji, J. Ji, *Macromol. Biosci.* **2013**, *13*, 483–493.
- [222] C. M. Preuss, A. S. Goldmann, V. Trouillet, A. Walther, C. Barner-Kowollik, *Macromol. Rapid Commun.* **2013**, *34*, 640–644.

- [223] C. N. LaFratta, J. T. Fourkas, T. Baldacchini, R. A. Farrer, *Angew. Chem. Int. Ed.* **2007**, *46*, 6238–6258.
- [224] S. Maruo, J. Fourkas, *Laser & Photon. Rev.* **2008**, *2*, 100–111.
- [225] T. G. Leong, A. M. Zarafshar, D. H. Gracias, *Small* **2010**, *6*, 792–806.
- [226] M. Malinauskas, M. Farsari, A. Piskarskas, S. Juodkasis, *Phys. Rep.* **2013**, *533*, 1–31.
- [227] A. S. Quick, H. Rothfuss, A. Welle, B. Richter, J. Fischer, M. Wegener, C. Barner-Kowollik, *Adv. Funct. Mater.* **2014**, *24*, 3571–3580.
- [228] M. Kaupp, A. P. Vogt, J. C. Natterodt, V. Trouillet, T. Gruending, T. Hofe, L. Barner, C. Barner-Kowollik, *Polym. Chem.* **2012**, *3*, 2605–2614.
- [229] C. Boyer, V. Bulmus, P. Priyanto, W. Y. Teoh, R. Amal, T. P. Davis, *J. Mater. Chem.* **2009**, *19*, 111–123.
- [230] M. Bruns, C. Barth, P. Brüner, S. Engin, T. Grehl, C. Howell, P. Koelsch, P. Mack, P. Nagel, V. Trouillet, D. Wedlich, R. G. White, *Surf. Interface Anal.* **2012**, *44*, 909–913.
- [231] E. H. Lock, D. Y. Petrovykh, P. Mack, T. Carney, R. G. White, S. G. Walton, R. F. Fernsler, *Langmuir* **2010**, *26*, 8857–8868.
- [232] O. Pop-Georgievski, N. Neykova, V. Proks, J. Houdkova, E. Ukraintsev, J. Zemek, A. Kromka, F. Rypáček, *Thin Solid Films* **2013**, *543*, 180–186.
- [233] F. Binns, J. A. G. King, S. N. Mishra, A. Percival, N. C. Robson, G. A. Swan, A. Waggett, *J. Chem. Soc. C* **1970**, 2063–2070.
- [234] J. Fischer, J. B. Mueller, J. Kaschke, T. J. A. Wolf, A.-N. Unterreiner, M. Wegener, *Opt. Express* **2013**, *21*, 26244–26260.
- [235] C. Strazielle, H. Benoit, O. Vogl, *Eur. Polym. J.* **1978**, *14*, 331–334.
- [236] A. A. Gorbunov, L. Y. Solovyova, V. A. Pasechnik, *J. Chromatogr. A* **1988**, *448*, 307–332.
- [237] A. A. Gorbunov, A. M. Skvortsov, *Polymer* **1991**, *32*, 3001–3005.
- [238] T. Gruending, M. Guilhaus, C. Barner-Kowollik, *Anal. Chem.* **2008**, *80*, 6915–6927.

- [239] K. Parry, A. Shard, R. Short, R. White, J. Whittle, A. Wright, *Surf. Interface Anal.* **2006**, *38*, 1497–1504.
- [240] J. Scofield, *J. Electron Spectrosc. Relat. Phenom.* **1976**, *8*, 129–137.
- [241] S. Tanuma, C. J. Powell, D. R. Penn, *Surf. Interface Anal.* **1994**, *21*, 165–176.
- [242] C. M. Herzinger, B. Johs, W. A. McGahan, J. A. Woollam, W. Paulson, *J. Appl. Phys.* **1998**, *83*, 3323–3336.

Curriculum Vitae

Date of Birth: June 20th, 1986
Place of Birth: Nagold, Germany
Nationality: German

Education

01/2011 - 04/2014 **Doctoral Studies in Chemistry**
Under the Supervision of Prof. Dr. Barner-Kowollik
Karlsruhe Institut of Technology (KIT), Germany
"Modular Modification of Polymeric Microspheres"

08/2012 - 10/2012 **Research Period**
Under the Supervision of Prof. Dr. Stenzel
University of New South Wales, Sydney, Australia

11/2010 **Diploma in Chemistry**
Under the Supervision of Prof. Dr. Barner-Kowollik
Karlsruhe Institut of Technology (KIT), Germany
"Photo-Induced Conjugation of Dithioester- and Trithiocarbonate-
Functional RAFT-Polymers with Olefins"

10/2005 - 11/2010 **Studies in Chemistry**
Universität Karlsruhe (TH) (later: Karlsruhe Institut of Technology
(KIT)), Germany

06/2005 **High School Certificate**
Nagold, Germany

Professional Experience

since 01/11	Institut für Technische Chemie und Polymerchemie Karlsruhe Institute of Technology (KIT), Germany Scientific Coworker
09/2010 - 12/2010	Fraunhofer Institute, Pfinztal, Germany Complementary Scientist
07/2009 - 08/2009	Group of Prof. Dr. Barner-Kowollik Universität Karlsruhe (TH), Germany Complementary Scientist
11/2008 - 01/2009	Group of Prof. Dr. Wilhelm Universität Karlsruhe (TH), Germany Student Assistant
08/2008 - 09/2008	Alfa Aesar GmbH & Co. KG, Karlsruhe, Germany Temporary Job

Publications and Conference Contributions

Peer Reviewed Publications*

- 1. Photo-Induced Conjugation of Dithioester- and Trithiocarbonate-Functional RAFT Polymers with Alkenes[§]**
T. Gruending, M. Kaupp, J. P. Blinco, C. Barner-Kowollik, *Macromolecules* **2011**, *44*, 166–174.
- 2. Orthogonal Ligation to Spherical Polymeric Microparticles: Modular Approaches for Surface Tailoring**
A. S. Goldmann, L. Barner, M. Kaupp, A. P. Vogt, C. Barner-Kowollik, *Prog. Polym. Sci.* **2012**, *37*, 975–984.
- 3. Modular Design of Glyco-Microspheres via Mild Pericyclic Reactions and their Quantitative Analysis**
M. Kaupp, A. P. Vogt, J. C. Natterodt, V. Trouillet, T. Gruending, T. Hofe, L. Barner, C. Barner-Kowollik, *Polym. Chem.* **2012**, *3*, 2605–2614.
- 4. A Facile Route to Boronic Acid Functional Polymeric Microspheres via Epoxide Ring Opening**
A. P. Vogt, V. Trouillet, A. M. Greiner, M. Kaupp, U. Geckle, L. Barner, T. Hofe, C. Barner-Kowollik, *Macromol. Rapid Commun.* **2012**, *33*, 1108–1113.
- 5. (Ultra-)Fast Catalyst-Free Macromolecular Conjugation in Aqueous Environment at Ambient Temperature**
M. Glassner, G. Delaittre, M. Kaupp, J. P. Blinco, C. Barner-Kowollik, *J. Am. Chem. Soc.* **2012**, *134*, 7274–7277.

*The publications marked with a § were accomplished during the Diploma thesis. All other publications and contributions stem from the course of the current thesis.

6. **Access to Intrinsically Glucoside-Based Microspheres with Boron Affinity**
A. P. Vogt, T. Tischer, U. Geckle, A. M. Greiner, V. Trouillet, M. Kaupp, L. Barner, T. Hofe, C. Barner-Kowollik, *Macromol. Rapid Commun.* **2013**, *34*, 916–921.
7. **Photo-Sensitive RAFT-Agents for Advanced Microparticle Design**
M. Kaupp, T. Tischer, A. F. Hirschbiel, A. P. Vogt, U. Geckle, V. Trouillet, T. Hofe, M. H. Stenzel, C. Barner-Kowollik, *Macromolecules* **2013**, *46*, 6858–6872.
8. **Photochemical Design of Functional Fluorescent Single-Chain Nanoparticles**
J. Willenbacher, K. Wuest, J. O. Mueller, M. Kaupp, H.-A. Wagenknecht, C. Barner-Kowollik, *ACS Macro Lett.* **2014**, *3*, 574–579.
9. **Photo-Induced Functionalization of Spherical and Planar Surfaces via Caged Thioaldehyde End-Functional Polymers**
M. Kaupp, A. Quick, C. Rodriguez-Emmenegger, A. Welle, V. Trouillet, O. Pop-Georgievski, M. Wegener, C. Barner-Kowollik, *Adv. Funct. Mater.* **2014**, DOI: 10.1002/adfm.201400609.

Conference Contributions[†]

1. **Epoxide Microspheres: A Versatile Material for Various Surface Modifications**
A. P. Vogt, M. Kaupp, V. Trouillet, A. M. Greiner, U. Geckle, L. Barner, T. Hofe, C. Barner-Kowollik
Warwick Polymer Conference 2012, Coventry, United Kingdom.
2. **XPS-Charakterisierung oberflächenmodifizierter Epoxid-Mikropartikel**
V. Trouillet, A. P. Vogt, M. Kaupp, A. M. Greiner, U. Geckle, L. Barner, T. Hofe, C. Barner-Kowollik
Angewandte Oberflächenanalytik AOFA 17 2012, Soest, Germany.
3. **Photo-Sensitive RAFT Agents for Advanced Glyco-Material Design**
M. Kaupp, A. Hirschbiel, A. P. Vogt, V. Trouillet, T. Hofe, M. Stenzel, C. Barner-Kowollik
European Polymer Congress EPF 2013, Pisa, Italy.

[†]The presenter is underlined.

4. Advanced Microsphere Design via Thermal and Light Triggered Ligation Chemistries

A. P. Vogt,[‡] M. Kaupp,[‡] V. Trouillet, T. Tischer, U. Geckle, A. M. Greiner, A. F. Hirschbiel, M. H. Stenzel, L. Barner, T. Hofe, C. Barner-Kowollik

Makromolekulares Kolloquium 2014, Freiburg, Germany.

Invited Talks

1. Non-demanding and modular modification of epoxy-functionalized polymeric microspheres

University of Sydney, Key Centre for Polymers & Colloids, Sydney, Australia, invited by Prof. S. Perrier, 10/2012.

2. Non-demanding and modular modification of epoxy-functionalized polymeric microspheres

Queensland University of Technology, Brisbane, Australia, invited by Dr. J. Blinco (ECARD Lecturer), 11/2012.

[‡]Authors contributed equally.

Danksagung – Acknowledgements

Zuallererst möchte ich Prof. Dr. Christopher Barner-Kowollik für die Überlassung dieses interessanten Themas, sein stetes Interesse, allzeitige Unterstützung, gelebte Motivation und Vertrauen in meine Fähigkeiten danken.

I would like to thank Dr. Andrew P. Vogt for our valuable joint work on the challenging topic of microspheres.

Dr. Thorsten Hofe von PSS danke ich für seine Unterstützung, seine Expertise und die vielen konstruktiven Treffen während unserer Zusammenarbeit. Natürlich gilt mein Dank auch allen weiteren Mitarbeitern von PSS, die Material und Messergebnisse für mich beigesteuert haben.

Vielen, vielen Dank an Vanessa Trouillet für all die XPS-Messungen und die Bearbeitung der Rohdaten. Deine Messungen und unsere Gespräche haben diese Arbeit weit voran gebracht.

Udo Geckle möchte ich für die REM-Bilder danken. Auch wenn der Großteil der Bilder nun im Appendix steckt, waren sie doch immer wichtig.

Dem Fraunhofer-Institut für chemische Technologie (ICT) in Pfinztal, insbesondere Dr. Bea Tübke, danke ich für die Elementaranalysen.

Dr. Alexandra Greiner danke ich für die vielen Fluoreszenzmikroskopieaufnahmen. Schade, dass die gute Zusammenarbeit (noch) nicht zu einer gemeinsam veröffentlichten Arbeit gereicht hat.

Alexander Quick und Dr. Alexander Welle danke ich für das Laser-Schreiben der Oberflächen und deren ToF-SIMS Messung. Das sind einfach immer tolle Bilder.

I would like to thank Dr. César Rodríguez-Emmenegger and Dr. Ognen Pop-Georgievski for the PDA-coating and the fruitful discussions.

Ich danke dem Karlsruhe House of Young Scientists (KHYS) für die finanzielle Förderung meines Auslandsaufenthaltes an der University of New South Wales (UNSW) in Sydney, Australien. Prof. Dr. Martina Stenzel danke ich dafür, mich in Australien betreut zu haben.

Für weitere Unterstützung bei gemeinsamen Projekten danke ich Dr. Till Gründling, Jens

Natterodt, Dr. Anja Goldmann, Dr. Leonie Barner, Dr. Mathias Glassner, Dr. Guillaume Delaittre, Prof. Dr. Martin Wegener und Astrid Hirschbiel. This thank you includes Dr. James Blinco.

Jan Müller, Johannes Willenbacher, Marcel Langer, Alexander Hähnel und Alexander Quick danke ich für das Korrekturlesen dieser Arbeit. Verbliebene Rechtschreibfehler gehen auf Euch ;-).

Danke an das "Masse-Team", Kai und Astrid, für die Hilfe beim gemeinsamen Kampf gegen die Maschine.

Allen Kollegen danke ich für mehr als nur gute Zusammenarbeit. Die gute Atmosphäre und der Zusammenhalt in unserer Gruppe sind großartig. Dem "kleinen" Büro, insbesondere Alexander und Astrid, danke ich dafür, auch während des Schreibens dieser Arbeit immer für gute Stimmung gesorgt und mich ertragen zu haben.

Mit Thomas Tischer verbindet mich ein gemeinsamer Weg seit dem Quali. Von Dir habe ich viel gelernt, wir haben viel erlebt, viel gelacht und nun werden wir zusammen zwei Buchstaben erhalten. Und alle so "yeah".

Christiane und Thomas danke ich für die gemeinsame Feier die jetzt ansteht.

Meinen Freunden David, Claudi und dem ganzen Fuchsrudel danke ich für die tolle Zeit während des Studiums und danach.

Auch während der Promotion habe ich gute Freunde kennen gelernt, dafür vielen Dank und tack så mycket an Corinna, Susanne, Jan, Kim und Johannes.

Meiner Mutter, meiner Oma, meinen Verwandten und Freunden und insbesondere meiner Schwester Nadine danke ich für die großartige Unterstützung bis hierhin. Traurig macht mich nur, dass ich diese Leistung nicht mehr meinem Vater zeigen darf.

Das Ende dieser Arbeit markiert auch das Ende vieler Geschichten, Ereignisse und Erfahrungen. Allen die mich auf diesem Weg für ein kürzeres oder langes Stück begleitet haben möchte ich abschliessend vielen Dank zukommen lassen und einen erfüllten weiteren Lebensweg wünschen.